EFFECTS OF STORMS ON SHORT AND MEDIUM-TERM MORPHODYNAMICS OF A TIDE-DOMINATED COASTAL REGION

Dissertation

zur Erlangung des Doktorgrades

der Mathematisch-Naturwissenschaftlichen Fakultät

der Christian-Albrechts-Universität zu Kiel

vorgelegt von

Talal Etri

Kiel

October 2007

Referent:	Prof. Dr. Roberto Mayerle
Koreferent:	Prof. Dr. Franciscus Colijn
Tag der mündlichen Prüfung:	3. December 2007
Zum Druck genehmigt:	Kiel, December 2007

Der Dekan:	Prof. Dr. Jürgen Grotemeyer

Acknowledgements

First of all I would like to thank GOD for giving me the effort to do this work.

This thesis arose in part out of years of research that has been done since I came to Coastal Research Laboratory (CORELAB). By that time, I have worked with a great number of people whose contribution in assorted ways to the research and the making of the thesis deserved special mention. It is a pleasure to convey my gratitude to them all in my humble acknowledgment.

In the first place I would like to record my gratitude to my advisor, Professor Roberto Mayerle, for his constant encouragement, support and invaluable suggestions. Without his help, this work would not be possible.

Above all and the most needed, he provided me unflinching encouragement and support in various ways. His truly scientist intuition has made him as a constant oasis of ideas and passions in science, which exceptionally inspire and enrich my growth as a student, a researcher and a scientist want to be. I am indebted to him more than he knows.

Collective and individual acknowledgments are also owed to my colleagues at CORELAB whose present somehow perpetually refreshed, helpful, and memorable. Many thanks go in particular to Dr. Peter Wepen, Dr. Kalle Runte, Dr. Klaus Ricklefs, Dr. Jort Wilkens, Dr. Poerbandono, Dr. Gatot Pramono, Dr. Wiwin Windupranata, Dirk Schulz, Maryam Rahbani, Ilgar Özgürel and Jose Fernandez for giving me such a pleasant time when working together with them since I knew them.
My special thanks go to My brother Dr. Tareq Etri, Prof. Rangaswarni Narayanan, Dr. Carlos Escobar, Leslie Malick and Nestor Jimenez. Without them the thesis would be unintelligible to read at all. I am also very grateful to Katherine Rosin and Gerd Bruss for the translation of the thesis abstract to German language.

I am deeply and forever indebted to my parents for their love, support and encouragement throughout my entire life. I am also very grateful to my wife Salwa Sliman for here support during my work. Also my sincere thanks go to my brothers, sisters and my wife's family.
Finally, I would like to thank everybody who was important to the successful realization of thesis, as well as expressing my apology that I could not mention personally one by one.

Notation

Symbol	Description	Unit
Δt	Computational time step	[s]
Δx	The length of the grid cells in x-direction	[m]
Δy	The length of the grid cells in y-direction	[m]
λ_x	Sediment transport representativity factor in x-direction	[-]
λ_y	Sediment transport representativity factor in y-direction	[-]
ν	Horizontal eddy viscosity	$[\frac{m^2}{s}]$
Ω	Angular speed of rotation of the earth	$[\frac{deg}{s}]$
ϕ	Geographic latitude	[degree]
ρ_d	Sediment dry density	$[\frac{kg}{m^3}]$
ρ_s	Sediment density	$[\frac{kg}{m^3}]$
ρ_w	Water density	$[\frac{kg}{m^3}]$
σ	The vertical direction of the coordinate system	[-]
$\tau_{cr,s}$	Critical bed shear stress for sedimentations	$[\frac{N}{m^2}]$
$\tau_{cr,e}$	Critical bed shear stress for erosion	$[\frac{N}{m^2}]$
τ_w	Bed shear stress due to waves	$[\frac{N}{m^2}]$
τ_c	Bed shear stress due to current	$[\frac{N}{m^2}]$
τ_{max}	Maximum bed shear stress	$[\frac{N}{m^2}]$
τ_m	Combined wave-current bed shear stress	$[\frac{N}{m^2}]$
Θ	Wave direction	$[^o$N]

ξ, η	Horizontal curvilinear coordinates	[m]
ζ	Water level above some horizontal plane of reference	[m]
C_r	Courant-Friedrich-Levy number	[-]
d	water depth below some horizontal plane of reference	[m]
d_{50}	Median grain diameter sand	[μm]
d_{min}	Minimum depth for sediment calculation	[m]
E	Non-local sink term due to evaporation	[-]
f	Frequency	[H_z,$\frac{1}{s}$]
f	Coriolis parameter	[H_z,$\frac{1}{s}$]
F	Fetch length	[m]
f_{mor},Morfac	Morphological scale factor	[-]
f_u,f_v	Coriolis coefficient (inertial frequency)	[$\frac{1}{s}$]
F_ξ	Turbulent momentum flux in ξ-direction	[$\frac{m}{s^2}$]
F_η	Turbulent momentum flux in η-direction	[$\frac{m}{s^2}$]
F_ξ, F_η	Horizontal Reynold's stresses	[$\frac{m}{s^2}$]
g	Acceleration due to gravity	[$\frac{m}{s^2}$]
$G_{\xi\xi}$	Coefficient used to transform curvilinear to rectangular coordinates	[m]
$G_{\eta\eta}$	Coefficient used to transform curvilinear to rectangular coordinates	[m]
h	Water depth	[m]
H	Wave height	[m]
H_s	Significant wave height	[m]
H_ϕ	Representative wave height	[m]
$h_{ref.}$	van Rijn's reference height factor	[m]
M_ξ	Source or sink of momentum in ξ-direction	[$\frac{m}{s^2}$]
M_η	Source or sink of momentum in η-direction	[$\frac{m}{s^2}$]

P	The non-local source term of precipitation	[-]
P_ξ	Gradient hydrostatic pressure in ξ-direction	$[\frac{kg}{m^2 s^2}]$
P_η	Gradient hydrostatic pressure in η-direction	$[\frac{kg}{m^2 s^2}]$
P_x, P_y	Horizontal pressure	$[\frac{N}{m^2}]$
Q	Global source or sink per unit area	$[\frac{m}{s}]$
q_{in}	The local sources of water per unit of volume	$[\frac{1}{s}]$
q_{out}	The local sinks of water per unit of volume	$[\frac{1}{s}]$
S_x	Total sediment transport in x-direction per unit width	$[\frac{m^2}{s}]$
S_y	Total sediment transport in y-direction per unit width	$[\frac{m^2}{s}]$
t_d	Wind duration	[s]
u	Wind velocity	$[\frac{m}{s}]$
u	Flow velocity in the ξ- direction	$[\frac{m}{s}]$
v	Flow velocity in the η- direction	$[\frac{m}{s}]$
V_{1990}	Wet volume below MSL of a sub-domain in 1990	$[m^3]$
V_i	Wet volume below MSL of a sub-domain in year i	$[m^3]$
$V_{rel,i}$	Relative wet volume below MSL of a sub-domain in year i	[-]
w_s	Settling velocity for cohesive sediment	$[\frac{mm}{s}]$

Abstract

Relevance of storm events on the morphodynamics
A storm event over shallow nearshore coastal waters or shallow inland water bodies can generate large water fluctuations if the storm is sufficiently strong. It can cause both a rise (set-up) and fall (set-down) of the water level. Generally, as a result of the water level fluctuations and the associated changes in the wave conditions the morphology will change at temporal and spatial scales.
The main concern of this work is to study the storm events and their effects on the short- and the medium-term morphological developments in the central Dithmarschen Bight, German North Sea. In this study, the morphological changes on the short- and the medium-term will be a result of a singular event from a few hours to days and from a few weeks to months, respectively.

Dithmarschen Bight morphodynamic model
In previous works, the individual process models (flow, wave and sediment transport) have been extensively calibrated and validated against measurements.
In this work a morphodynamic model for the Dithmarschen Bight region has been setup. The morphodynamic model is based on Delft3D model developed by WL | Delft Hydraulics in which the on-line approach was applied. The Dithmarschen Bight morphodynamic model implies a morphological acceleration factor. Moreover, the sediment transport model concerns the sediment distribution for cohesive and non-cohesive sediments for the Dithmarschen Bight.

Modelling of the short-term morphodynamics
In the short-term morphodynamic model the simulations were obtained by nesting the Dithmarschen Bight Model (DBM) in the German Bight Model (GBM), which in turn is nested in the northwest European Continental Shelf Model (CSM). For the Dithmarschen Bight model the bathymetry update takes place every computing time step of the flow simulation and the analysis was focused on two severe events that took place in January 1994 and December 1999.

Modelling of the medium-term morphodynamics
In the medium-term morphodynamic model an input filtering approach has been applied in which a limited number of representative conditions by means of tides, wave climates and storm conditions were defined. The interactions between the flow, sediment and wave models were obtained every time step of the flow model, however, the bathymetric update will take place each morphological acceleration factor value.

Analysis of modelled short-term morphodynamics
The performance of the short-term morphodynamic model showed that the maximum morphological changes take place during the storm event (the peak of the storm) with about 1m depth of erosion in the Tertiussand sandbank at most. It has been also noted that the morphological changes due to the tide alone were relatively small within the period considered.
The morphological changes due to the two storms events indicate that more significant changes took place during the storm of December 1999 and lower morphological activity was observed from the storm of January 1994.

Analysis of modelled medium-term morphodynamics
The medium-term morphodynamic model showed that the tide is the main driving force for the initiation of the tidal channels and the storms are responsible for the erosion of the tidal flats. The model also showed no indication that the storm sequences and the chronology of the wave climates have major effects on the morphodynamics for the simulation period.
The evaluation of the differences between the cases simulated including only the tides and those including tides and storms together, showed that there are increases in erosion and sedimentation of about 0.4m in the Tertiussand sandbank and about 1m in the Piep tidal channel after including the storms.

Zusammenfassung

Die Bedeutung von Sturmereignissen für die Morphodynamik
In flachen Küsten- oder Binnengewässern können durch ausreichend starke Sturmereignisse groβe Veränderungen im Wasserkörper hervorgerufen werden. Sie können sowohl einen Anstieg (set-up) sowie ein Abfallen (set-down) des Wasserstandes bewirken. Generell führen diese Fluktuationen und die damit einhergehenden Änderungen des Seegangs zu einer Veränderung der Morphologie in verschiedenen räumlichen sowie zeitlichen Skalen.
Das Hauptanliegen dieser Arbeit ist die Untersuchung von Sturmereignissen und deren Auswirkungen auf die kurz- bis mittelfristigen morphologischen Entwicklungen in der zentralen Dithmarscher Bucht der Deutschen Nordsee. In dieser Studie werden die kurz- bzw. mittelfristigen morphologischen Veränderungen durch Einzelereignisse von wenigen Stunden bis Tagen bzw. von kontinuierlichen Vorgängen innerhalb weniger Wochen bis Monaten sowie deren Kombination verursacht.

Morphodynamisches Modell Dithmarscher Bucht
In vorangegangenen Studien wurden die einzelnen Prozessmodelle (Strömung, Seegang und Sedimenttransport) umfangreich kalibriert und gegen Messungen verifiziert. In der vorliegenden Arbeit wurde ein morphodynamisches Modells für die Dithmarscher Bucht aufgebaut. Es basiert auf dem Delft3D Modell, entwickelt von WL | Delft Hydraulics, unter Anwendung des "online" Ansatzes. Besonderheiten sind die Anwendung eines Beschleunigungsfaktors im morphodynamischen Modell sowie die Unterscheidung in der Verteilung von kohäsiven und nichtkohäsiven Sedimenten im Sedimenttransportmodell.

Modellierung der kurzfristigen Morphodynamik
Für das Modell zur Simulation der kurzfristigen Morphodynamik wurden folgende Modelle ineinander "genested": das "Dithmarscher Bucht Modell" (DBM) in das "Deutsche Bucht Modell" (GBM) und das GBM in das "Northwest European Continental Shelf Model" (CSM). Im Modell der Dithmarscher Bucht für kurze Zeiträume erfolgt die Aktualisierung der Bathymetrie bei jedem Rechen-Zeitschritt des Strömungssmodells. Der Fokus der Auswertungen war auf die beiden schweren Sturmereignisse vom Januar 1994 und Dezember 1999 gerichtet.

Modellierung der mittelfristigen Morphodynamik
Für das Modell zur Simulation der mittelfristigen Morphodynamik wurde ein Filter angewendet in dem eine eingeschränkten Anzahl repräsentativer Eingangswerte in Bezug auf Gezeiten, Seegangsklimate und Sturmbedingungen definiert wurden.

Der Austausch der Informationen zwischen Strömungs-, Seegangs- und Sedimenttransportmodell erfolgte an jedem Zeitschritt des Strömungsmodells, wohingegen die Aktualisierung der Topographie entsprechend dem morphologischen Beschleunigungsfaktor durchgeführt wurde.

Analyse der modellierten kurzfristigen Morphodynamik
Die Ergebnisse der Simulationen der kurzfristigen Morphodynamik zeigen, dass sich die gröβten morphologischen Veränderungen während der Sturmereignisse (zum Höhepunkt des Sturmes) ereignen, mit Höchstwerten um 1m im Bereich des Tertiussandes. Des Weiteren wurde deutlich, dass unter den gegebenen Modellbedingungen die morphologischen Veränderungen aufgrund der Gezeitenwirkung allein relativ klein blieben. Ein Vergleich der Topographieänderungen während der beiden Sturmereignisse zeigte signifikante Veränderungen während des Sturms im Dezember 1999 und eine geringere morphologische Aktivität während des Sturms im Januar 1994.

Analyse der modellierten mittelfristigen Morphodynamik
Die Simulationen zur mittelfristigen Morphodynamik machten deutlich, dass die Gezeiten die Hauptantriebskraft für die Ausbildung und Umlagerung von Prielen sind und dass Sturmereignisse hauptsächlich für die Erosion der Wattflächen verantwortlich sind.
Die Ergebnisse gaben keine Hinweise darauf, dass die zeitliche Abfolge der Sturmsequenz innerhalb der gegebenen Simulationsperiode, eine Auswirkung auf die Morphodynamik hat. Eine Auswertung der Unterschiede zwischen Simulationen mit reiner Gezeitenwirkung und solchen mit Gezeiten und gleichzeitigem Sturmereignis zeigte, dass sich unter zusätzlicher Sturmeinwirkung eine erhöhte Erosion und Sedimentation von etwa 0,4m am Tertiussand und von etwa 1m im Piep-Priel ergaben.

Contents

List of Figures

List of Tables

Chapter 1

Introduction

1.1 General problem definition

Coastal morphological changes take place at a variety of spatial and temporal scales, from small-scale ripple formation at a time of minutes to the evolution of entire coastal systems at historical and geological time scales (De Vriend, 1998). Dynamic coastal systems often show complex, non-linear morphological changes. Erosion, transport and deposition of sediment often involve long-term processes, that make possible the morphological evolution of sedimentary coasts as a result of counteracting processes of sediment supply and removal. A shoreline may adapt a stat of equilibrium in the cross- or long-shore direction once these processes are in balance. However, external factors, such as storms, often induce morphodynamic change away from an equilibrium state (IPCC, 2007).

The impact of strong storms over large coastal areas obviously produce high waves and surges. The greatest and most dramatic changes occur during storms. Coastal systems also are constantly remolded under the action of waves, wind and tides. Thus, the study of storm effects is extremely important for the knowledge of coastal hazards and also, to improve coastal management projects (Reyes, et al., 1999). Several field surveys have demonstrated that the coastal regions tend to recover after storms, though, this recovery processes have not been investigated extensively and are not well understood. In some cases the post-storm recovery can last from 4 to 5 years or even larger (Zhang et al., 2002).

The evaluation of the morphological changes is a matter of available bathymetric measurements for the considered temporal and spatial scales. Due to the fact that bathymetric measurements are not only expensive but also not easy, it is very difficult to obtain the necessary field data immediately before and after a storm event. Because of the growth of knowledge and our understanding of the different coastal processes and the progress in the utilization of computers, researchers are able to develop and set-up complex numerical models to study the morphology of the nearshore regions. Hence, the analysis and the detailed prediction of the morphological changes involving tidal inlets, river mouths, estuaries and bays require the use of advanced process-based morphodynamic models is now possible.

In this work, storms and their relevance for the morphological evolutions at the central Dithmarschen Bight have been studied through the advantage of the morphodynamic models. This study mainly addresses two problems; (1) How can we capture, in short-term, the storm developments and its impact on the morphological changes during the event itself (few hours to weeks)?, and (2) How do the storm events, in medium-term, affect the morphological changes after the event has taken place (few weeks to months) and how the system will recover from these effects?

On the basis of previous studies, a short- and a medium-term morphodynamic model has been set-up by combining calibrated and validated individual process models for flow, wave and sediment transport. The applied morphodynamic model is based on coupled flow, wave and sediment transport models via a bed evolution model. In the short-term morphodynamic model, the influence of storm events on morphological developments was investigated on the basis of a real time hindcast principle of the storm events.

In order to limit the computational requirements of the medium-term morphodynamic model, input reduction was applied for the tidal, wave and local wind driving conditions. The representative forcing conditions obtained by these techniques should result in approximately the same morphological changes as it would be expected under actual conditions over the same simulation period.

1.2 Aims and Objectives

The main aim of this work is to analyze the morphological developments due to storm events over short-term (days to month) and medium-term (months to one year) periods. Therefore, the main objectives are as follows:

- to have a clear and detailed understanding about the morphological evolution due to storm events on the short and medium-term in the study area,
- to differentiate between the effects of several storm events and their characteristics in the morphological developments,
- to study the recovery process after the storm and how long it could take to recover from the post-storm morphological changes,
- to study the effect of the storm sequences (chronology) on the changes in the morphology, and
- to study the effect of the wave climates and their sequences on the morphological developments.

1.3 Structure of the Thesis

Chapter 1
This chapter includes an introduction of the study, the motivations behind the thesis and, the main aim and objectives of this work.

Chapter 2
In this chapter literature review is presented. In addition, descriptions of the most recent approaches regarding the use of numerical morphodynamics modelling are given.

Chapter 3
This chapter presents the general characteristics of the Dithmarschen Bight region. The hydrodynamic processes and sediment properties and, processes will be addressed. The available data, that will be used as input and for assessing the performance of the Dithmarschen Bight morphodynamic model, are described.

Chapter 4
In this chapter the set-up of the Dithmarschen Bight morphodynamic model is presented. The description covers the definition of the model extent, grid, bathymetry and boundary conditions. The set-up of the models for the simulation of flow, waves, sediment transport and morphological evolution on the short- and medium-term is presented.

Chapter 5
In this chapter the results of the simulations of the short-term morphodynamic model for the Dithmarschen Bight are presented. Also, the effects of the storm events on the morphological changes are described. Additionally the selection of storms has been studied in more detail.

Chapter 6
The chapter presents the results of the numerical investigations of the effect of the storms on the medium-term morphological changes. The chapter describes the model set-up, representative tide conditions and simulation scenarios for wind and wave conditions. A conclusion at the end of the chapter with model results and analysis are presented.

Chapter 7
This chapter presents a summary of the outcome of the work and the main recommendations regarding future studies and analysis.

Chapter 2

Literature review

2.1 Introduction

In the recent past, numerical models have gained ground in improving our understanding of the coastal dynamics and assessment of consequences of human impacts. These models also have been developed for applications to coastal regions.
The model compiles modules for solution of flow, wave, sediment transport and morphological evolution.

Models based on hydrodynamic processes are being widely applied and successfully validated for the prediction of currents, water levels and waves at the engineering time and spatial scales. On the other hand, models for sediment dynamics and morphodynamic models are in the process of development.
This chapter will review the main morphodynamic model for coastal regions. Details of the different time scales in the modelling process are also discussed. Finally the most recent morphodynamic model that has been set-up and the proposed model to the area of interest are presented.

In this study short-term is defined as the time scale of several days up to a month, medium-term as several months up to years and long-term as several decades up to centuries. This time scale of the morphological changes is related to the time span proposed by De Vriend, 1997 (Fig. 2.1). On the short and medium-terms the morphological changes are considered in terms of the evolution of channels, tidal ridges, shoals (sandbanks) and tidal flats.

Multidimensional coastal evolution models usually start from a number of more or less standard models of constituent physical processes like wave, currents, and sediment transport. These basic models can be summarised in three models as the following: Short-term morphodynamic (STM), Medium-term morphodynamic (MTM), and Long-term morphological models (LTM). A more detailed description of these models can be found in Fig. 2.2.

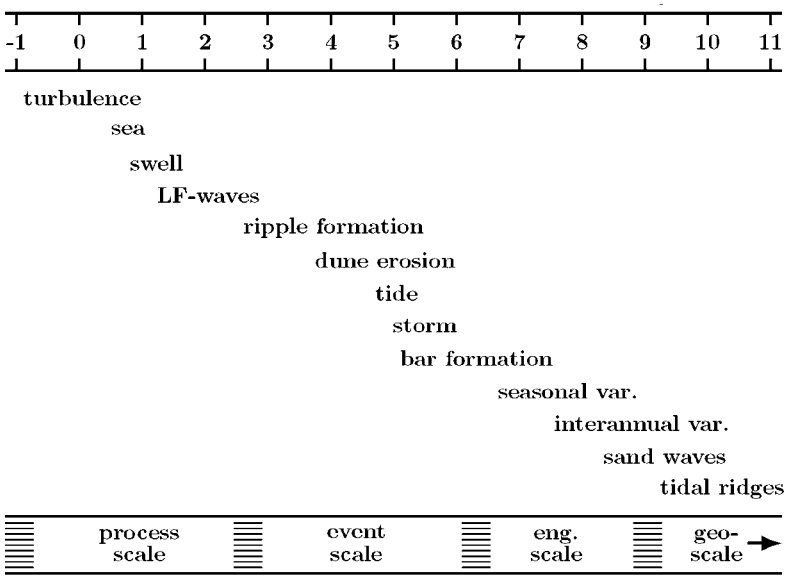

Figure 2.1: Scale range in coastal morphology, where T_m is morphological time scale in sec. (after De Vriend, 1997)

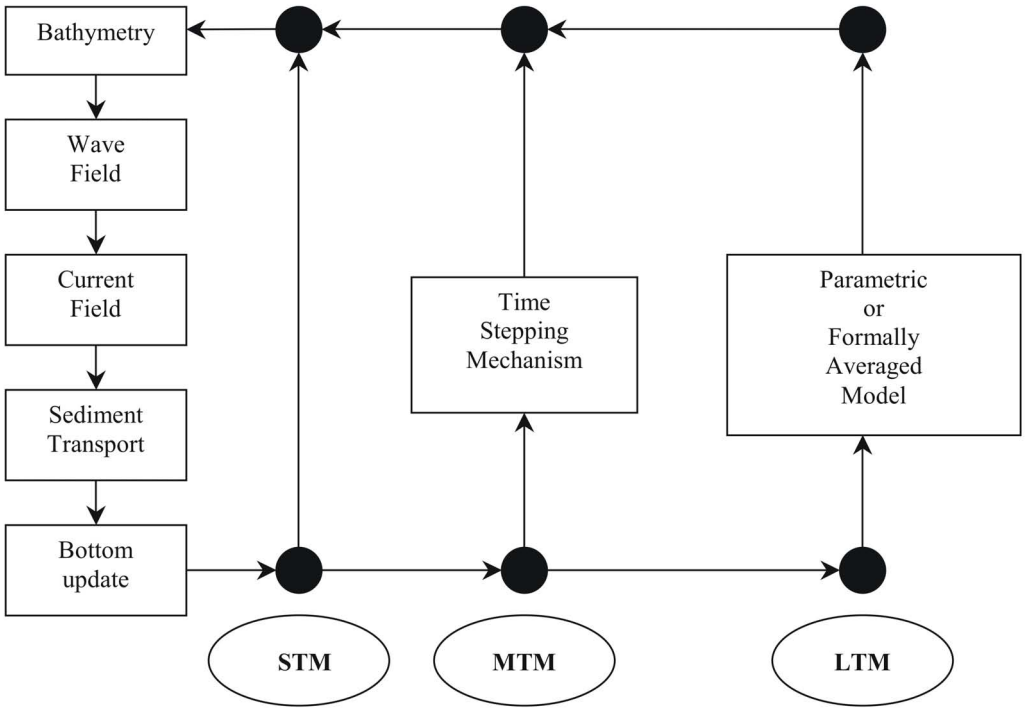

Figure 2.2: Basic morphological model concepts

2.2 Short-term morphodynamics (STM)

2.2.1 General concepts

The basic idea of this model is that the hydrodynamic and sediment transport computation are based on the updated bed topography at every location and time step (De Vriend, 1987).
The series of constituent process models that forms an STM-model is an essential element in all-morphological modelling approaches. The composition of this series is far from trivial and determines to a high extent the quality of the final results (De Vriend, 1987). In this type of models the coupling procedure of flow, wave, sediment transport and bottom evolution takes place every computing time step for the flow model. These models are coupled and the bed topography is updated at every time step.

2.2.2 Wind-wave generation and degeneration

Wind blowing over the surface of a water body will transfer energy to the water in the form of a surface current and by generating waves on the water surface. The first question is, how does a horizontal wind initiate the formation of waves on an initially flat water surface. This process is best explained by a resonance model proposed by Phillips (1957 and 1960). There are turbulent eddies in the wind field that exert fluctuating pressure on the water surface. These pressure fluctuations vary in magnitude and frequency and they move forward at a wide range of speeds. The pressure fluctuation cause water surface undulations to develop and grow. The key to their growth is that a resonant interaction occurs between the forward moving pressure fluctuation and the free waves that propagate at the same speed as the pressure fluctuations (Sorensen, 2006).

The significant wave height and period as well as the resulting spectrum of wind-generated wave depend primarily on the distance over which the wind blows F (fetch length), the wind velocity u (10 m above the reference) and the duration of the wind t_d. As is demonstrated in Fig. 2.3, if the wind duration exceeds the time required for waves to propagate the entire fetch length, the waves will grow along the path OAB and their characteristics at the end of the fetch will depend on the fetch and the wind velocity. This is known as the fetch limited condition. If the duration is less, wave growth reaches only the path OAC and wave generation is duration limited. If both the fetch and duration are sufficiently large, the curve OAB becomes essentially horizontal at the downwind end and a fully developed sea is generated for that wind velocity. Note that as the waves grow, the component periods and thus the component group celerities continually increase along the fetch so an average group celerity would have to be used to determine if waves are fetch or duration limited (Sorensen, 2006).

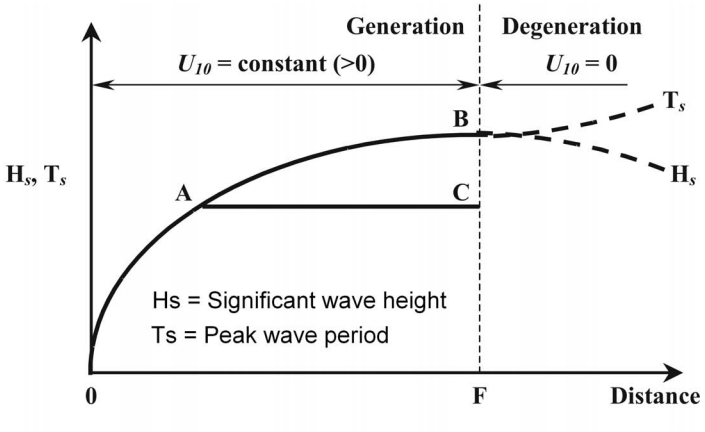

Figure 2.3: Idealized wave growth and decay for a constant wind velocity (after Sorensen, 2006)

2.3 Medium-term morphodynamics (MTM)

Medium-term morphodynamic models are not likely to be able to cover time spans, which are much larger than the inherent time scale of the relevant morphological evolution. The described process is non-linear and the input conditions are uncertain and include extreme events. Therefore the predictability of morphological evaluation must be expected to decrease as the time span increases. However, the quantification of this statement is still a research issue (De Vriend 1993).

This is the justification for a medium-term model, which neither goes into the details of small-scale processes nor extends into the scales far beyond those of interest. It also gives access to powerful mathematical techniques based on scale separation and perturbation methods (De Vriend et al., 1993). Therefore one of the key elements in medium-term modelling is reduction of information. It involves essentially four levels (see Fig. 2.4), which concerns the input, the physical system or its model, the output and the interpretation or generalization.

2.3.1 Tide input filtering

To find out the representative tide, the following matters should be taken into account (Latteux, 1995):

- The long-term distribution of tidal range
- The relation between tidal range and tidal current, from analytical, or by numerical models, or field measurements
- The relationship between the current velocity, the water depth, and the sediment transport.

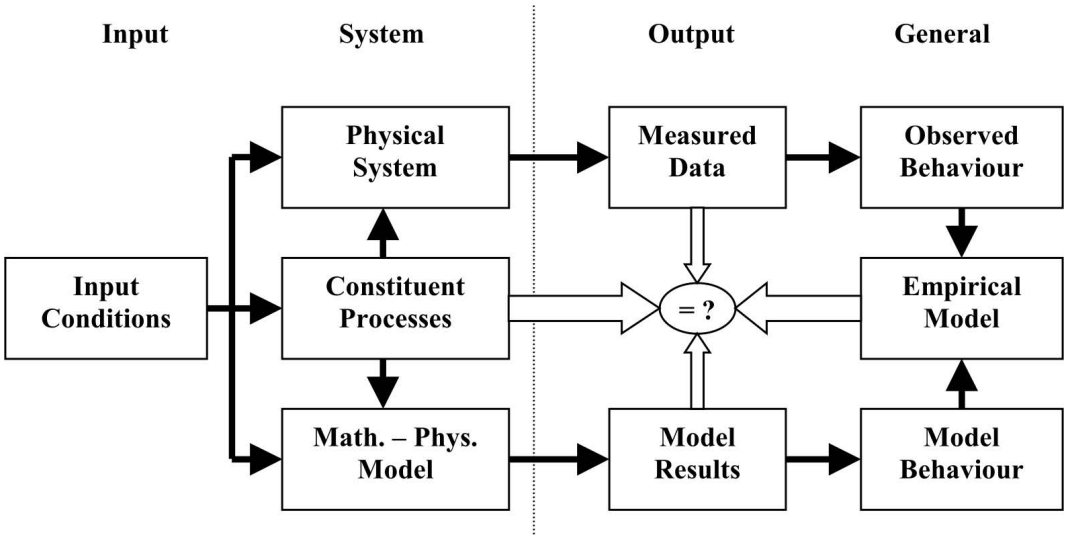

Figure 2.4: Aggregated flow chart of medium-term prediction process (after De Vriend et al., 1993)

After that it is possible to determine one representative tide (morphological tide). This tide must lead to the same elementary (flood and ebb) and residual transport (intensity and direction) as the sum of these transports for each class of tide, weighted by its frequency of occurrence that represents the average actual transport. It will be possible to determine a set of representative tides (number, tide range and weighting factor for each tide) for which the effect on the bed will be similar to the effect of the actual set of natural tides (Latteux, 1995).

The physical system which is intended to be simulated, is a fully coupled system where flow, sediment transport and morphological changes are permanently interacting. This interaction requires, that the flow is continually re-computed as the bed evolves. This is a prohibitively time consuming requirement which can be relaxed by using the difference in the time scales between hydrodynamics and morphodynamics. According to Latteux (1995) the following methods may be used since the bed changes are not too significant:

- Disregard the effect of bed evolution on flow at the very short-term. In this simple method the flow and then the sediment transport is kept without any modification as long as the bed evolution remains small enough;
- Adjust the flow to the new topography by a continuity correction assuming that there is no surface changes or current deflection due to these bed changes. The new velocity is computed from the initial flow discharge and from the new water depth, then considering the bed changes which occurred in the meanwhile this is only valid under the assumption that the flow direction is less sensitive to bed topography than its velocity;
- Compute the flow perturbations induced by the bed changes assuming that there is no surface changes or current deflection no free surface changes. Additionally assuming that these perturbations are weak enough, linearization of

the shallow water equations makes it possible to compute them from a Poisson equation (Hauguel, 1978 and Latteux, 1995).

The number of morphological time steps would really be huge if each involved tide in this medium-term process had to be simulated in detail. In order to reduce the number of morphological time steps, four very pragmatic methods have been developed and tested at the National Hydraulic Laboratory, France (Laboratoire National d' Hyraulique) (Latteux, 1987, 1990) and are described below:

- Straightforward extrapolation:
  This method assumes that the flow is not modified as long as the bed changes do not exceed a given threshold. The results of computed bed changes on a first tide, with a fixed bed, is then extrapolated for n number of tides such that the maximum evolution over these n tides is equal to this threshold. N is called the filtering coefficient. This method is very simple and cheap. However, as it is not centred in time (bed changes over n tides are computed from the first one) it leads rapidly to instabilities if the filtering coefficient is too large. Moreover, as this extrapolation is more or less an Eulerian artefact it can not reproduce the propagation of bed forms;

- Time-centered extrapolation:
  The idea is still to extrapolate to n tides from the results obtained on one of them. However this tide is no longer the first one, but more or less the one in the middle using a predictor correction approach. In the first trial the straightforward extrapolation method is used to derive a first guess of the bed changes over n tides. Then sediment transport is computed over the tide n+1 after considering the effect of this bed evolution on hydrodynamics for example by using the continuity correction. Then the average of the bed changes computed in the first trail over the first tide and afterwards over the tide n+1 which, leads to better time-centered estimation of the average change over these n tides. This method is like the previous method but, it is more accurate and less unstable as it is time centered. On the other hand just as the first method it does not allow for the propagation of bed forms;

- Lengthening of the tide:
  N successive tides are simulated by a single one extended n times. From the other point of view, it consist of lumping together the same phases of the successive tides after computation of hydrodynamics at the proper time scale. A longer time step can be used in morphological simulation as the hydrodynamics varies much more slowly. At each long time step the bed evolution is no longer negligible and the flow conditions are adjusted via the continuity correction;

- Expansion of sediment transport as a function of bed evolution:
  This method is based on the assumption that neither flow lines, nor free surface are disturbed by bed changes as long as these changes are small compared to the water depth. In that case the flow rate is the same during the first tide and the n+1 tide. (Latteux, 1995).

2.3.2 Wave input filtering

2.3.2.1 Wave-current interaction

For the sediment transport (as bed or suspended load material) which affects the water column, the effect of wave-current interaction (WCI) should be taken into account. In general the transport characteristics present in the situation of both waves and currents are significantly different from those without wave's effect. Therefore additional processes could happen when the wave action takes place. These processes have the following effects (Delft3D-Flow manual, 2006):

- vertical mixing due to the turbulence generated near the surface by whitecapping and wave breaking, and near the bottom due to energy dissipation in the bottom;

- generation of net mass flux, which will have effects on the current profile, especially in cross-shore direction;

- generation of long-shore currents and cross-shore set-up in the surf zone due to variations in the wave-induced momentum flux (radiation stress). In case of irregular surf zone a generation of bathymetry strong circulation (rip currents) could be generated;

- development of bed shear stress will affect the stirring up of sediments and increases the bed friction.

Some of these processes act at a specific location or interface such as the development of bed shear stress or wave breaking at the surface. From the other point of view, the other processes have a certain distribution over the vertical such as the energy dissipation due to bottom friction in the wave boundary layer (Soulsby et al., 1993 and 1995).
To derive the effect of the wave-induced forces, the continuity equation and the momentum equations are averaged over the wave period. Additionally the wave-current interaction terms and their possible profile in the vertical are described in the following paragraphs:

- Radiation stress gradients:
  The wave-induced force can be expressed in the wave parameters of the wave model being applied. For linear wave theories the refraction can be derived analytically. To count for wave dissipation due to bottom friction, wave breaking and whitecapping and wave growth due to wind one can rely on mild slope formulation with dissipation terms (Dingemans et al., 1987).

- Stokes drift and mass flux:
  Fluid particles in surface waves describe an orbital motion. The net horizontal displacement for a fluid particle is not zero in shallow waters. This wave induced drift velocity (Stokes-drift) is always in the direction of wave propagation. A particle at the top of the orbit beneath a wave crest moves slightly faster in the forward direction than in the backward direction beneath a wave

trough. This drift leads to additional fluxes in the wave averaged continuity equation (Delft Hydraulics wave manual, 2006).

- Streaming:
  The wave-induced current in the wave boundary layer directed in the wave propagation direction (Streaming) is modelled as a time-averaged shear-stress which results from the fact that the horizontal and vertical orbital velocities are not exactly 90^o out of phase. It is based on the wave bottom dissipation and is assumed to decrease linearly to zero across the wave boundary layer (Fredsoe and Deigaard, 1992).

- Wave-induced turbulence:
  The vertical mixing processes are enhanced by the wave actions. This can best be accounted for by adding the wave energy production and dissipation terms in the turbulence model. The two main sources of wave energy decay that are included are wave breaking, whitecapping and bottom friction due to the oscillatory wave motion in the bottom boundary layer (Deigaard et al., 1986).

- Increase of the bed shear-stress by wave:
  The boundary layers at the bed associated with the wave and the current interact non-linearly. This has the effect of enhancing both the mean and oscillatory bed shear stresses. In addition the current profile is modified, because the extra turbulence generated close to the bed by the waves appears to the current as being equivalent to enhanced bottom roughness. The bed shear stress due to the combination of waves and currents is enhanced beyond the value, which would result from a linear addition of the bed shear stress due to waves ($\vec{\tau_w}$) and the bed shear stress due to current ($\vec{\tau_c}$). For sediment transport modelling it is important to predict the maximum bed shear stress ($\vec{\tau_{max}}$) because the current velocity and the turbulent diffusion are determined by the combined wave-current bed shear stress ($\vec{\tau_m}$) (Delft Hydraulics wave manual, 2006).

The overall wave conditions in an area such as wave height, period and direction vary randomly with time (occurrence of calms and storms). Moreover the local sea state for given overall conditions can be more or less irregular (local variation of wave height, period and direction). At the scale of morphological evolution of interest, overall randomness has to be taken into account via, the boundary conditions. In this context wave input filtering concerns only overall randomness. Therefore local irregularity should be included in the wave model concept.

The objective of wave input filtering is to represent the wave climate by a small number of representative conditions with which we can derive the wave model in our deterministic model system in order to estimate medium-term mean transports and bed evolutions. So far two approaches have been developed which can be called multiple and single representative wave approaches (MRW and SRW), respectively (De Vriend et al., 1993).

2.3.2.2 Single representative wave (SRW)

Both the longshore power and the stirring parameter have to be reproduced by the set of representative conditions. This means that we have to meet the two requirements simultaneously, for which we need two degrees of freedom. Steijn (1989 and 1992) suggested a procedure in which the direction sectors are preset whilst the representative wave height per sector and the weight factor in the transport computation are the degrees of freedom. This approach was tested in various practical cases and found to work reasonably well in rather simple situations with no wide variety of transport mechanisms (De Vriend et al., 1993).

The basic idea for this approach is to combine results of wave computations for a number of sectors to yield a single set of representative wave parameters which is put into the flow and sediment transport models (Chesher and Miles, 1992). Clearly, this would lead to a considerable saving in time and computational expense, since the flow and sand transport models would need to be run once only (De Vriend et al., 1993).
As stated before waves affect sediment transport in two main ways:

- The waves generate and affect currents, then they stir up the sediment, which is subsequently adverted away by the flow;
- The latter mechanism is exploited in the SRW concept, since the stirring is independent of direction.

The schematization procedure comprises the following steps:

- Definition of the wave direction sectors;
- Selection of a representative wave height, H_ϕ, for each sector on the basis of the weighting algorithm (De Vriend et al., 1993)

$$H_\phi = \left[\frac{\sum f H^n}{\sum f} \right]^{\frac{1}{n}} \tag{2.1}$$

where
H is the wave height, f is the frequency of occurrence and n is an exponent of the wave height in the sand transport formula.

- Wave model runs for each chosen wave height from each sector;
- Weighted averaging over the sectors with suitable weighting factors.

Since the wave conditions have a strong influence on the character and the magnitude of the sediment transport, the choice of these weighting factors depends on what is considered as the most relevant type of transport for example rippled-bed transport or sheet flow. The decision, on which type is the most relevant, is not always clear (De Vriend et al., 1993).

2.3.2.3 Multiple representative wave approach(MRW)

The multiple representative wave approach (MRW) is described extensively by Steijn (1989 and 1992). It starts from measured wave heights and directions (wave or wind data) and reduces those to a limited number of combinations of wave height and direction inputs at the model boundary plus the weight factor applied to the results of each of them in the calculation of medium-term mean transports and bed evolution (De Vriend et al., 1993). The criteria applied to determine these representative conditions and the corresponding weight factors refer to the two most prominent effects of waves on the transport:

- The bulk longshore drift, for which the longshore power is a useful yardstick (SPM, 1984);
- The stirring of sediment, which is then carried along with the ambient current. Here we are using the stirring parameter as yardstick.

Being a surf zone the longshore power parameter can be evaluated using the shallow water approximation to yield proportionality with significant wave height and $\sin 2\phi$ in the point under consideration in which ϕ is the angle of the wave incidence with respect to the shore normal. The stirring parameter indicates the magnitude of the wave contribution to the bottom friction (De Vriend et al., 1993).

2.3.2.4 Concomitance of tides and waves

It is not always possible to consider the tides and the waves separately, if both of them are important for the transport. Firstly, there will be interaction via the effect of the water level variation on the wave-induced sediment stirring. Secondly, the relative importance of waves and tides will vary in space (deep channels versus shoals) and time. Both can lead to rather complex residual effects (De Vriend et al., 1993).
In order to take such effects into account a single representative tide in combination with a single representative wave per sector may be not enough. For complex topographies we should think of the two tides (neap, or mean and spring) and three representative wave conditions (calm, mean and storm) per sector (De Vriend et al., 1993).
Steijn and Hartsuiker (1992) and Van Overeem et al. (1992) give an example of what could happen if only the rather moderate wave, which represents the whole wave climate, is taken into account. They show that the intermittence of storms and calmer periods playing an important role in the sediment circulation pattern around the outer delta of a tidal inlet (De Vriend et al., 1993).

2.3.2.5 Wave chronology effects on morphology

In this section the problem of stochastic wave input and its effect on the morphology response is addressed. This problem is often referred as wave chronology or wave event sequencing. Wave chronology effects are conceptually different from the effects of physical processes. Physical processes cause the development of actual

seabed levels, whereas chronology effects refer to differences between future possible seabeds that result from different possible wave sequences (Southgate, 1995).

The response of the morphology to the hydrodynamic driving forces is strongly non-linear. This is most obviously, but not exclusively, apparent through the high-power relationship of sediment transport rate to the prevailing current and wave orbital velocity. It is thus non-linear response that renders the effects of wave chronology, and in principle the chronology of any random driving force, which is potentially important for nearshore morphological response. If the response was linear, it would be independent of the sequencing of wave conditions and will depend only on the overall statistics of the whole wave sequence. It is noted in passing that the non-linear response is also the reason for possible limitations on the range of predictability of morphodynamic response through chaotic behaviour for deterministic driving forces such as tides (Southgate, 1995).

Considerations of the chronology of random forces for which future sequencing is necessarily unpredictable. However, wave conditions are predictable for a limited time, which corresponds to the predictability of future meteorological conditions or the time of travel of distantly generated waves. Another issue worth mentioning, is that of the correlations between the values of wave statistics defined over ranges of time with corresponding values at other similar ranges of time. The seasonal variability is the most obvious example of these cyclic variations in wave conditions and one would expect for example a positive correlation between one winter season and the next. A methodology for determining wave chronology effects needs to take account of both the initial period of predictable wave behaviour and the variations of wave statistics over cycles shorter than the length of the total wave sequence (Southgate, 1995).

In conclusion, the effect of the wave chronology is poorly studied. Therefore the study of the wave chronology provides a means both for understanding their effects and predicting these effects in practical engineering problems involving medium timescale changes to coastal morphology (Southgate, 1995).

2.3.3 Available medium-term morphodynamics models

Morphodynamic models applied for coastal areas consist of coupled flow, sediment transport, wave and bottom updating models. Therefore the main factor when we deal with the morphological models, is the bottom update models. In the previous and more recent time, several approaches have been used in this manner, starting with the classical tide-averaging approach in combination with the continuity correction, an extension of continuity correction method (RAM) and the most recent approach, on-line or morphological factor approach. The three mentioned approaches are based on finite differences method. An example implementing these approaches is DELFT3D package from WL | Delft Hydraulics, The Netherlands (Delft3D-Flow Manual, 2006).
There is also another morphodynamic models use the bottom-evolution equation on the bases of finite-element method. TIMOR package from University of Darmstadt,

Germany applies this method (Zanke et al., 2002).

2.3.3.1 Tide-averaging model with continuity correction approach - Classical model

This approach is based on the fact that morphological changes take place over far longer time-scales than changes in the hydrodynamics. Thus, morphological changes within a single cycle are usually very small compared to the trends over a longer period, and such small changes do not affect the hydrodynamics or sediment transport patterns significantly (Roelvink, 2006). Therefore it is acceptable to consider a fixed bed during the computation of the hydrodynamics and sediment transport over a tidal cycle. The rate of change of the bed level is computed from the gradient in the tidally averaged transport.

As illustrated in Fig. 2.5, the wave-current interaction is solved over a tidal cycle, starting from a given bathymetry, using an iterative approach. The resulting flow and wave fields are then fed into a transport model, which computes bed load and suspended load transport over the tidal cycle. The averaged results is applied to compute bed changes. The updated bathymetry is looped back to the transport model through the continuity correction or to the full hydrodynamic model.

The continuity correction is a frequently applied method to adjust the flow field after small changes in the bathymetry. The flow pattern is assumed not to vary for small bottom changes, and therefore the local flow rate can be assumed to be constant. Adaption of sediment transport field is now simply a matter of adjusting the velocity and orbital velocity and recomputing the sediment transport. In the case of tidal flow conditions, a number of velocity and wave fields based on the original bathymetry are stored, and when the depth changes, the adapted transport field is computed for number of time points in the tidal cycle and subsequently averaged. This average transport field is then used in the sediment balance.

Limitations of the continuity correction approach

- The method still requires full transport computations through the tidal cycle, which can be time consuming when suspended sediments transport needs to be accounted for.
- The morphological time step is often dominated by shallow grid cells, which are usually not of interest. This means that typically after some 5-20 continuity steps, the full hydrodynamic model has to be run on the updated bathymetry.
- The main limitation of the continuity correction is the assumption that the flow rate and pattern remain constant in time. In the case of shallow areas becoming shallower, the flow velocity will keep increasing under continuity correction, whereas in reality the flow will go around the shallow area due to the increase of friction.

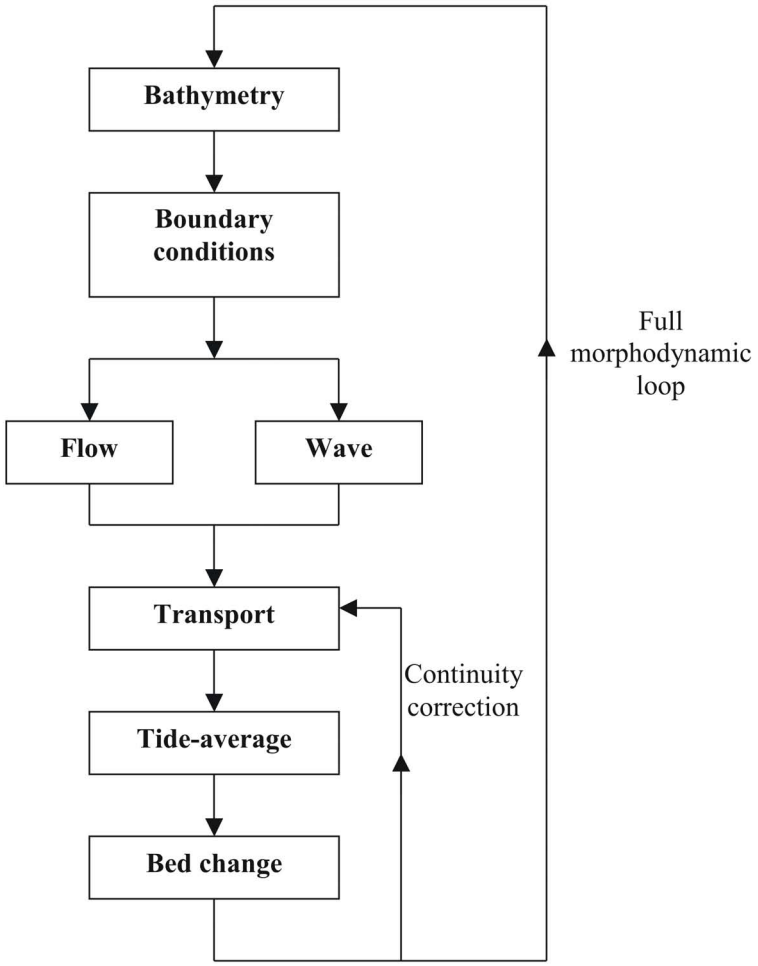

Figure 2.5: Flow diagram of tide-averaging morphodynamic model (adapted after Roelvink, 2006)

Dithmarschen Bight morphodynamic model by Wilkens (2004)

A two-dimensional fully coupled depth-averaged morphodynamic model, including models of currents, wave, sediment transport and bottom evolution, were set-up by Wilkens (2004) to predict the medium-scale morphological evolution in the Dithmarschen Bight. Simulations, which cover a ten-years period, have been carried out with fully coupled models using continuity correction method for the bottom update. The representative approach for simulating medium-scale morphodynamics has been applied for the hydrodynamic model (tide), swell, wind and storm conditions as follows:

- The method for selection of representative tidal conditions has been applied on the basis of the method proposed by Steijn (1992) and Latteux (1995).
- Since long-term wave measurements are not available for the medium-scale morphodynamic set-up of Wilkens (2004), wave statistics from observations

near the Island Sylt have been used (described in Section 3.2.3).

- The representative wind conditions, the synoptic wind data (described in Section 3.2.3) served as the basis for the statistical analysis of the wind conditions for the Dithmarschen Bight MTM.
- For the representative swell and wind climates, first have been estimated and later have been adjusted in the calibration stage.
- The storm effects have been included in the Dithmarschen Bight MTM through the representative wave and wind conditions.

Tables 2.1 and 2.2 summarize the original (without any adjustments) and the adjusted swell and the wind climate, respectively that have been imposed at the open boundaries of the Dithmarschen Bight morphodynamic model set-up by Wilkens (2004).
Wilkens (2004) concluded that the reduction of the representative swell and wave climates by 50% in terms of the significant wave heights and the wind speeds led to significant improvements in terms of medium-scale morphodynamic prediction. As shown in Table 2.1 50% reduction of 22.5 m/s (strong squall or 9 Beaufort[1]) leads to 11.25 m/s (fresh wind or 6 Beaufort[1]). In other words the direct effects of the storms have been eliminated or in good cases have been significantly decreased within the used morphodynamic model.

The model set-up by Wilkens gives a good representation of the medium-scale morphodynamics of the Dithmarschen Bight and it can be applied for realistic modelling of the medium-scale morhophological evolution. It can be seen from Fig. 2.6 that the results of the model prediction of the medium-term morphodynamics in the study area showed some significant changes. Enhanced by the breakthrough of the channel over the tidal flat Tertiussand, the adjacent tidal channels Norderpiep and Suederpiep showed a narrowing and deepening. The predicted new channel is located at the western end of the northern sub-channel of the Piep and thus forms an extension of this sub-channel. Therefore the morphodynamics of the Piep are subject to changes as well (Wilkens, 2004).

The northern channel seems to change its orientation to create a smoother connection, resulting in erosion of the submerged bar in the Piep. Although the model predicts some rather extensive changes in the morphology of the area, they do not seem to be unrealistic. Considering that the model showed rather good results on the medium scale in the calibration and validation, together with the fact that the underlying individual process models were also subjected to extensive calibration and validation studies, the model results appear to be reliable. The prediction has been based on the optimised representative conditions for tides, swell and wind as described in Table 2.2 (Wilkens, 2004).

[1]According to DWD (German Weather Service), Germany

Table 2.1: Combined climate for swell and wind before adjustment (after Wilkens, 2004)

$\mathbf{H_s(m)}$	θ (^{o}**N**)	$\mathbf{U}_w$ **(m/s)**	θ_w (^{o}**N**)	**Probability** (%)
0.20	300	2.50	180	4.43
0.20	300	7.50	240	7.97
0.20	300	12.50	255	3.09
0.20	300	17.50	270	0.48
1.00	300	2.50	180	20.22
1.00	300	7.50	240	36.35
1.00	300	12.50	255	14.09
1.00	300	17.50	270	2.19
1.00	300	22.50	300	0.22
2.00	270	2.50	180	3.05
2.00	270	7.50	240	5.48
2.00	270	12.50	255	2.12
2.00	270	17.50	270	0.33

Table 2.2: Combined climate for swell and wind after adjustment

$\mathbf{H_s(m)}$	θ (^{o}**N**)	$\mathbf{U}_w$ **(m/s)**	θ_w (^{o}**N**)	**Probability** (%)
0.10	300	1.25	180	2.22
0.10	300	3.75	240	3.99
0.10	300	6.25	255	1.09
0.10	300	8.75	270	0.24
0.50	300	1.25	180	10.11
0.50	300	3.75	240	18.18
0.50	300	6.25	255	7.05
0.50	300	8.75	270	1.09
0.50	300	11.25	300	0.11
1.00	270	1.25	180	1.53
1.00	270	3.75	240	2.74
1.00	270	6.25	255	1.06
1.00	270	8.75	270	0.17

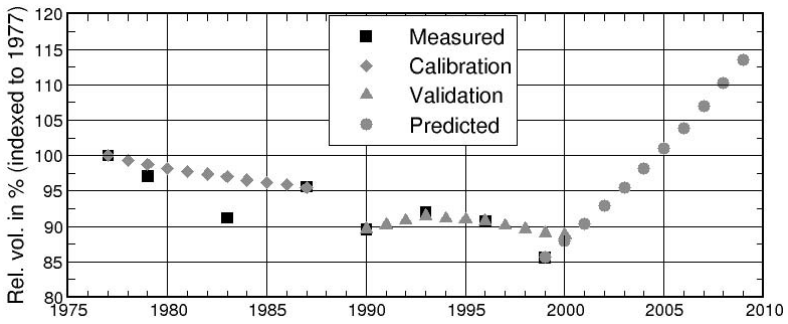

(a) Tertiussand

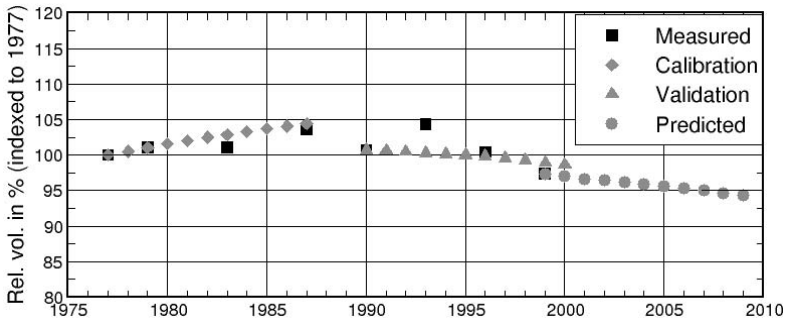

(b) Suederpiep

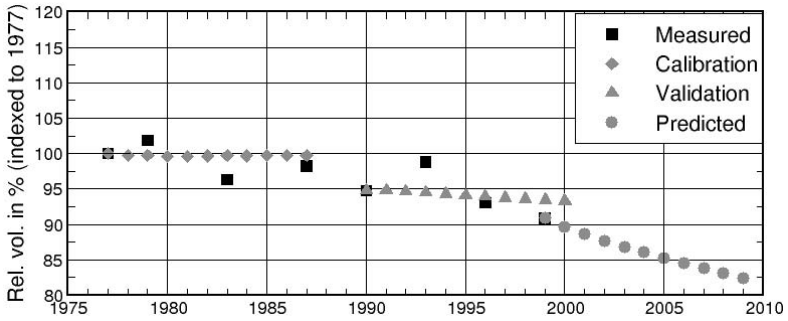

(c) Norderpiep

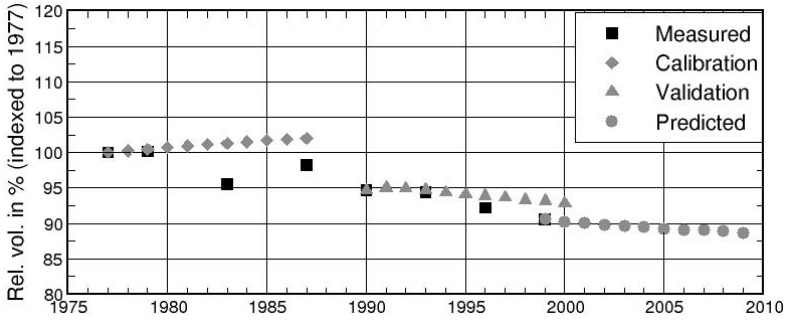

(d) Piep

Figure 2.6: Model results of the Dithmarsche Bight MTM by Wilkens (after Wilkens, 2004)

2.3.3.2 On-line model with morphological factor approach

The most recent morphodynamic model (on-line with morphological factor) is simulating the morphological evolution by coupling the process-based models for flow and sediment transport model with the wave model (see Fig. 2.7). In the case of the solution of the advection-diffusion for the sediment transport has to be done with comparable time steps as the flow solver. The updating of the bottom takes very little computation time. However, this method does not take into consideration the difference in time scales between the flow and morphology. Therefore, as Lesser et al.(2004) described, a simple device can be used, called the morphological factor. This factor simply increases the depth change rates by a constant factor so that after a simulation over one tidal cycle we have in fact modelled the morphological changes over n cycles. This is similar to the concept of the elongated tide proposed by Latteux (1995), where the combination with continuity correction is applied (Roelvink, 2006).

An important difference between the on-line approach and the continuity correction approach is that in the first approach the bottom evolution is computed in much smaller time steps, even when relatively large values of morphological factor are used (Roelvink, 2006). For example if we use a morphological factor of 60, this means after computing 12 tidal cycles we have covered approximately one year of morphological changes. In a typical flow model we would apply a time step of 1 min and the update of the bathymetry will be every morphological hour. In comparison with a tide-averaging approach (continuity correction) we would have to take steps of a month in order to cover the same time period while calculating through the same number of tide cycles. Even when applying 10 continuity steps in between each full morphological step this still means a 3 day time step which takes 10 times as many as the transport computations (Roelvink, 2006).

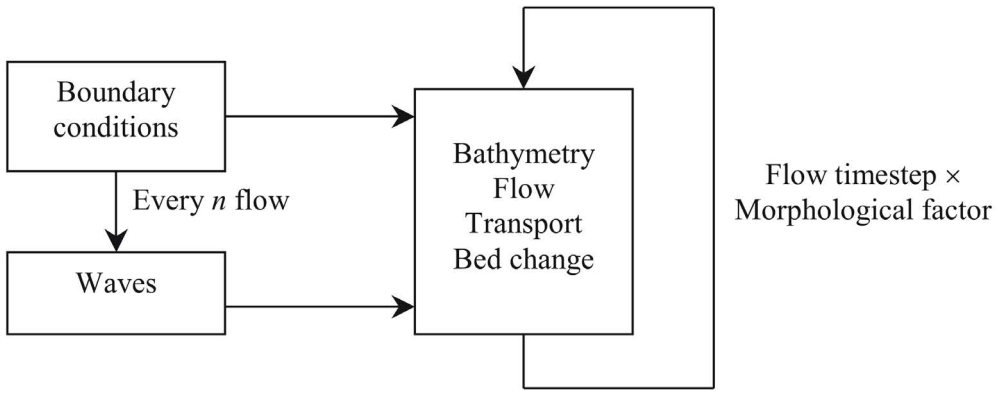

Figure 2.7: Flow diagram of on-line morphological model (adapted after Roelvink, 2006)

An advantage of the on-line with morphological factor approach is that short-term processes are coupled at flow time-step level, which makes it easy to include various interaction between flow, sediment and morphology and as a result of that less data will be required to store between these processes. Moreover, the treatment of areas that may be drying or wetting also becomes more straightforward, and especially in these areas it is of a great advantage to take many small morphodynamic timesteps. In comparison with the continuity correction approach the advantage is that no continuity correction is required and therefore processes in shallow water are represented more accurately (Roelvink, 2006).

2.4 Long-term morphodynamics (LTM)

In this type of model the underlying equations describe the morphodynamics in an integrated manner instead of on the basis of the process-resolving method of the first two model types (De Vriend et al., 1993).
Long-term (behavior-oriented) models are usually much simpler than process-based models of the same phenomenon. As a consequence, they are more suited for model fitting instead of computing the behaviour straightforwardly from a mathematical system with present parameters and maybe even some aspects of the mathematical system are derived from the behaviour, which we want the model to exhibit. This means that we can make use of the theoretical framework and the gamut of techniques, which have been developed for parameter identification and model fitting in other fields (De Vriend et al., 1993).

Chapter 3

Characteristics of the selected site for study-Dithmarschen Bight

3.1 Introduction

To study the effects of the storms on the short and the medium-term morphodynamics of a tidally-dominated coastal environment, the central Dithmarschen Bight has been chosen to be considered as a case study. The Dithmarschen Bight is a part of the Greater North Sea, which is situated on the continental shelf of north-west Europe (see Fig. 3.1). It is open to the Atlantic Ocean to the north via the Channel and to the south-west it is connected to the Baltic Sea to the east. The open North Sea is often divided into the relatively shallow southern North Sea (including the Southern Bight and the German Bight), the central North Sea, the northern North Sea, the Norwegian Trench and the Skagerak. The shallow Kattegat is seen as a transition zone between the Baltic and the North Sea. The Greater North Sea, including its estuaries and fjords, has a surface area of about 750 000 km^2 and a volume of about 94 000 km^3(OSPAR, 2000).

The Dithmarschen Bight is located in the Wadden Sea at the south-east part of the German North coast between the Elbe and the Eider estuaries in the South and the North, respectively. The area consists of several tidal channels like Piep, Suederpiep and Norderpiep, tidal flats and exposed sandbanks like Tertiussand and Trischen (see Fig. 3.12). The maximum water depths in the channels are of the order of 23m, and approximately 50% of the area is intertidal (Wilkens and Mayerle, 2005). Applying the classification by Hayes (1979), the outer western part falls within the classification slightly tidally dominant. The sheltered eastern part classifies within the highly tidally-dominated. The classifications as indicated in Fig. 3.2 are considering mean values of tidal range and wave heights (Wilkens and Mayerle, 2005).

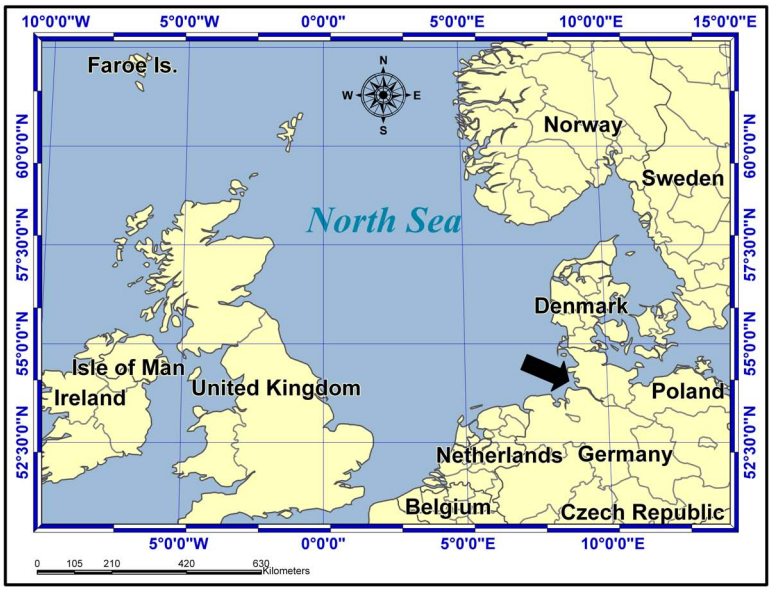

Figure 3.1: Location of the Dithmarschen Bight

3.2 Hydrodynamic processes

3.2.1 Tidal conditions

Tidal oscillations in the North Sea are determined by its dimensions and the progressive semi-diurnal tides entering from the Atlantic Ocean. The tidal flow is deflected by the Coriolis force, resulting in three amphidromic points. Tidal conditions in the central Dithmarschen Bight depend primarily on the rotation of the semi-diurnal tidal wave around the amphidromic point in the south eastern part of the North Sea (Toro et al., 2005).
According to Asp (2004), the area is characterized by a semi-diurnal tide with a tidal period of about 12 hrs and 24 min. The mean tidal range varies from about 3.1 m to 3.4 m between the mouth of the Elbe estuary in the south and the Eiderstedt peninsula in the north. With reference to N.N. (German Reference Datum, Normal Null), the mean high and low water levels close to the coastline are +1.6 m and -1.6 m, respectively. Analysis of a long time series of water level measurements reveals that the mean tidal range in the study area is about 3.2 m, with neap and spring tidal range of about 2.8m and 3.5m, respectively (Toro et al., 2005).

3.2.2 Currents

Toro et al. (2005) have preformed selective measurements of current velocities over several cross-sections using acoustic profiles from moving vessels. Additionally current velocity measurements over the water column were provided by moored devices. These measurements covered a wide range of conditions typical for the study area. The measurements from ship-based devices provided a good description of the spa-

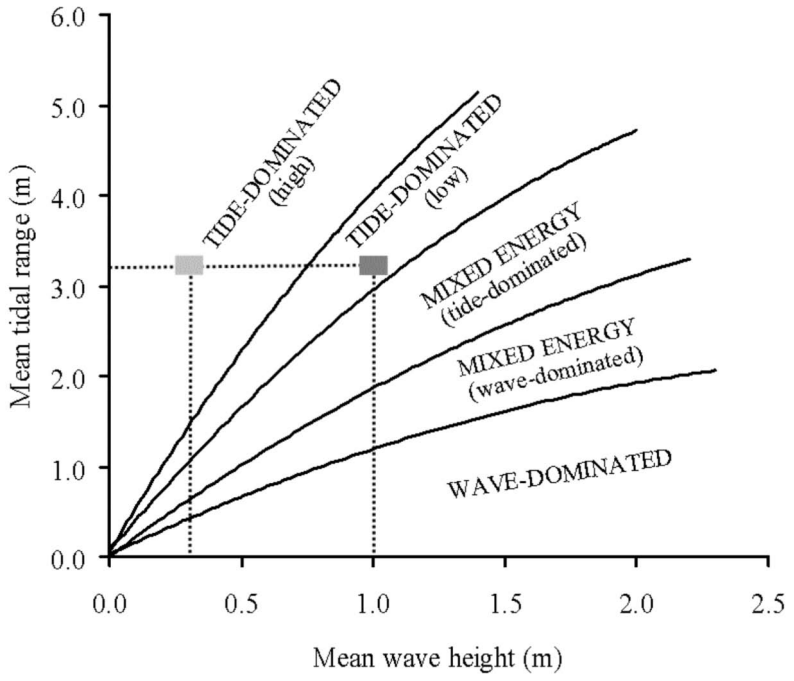

Figure 3.2: Classification of Dithmarschen Bight (after Wilkens, 2004)

tial variation of current velocities. Measurements were taken from a variety of tidal conditions under relatively calm weather conditions.
The maximum values of point and depth-averaged current velocity in the main tidal channels were found to be about 2.8 m/s and 1.7 m/s, respectively. The vertical distribution of current velocity was also found to be fairly uniform at all locations surveyed due to low bed roughness.

3.2.3 Wave conditions

The wave conditions in the area are mainly dependent on the swell waves approaching from the open North Sea as well as on the locally generated wind waves (Wilkens, 2004).
Toro et al. (2005) studied wave data from several wave buoys provided by the Coastal Research Station of the Lower Saxony Board of Ecology (CRS) on Norderney, the Regional State Office for Rural Areas in Husum (ALR) and the German Federal Maritime and Hydrographic Agency in Hamburg (BSH) to investigate wave characteristics in the study area. The wave data show that, the wave energy in the easter part of the domain is dominated by locally generated wind waves as the major swell energy is dissipated along the edge of the outer tidal flats. The limited depths to the east of this location are responsible for energy dissipation due to wave-breaking, bottom friction, refraction and diffraction. Maximum wave height some 10 km westward of the outer tidal flats were found to be about 3.5 m (Toro et al., 2005).

3.2.3.1 Short-term wave measurement

During September 1996 short-term measurements at five locations in the Dithmarschen Bight have been carried out (Niemeyer et al., 1995). Fig. 3.3 shows the location and the significant wave heights for the five measurement locations.

Some other wave measurements taken at the nearby island Sylt was also available (70 to 100 km north of the study area) between 1986 and 1993 (BMFT, 1994). The measurements were taken by a wave buoy about 5 km offshore at the center from the island (Wilkens, 2004).

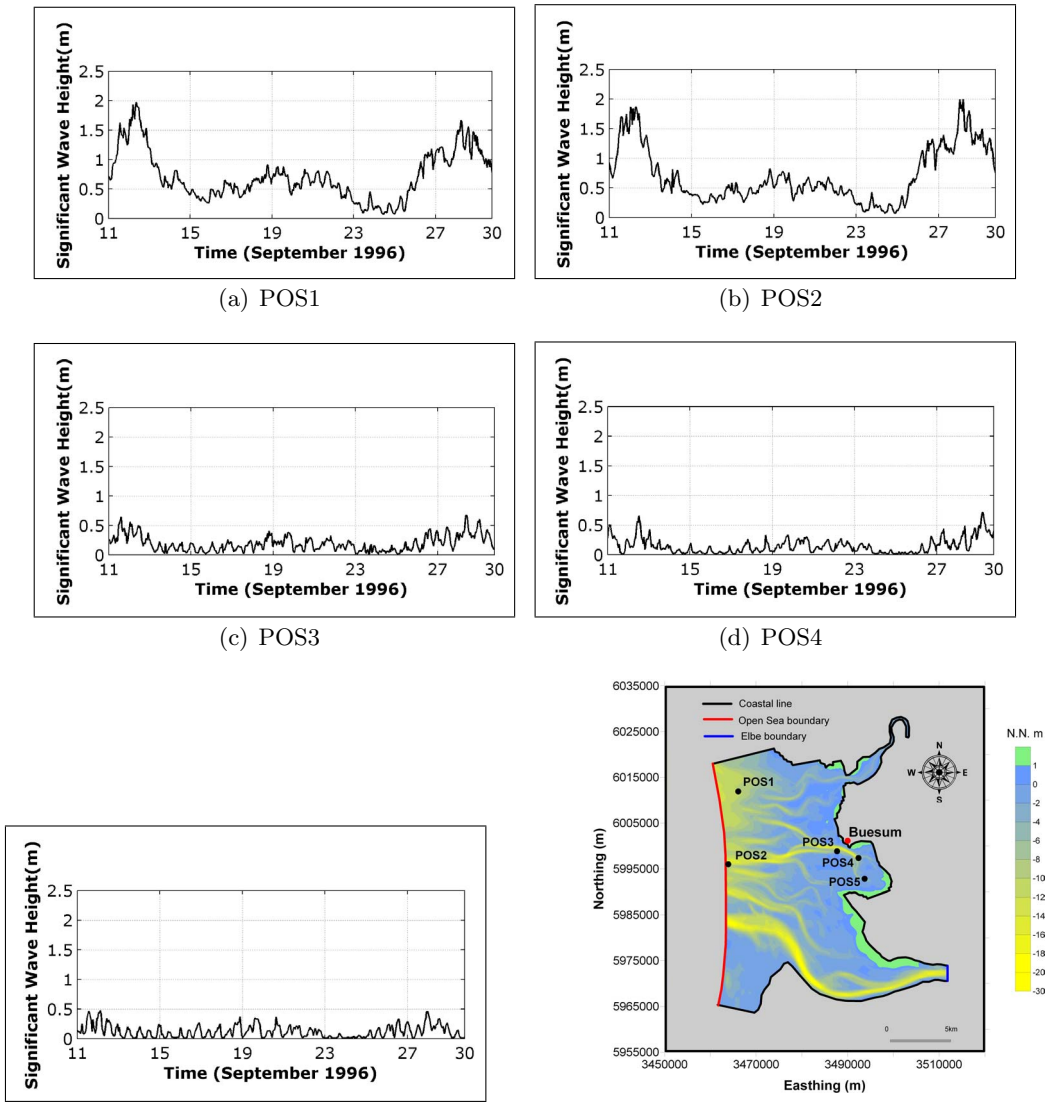

Figure 3.3: Significant wave heights from the measurements during 1996 at five wave buoys

Fig. 3.4 shows the probability of occurrence per wave height and direction at Sylt Island. The average water depth at the location of the buoy is around 13m and Fig. 3.4 shows that the highest probability for wave height between 1 and 2m and for waves coming from West-North direction. The highest wave height recorded was about 5.5m with a direction of 330 °N and more than 65% of the waves are between the sectors 240 and 330 °N.

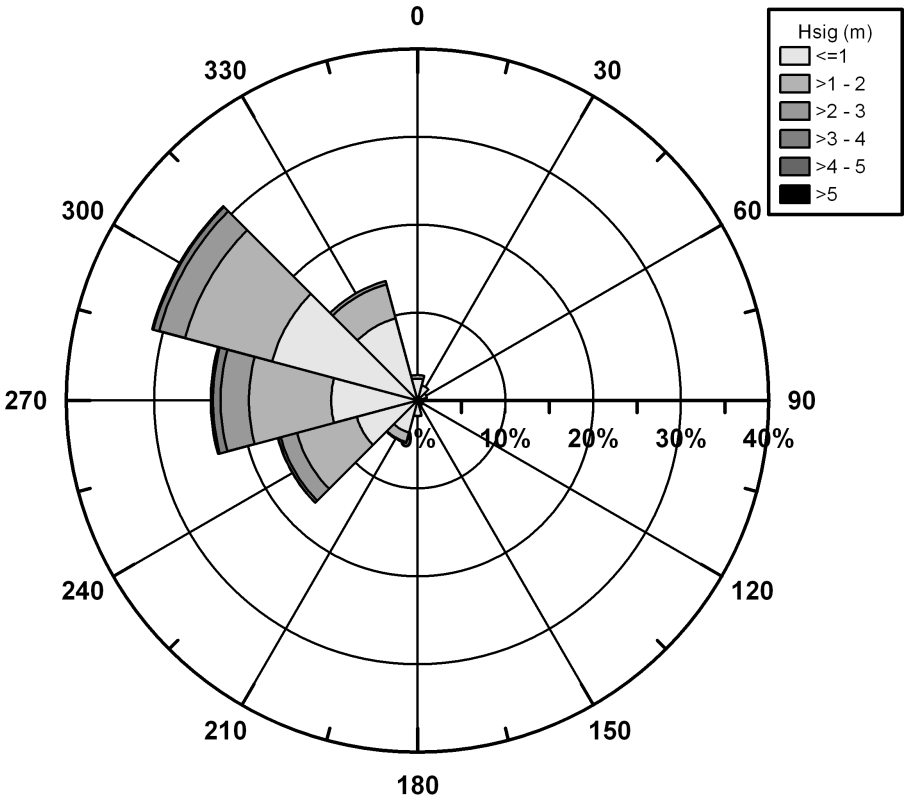

Figure 3.4: Wave rose nearby island Sylt

3.2.3.2 Long-term hindcast data

Another wave data set for long-term hindcast uses available wave data for 40 years in the frame work project HIPOCAS. The project HIPOCAS (**HI**ndcast of Dynamic **P**rocesses of the **O**cean and **C**oastal **A**rea**S** of Europe) has been funded by European Union (EVK2-CT-1999-00038) to cover a period of time between 1958 to 2001.

The project tries to solve the problem of collection of long-term information on prevailing environmental conditions to assess the climate and plan the sustainable development of the economic activities in European waters (Weiβe et al., 2003).

The objective of the HIPOCAS project is to obtain a 40-year hindcast of wind, wave, sea-level and current climatology for European waters and coastal seas for application in coastal and environmental decision processes.

The data are provided on a 50 × 50 km grid and has been used in the project to force the wave and ocean models. Wave models have been used in the North Sea, the North East Atlantic south of UK, including Azores and Canary islands, Irish Sea, and the Mediterranean sea, see Fig.3.5, (Soares et al., 2002).

The wave models that have been used are based on the last version of WAM model, which is used with nested grids in order to produce high-resolution information in coastal waters. In the North Sea the model takes account of the tidal changes that will influence wave predictions (Soares et al., 2002).

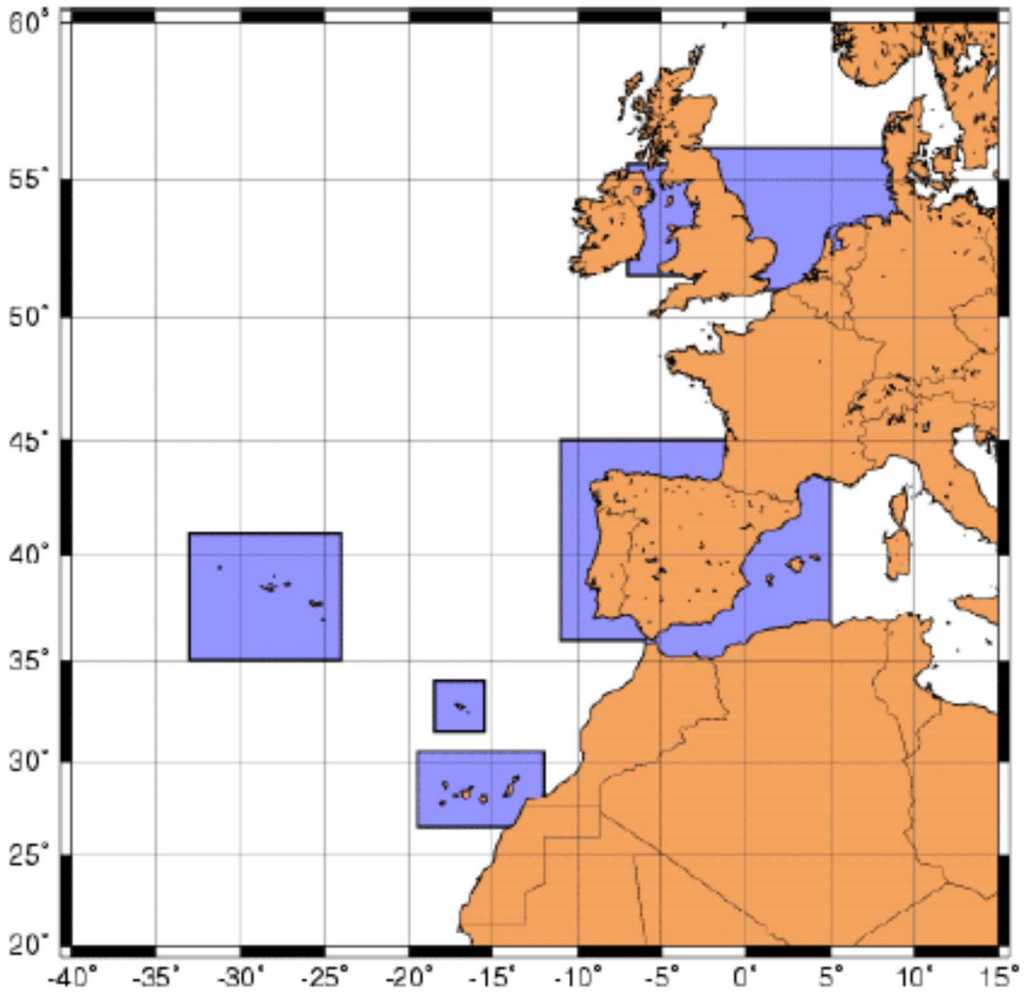

Figure 3.5: Details of wave hindcast areas of HIPOCAS project (after Soares et al., 2002)

Measurements are only available for the last decades of the hindcast and an effort to compile reliable wave measurements and preliminary hindcasts are being carried out. Also extensive verifications in open waters with the available satellite data have been carried out (Soares et al., 2002).

For the study area (Dithmarschen Bight region), wave data at 21 points along the western open-sea boundary are available from the North Sea hindcast of the HIPOCAS wave model (see Fig.3.6).

Statistical analysis related to the probability of occurrence has been carried out at each of the 21 locations. As an example, Table 3.1 shows the probability of occurrence per wave direction and significant wave height at Station P7.

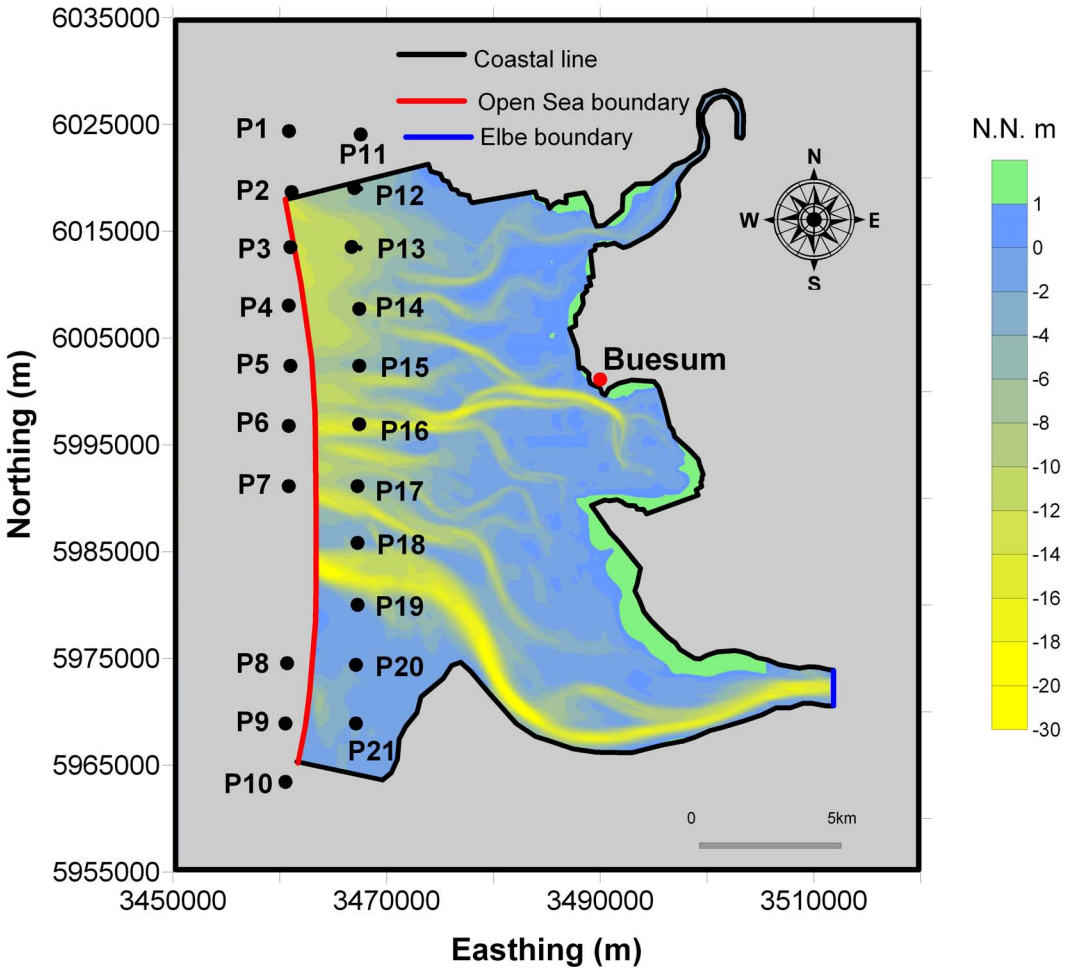

Figure 3.6: Location of wave hindcasts stations in the Dithmarschen Bight

Table 3.1: Probability of occurrence (%) per wave direction and significant wave height at Station P7

Dir.(^{o} N) **H_s (m)**	**0**	**30**	**60**	**90**	**120**	**150**	**180**	**210**	**240**	**270**	**300**	**330**	**Total**
0.125	0.20	0.16	0.18	0.26	0.41	0.33	0.17	0.15	0.24	1.27	1.48	1.14	**5.99**
0.375	1.10	0.98	1.50	2.10	1.73	0.83	0.63	0.80	1.49	4.28	5.83	3.46	**24.72**
0.625	0.98	0.63	1.25	1.58	1.07	0.40	0.36	0.53	1.61	5.49	6.28	3.73	**23.92**
0.875	0.46	0.41	0.76	0.93	0.47	0.15	0.13	0.29	1.26	4.45	4.24	2.05	**15.61**
1.125	0.26	0.20	0.37	0.43	0.16	0.04	0.03	0.10	0.88	3.43	2.80	1.32	**10.02**
1.375	0.11	0.09	0.14	0.14	0.03	0.00	0.01	0.04	0.40	2.67	1.94	0.77	**6.36**
1.625	0.05	0.03	0.03	0.06	0.01	0.00	0.00	0.01	0.18	1.90	1.55	0.46	**4.27**
1.875	0.02	0.01	0.01	0.01	0.00	0.00	0.00	0.00	0.07	1.26	1.09	0.26	**2.74**
2.125	0.01	0.00	0.00	0.00	0.00	0.00	0.00	0.00	0.02	0.85	0.90	0.14	**1.93**
2.375	0.00	0.01	0.01	0.00	0.00	0.00	0.00	0.00	0.01	0.61	0.72	0.07	**1.42**
2.625	0.00	0.00	0.00	0.00	0.00	0.00	0.00	0.00	0.00	0.35	0.56	0.03	**0.94**
2.875	0.00	0.00	0.00	0.00	0.00	0.00	0.00	0.00	0.00	0.24	0.40	0.01	**0.64**
3.125	0.00	0.00	0.00	0.00	0.00	0.00	0.00	0.00	0.00	0.16	0.28	0.00	**0.44**
3.375	0.00	0.00	0.00	0.00	0.00	0.00	0.00	0.00	0.00	0.12	0.23	0.00	**0.34**
3.625	0.00	0.00	0.00	0.00	0.00	0.00	0.00	0.00	0.00	0.07	0.15	0.00	**0.22**
3.875	0.00	0.00	0.00	0.00	0.00	0.00	0.00	0.00	0.00	0.05	0.09	0.00	**0.14**
4.125	0.00	0.00	0.00	0.00	0.00	0.00	0.00	0.00	0.00	0.03	0.08	0.00	**0.11**
4.375	0.00	0.00	0.00	0.00	0.00	0.00	0.00	0.00	0.00	0.02	0.05	0.00	**0.07**
4.625	0.00	0.00	0.00	0.00	0.00	0.00	0.00	0.00	0.00	0.02	0.03	0.00	**0.05**
4.875	0.00	0.00	0.00	0.00	0.00	0.00	0.00	0.00	0.00	0.01	0.03	0.00	**0.04**
5.125	0.00	0.00	0.00	0.00	0.00	0.00	0.00	0.00	0.00	0.00	0.00	0.00	**0.00**
5.375	0.00	0.00	0.00	0.00	0.00	0.00	0.00	0.00	0.00	0.00	0.00	0.00	**0.00**
Total	**3.20**	**2.51**	**4.25**	**5.51**	**3.87**	**1.77**	**1.34**	**1.94**	**6.16**	**27.28**	**28.73**	**13.44**	**100.00**

3.3 Meteorology

Storm surges, resulting from extreme meteorological events, lead to a temporary increase in water levels in the near-coast region. The magnitude of a surge depends primarily on the size, intensity and movement of the storm responsible, and will be influenced also by the shape of the coastline, local bathymetry and the state of astronomical tide. Since the wind-induced water level set-up is inversely proportional to the local water depth, shallow tidal flat areas of the Dithmarschen Bight are strongly affected by storms (Toro et al., 2005).
Storm surges exceeding 1.5 m at the mouth of the Elbe annually take place mainly in December, with over 60% occurring from November to January and over 80% from October to February (Toro et al., 2005).
The frequency and severity of storms have increased for the last 30 years. In the analysis of 25 most severe storm surges since 1920 were storm surges defined as water level increases higher than 3m above N.N. (German Reference Datum, Normal Null), 21 took place after 1960 (Hofstede, 1997).

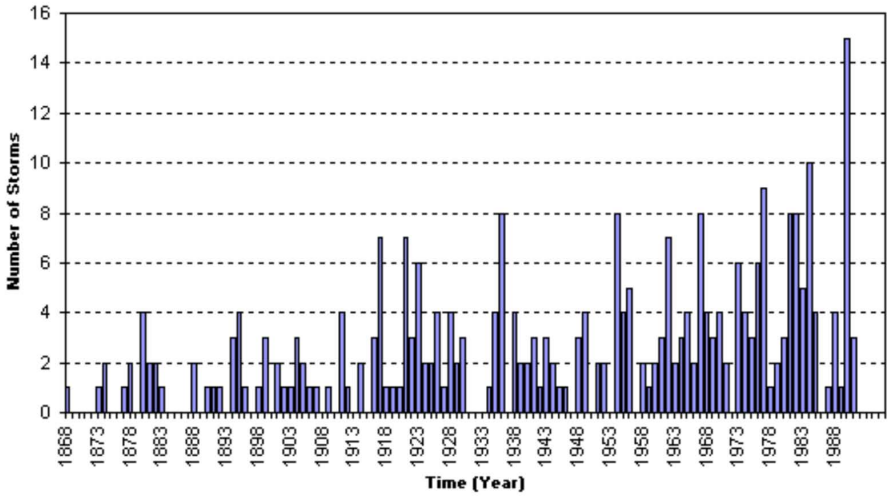

Figure 3.7: Frequency of storm surges at Büsum (after Kesper, 1992)

Fig. 3.7 shows a significant increase in the storm surges during the period between 1868 and 1992. It is clear that at the beginning of the period up to 4 storm surges took place and up to 15 storm surge at the end of the period. It is obvious that due to the influence of strong winds the tides of the North Sea can rise to extreme heights. The resulting storm surges cannot be generally defined by the height of their water levels since these vary from place to place as a function of wind direction and local tidal range. For the Dithmarschen Bight a light storm surge is defined when the maximum water level reached between 10 times a year and once every two years. A severe storm surge occurs once every two to twenty years, and the peak water levels of a very severe storm surge are reached once in every twenty years or even more infrequently (Ehlers, 1988). In summary, the Dithmarschen Bight climate

is characterised by the wide variation in the wind direction and speed, high level of cloud coverage and relatively high precipitation.

PRISMA wind data set

PRISMA wind dataset consist of observed wind field, meticulously modelled and interpolated over a grid with a regular mesh spacing of 42 km and a time resolution of 3 hours. In addition to measuring winds the observed surface pressure data are used to generate a synoptic scale wind field by means of the geostrophic wind equation (Benkel et al., 2005 and Luthardt, 1987). PRISMA datasets have been generated from measurements free of forcast errors and they also have relatively sharply defined land-sea mask in the speed of the wind (Nielinger, 1998). The measurements used to generate the PRISMA datasets have been gathered from ships, platforms and coastal synoptic station. Therefore the wind data is also applicable for the short-term morphodynamic.
Based on the synoptic data Wilkens(2004) analyzed the wind climate in the Dithmarschen Bight for the period between 1989 and 2000. The results are summarized in the wind rose of Fig. 3.8 and in the probability of occurrence of Table 3.2. It is easily noticeable that the dominance of the winds is from the sector southwest-west. This dominance holds for all of the wind velocity intervals. The wind direction ranges between 200 and 280^o for approximately 40% of the time.

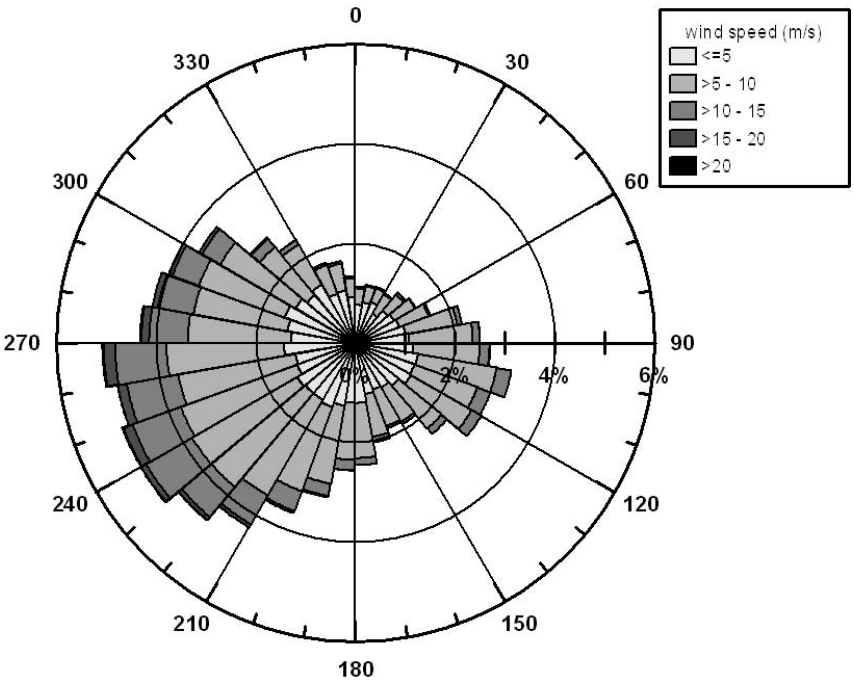

Figure 3.8: Probability of occurrence of wind speed and directions based on PRISMA data at the Dithmarschen Bight (after Wilkens, 2004)

Table 3.2: Probability of occurrence (%) per wind direction and wind speed (after Wilkens, 2004)

θ_w(^{o} N) U_w (m/s)	**0**	**30**	**60**	**90**	**120**	**150**	**180**	**210**	**240**	**270**	**300**	**330**	**Total**
0.00-5.00	2.29	1.17	2.19	2.16	3.25	2.26	2.95	2.50	2.57	2.43	1.78	1.58	**27.67**
5.00-10.0	1.37	1.44	1.23	4.01	3.36	3.56	3.42	6.61	7.67	6.88	6.47	3.73	**49.76**
10.0-15.0	0.03	0.07	0.00	1.03	1.34	0.41	0.38	2.95	4.55	4.55	2.95	1.03	**19.28**
15.0-20.0	0.00	0.00	0.00	0.00	0.03	0.00	0.07	0.51	0.82	1.06	0.45	0.00	**2.95**
20.0-25.0	0.00	0.00	0.00	0.00	0.00	0.00	0.00	0.03	0.00	0.10	0.21	0.00	**0.33**
Total	**3.70**	**3.22**	**3.42**	**7.19**	**7.98**	**6.23**	**6.82**	**12.60**	**15.62**	**15.03**	**11.85**	**6.34**	**100.00**

3.4 Salinity and water temperature

The seasonal variation in salinity and temperature throughout the study area were analyzed within the framework of the PROMORPH project, as mentioned before (Mayerle and Zielke, 2005). Vertical profiles of salinity and temperature were measured at 3-monthly intervals during the year 2000 within the study area. The results show that the vertical salinity distributions are fairly uniform throughout the year, because of the water column in this relatively shallow area is always well-mixed due to strong tidal currents. The salinity values range from about 20‰ to 28‰ indicating that the influence of coastal freshwater run-off derived mainly from the discharge of the Elbe estuary in the south (Toro et al., 2005).
The maximum variation in salinity throughout the year is found to be between 7 and 8 ‰ (Toro et al., 2005). This variation in salinity level is most probably a result of seasonal variations in the freshwater discharge of the Elbe and Eider eastuaries in combination with prevailing meteorological conditions. Measurements carried out in the area as part of the research project TRANSWATT (Sündermann et al., 1999) support these results. The results have clearly shown that the salinity distribution in the Dithmarschen Bight is highly dependent on the magnitude of riverine discharges and local wind conditions.

The seasonal variation in water temperature was found to be in the range of 6-7 °C in March and between 16 to 17 °C in September and the spatial variations were found to be negligible (Toro et al., 2005). The uniform vertical profiles of salinity and temperature in the study area is indicative of the well-mixed conditions without flow stratification due to density effects.

3.5 Characteristics of sediments

In the Dithmarschen Bight intensive sediment movements occur frequently owing to the wind-induced current, tides and wave actions. Sea swell is an especially effective agent for suspension. This will lead to changes in seabed topography and may also result in suspension of contaminants adsorbed to the settled particulate matter and their transportation and elsewhere.
The following paragraphs describe the recent sediment deposits, seabed surface sediments and material transported in suspension.

3.5.1 Recent sediment deposits

The composition of the sediment deposits correspond mainly to the recent tidal flat sediments (Ricklefs and Asp, 2005). The layer thickness of the intertidal deposits is up to about 20 m on the tidal flats (Asp, 2004). Fig. 3.9 shows the distribution of the layer thickness of sediment deposits in central Dithmarschen Bight. The thickness of sediment deposits above the Early Holocene Layer (EHL) is as high as 16m along the channel banks and goes down to nearly zero towards the deeper parts of the channels (Asp, 2004).

The early Holocene consolidated cohesive sediments form a natural base that delays or even prevents erosion of the tidal channels, thereby restricting morphological changes to lateral displacements (Asp, 2004). In the central and deeper parts of the tidal channels where shear stresses are generally larger the sediment deposits have been entirely eroded and the EHL shows (Asp, 2004).

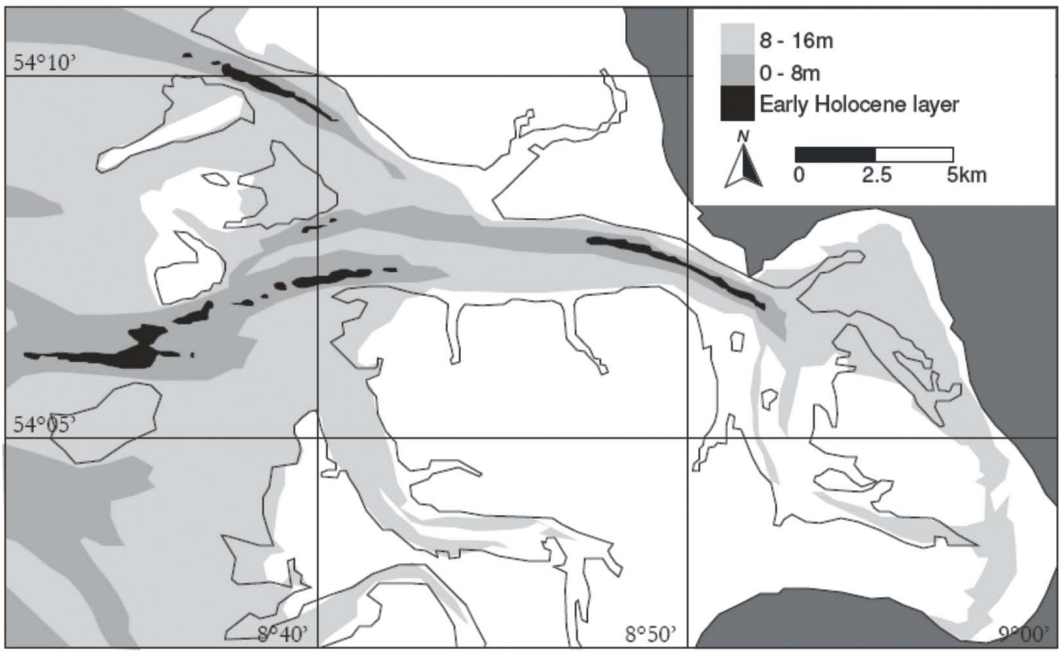

Figure 3.9: Thickness of the potentially mobile sediment layer above EHL (after Asp, 2004)

3.5.2 Seabed surface sediments

On the basis of side-scan sonar images and grab samples Vela-Diez (2001) mapped the distribution of seabed surface sediments in the tidal channels. Fig. 3.10 shows the distribution of the seabed sediments and mud as well as the identified zones of consolidated deposits were identified. Consolidated fine-grained sediments were found to show at a number of deeper locations in the channels. The sand is mainly very fine to fine with isolated patches of medium sands (Poerbandono and Mayerle, 2005).
An analysis of mud content (less than 63 μm) of seabed sediment grab samples collected in the less exposed tidal channels was carried out. Mud was found in all samples. The measurements indicate that the percentage of fines in the sediments of the sampling area is generally greater than 5%, attaining maximum values of 75% to 80%. Moreover, values exceed 10% in about 50% of the samples (Poerbandono and Mayerle, 2005).

The characteristics of seabed surface sediments in the intertidal areas have been studied by Reimers (2003). He found that the characteristic median sediment size

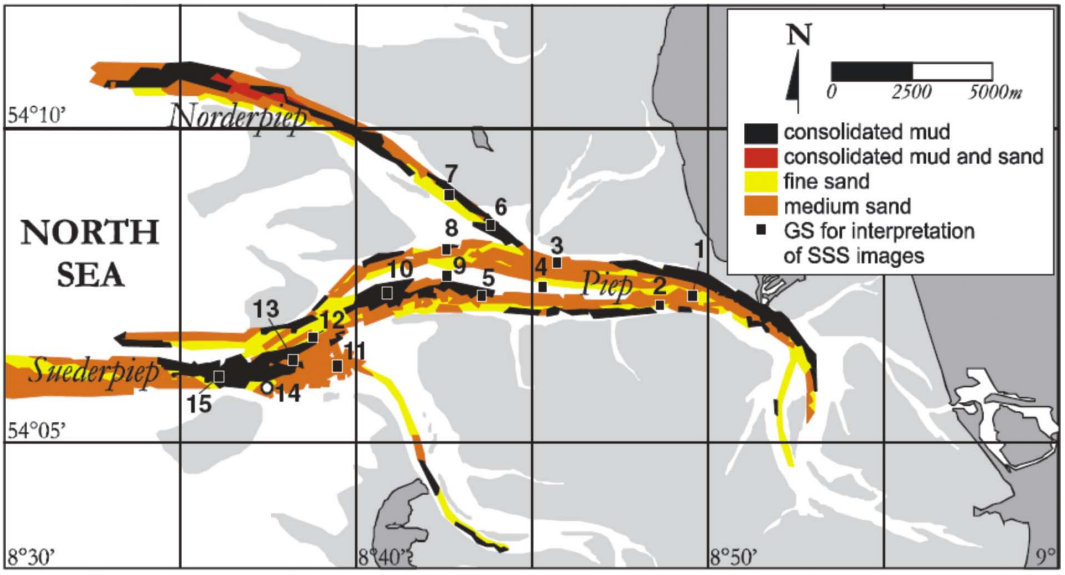

Figure 3.10: Seabed surface sediment distribution in the main tidal channels (after Vela-Diez, 2001)

ranges from fine sand ($d_{50} \approx 230$ μm) to coarse silt (($d_{50} \approx 70$ μm)). Fine sands are found mainly at the supratidal sites and on the exposed sandbanks of Blauort, Bielshovenersand and Blauortsand (Fig. 3.11 (Poerbandono and Mayerle, 2005)).
A clear gradual decrease in the grain size of the seabed sediments from the outer regions to the inner tidal flat regions, changing from coarse sand (grain size of about 355 μm) to coarse silt (grain size of about 38 μm) has been identified (Ricklefs and Asp, 2005).
In the more exposed outer regions in the proximity of the main tidal channels the content of fines (less than 63 μm) is generally less than 5%. Towards the inner parts of the Dithmarschen Bight the content of fines increases to between 50% and 100% (Ricklefs and Asp, 2005).

3.5.3 Material transported in suspension

The characteristics of the material transported in suspension were investigated by Poerbandono (2003). It was found that the material transported in suspension is much finer than those in the seabed sediments in the tidal channels and on the tidal flats. Besides, the sandy material on the seabed is seldom found in suspension. In general, the mean grain-size of suspended materials were up to 5 times smaller than those of seabed material (Poerbandono and Mayerle, 2005).

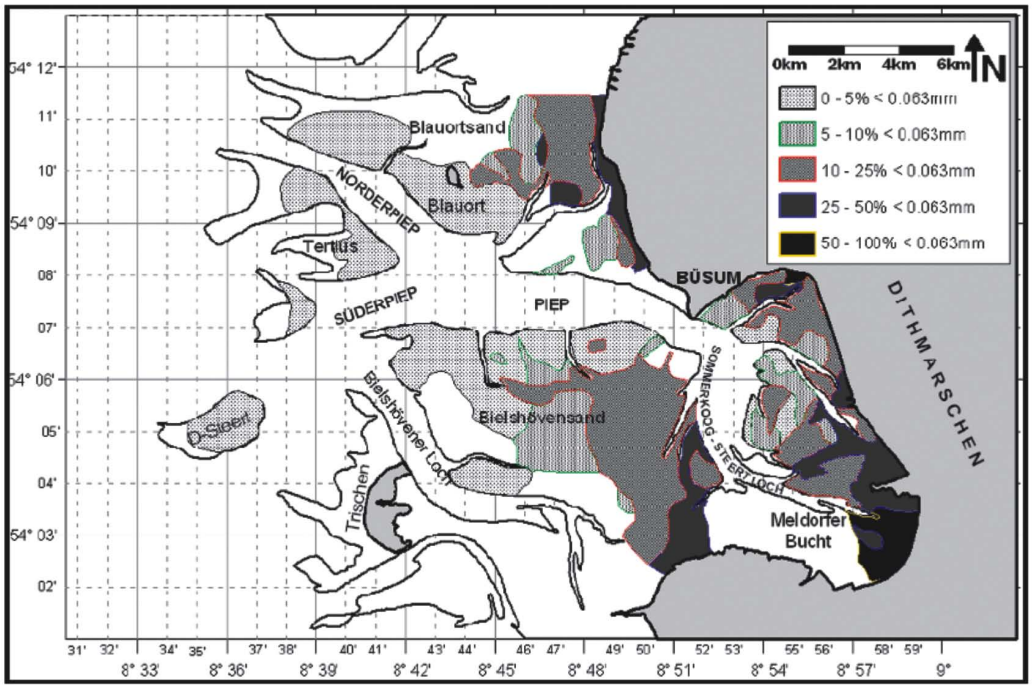

Figure 3.11: Seabed surface sediment distribution on the tidal flats (after Reimers, 2003)

3.6 Morphology and morphodynamics

The central Dithmarschen Bight contains several primary and secondary channels which are divided by a number of shoals and tidal flats (see Fig. 3.12).
The channel system consists of the main channel Piep. The channel Piep splits into two channels in the western direction into Norderpiep and Suederpiep channels. Towards the East, the Piep bends in a southern direction near Buesum, after which it spreads over the Meldorf Bight through several smaller channels (Wilkens, 2004).

From the Suederpiep the smaller channel Bielshoevener Loch branches in a southeastern direction. Between the Norderpiep and Suederpiep, the exposed sandbank Tertiussand can be found. The flat Blauortsand, located north of the Norderpiep and Piep, forms the northern limit of the study area. In the middle of the domain is the flat Bielshoevensand, which marks the southern limit of the investigated area, together with the shoal D-Steert (Wilkens, 2004). The morphology of the Dithmarschen Bight is rather dynamic. Therefore the morphological changes in short-term (weeks to months) and in long-term (years and decades) are discussed in details in the following paragraphs.

3.6.1 Long-term Morphological changes

In the following, the morphodynamic behaviour for the study area over several decades is described. In 2005 Ricklefs and Asp have studied the morphological

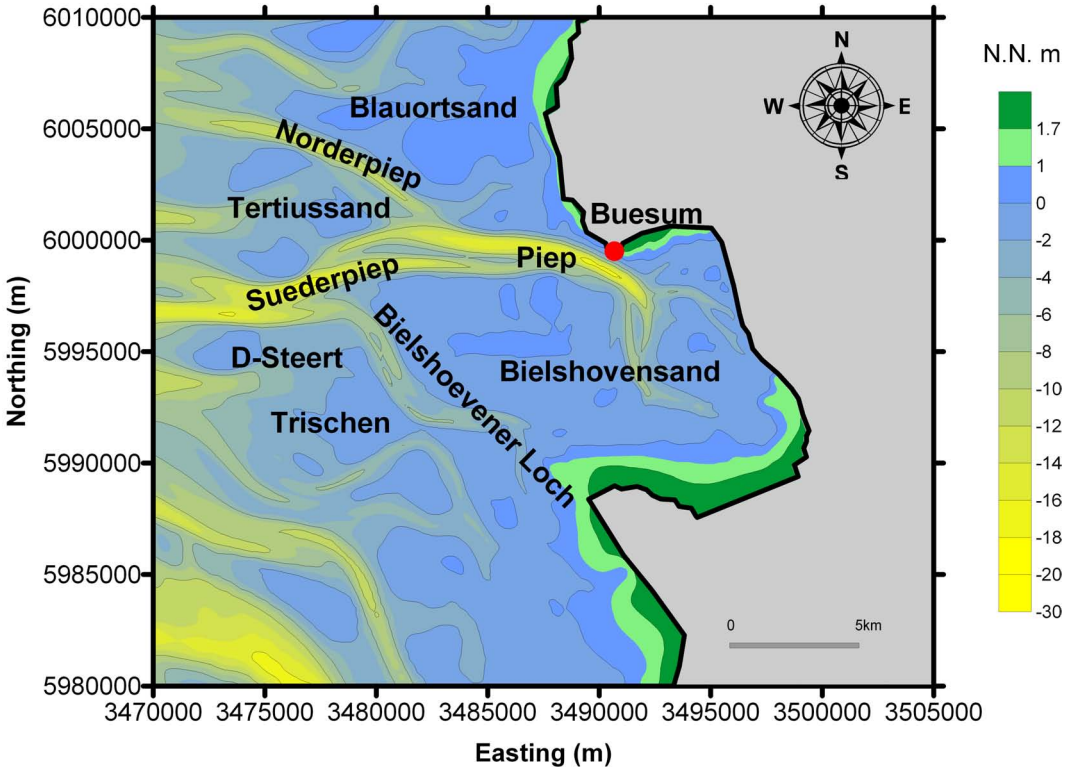

Figure 3.12: Morphological features in the Dithmarschen Bight (Bathymetry 1990)

changes in Dithmarschen Bight based mainly on bathymetric data collected by the German Federal Agency for navigation and Hydrography (BSH) in the course of annual surveys over a period of almost 30 years. Fig. 3.13 shows the elevation difference between the 1977 and 1996 bathymetries.

It can be seen that in this time span some smaller tidal channels silted up. Following the Piep channel further toward the west, significant departure in the depositional trends on either side of the mid channel shoal can be observed. While erosion prevails south of the shoal, a tendency towards accretion is observed along the northern slope and on the shoal itself. However, despite this internal reshaping, the reach and deposition of the central Piep channel remain relatively stable (Ricklefs and Asp, 2005).

Compared to the relatively stable central part of the study area, the more westerly and most exposed regions are characterized by intense erosion and re-deposition processes. Hydrodynamic forces have driven the outer sandbanks such as Tertiussand and D-Steert landwards(Ricklefs and Asp, 2005). In the case of Tertiussand, the migration has produced a compressed morphology. The reason for this is that the sandbank is trapped like a wedge between the two bordering banks. This wedge-like advance also forces the inlet of the Norderpiep to the north, as clearly recorded by the erosion along the northern and accretion along the southern bank (Ricklefs and Asp, 2005).

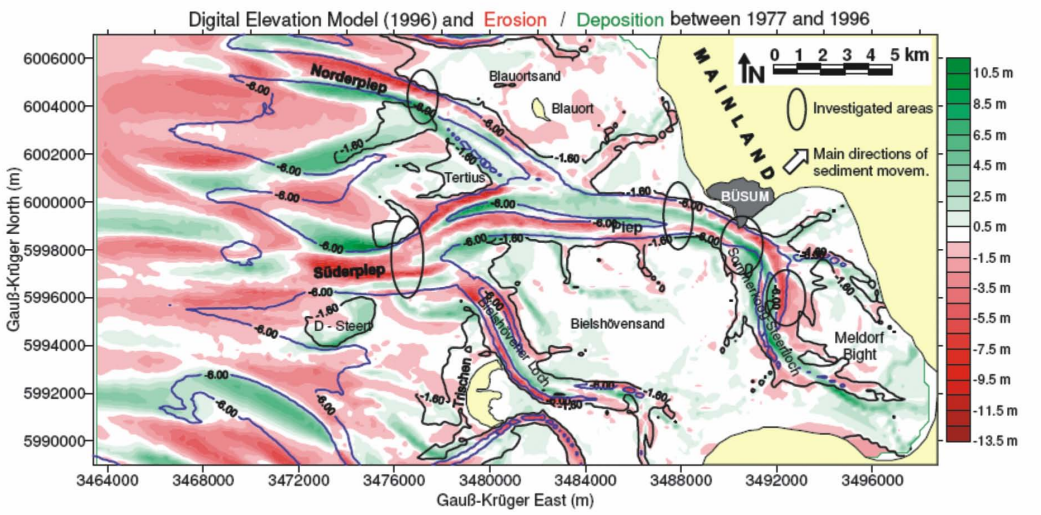

Figure 3.13: Overview of long-term morphological changes in Dithmarschen Bight (after Ricklefs and Asp, 2005)

In contrast to evolution of the northern channel, the situation in the Suederpiep is more complex. Here, the channel is bifurcated, as it is shown as cross-section B-Suederpiep and Seegatt-S in Fig. 3.14, over wide stretches. At the section Seegatt-S the stronger morphodynamic response of the southern, flood-dominated channel is associated with increased meandering. In both cases a northward migration of the mid-channel shoal and the northern channel section is observed. This northward migration in combination with the ebb-domination of northern channel, results in erosion along the flanks of the Tertiussand sandbank (Ricklefs and Asp, 2005).

In summary, the outer region of the study area, west of the bifurcation of the Piep channel into the Norderpiep and Suederpiep, is exposed to intense erosion processes. Landward migration of sandbanks, vertical accretion, especially of those parts of sandbanks which border the channels, and erosion tendencies in the channels are typical for this area. On the other hand the central part of the study area has remained relatively stable and is characterized by minor internal reshaping processes (Ricklefs and Asp, 2005).

3.6.2 Short-term Morphological changes

To identify the seasonal effects and effects of singular events, analysis related to the short-term morphological changes based on bathymetric surveys has been studied by Ricklefs and Asp (2005) as for the long-term morphodynamics (described in section 3.6.1).

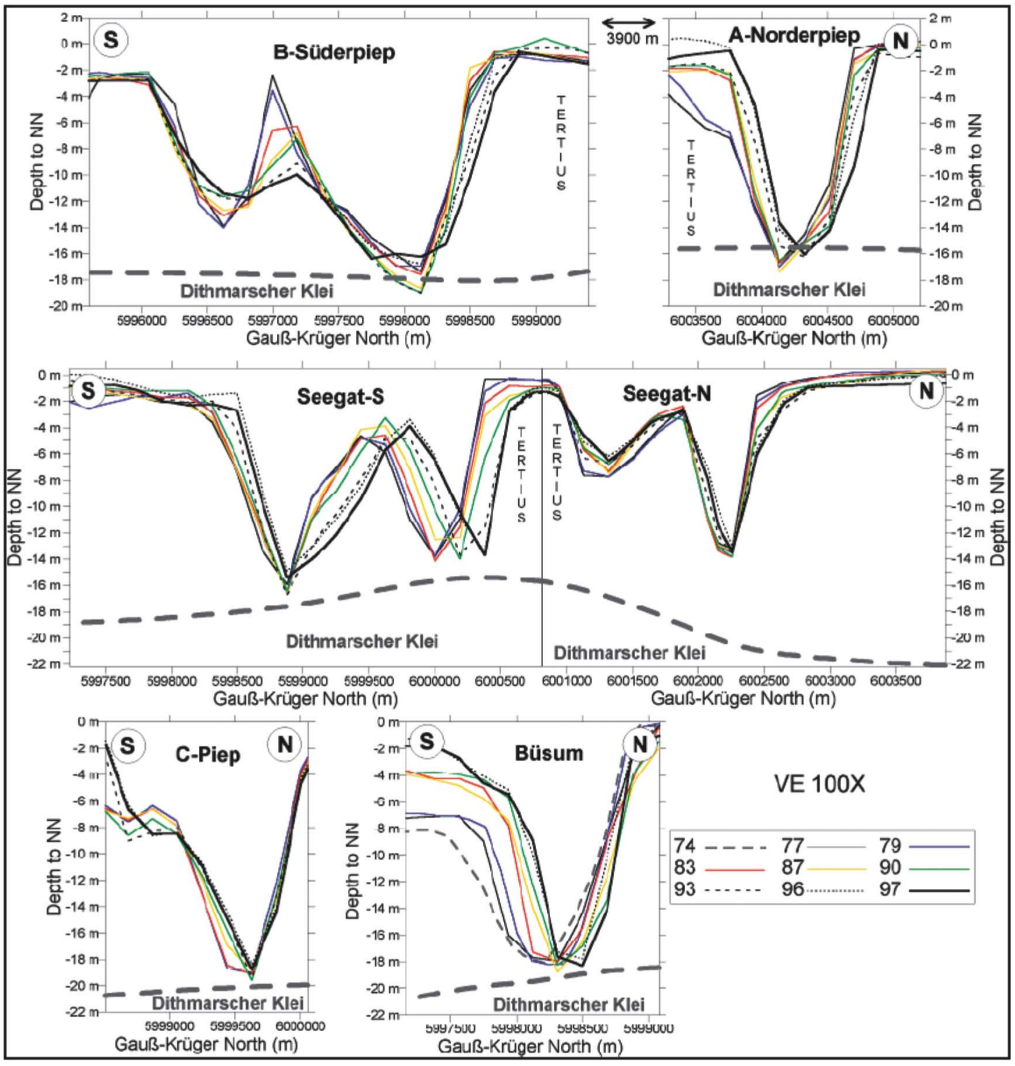

Figure 3.14: Annual to decadal morphological evolution along several channel cross-sections relative to the depth of Dithmarschen Klei (after Ricklefs and Asp, 2005)

The results of bathymetric measurements as shown in Fig. 3.16 to 3.18 has been carried out between summer 2000 and summer 2003 at cross-section in tidal channels illustrated in Fig. 3.15. The results confirm the tendency for a general northward migration of the Norderpiep channel. However, Fig. 3.16 reveals localized accretional and erosional phase. A temporal analysis of these variations shows that deposition prevails from winter to summer, and erosion from summer to winter. They found that the Norderpiep channel in this region can be considered to be in dynamic stability with seasonal variations and the superposition of a tendency towards northward migration in the longer-term.

Fig. 3.17 shows the bathymetric measurements along a cross-section in Suederpiep tidal channel. It can be seen that the cross-section can be considered to be relatively stable in the period from summer 2000 to spring 2003. Depth variations of 1-2m were monitored without showing any clear evolutionary trend. Persistent erosion is only observed along the northern embankment of Tertiussand sandbank (Ricklefs and Asp, 2005).

The cross-section in the Piep tidal channel (Fig. 3.18) is located approximately three nautical miles west of the town Buesum. It covers the eastern junction of the main Piep tidal channel and its southern flood dominated branch called Dwarsloch. The data shows this cross-section to be morphologically very stable. Although maximum depth changes of up to 3 m were measured, they more commonly remain below 0.5 m on short time scales. A comparison of data from June, September and December 2000 suggests deposition from summer to winter. This trend, however, reverses in the period from December 2000 to May 2001 when erosion occurred from winter to summer instead (Ricklefs and Asp, 2005).

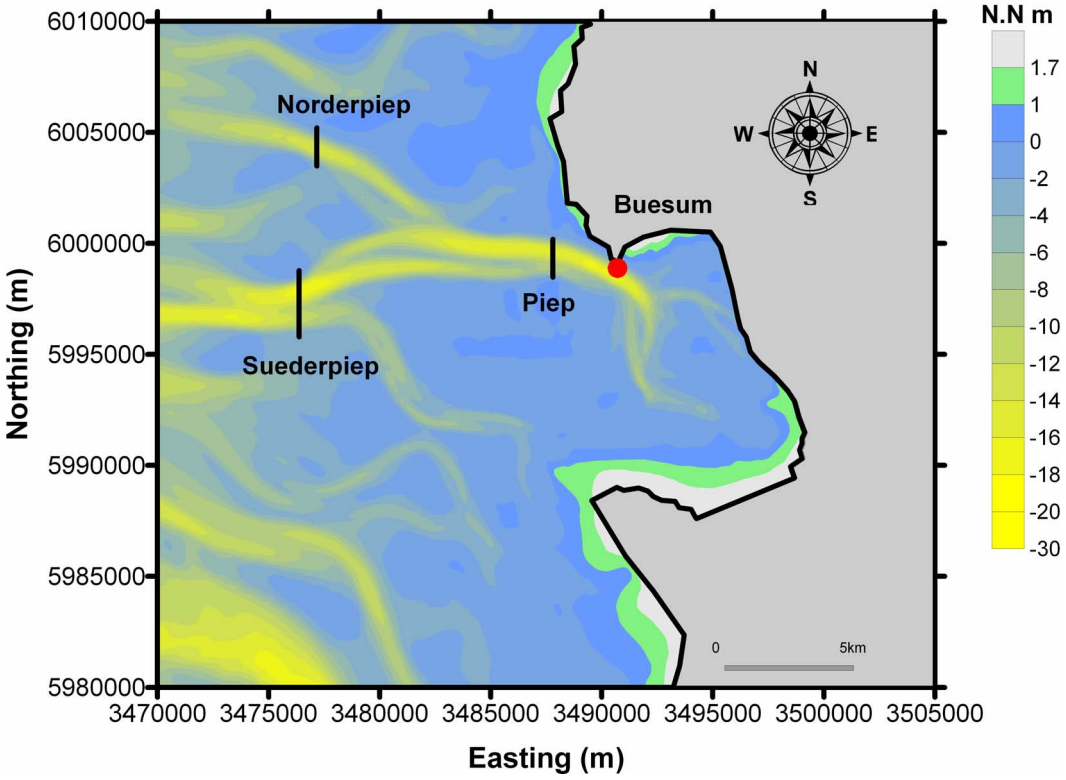

Figure 3.15: Location of cross-sections in tidal channels

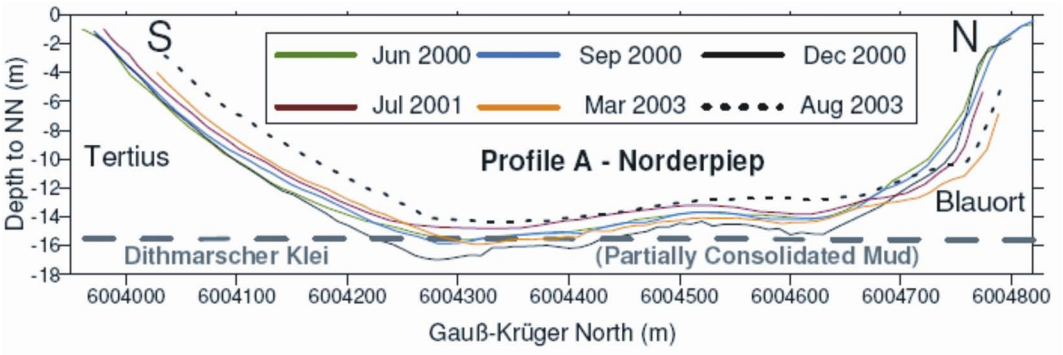

Figure 3.16: Bathymetric measurements along cross-section in Norderpiep tidal channel (after Ricklefs and Asp, 2005)

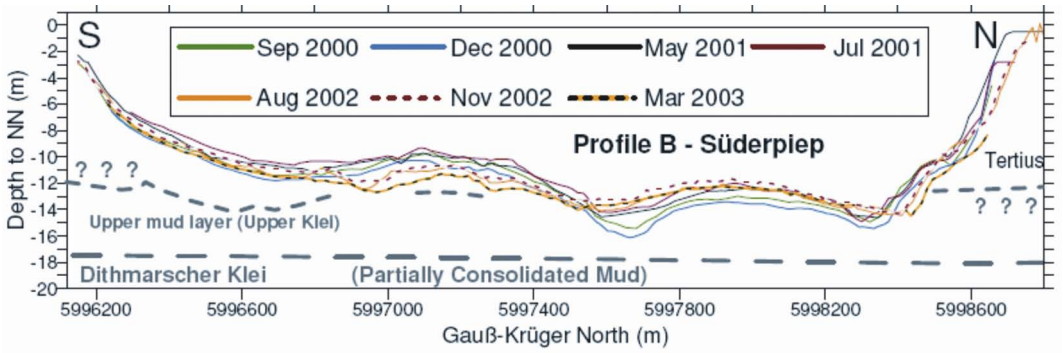

Figure 3.17: Bathymetric measurements along cross-section in Suederpiep tidal channel (after Ricklefs and Asp, 2005)

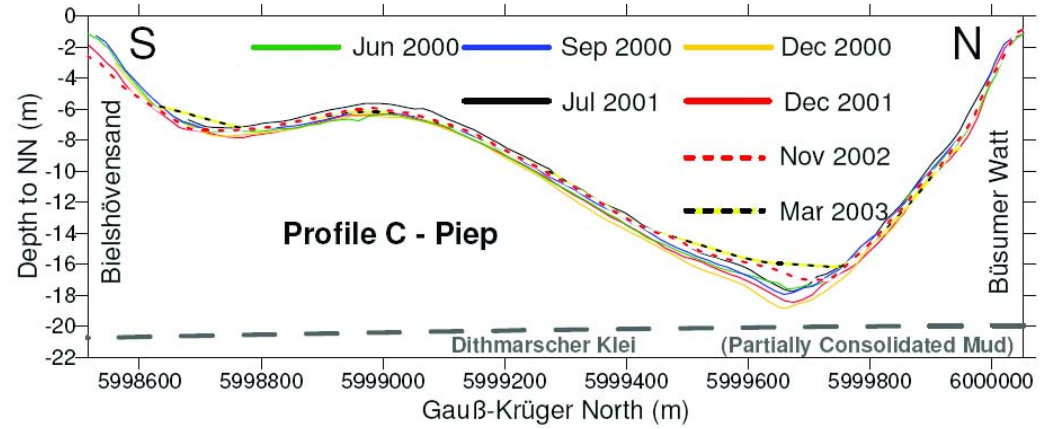

Figure 3.18: (Bathymetric measurements along cross-section in Piep tidal channel (after Ricklefs and Asp, 2005)

Chapter 4

The Dithmarschen Bight morphodynamic model

4.1 Introduction

To investigate the morphological changes due to storms, in short-term and medium-term, a numerical model was set up. In this chapter the set-up of the morphodynamic model covering the Dithmarschen Bight is described. In Section 4.2 the definition of the model domain is presented. This is followed by the description of the model components for flow, waves, sediment transport and morphodynamics in Sections 4.3 to 4.6. In Section 4.7 the results are discussed.

The model is based on the DELFT3D modeling package developed by WL|Delft Hydraulics. Because most of these models have been described elsewhere, the description of each is given in further detail in Appendix C.

4.2 Model domain

The model domain is defined as the area in which the physical processes will be simulated. For the Dithmarschen Bight morphological model, the domain will be identical for all of the applied sub-models.
Since the domain definition is the first and the most important step for the model set-up, one should take into account on one hand the area of interest (the area that will be taken into consideration when evaluating the model results and analysis) and the location of the open sea boundaries, and on the other hand, the computational requirements for the selected area.
Based on the previous description, the model of the Dithmarschen Bight as well as the area of interest have been defined. Fig. 4.1 shows the entire Dithmarschen Bight domain and also the area of interest. This includes of the tidal channels Norderpiep, Suederpiep and Piep connected to the sandbank Tertiussand.
The open sea boundaries have been selected away from the area of interest to ensure that the hydrodynamics, sediment dynamics and morphodynamics are well captured.

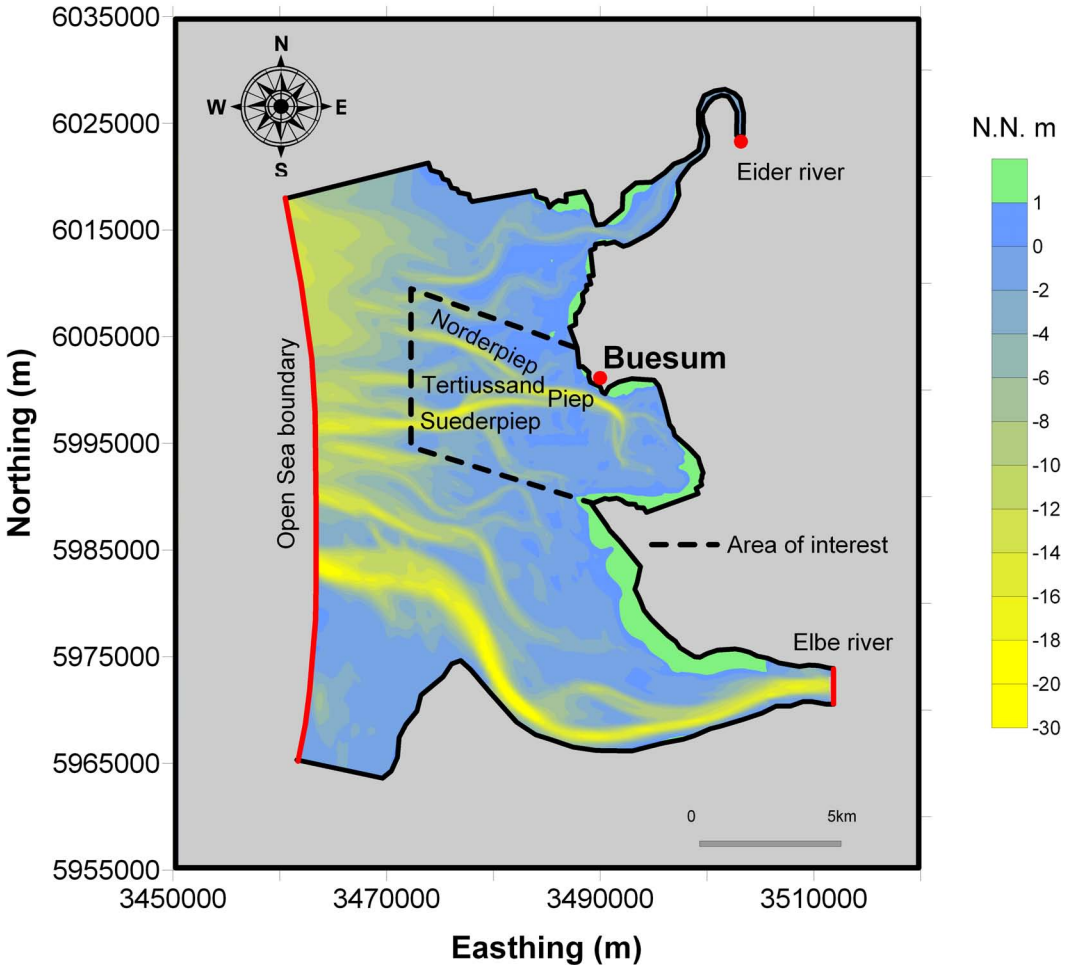

Figure 4.1: Model domain of the Dithmarschen Bight and the area of interest (Bathymetry 1990)

4.2.1 Model grid

For the simulation of short term events, as it is not possible to combine all model restrictions (see Appendix C) within one grid for an area as large as the Dithmarschen Bight, a detailed model was nested into two larger models.
Fig. 4.2 and Fig. 4.3 show the three models' nesting sequence and the computational grid of the Dithmarschen Bight Model, respectively. The first model (CSM) covers the north-west European Continental Shelf, the second model (GBM) covers the German Bight region and the third and more detailed model (DBM) covers the Dithmarschen Bight area. More detailed description of the three model's grids will be found in Table 4.1.
For simulation of the morphodynamics on the medium-term representative tide and wave conditions are used and there is no need for the nesting sequence. Therefore only one grid for the Dithmarschen Bight Model has been considered. The grid spacing varies from 45 m to 648 m with a total number of cells of about 43,000.

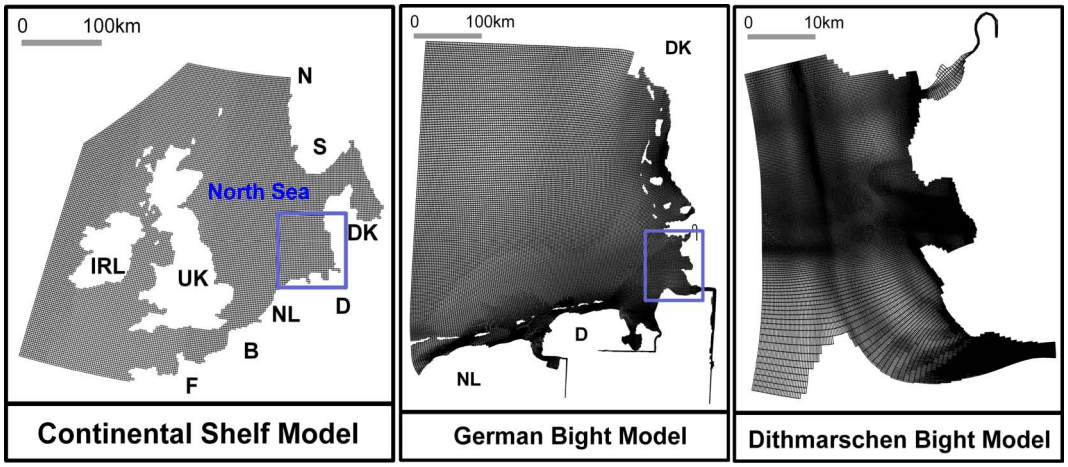

Figure 4.2: Nesting sequence from Continental Shelf Model to the Dithmarschen Bight Model

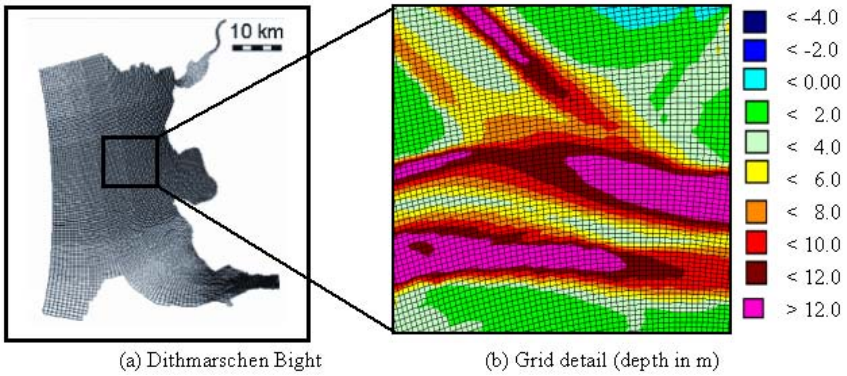

Figure 4.3: Computational grid of the Dithmarschen Bight Model

Continental Shelf Model (CSM)

The CSM model was developed by Verboom et al. (1992). The model domain is located between 48^{o}N and 62^o 20$'$N and 12^{o}W and 13^{o}E. The computational grid has a resolution of 5$'$ in the north-south direction and 7.5$'$ in the east-west direction. The model is driven by astronomical constituents along the open sea boundaries. The diurnal and semi-diurnal harmonic constituents are considered (M2, S2, N2, K2, O1, K1, Q1, P1, NU2 and L2). Synoptic wind and pressure fields are interpolated to the CSM grid. The full documentation of the model set-up and validations can be found in Verboom et al. (1992).

German Bight Model (GBM)

The German Bight model (GBM) is nested into the Continental Shelf Model (CSM). At the open boundaries of the GBM water levels are obtained from simulations with the CSM. The modelled area of the GBM is located between 53^{o}N and 56^{o}N and

5.3^{o}E and 9^{o}E. Synoptic wind and pressure fields are interpolated to the GBM grid. The GBM was originally developed by WL|Delft Hydraulics and later improved within the project PROMORPH (Mayerle and Zielke, 2005).

Table 4.1: Properties of the grids for CSM, GBM and DMB Models

Model	**Area (km^2)**	**Cells**	**Grid cells spacing (m)**
CSM	1425950	34400	7766-9576
GBM	54067	59890	262-1922
DBM	1440	240383	22-342

4.2.2 Model bathymetry

The bathymetry, that has been used for the three different models, was generated from measuring bathymetric data as described in Chapter 3, section 3.6.1. As typically found, quality bathymetric data is still lacking covering of the entire domain. Therefore the gaps have been filled in with data from other years. The sensitivity study conducted for the DBM bathymetric data showed the model needs from a few months up to about one year to adjust to the starting bathymetry. To avoid uncertainty of the bathymetry, one simulation with measured bathymetric data has been carried out for one year and the final adjusted bathymetry has been used in the Dithmarschen Bight Model as the starting bathymetry.

4.2.3 Boundary conditions

Three open boundaries have been defined for the Dithmarschen Bight model. Two open boundaries have been defined for the Elbe and the Eider rivers as water levels and point discharge, respectively. The third open sea boundary has been located at the western, northern and the southern regions of the domain as water levels or current velocity (see Fig.4.1). More details through the following sections will explain the open sea boundaries, that have been used for the short- and medium-term models.

4.3 Flow model set-up

In this section the set-up of the flow model is described. More details about the flow model of DELFT3D modelling systems is given in Appendix C.
The set-up procedure, the results of sensitivity studies for the main numerical and the physical parameters, and the calibration and validation of the flow model against field data, are fully documented by Palacio et al. (2005).
Early in the year 2000, Palacio et al. managed to set-up a flow model in the Meldorf Bight (includes the area of interest) as part of investigations carried out at the Coastal Research Laboratory (CORELAB) of the University of Kiel in Germany,

in conjunction with the research project entitled "Prediction of Medium-Scale Morphodynamics - PROMORPH " funded by the German Ministry of Education and Research from January 2000 to December 2002 (Mayerle and Zielke, 2005).
The depth-integrated two-dimensional flow model was employed, calibrated and validated by considering several approaches for defining the open sea boundaries through nesting sequences (Fig. 4.2), by imposing astronomical tides, and finally by applying measured water levels from the closest gauges.
A detailed investigation with respect to several flow model parameters and settings were carried out. The variability of the computed water levels and velocities at several monitoring points with respect to time step, grid resolution, eddy viscosity, wind speed, bottom roughness and morphology were investigated.
Fig. 4.5 and 4.6 show the comparison between the measured and the modelled water levels for different open sea boundary condition approaches at six locations (for the location see Fig. 4.4).
Additional comparisons between a 3D versus 2Dh model results have been carried out by Palacio et al. (2001). In this case the 2Dh model was extended to 10 layers in the vertical direction. The vertical grid size variation was chosen to follow a logarithmic distribution, in order to reproduce the expected vertical flow profiles more adequately. Comparisons between results of 2Dh and 3D model approximations show only minor differences in terms of water levels at several locations and flow discharges at several cross-sections (Palacio et al., 2001). Therefore, the two-dimensional depth-integrated approach has been applied in this study.

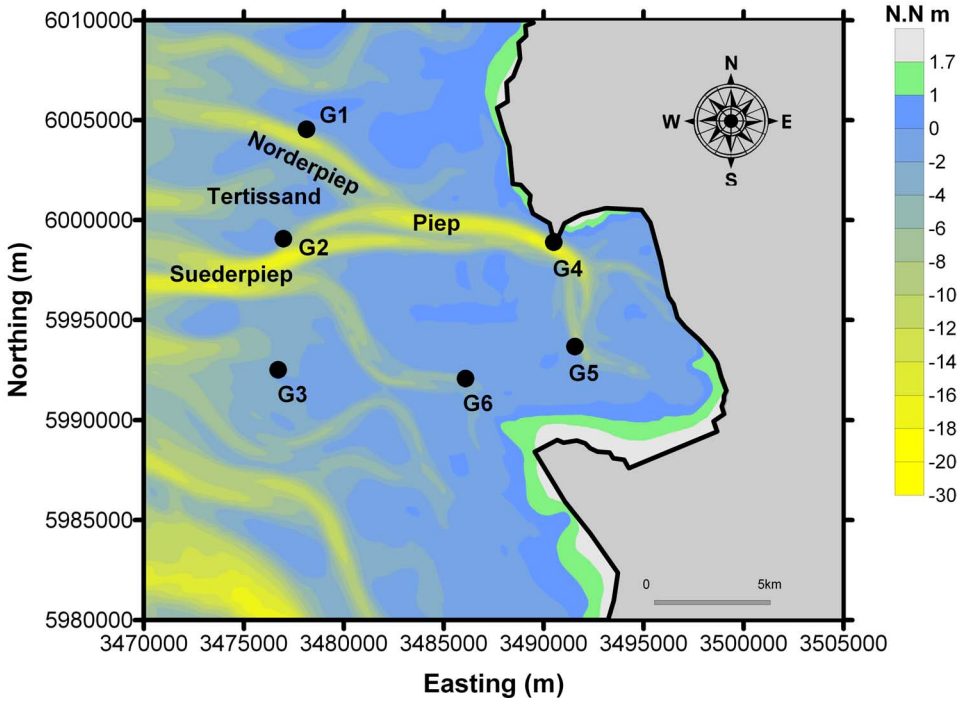

Figure 4.4: Location of observation stations G1 to G6

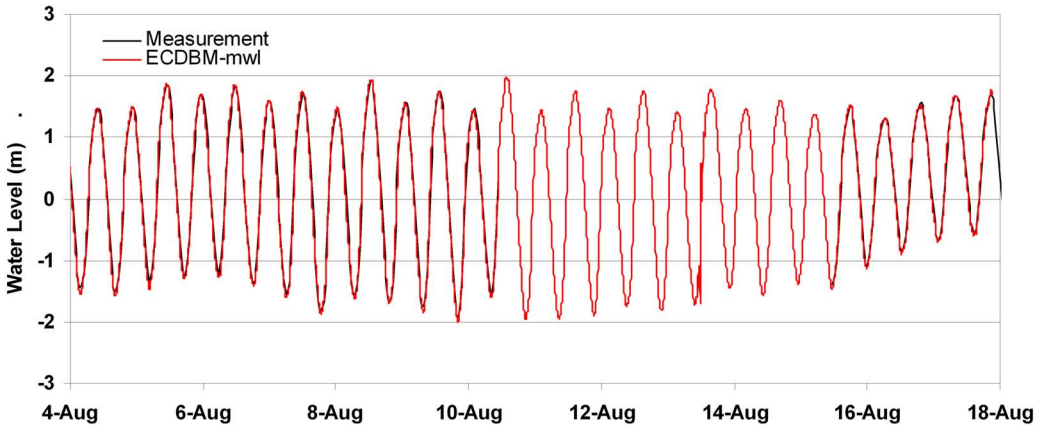

(a) Gauge Station G1 (Blauort)

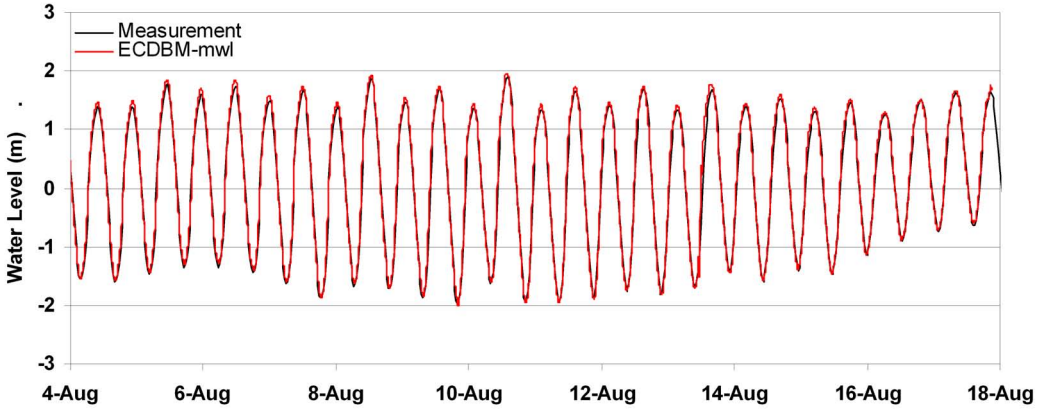

(b) Gauge Station G2 (Tertius)

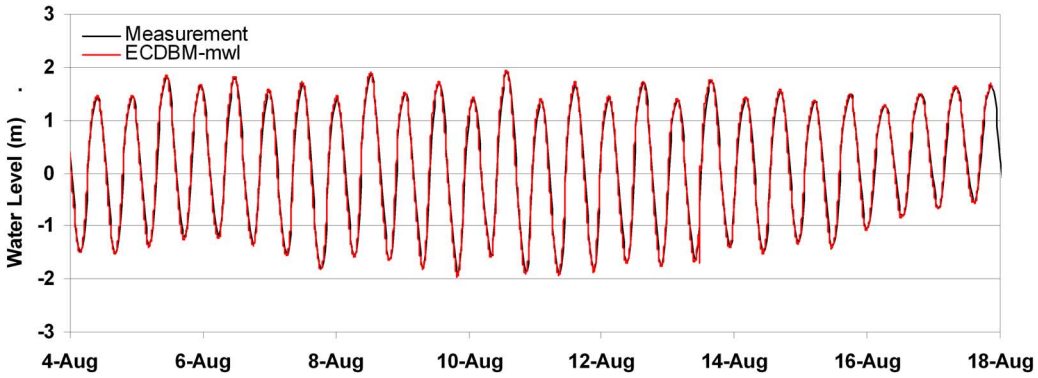

(c) Gauge Station G3 (Trischen)

Figure 4.5: Measured vs. modeled water levels at G1 to G3 stations (after Palacio et al., 2005)

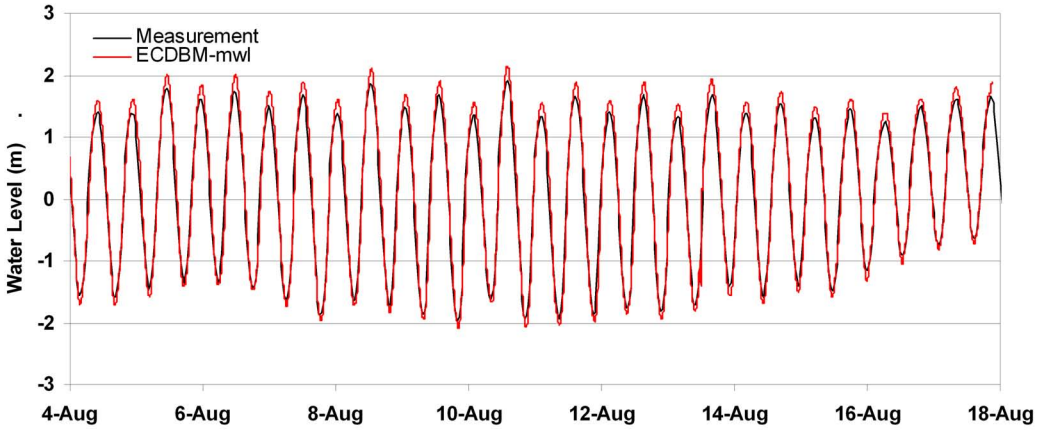

(a) Gauge Station G4 (Buesum))

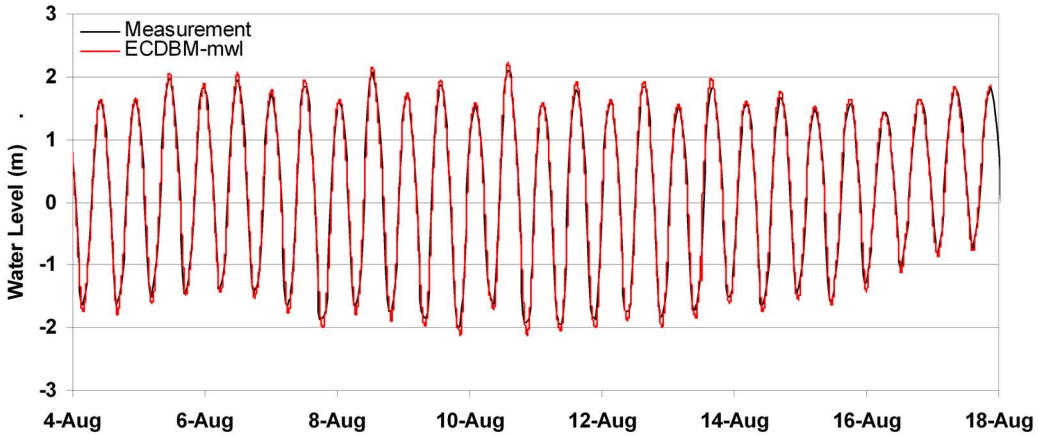

(b) Gauge Station G5 (Steertloch)

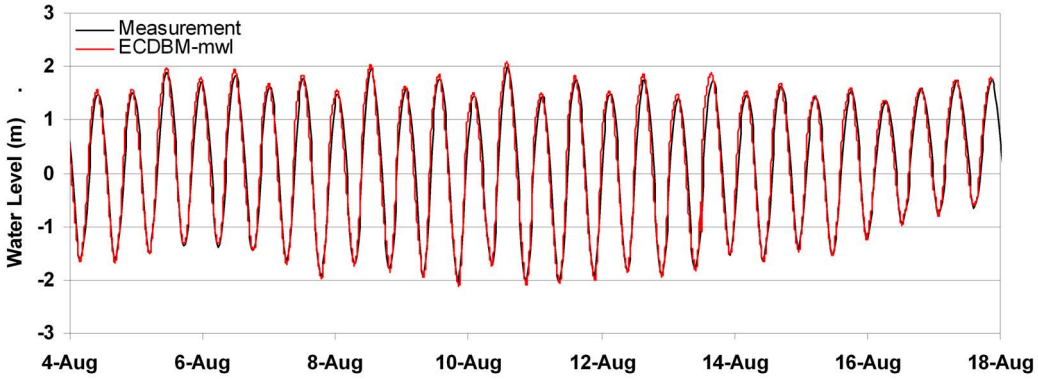

(c) Gauge Station G6 (Flackstorm)

Figure 4.6: Measured vs. modeled water levels at G4 to G6 stations (after Palacio et al., 2005)

4.4 Wave model set-up

To include the effects of the waves on the flow simulation, the wave model has been coupled with the flow model. This leads to the inclusion of computed water levels and flow velocities in the wave model. As is mentioned in Section 4.2, the grid for the wave model will be the same as for the flow model.

Wilkens and Mayerle (2001) set up a wave model (SWAN model) for the central Dithmarschen Bight. The calibration of the coupled flow-wave model, was carried out on the basis of a one-month measurement campaign (September 1996) using five wave rider buoys (data from Niemeyer, 1995, Section 3.2.3).

The two outer western buoys, POS1 and POS2 (Fig. 3.3(f)), were used for defining the swell boundary conditions and the inner buoys were used for evaluation of the model results. A comparison has been made between the results of the applied wave model.

Another set of wave boundary conditions has been generated from a larger coupled flow-wave model, which covers the entire German Bight. This model has been forced locally by wind only (wind data from PRISMA data set, Section 3.3) and has been calibrated with the measurements of the two outer western wave buoys (POS1 and POS2).

In general the wave model produced good results, especially when the complex conditions are taken into account. The larger discrepancies are mainly under very calm conditions. The overall results showed that the predicted wave breaking takes place in the areas where wave breaking is observed. Additionally, the boundary conditions based on the two western wave buoys proved to be acceptable.

The generation of boundary conditions with the larger German Bight model showed good results for 80% of the measurement period, where the discrepancies were below 15-20% of the measured wave height and 5-10^o in the wave direction. During the other 20% the directional discrepancy was about 30^o and the wave height discrepancy up to 40% of the measured value.

For example the Fig.4.7 shows the measured and computed wave heights at POS2 for SWAN model. It is clear that, the model results from SWAN model show a good agreement with the measurements in terms of significant wave height.

Wilkens et al. (2005) investigated the accuracy of applications of four wave models (HISWA, SWAN, TOMAWAC and COWDADIS) to be used as modules for the morphodynamic models of central Dithmarschen Bight. According to the quality index, proposed by Van Rijn et al. (2003) in Table 4.2, the performance of the four wave models vary between reasonable and good. The obtained root mean absolute error (RMAE) values and scatter plots confirm the finding based on the time series comparison (Wilkens et al., 2005).

Fig. 4.8 shows scatter plots of the modelled and measured significant wave heights at the three eastern wave buoys (POS3, POS4 and POS5) for the models COWADIS, HISWA and SWAN. Moreover Fig. 4.9 shows also the scatter plots but for POS1, POS2 and POS3 wave buoys (for the wave buoy locations, see Fig. 3.3(f)). It can be seen that the SWAN wave model provides better results compared to the remaining three wave models.

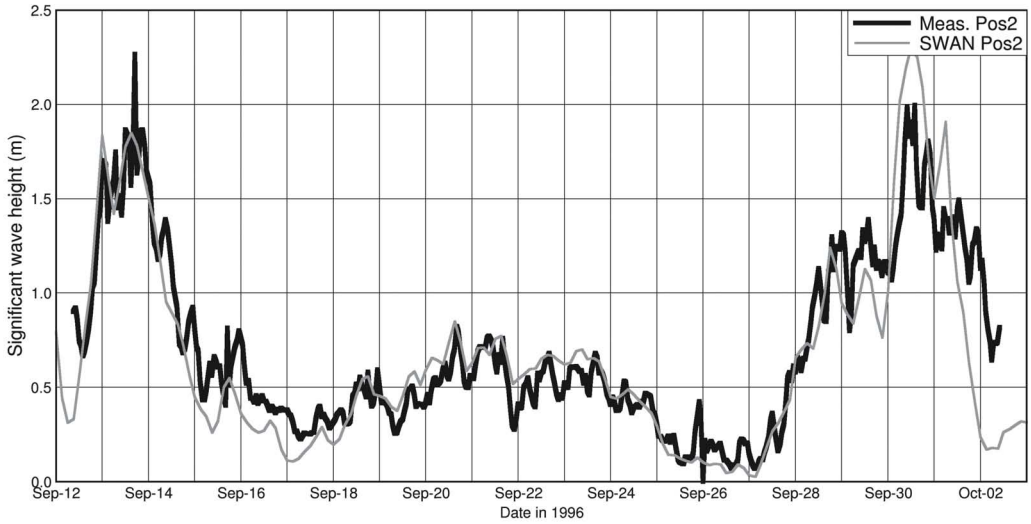

Figure 4.7: Measured and modelled significant wave heights at POS2 station (after Wilkens et al., 2005)

Table 4.2: Quality of simulation wave heights (after Van Rijn et al., 2003)

Qualification	**RMAE value**
Excellent	< 0.05
Good	0.05-0.10
Reasonable / Fair	0.10-0.20
Poor	0.20-0.30
Bad	> 0.30

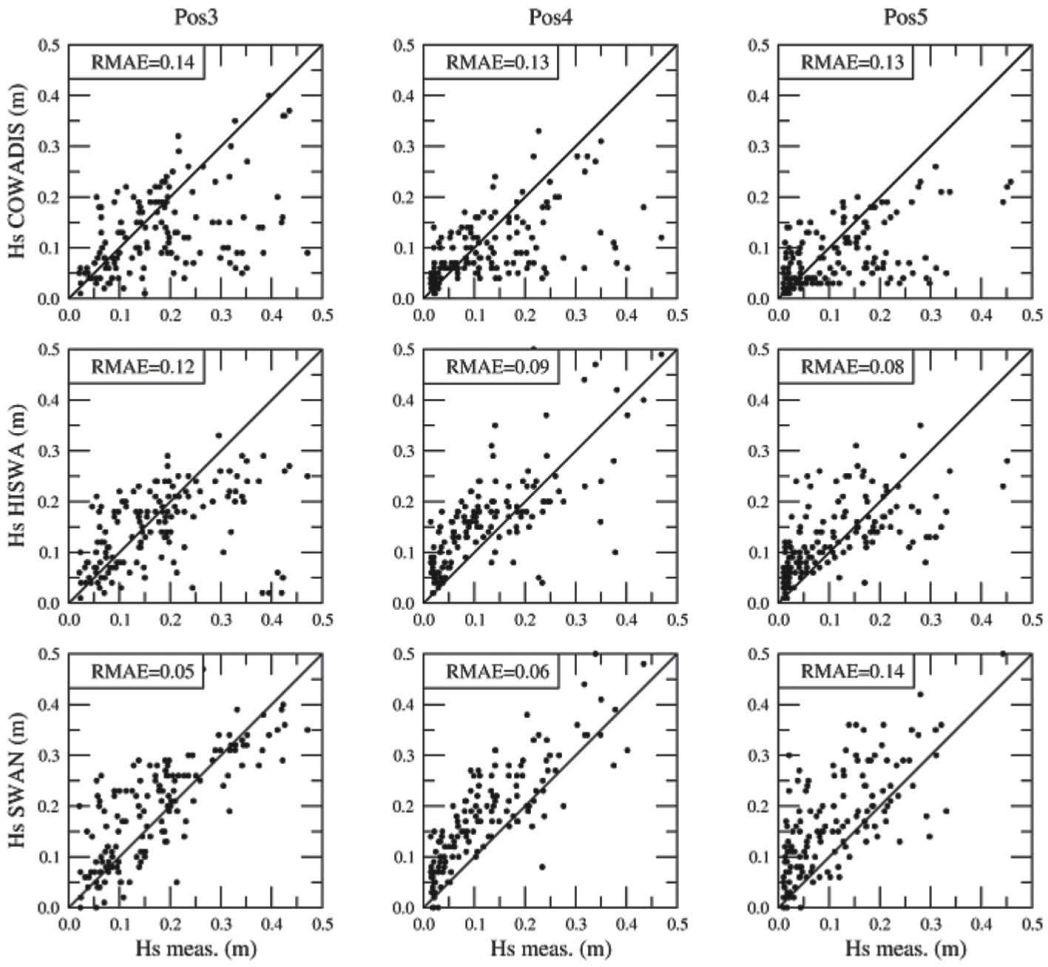

Figure 4.8: Modelled vs. Measured wave heights at POS3, 4 and 5 for COWADIS, HISWA and SWAN wave models (after Wilkens et al., 2005)

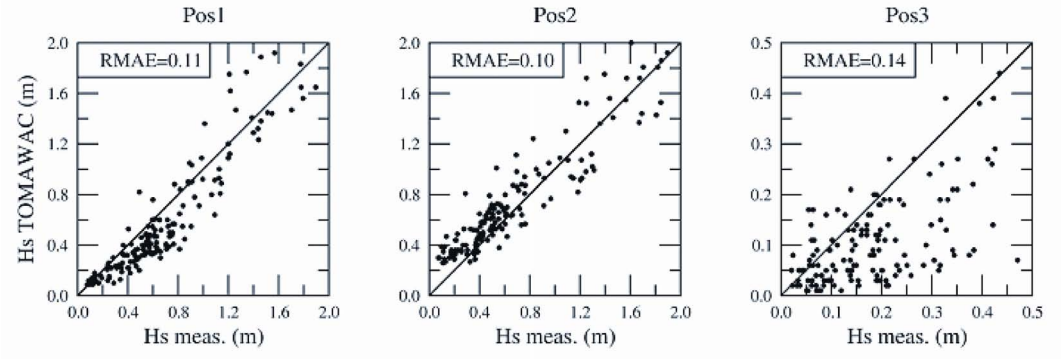

Figure 4.9: Modelled vs. Measured wave heights at POS1, 2 and 3 for TOMAWAC wave model (after Wilkens et al., 2005)

4.5 Sediment model set-up

In the last few years, several sediment transport models have been set up for the Dithmarschen Bight region. In the following paragraphs the description of the most recent models will be presented. It includes the models proposed by Winter and Mayerle (2003), Poerbandono and Mayerle (2003), and Escobar and Mayerle (2007)

4.5.1 Sediment transport model by Winter and Mayerle (2003)

In the framework of the German government funded research project PROMORPH, a large number of suspended sediment transport measurements at several cross-sections and longitudinal transects of a tidal channel system in the German Bight have been carried out to enhance model development. The model, that has been set up by Winter and Mayerle, computes the bed load transport based on algebraic formula and separately accounts for the suspended load transport by solving a 2Dh advection-diffusion equation for the suspended sediment concentration.
Three algebraic sediment transport formulas of Van Rijn (1984), Bijker (1971) with local waves and Bijker (1971) without local waves were tested. This use done to analyse the model sensitivity to variations in physical input parameters such as the grain size, the bottom roughness and the calibration coefficients. Comparisons between the results of prediction and observations have been performed in terms of time series of suspended sediment concentrations with different hydrodynamic conditions. The direct comparison between measured and computed concentrations shows the model suitability to this domain. The validation of the model at different points in time and space without additional tuning of the model parameters shows reliable results. The evaluated results at three cross-sections (see Fig. 4.10) for the optimized Bijker formula revealed a good agreement (Winter and Mayerle, 2003) (see Fig. 4.11).

4.5.2 Sediment transport model by Poerbandono and Mayerle (2003)

Some additional measurements were taken in the Dithmarschen Bight between the years 1999-2002. Fifty field measuring campaigns, most of them covering complete tidal cycles, have been conducted at several cross-sections to cover a large part of the domain under different tidal and wind conditions. The measurements were taken by using combined devices of CTD (Conductivity, Temperature, Depth) and optical transmission sensors with water samples. More than 500 water samples and 3800 transmissivity profiles have been collected. Additionally stationary and vessel mounted direct reading ADCP's (Acoustic Doppler Current Profilers) were used for measuring velocity profiles and acoustical backscatter. Water samples have been analysed for grain size using a laser granulometer and suspended matter concentrations.
This extensive data set from the measurements has been used by Poerbandono to extend the calibration and the validation of Winter and Mayerle's (2003) numerical sediment transport model. The results produced by the sediment transport model at cross-sections T1, T2 and T3 (the same as those in Winter and Mayerle), utilizing

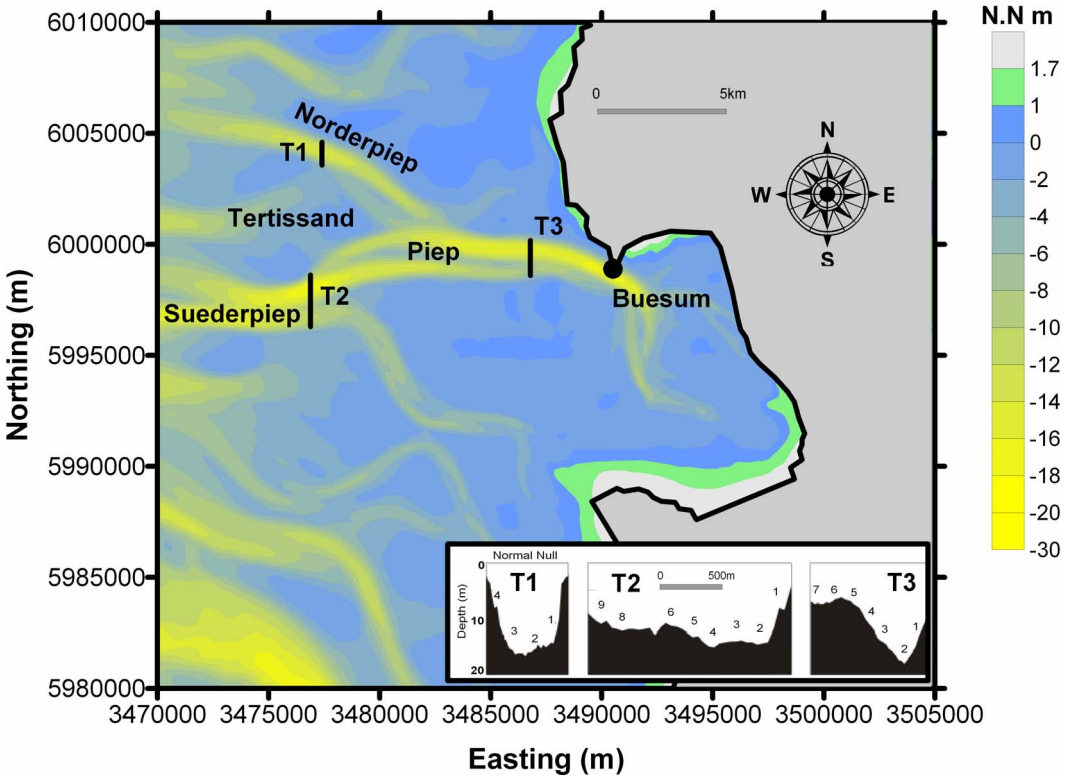

Figure 4.10: Location of cross-sections for Winter & Mayerle, 2003

the Bijker (1971) formula fared slightly better than those produced by the Van Rijn (1984) formula (see Fig. 4.12).

The sediment grain sizes for non-cohesive sediments and equivalent roughness sizes were uniform for the entire domain (d_{50} of 100μm, d_{90} of 150μm and k_s of 0.2m). Moreover cohesive sediments have been not taken into account, for the two sediment transport models (Winter and Mayerle, 2003 and Poerbandono and Mayerle, 2003).

4.5.3 Sediment transport model by Escobar and Mayerle(2007)

The sediment transport model developed by WL|Delft Hydraulics has been improved in the last few years. Nowadays the Delft3D sediment transport models support both bed load (non-cohesive) sediments and suspended load (cohesive and non-cohesive) sediments.
Escobar (2007) studied the relationship between equilibrium grain size and flow-wave energy levels. The computed grain sizes were used in his model for the prediction of sediment transport as well as for defining bed forms and associated roughness under tidal flow conditions. His approach has been verified by using measured and modelled sediment sizes, bed form dimensions and suspended sediment concentrations. He concluded that the accuracy of the implemented sediment transport model utilizing a roughness map created by means of a constant Chezy coefficient (this is the same map that has been used in the two previous sediment transport models) could

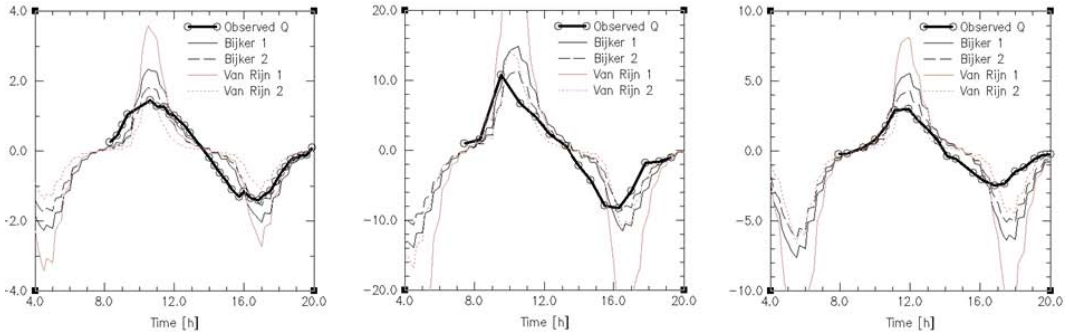

Figure 4.11: Observed and computed suspended sediment load (10^3 kg/s) at T1, T2 and T3 cross-sections (after Winter & Mayerle, 2003)

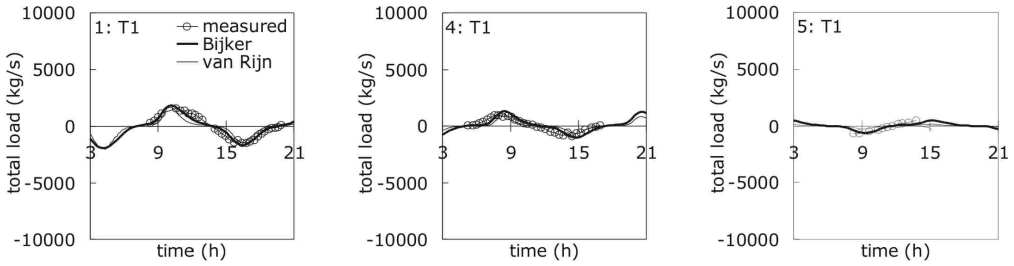

(a) Cross section T1, data set 1, 22 March 2000, tidal range 4m

(b) Cross section T1, data set 4, 12 Sep. 2000, tidal range 3.3m

(c) Cross section T1, data set 5, 5 Dec. 2000, tidal range 2.3m

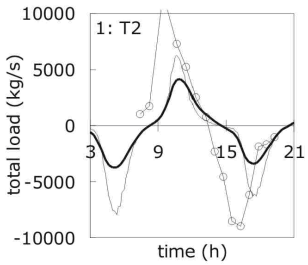

(d) Cross section T2, data set 1, 21 March 2000, tidal range 4.1m

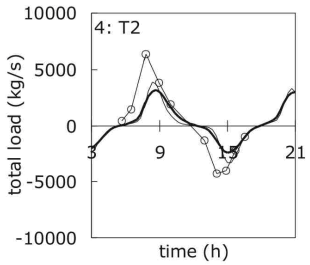

(e) Cross section T2, data set 4, 12 Sep. 2000, tidal range 3.3m

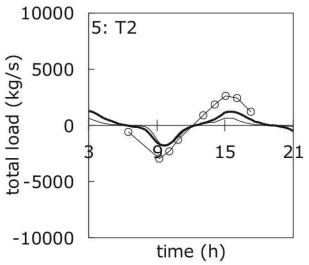

(f) Cross section T2, data set 5, 5 Dec. 2000, tidal range 2.3m

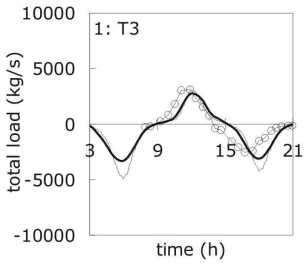

(g) Cross section T3, data set 1, 23 March 2000, tidal range 4.2m

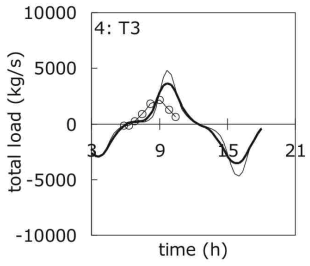

(h) Cross section T3, data set 4, 13 Sep. 2000, tidal range 3.5m

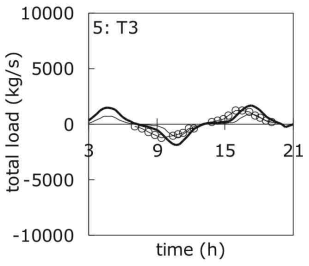

(i) Cross section T3, data set 5, 6 Dec. 2000, tidal range 2.5m

Figure 4.12: Observed and computed suspended sediment load (kg/s) at T1, T2 and T3 cross-sections (after Poerbandono & Mayerle, 2003)

be improved by about 35% by using roughness maps obtained through his improved sediment transport model. Further improvements of about 25%, 15%, and 10% resulted from the inclusion of cohesive sediments, new roughness, and other factors such as the sediment availability, respectively (Escobar and Mayerle, 2007).
Fig. 4.14 to 4.16 show comparisons between measured and modelled depth-integrated suspended sediment concentrations obtained from this sediment transport model as well as their respective RMAE (root mean absolute error) values at the cross-sections T1, T2 and T3.

4.5.4 Discussion of sediment transport models

As already mentioned in the second chapter and the previous sections, in the models of Winter and Mayerle (2003) and Poerbandono and Mayerle (2003), the presence of cohesive sediments has been ignored and a uniform grain size distribution was used. Wilkens, 2004 (applying the same sediment transport model) concluded that defining multiple grain sizes could give a better representation. Nonetheless, good results were obtained for sediment transport modelling within uniform grain sizes and in the medium scale morphodynamic modelling.
These improvements in the representation of physical phenomena (sediment sizes, bed roughness and sediment availability) may lead to a better description of the morphodynamics. Therefore, based on the sediment transport model that has been improved by Escobar and Mayerle (2007), the sediment distribution for cohesive and non-cohesive sediment for the Dithmarschen Bight model is described in Fig. 4.13.

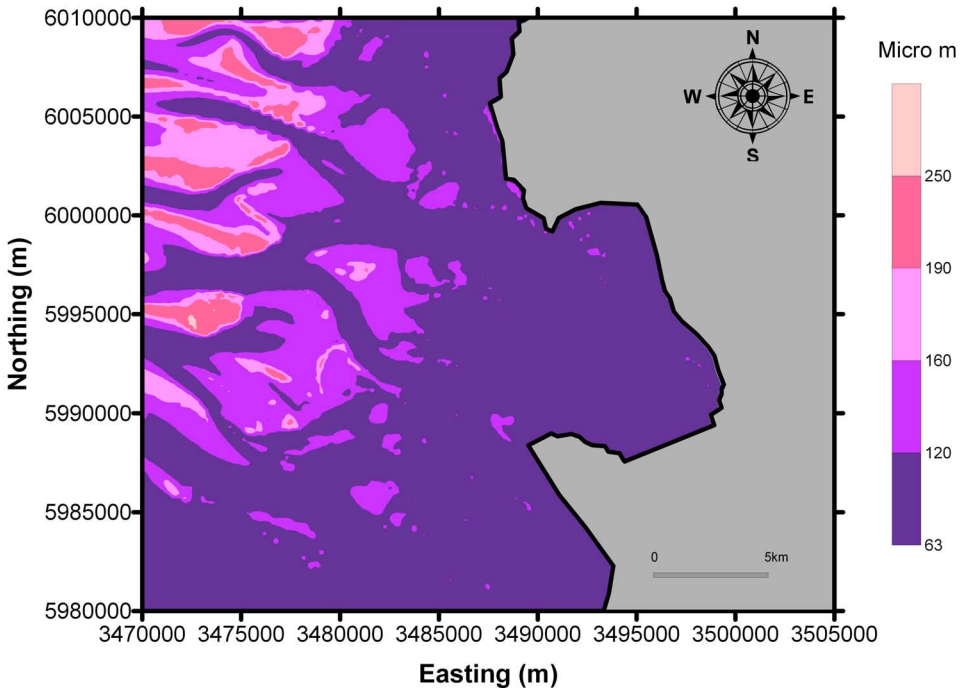

Figure 4.13: Grain size distribution in the Dithmarschen Bight (μm) proposed by Escobar, 2007

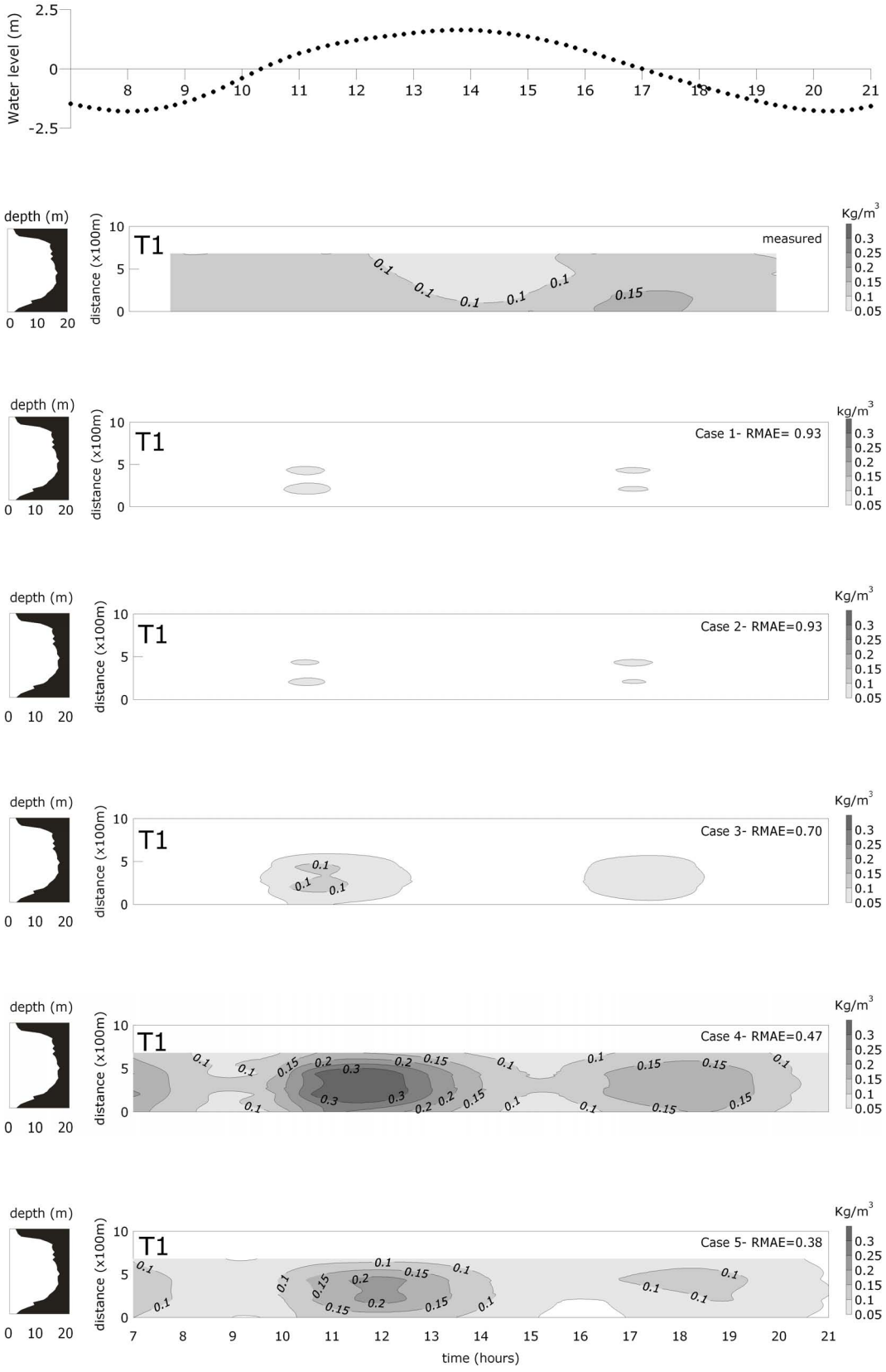

Figure 4.14: Depth-integrated suspended sediment concentrations at cross section T1 (after, Escobar, 2007)

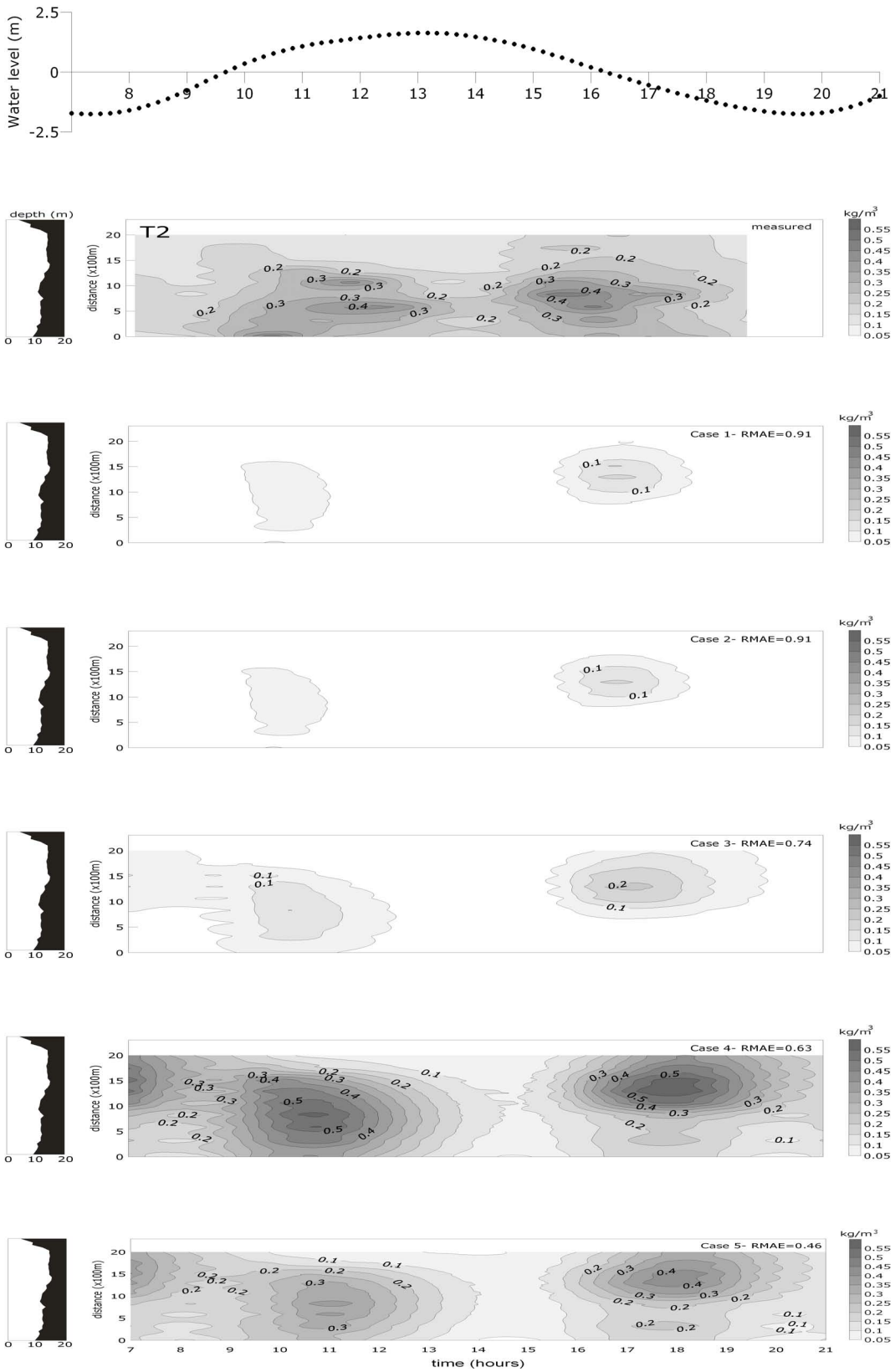

Figure 4.15: Depth-integrated suspended sediment concentrations at cross section T2 (after, Escobar, 2007)

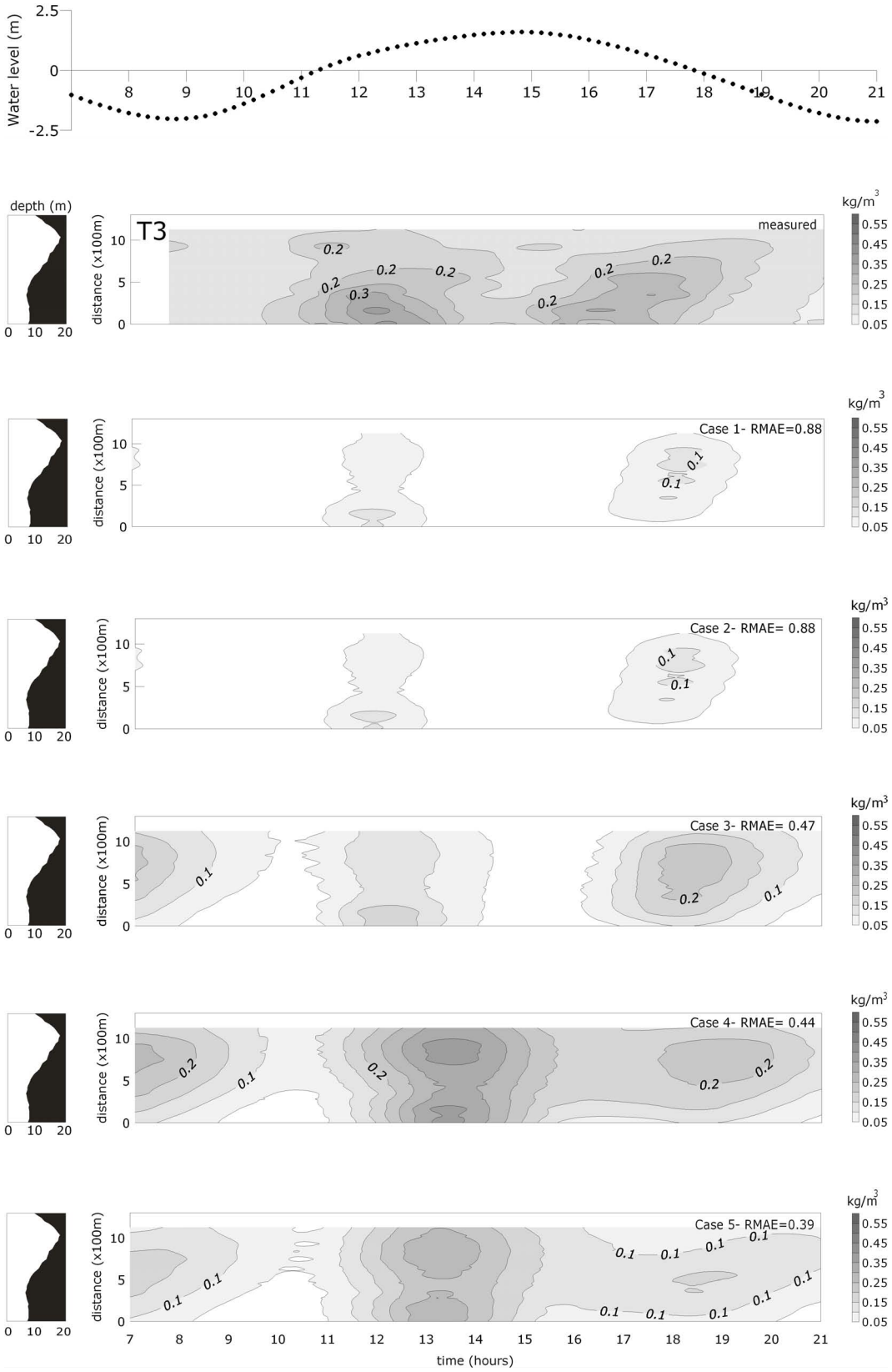

Figure 4.16: Depth-integrated suspended sediment concentrations at cross section T3 (after, Escobar, 2007)

4.6 Morphodynamic model

For the short- and medium-term morphodynamic models, the open sea boundaries for the flow and the wave models will differ. For the short-term model the open sea boundaries will be imposed based on the nesting sequence. Simulations will be carried out considering the actual driving forces in terms of water levels, waves and winds that are imposed along the open boundaries.

The open sea boundaries for the medium-term morphological model will be imposed on the basis of representative flow and wave approaches. A more detailed description related to the nesting sequence will follow in Section 4.6.1, as will the representative flow and wave conditions in Chapter 6 and Appendix B.

The implementation of the morphological time scale factor (Morfac), on one hand, is achieved by simply multiplying the erosion and deposition fluxes from the bed to the flow and vice-versa by the Morfac at each morphological time-step (n time-steps for Morfac equals n). This allows accelerated bed-level changes to be incorporated dynamically into the hydrodynamic flow calculations (Delft3D-Flow manual, 2006).

Data reduction schemes, on the other hand, are used to express hydrodynamic processes. The use of schematised open-boundary conditions, which are considered as representative in terms of their cumulative morphological effect, is based on the concept of morphological or representative boundary conditions (Winter et al., 2006).

4.6.1 Short-term morphodynamic model

For the short-term morphodynamic model, the open-sea boundaries for the flow and wave models were obtained according to the nesting sequence shown in Fig. 4.2. In this way a better description of the variety of water level and swell during the storm are imposed along the open sea boundaries. Flow conditions along the open-sea boundaries of the investigation area were obtained by nesting the Dithmarschen Bight Model (DBM) in the German Bight Model (GBM), which in turn is nested in the north-west European Continental Shelf Model (CSM).

The open-sea boundary conditions for waves were obtained by nesting the DBM in the larger GBM. The GBM wave model is forced by wind only, neglecting incoming wave energy through the open-sea boundaries (Mayerle et al., 2005). From a sensitivity study it was concluded that the extra computational costs of additionally nesting the GBM in the CSM for improving wave boundary conditions were not justified due to only slight differences in wave parameters along the boundary of the DBM (Wilkens et al., 2005).

In the simulations of morphological changes in the study area for the considered storm events, morphodynamic updating was limited to the DBM model. Since this study has been carried out using a morphological model with an online approach implementing a morphological acceleration factor (Morfac), as described in Chapter

2, the Morfac is set to 1 for the short-term model and will vary in time for the medium-term model.

The Morfac is set to 1 for the short-term model in order to allow the model to capture the morphological development at every computing flow model time step. The Morfac corresponding to the medium-term model is selected as a function of time and wave climate in order to accelerate the computing time of the morphological model.

Fig. 4.17 shows the short-term morphological modelling scheme for the Dithmarschen Bight model. The simulation period for the CSM and the GBM will be for a 30 day simulation period. After that the output for the hydrodynamic and the wave conditions from GBM will be the input for the flow and wave model of the DBM. The bathymetry will be updated each time step of the flow simulations.

4.6.2 Medium-term morphodynamic model

As described in Chapter 2, the input filtering approach will be implemented in the medium-term morphodynamic model. For the flow and wave models, input filtering will be performed only for the open sea boundaries. More details for the representative tide and representative wave conditions, which are imposed in the medium-term morphodynamic model, are given in Sections 6.2.1.1 and 6.2.3. The basis of the theory behind the representative tide and wave conditions is described in Appendix B.

Fig. 4.18 shows the medium-term morphological modelling scheme for the Dithmarschen Bight model. The representative tide, wave and wind will be the input for the flow and wave model (these input conditions will be described in detail in Chapter 6). The interaction between the flow, sediment and wave models will be every n time step of the flow model, however the bathymetric update will take place each Morfac value. This meaning that if the Morfac equals 10, the bathymetric update will take place every 10 time steps.

4.7 Morphodynamics model performance

All of the models, described in the previous sections, have been calibrated and validated individually with respect to extensive measurements as well as under different conditions. On the basis of these procedures, these models could, therefore, be used to build a morphological model for the Dithmarschen Bight region for both short and medium-term. Table 4.4 and Table 4.5 show the parameters settings of the various model set-ups and it concludes with the most important parameters for each model used.

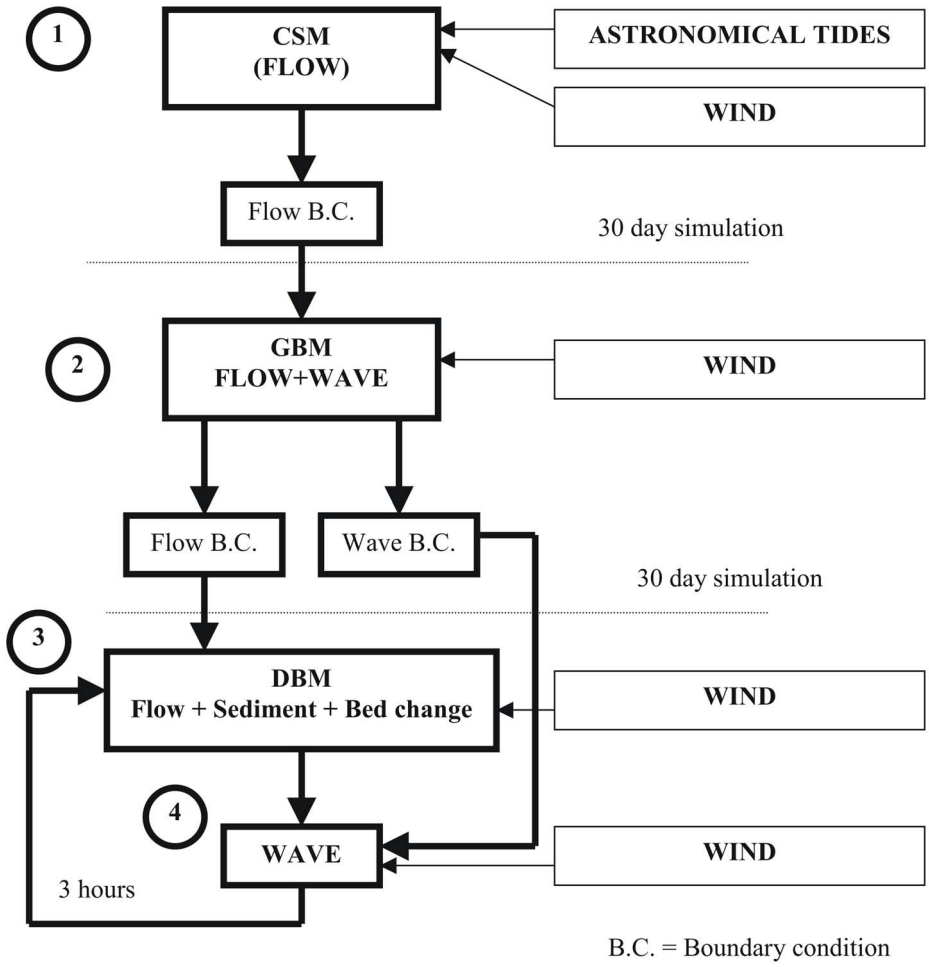

Figure 4.17: Scheme of the short-term morphological modelling for the Dithmarschen Bight model

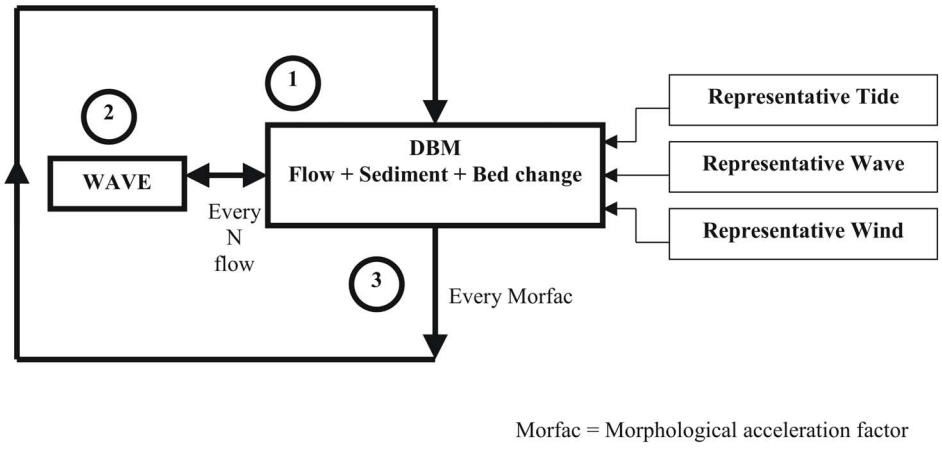

Figure 4.18: Scheme of the medium-term morphological modelling for the Dithmarschen Bight model

To assess the results from the morphodynamics model for the Dithmarschen Bight region, the Brier Skill Score (BSS) is proposed. The formulae is as follows:

$$BSS = 1 - \frac{\left\langle \left(|Z_{b,c} - Z_{b,m}| - \Delta Z_{b,m} \right)^2 \right\rangle}{\left\langle \left(Z_{b,0} - Z_{b,m} \right)^2 \right\rangle} \tag{4.1}$$

Where
Z_b = bed level
$\Delta Z_{b,m}$ = error of measured bed level (0.1 m for bed level in field conditions and 0.02 m for laboratory conditions)
$Z_{b,0}$ = initial bed level
index m = measured
index c = computed
$\langle .. \rangle$ = averaging procedure over time series

Van Rijn et al. (2003) asserts that the BSS is very suitable for the prediction of bed evolution. The baseline prediction for morphodynamic modelling well usually be that the initial bed remains unaltered. In other words, the initial bathymetry is used as the baseline prediction for final bathymetry. The BSS can be extremely sensitive to small morphological changes when the denominator is small compared to non-dimensional skill scores derived from proportionalities. The qualification of model performance is given in Table 4.3, where the ranges give a set of standards of models achievements.

Table 4.3: Qualification of error ranges of BSS parameter (after Van Rijn et al., 2003)

Qualification	**BSS**
Excellent	1.0-0.8
Good	0.8-0.6
Reasonable/Fair	0.6-0.3
Poor	0.3-0.0
Bad	Less than 0.0

The morphological analysis is mainly based on bathymetric data from the German Federal Maritime and Hydrographic Agency in Hamburg (BSH). It should be taken in account that the coverage of the bathymetric data varies strongly per year as well per space. A period of one month (August 1990), from the available bathymetric data, has been chosen to carry out the evaluation simulation for the Dithmarschen Bight morphodynamic model. For this period the bathymetric data are available before and after a storm at August 1990.

Fig.4.19 shows the available bathymetric data and the sub-domains, where the BSS factor is calculated. Fig.4.20 shows the wind speed at the center of the domain at August 1990. It is clear that the wind speed reached a speed of about 23 m/s within several days.

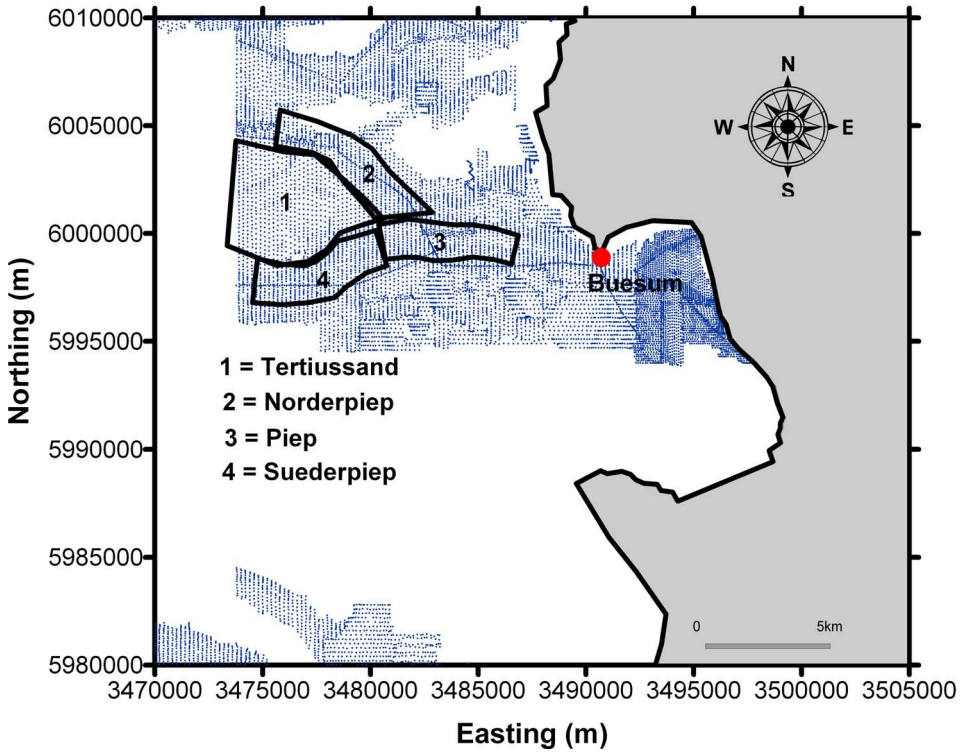

Figure 4.19: Available Bathymetric data before and after August 1990 storm

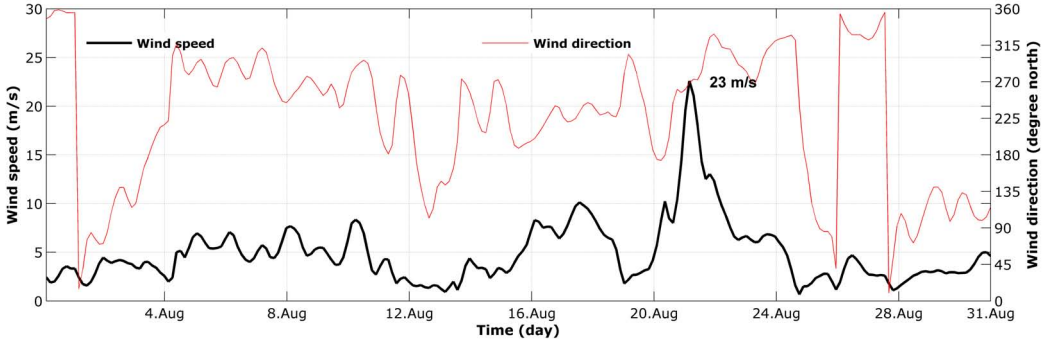

Figure 4.20: PRISMA wind speed and direction for Aug. 1990 at the center of DBM

The BSS factor has been calculated simply by applying equation4.1 at the four sub-domains for simulation results of one month (August 1990). Fig.4.21 shows the BSS values at Piep, Norderpiep. Suederpiep and Tertiussand sub-domains. It can be concluded that the model can simulate the morphodynamics at the Tertiussand sandbank and at the Suederpiep tidal channel very well (BSS values of 0.95 to 1.0). As for the other sub-domains the computed BSS at the Piep and Norderpiep are good considered (BSS values of 0.68 to 0.76).
Therefore the morphodynamic model of the Dithmarschen Bight region performs between Excellent and good in the area of interest.

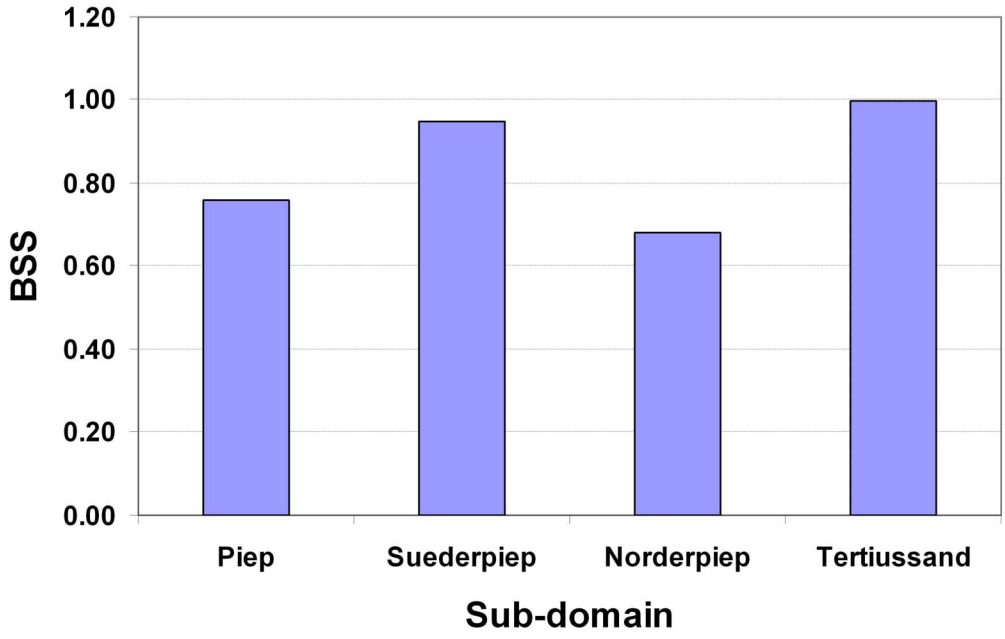

Figure 4.21: BSS values at sub-domains from one month simulation (August 1990)

Table 4.4: Dithmarschen Bight model parameter settings (Flow and Wave models)

Model	Parameter	Value	Description
Flow	Δt	60	Computational time step (s)
	ρ_w	1023	Water density (kg/m^3)
	g	9.813	Acceleration due to gravity(m/s^2)
	K	1	Horizontal eddy viscosity (m^2/s)
	White-Colebrook	map	Calculation of the Chezy coefficient (m)
	Threshold depth	0.1	Threshold depth for drying and flooding (m)
	ν	1	Horizontal eddy viscosity (m$^2/s$)
Wave			
	Directions	36	Number of bins in the directional space
	Frequency bins	24	Number of bins in frequency space
	Set-up	Not active	Wave-related water level set-up
	Forcing	Wave energy dissipation rate	Computation of wave forces
	Spectrum	JONSWAP	Shape of the wave spectrum
	Friction	JONSWAP	Type of bottom friction
	Friction Coefficient	0.067	The coefficient of the JONSWAP model(m^2/s3)
	Breaking	Battjes and Janssen (1978)	Energy dissipation due to depth-induced wave breaking
	Alpha	1.0	Coefficient for wave energy dissipation in the B&J model
	Gamma	0.73	Breaker parameter in the B&J model
	Wind	Active	Formulation for exponential wind growth
	White	Active	Formulation for whitecapping
	Quadruplets	Active	Quadruplet wave-wave interactions
	Refraction	Active	Refraction for wave propagation in spectral space
	Frequency	Active	Frequency shift for wave propagation in spectral space

Table 4.5: Dithmarschen Bight model parameter settings (Transport and Morphology models)

Model	**Parameter**	**Value**	**Description**
Transport			
	ρ_s(sand)	2650	Density of non-cohesive sediments (kg/m^3)
	ρ_d(sand)	1600	Dry density of non-cohesive sediments (kg/m^3)
	d_{50}	map	Median grain diameter sand (μm)
	ρ_s(mud)	1600	Density of cohesive sediments (kg/m^3)
	ρ_d(mud)	1600	Dry density of cohesive sediments (kg/m^3)
	w_s	1.6	Settling velocity for cohesive sediment (mm/s)
	$\tau_{cr,s}$	2.88	Critical bed shear stress for sedimentations (N/m^2)
	$\tau_{cr,e}$	0.89	Critical bed shear stress for erosion (N/m^2)
	Erosion	0.0001575	Sediment erosion rate for cohesive sediments (kg/m^2/s)
Morphology			
	f_{mor}	1 or 22	Morphological scale factor
	d_{min}	0.1	Minimum depth for sediment calculation (m)
	$h_{ref.}$	1	van Rijn's reference height factor (m)
	SEDTHR	0.05	Threshold sediment thickness (m)
	Ripple	2	Estimated ripple height multiplication factor

Chapter 5

Storm effects on short-term morphodynamics

5.1 Introduction

The effect of storm events on morphodynamics is still poorly understood due to a lack of suitable field data. Despite the fact that the driving forces can nowadays be measured and modelled fairly well, very little is known about the morphological developments resulting from the storm events. Besides the fact that bathymetric measurements are expensive, it is very difficult to obtain the necessary field data immediately before and after a storm event.

With the recent advancements in numerical models applied to coastal areas, however, simulations of wave-induced currents, sediment transport and bed elevation changes have been successfully carried out, thus offering an alternative means of improving our understanding of the underlying physical processes. These include the storms in January 1994 as well as the well-documented storm "Anatol" at the beginning of December 1999. Morphological changes during these storm events were analyzed with the consideration of the different driving forces.
In this chapter the state-of-the-art process-based model, that has been described in chapter 4, is applied to hindcast the morphological developments resulting from the previously mentioned storms in the study area on the German North Sea coast.

5.2 Selection of storms

In order to study the effects of storm events on the morphodynamics of the investigation area, two storm events were selected, namely, the storm of January 1994, and December 1999 (Anatol). These storms were selected due to their historical significance and the amount of destruction they caused on the German North Sea coast. Table 5.1 shows the main characteristics of the selected storm events.
In addition to that, simulation covering periods of about 12 months after the storms have been carried out to study the recovery of the system.

Table 5.1: Characteristics of the selected storm events

Storm event	**Max. wind speed**[1] **(m/s)**	**Tidal range**[2] **(m)**	**Storm surge**[2] **(m)**	**Sea state**[3]	**H_s remote from the coast**[2] **(m)**	**H_s close to the coast**[2] **(m)**
January 1994	22	3.2 Spring	4.6	High waves	4.8	1.05
December 1999	28	2.6 Neap	4.4	Very high waves	5.0	1.14

The wind data were obtained using the PRISMA interpolation model (Luthardt, 1987), described in Section 3.3. Hydrodynamic data were obtained by means of the nesting sequence described in Section 4.6.1. These storms were typical low-pressure areas moving from west to east across the central North Sea, causing strong onshore winds combined with a strong surge. Wind speeds during the selected storms ranged between 22 and 28 m/s (9 and 10 Beaufort scale). The wind directions were mainly westerly during the 1994 and 1999 storm events. Higher wind speeds and waves occurred during the storm Anatol in 1999.

5.2.1 December 1999 storm (Anatol)

The Anatol storm has been fully documented by the German weather service (DWD). The reports from the DWD (2000) showed that the Anatol storm has been classified as a hurricane with wind speed of more than 118 km/h. Moreover it was the most robust hurricane in the 90's. Wind speeds of up to about 184 km/h were recorded at the station List/Sylt (north-east of the German Bight).
A comparison of maximum annual averaged wind speeds observed during the main storms indicates that this storm was not just one of the strongest storms in the 90's, but since 1950 (see Fig. 5.2). The effects of the Anatol storm was not limited to on-shore but extended to off-shore areas. The records at the North Sea platform station, south-west North Sea (55.50^o N, 5.00^o E) showed wind speeds of about 180 km/h (see Fig. 5.3).

A defining characteristic of the Anatol storm (Hurricane), is that the German North Sea exhibits a very low pressure compared to other locations along the storm path (see Fig. 5.1). In northern Ireland, the pressure was recorded at about 985 hPa and then decreased dramatically by about 30 hPa in only 12 hours.

[1]Wind data from PRISMA data set
[2]Model results
[3]According to DWD (German Weather Service), Germany

Fig. 5.4 shows the wind velocity distribution during the Anatol storm over the North Sea. It can be seen that the wind velocities in the southeastern North Sea started to increase after December 3^{rd}, 09:00 UTC, and the wind direction gradually shifted from West-Southwest to West. But on December 4^{th}, 03:00 UTC, the low pressure area has passed and the wind attained moderate conditions.

One importantly peculiar characteristic of the Anatol storm was the abrupt increase and build up of the wind speed. It is noticeable from Fig. 5.5 that the wind speed reached 28 m/s in few hours during neap tide. Therefore, this storm combined both sudden increase in the wind speed and low water level.

The modelled water levels reach about 3m (above MSL) near to the coastline (Piep-Buesum location) and between 3 and 3.5m further out to sea (Tertiussand location). The average modelled storm surge reached 4.4m and the tidal range was about 2.6m considering to neap tide (see Fig. C.5 and Fig. C.6 in Appendix C).

On one hand, the modelled significant wave heights remote from and near to the coastline showed values of about 5m and 1.1m, respectively (see Fig. C.13 and Fig. C.14 in Appendix C). On the other hand, the modelled current velocities (see Fig. C.9 and Fig. C.10 in Appendix C) showed also high velocities remote from the coastline (about 1 m/s) and lower current velocities close to coastline (about 0.8 m/s).

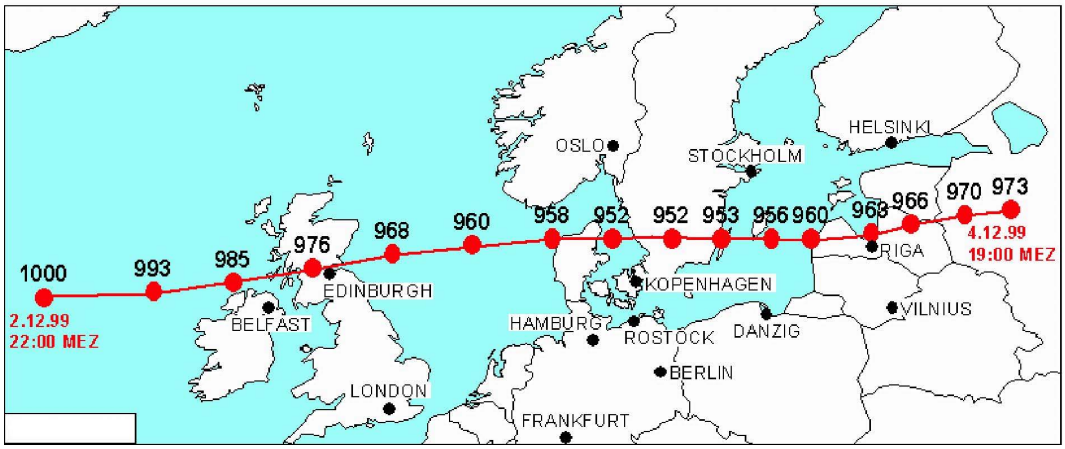

Figure 5.1: The path and air pressure (hPa) of Anatol storm in 3-h intervals (DWD,2000)

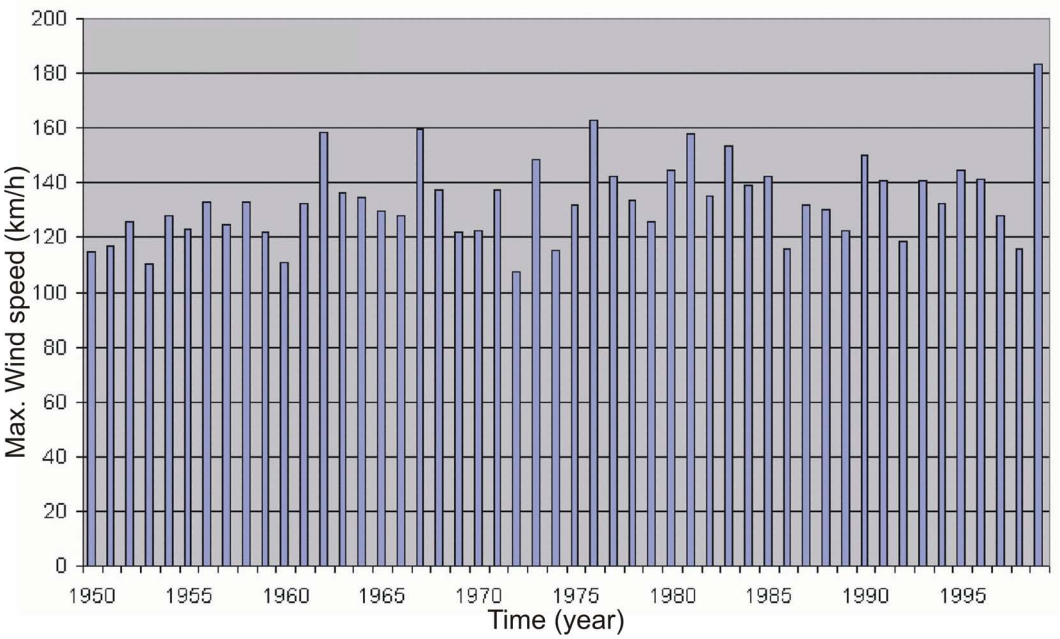

Figure 5.2: Annual maximum measured wind speed at List/Sylt station (DWD, 2000)

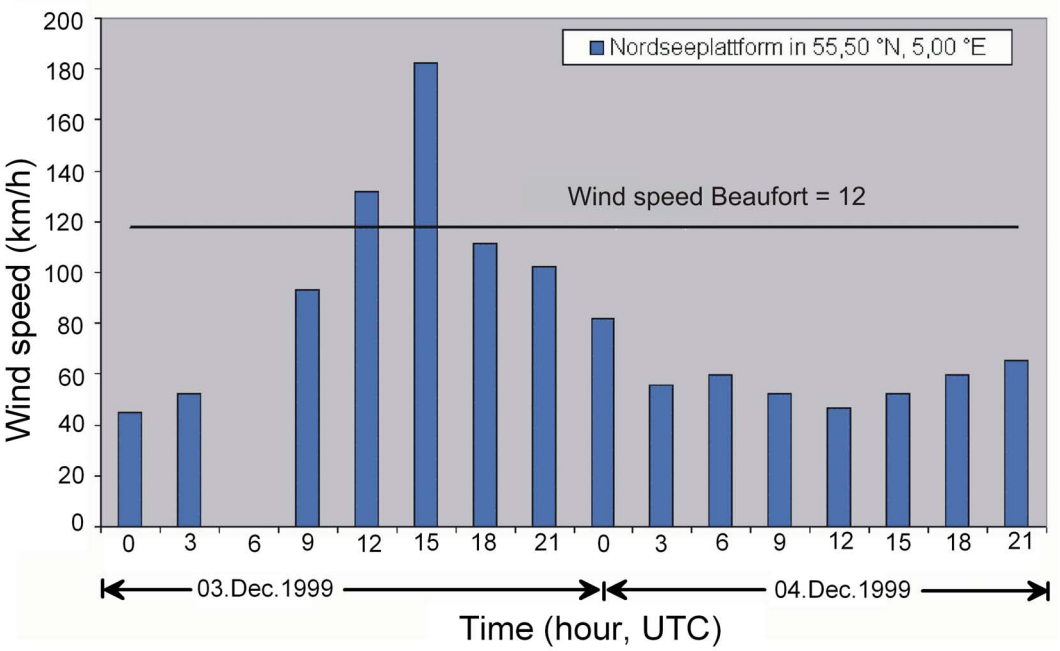

Figure 5.3: Mean wind speed at the North Sea platform station (adapted after DWD, 2000)

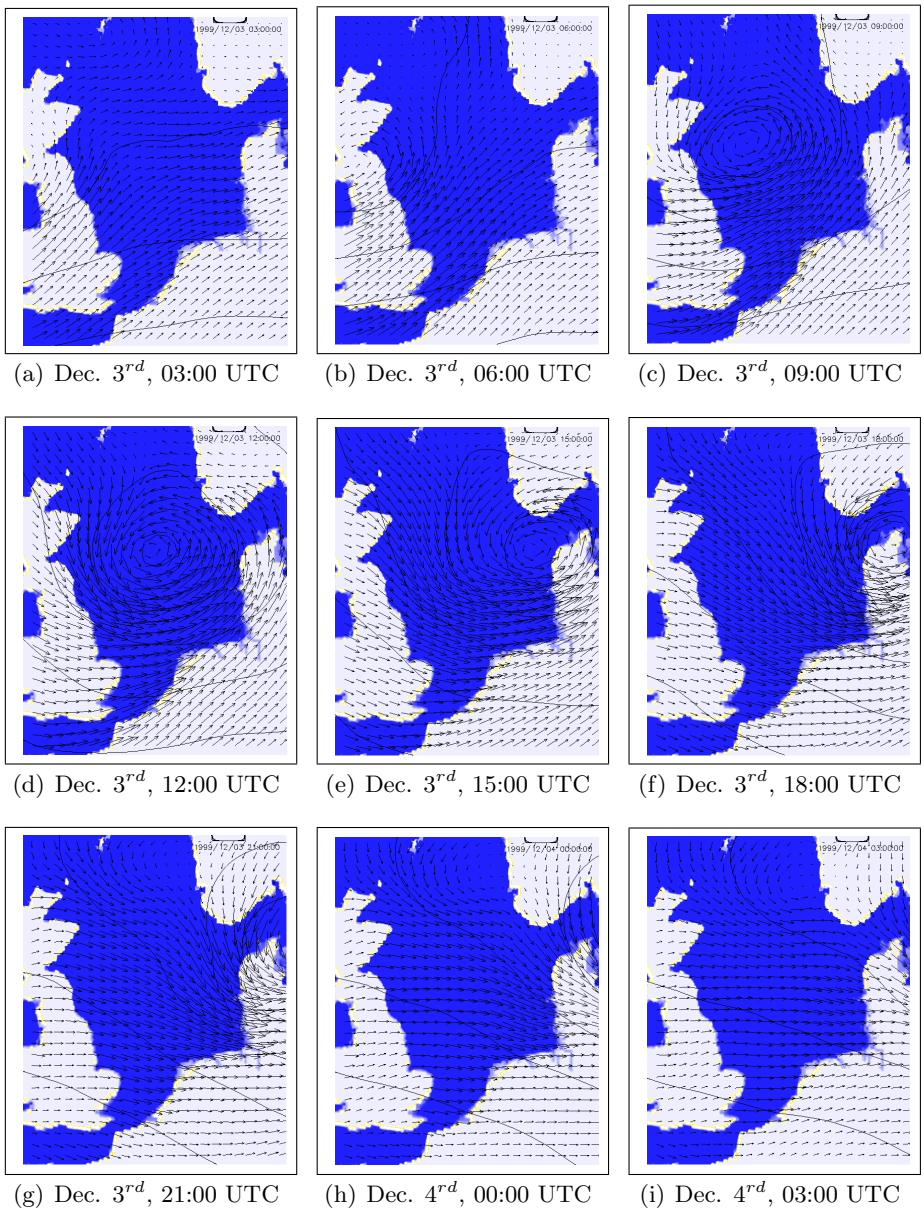

(a) Dec. 3^{rd}, 03:00 UTC (b) Dec. 3^{rd}, 06:00 UTC (c) Dec. 3^{rd}, 09:00 UTC

(d) Dec. 3^{rd}, 12:00 UTC (e) Dec. 3^{rd}, 15:00 UTC (f) Dec. 3^{rd}, 18:00 UTC

(g) Dec. 3^{rd}, 21:00 UTC (h) Dec. 4^{rd}, 00:00 UTC (i) Dec. 4^{rd}, 03:00 UTC

Figure 5.4: Wind velocity distribution during the 1999 storm over the North Sea including isobars, based on PRISMA data (after Wilkens, 2004)

5.2.2 January 1994 Storm

The storm of January 1994 has different characteristics in comparison with the Anatol storm. One important difference was the gradual increase of wind speed to reach a speed of about 22 m/s within several days during spring tide (see Fig. 5.6). Fig. 5.7 shows the wind velocity distribution during 1994 storm over the North Sea. It can be seen that the wind velocities in the west to the southeast North Sea start to increase after January 27^{th}, 00:00 UTC, and the wind moves from Northwest then West to Southwest. On January 29^{th}, 03:00 UTC, the low presure area has passed and the wind reduces to moderate conditions. In comparison with the Anatol storm, the 1994 storm took place even a much longer period of time (approximately 48 hours).
The modelled water levels showed an average storm surge in the order of 4.6m and a tidal range of 3.2m, which indicate that the storm occurred during spring tide (see Fig. C.3 and Fig. C.4 in Appendix C).
Similar to the Anatol storm, the significant wave heights reached about 4.8m remote from the coastline and about 1.1m near the coastline. However, for the 1994 storm, several peaks (about 3m) took place before and after the storm itself (see Fig. C.11 and Fig. C.11 in Appendix C).
With regard to the means of the magnitude of the current velocities of Anatol's storm the modelled current velocities for the 1994 storm showed similarity to the Anatol's storm (see Fig. C.7 and Fig. C.8 in Appendix C).

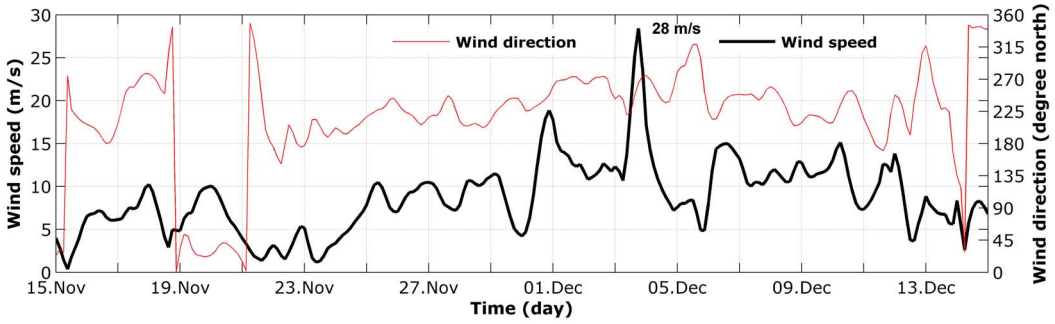

Figure 5.5: PRISMA wind speed and direction for 1999 Storm

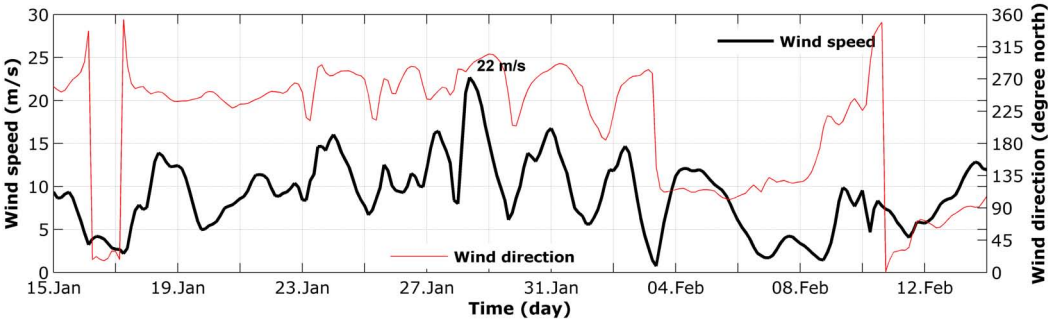

Figure 5.6: PRISMA wind speed and direction for the 1994 Storm

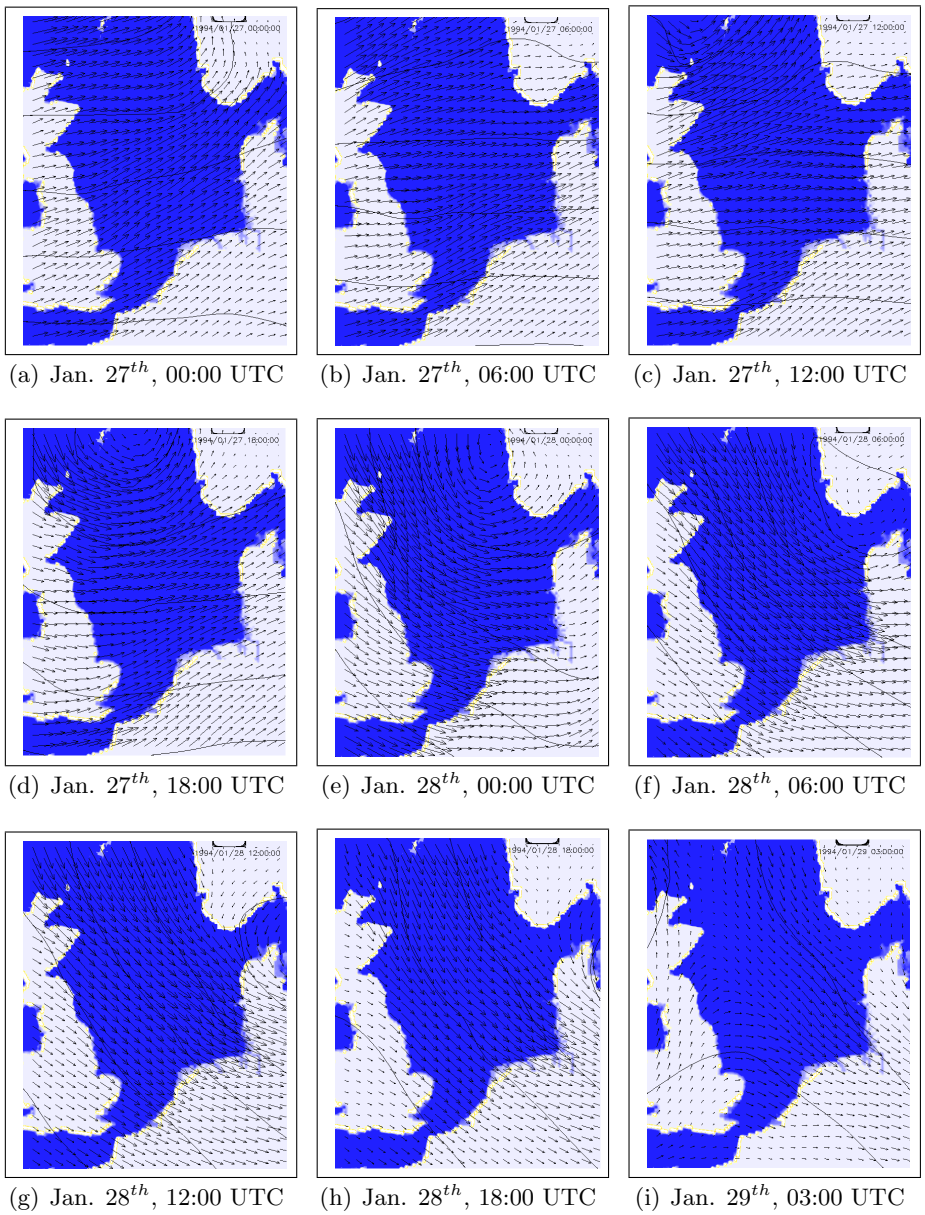

(a) Jan. 27^{th}, 00:00 UTC (b) Jan. 27^{th}, 06:00 UTC (c) Jan. 27^{th}, 12:00 UTC

(d) Jan. 27^{th}, 18:00 UTC (e) Jan. 28^{th}, 00:00 UTC (f) Jan. 28^{th}, 06:00 UTC

(g) Jan. 28^{th}, 12:00 UTC (h) Jan. 28^{th}, 18:00 UTC (i) Jan. 29^{th}, 03:00 UTC

Figure 5.7: Wind velocity distribution during the 1994 Storm over the North Sea including isobars, based on PRISMA data

5.3 Significance of the storm events on the morphodynamics

Morphodynamic model simulations covering the selected storm periods were carried out using forced water levels, waves and winds. The morphodynamic model, described in the Section 4.6.1, has been used. The wind conditions over the entire North Sea were determined using the synoptic PRISMA Model (Luthadt, 1987), described in Section 3.3. The open-sea boundaries for the flow and wave models were

determined according to a nesting sequence covering the entire North Sea (Section 4.6.1).

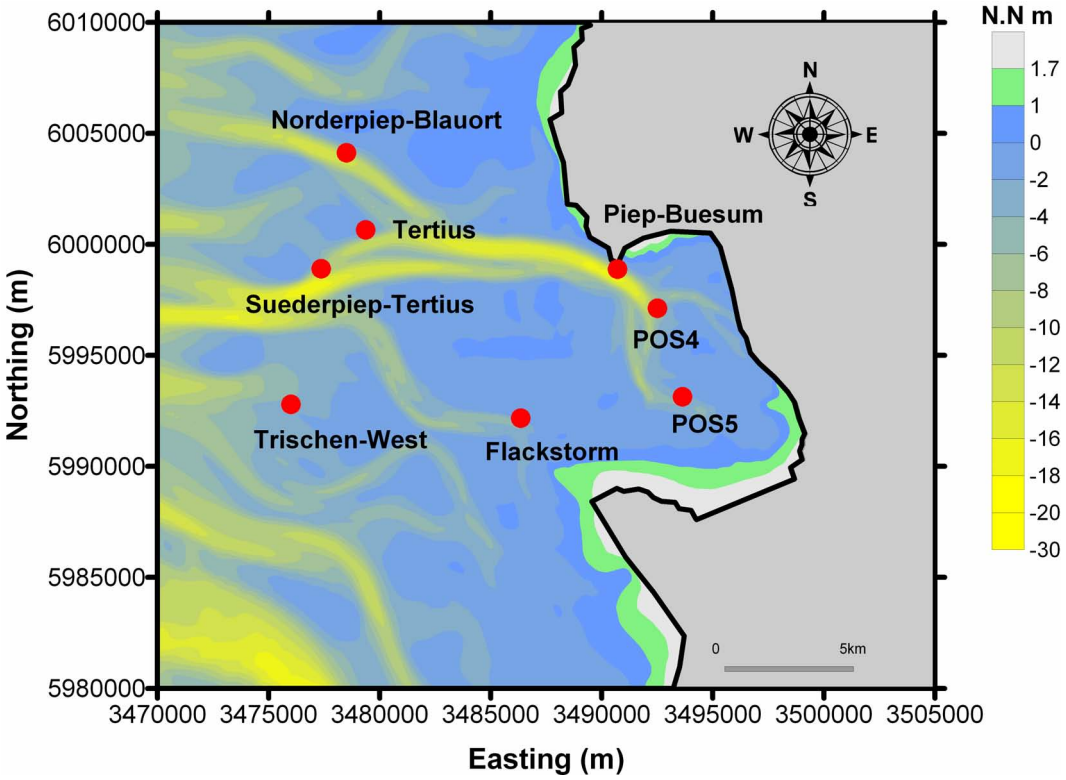

Figure 5.8: Location of the observation points (1990 bathymetry)

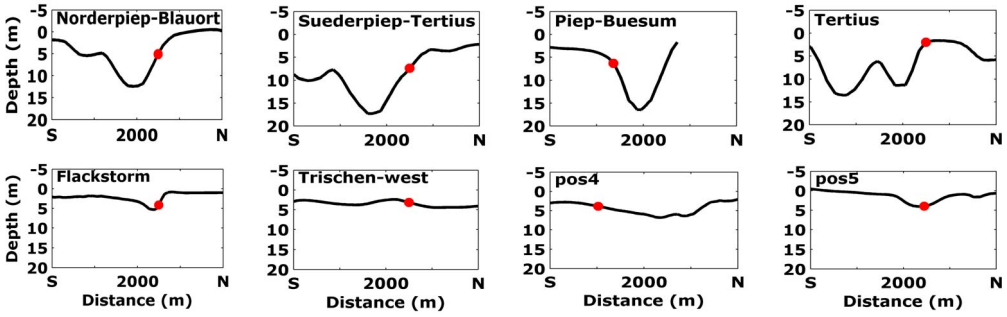

Figure 5.9: Cross-sections including the location of the observation points

To avoid initialization effects, sufficient warming up time was given to the hydrodynamics and morphodynamics. The simulations commenced a few days before the storms and covered a period of 30 days. In order to permit direct comparisons between the results, the same bathymetry (1990) was used initially (see Fig. 5.8 and 5.9).

To study the effect of the tide alone on the morphological changes, an additional simulation has been carried out for the selected storms. In this case swell and wind forcing were excluded from the boundary conditions in the morphodynamic simulation.
The temporal variation of water levels, current velocities, wave heights and shear stresses during the storms are shown at eight different locations (Appendix C) as illustrated in Fig. 5.8 and 5.9 (exposed sandbank, tidal channels and tidal flats).

The resulting morphological changes were evaluated according to changes in the wet volume below a reference level integrated over four large areas (listed 1 to 4 in Fig. 5.10). These areas consist of an exposed sandbank (Tertiussand), two tidal channels (Norderpiep and Suederpiep) in the central part of the domain, and a third tidal channel (Piep) in the relatively sheltered part of the domain. The bathymetric data for the year 1990 used at the beginning of the simulations was taken as the reference bathymetry in this analysis as follows:

$$V_{rel,i} = \frac{V_i}{V_{1990}} \times 100\% \tag{5.1}$$

where:
$V_{rel,i}$ = Relative wet volume below MSL of the sub-domain in year i.
V_{1990} = Wet volume below MSL of the sub-domain in 1990.
V_i = Wet volume below MSL of the sub-domain in year i.

Comparisons of the modelled volumetric changes over the four areas for the two storm events over the simulation period are shown in Fig. 5.11 and Fig. 5.12.

It is clear that the effect of the tide only (Astronomical tide) is very limited on the volumetric changes in the wet volume, for the period of the simulation, for both of the storms. On the other hand, the results indicate that erosion of the sandbanks was accompanied by deposition in the tidal channels for the storm simulations. It is evident from Fig. 5.11 and Fig. 5.12, that the least and the most significant morphological changes occurred during the storms of January 1994 and December 1999, respectively. This is probably due to the gradual increase in wind speed and higher water levels during the January 1994 event in contrast to the sudden increase in the wind speed combined with low water levels in December 1999.

The bed elevation changes during the January 1994 storm lie about midway between those resulting from the other event. Although this storm, which occurred during a spring tide, is also characterised by sudden changes in wind speed, the maximum wind speeds are lower than during the storm Anatol in December 1999.

Fig. 5.13 and 5.14 show the bed level changes at the end of the simulations in 1999 and 1994, respectively. Moreover, Fig. 5.15 shows the bed elevations differences between 1994 and 1999 storms at the end of the simulations. It can be noted that the storm 1999 showed about 20cm more erosion on the sandbanks and the

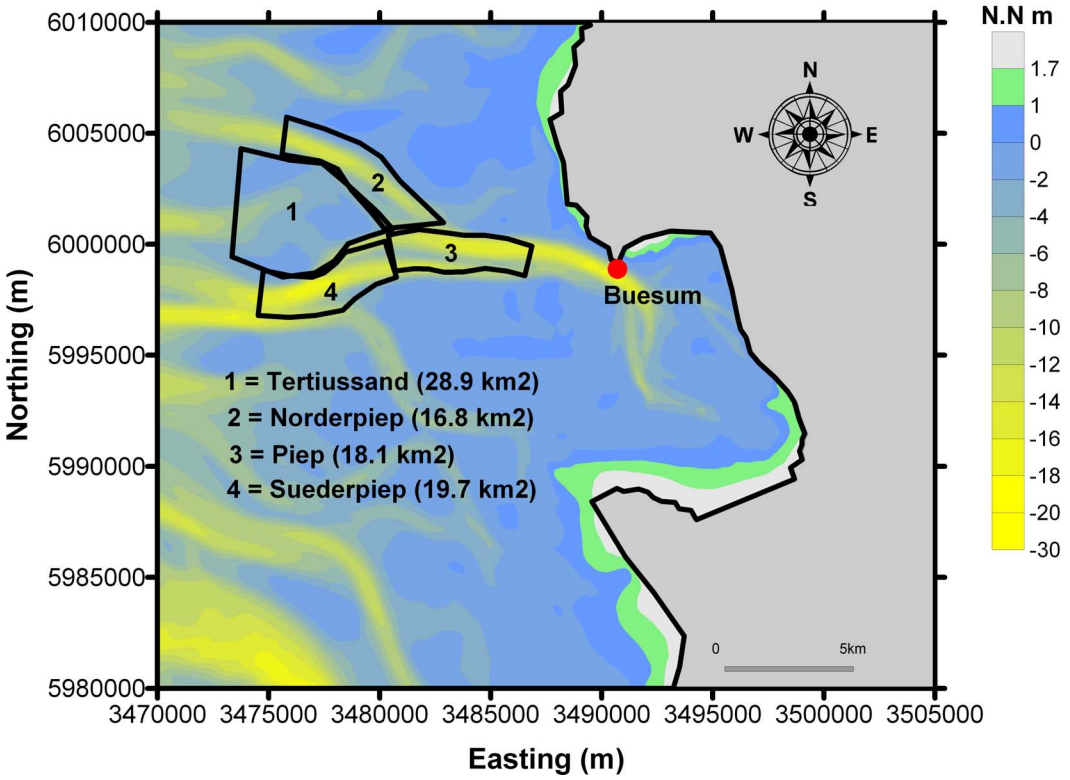

Figure 5.10: Location of the sub-domains (1990 bathymetry)

tidal flats, and about 10cm more depositions in the tidal channels compared to 1994 storm, especially in the Suederpiep tidal channel.

The spatial variations of bed elevation changes due to the storms are shown in Fig. C.23 to Fig. C.30 in Appendix C. It is obvious that erosion takes place primarily in the most exposed areas along the sandbanks and tidal flats predominantly in the outer region accompanied by material deposition in the tidal channels. The changes in bed elevation were found to be of the order of a few decimeters for both simulations.

It is remarkable to see high movements in the sea topography during both storms. Therefore it can be concluded that the main changes took place at the peak of the storms.
This is also confirmed by looking into the spatial variation of the bed shear stress for both of the storms. It can be seen from Fig. 5.16 and 5.17 that the maximum shear stress as well as the suspended sediment concentration are observed close to peak of the storm events (see Fig. 5.18 and 5.19).

It can be noted that close to the coast line, where the tide is most dominant, the bed shear stresses do not change much. On the other hand, in the most exposed areas, where waves are most dominant, the bed shear stresses reach their maximum at the peak of the storms (see Fig. C.15 to C.17 in Appendix C).

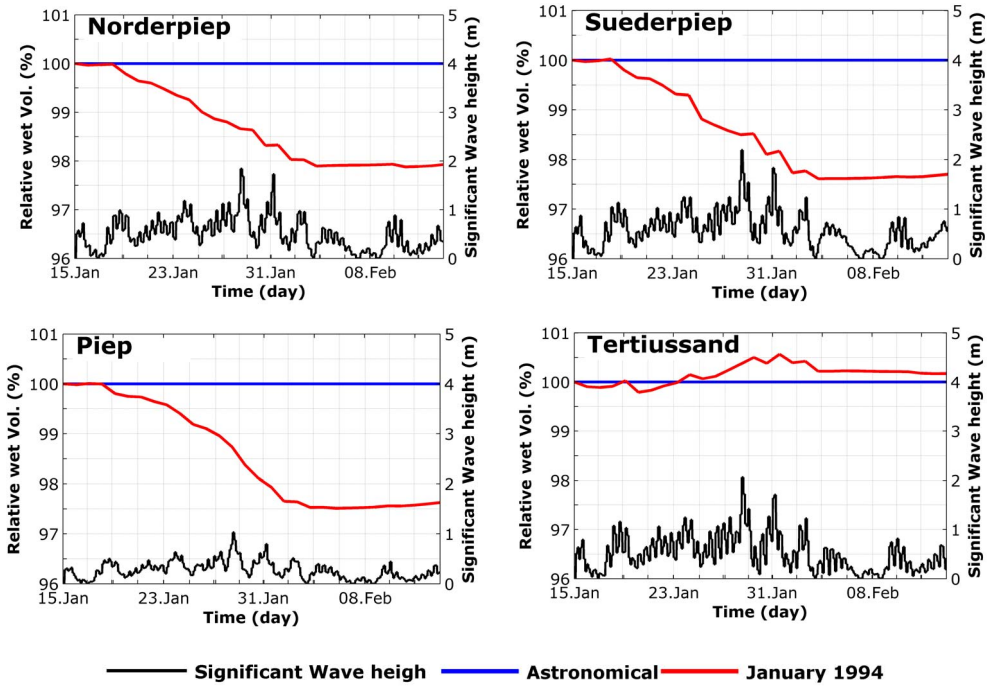

Figure 5.11: Relative wet volumes referred to at the beginning of the storm event (January 1994)

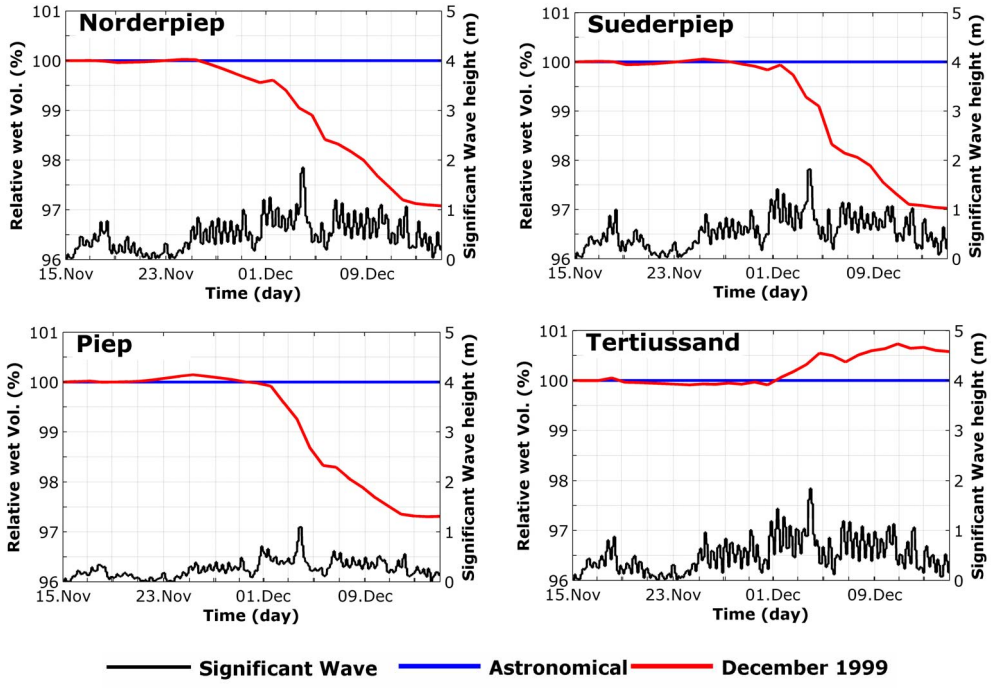

Figure 5.12: Relative wet volumes referred to at the beginning of the storm event (December 1999)

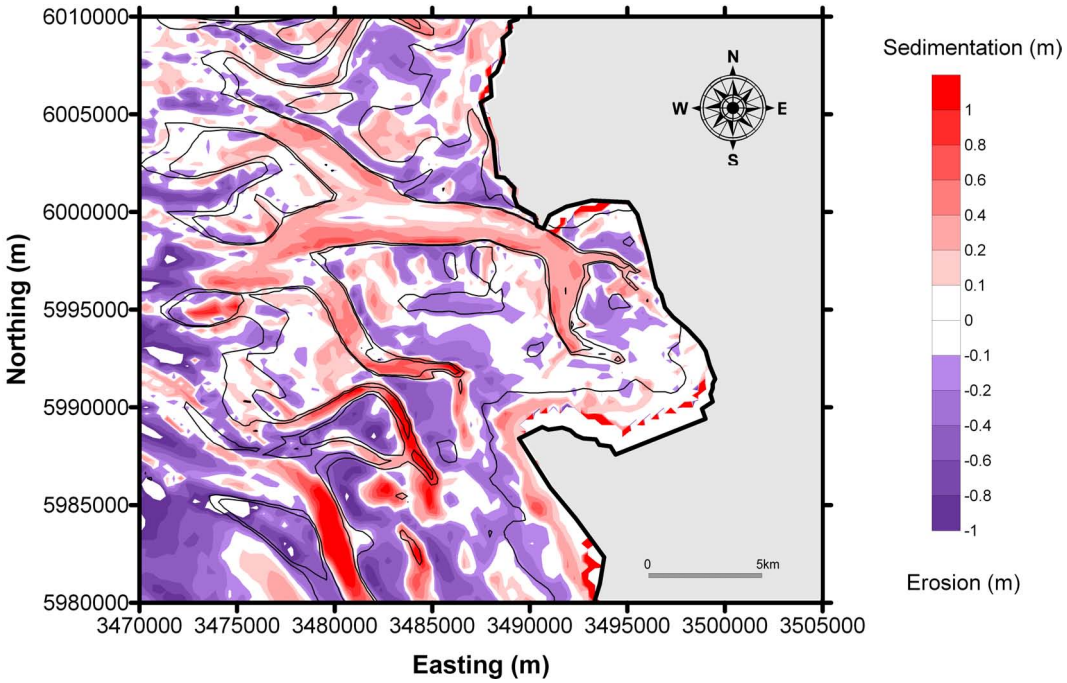

Figure 5.13: Bed level changes resulting at the end of the simulation 1994 Storm (14.Feb)

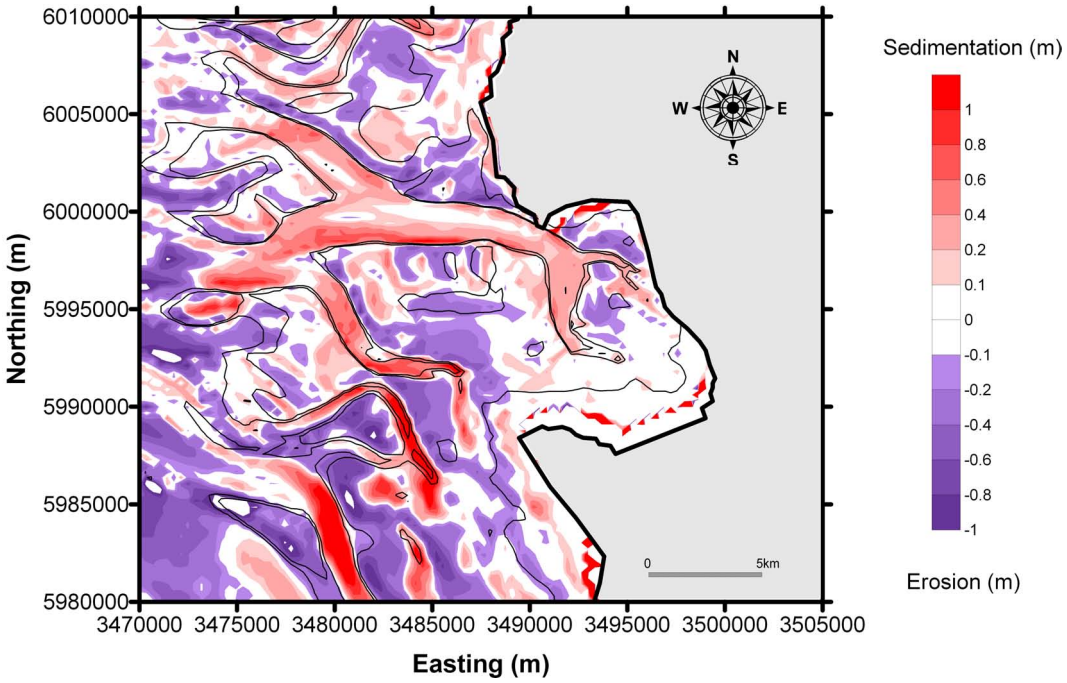

Figure 5.14: Bed level changes resulting at the end of the simulation 1999 Storm (15.Dec)

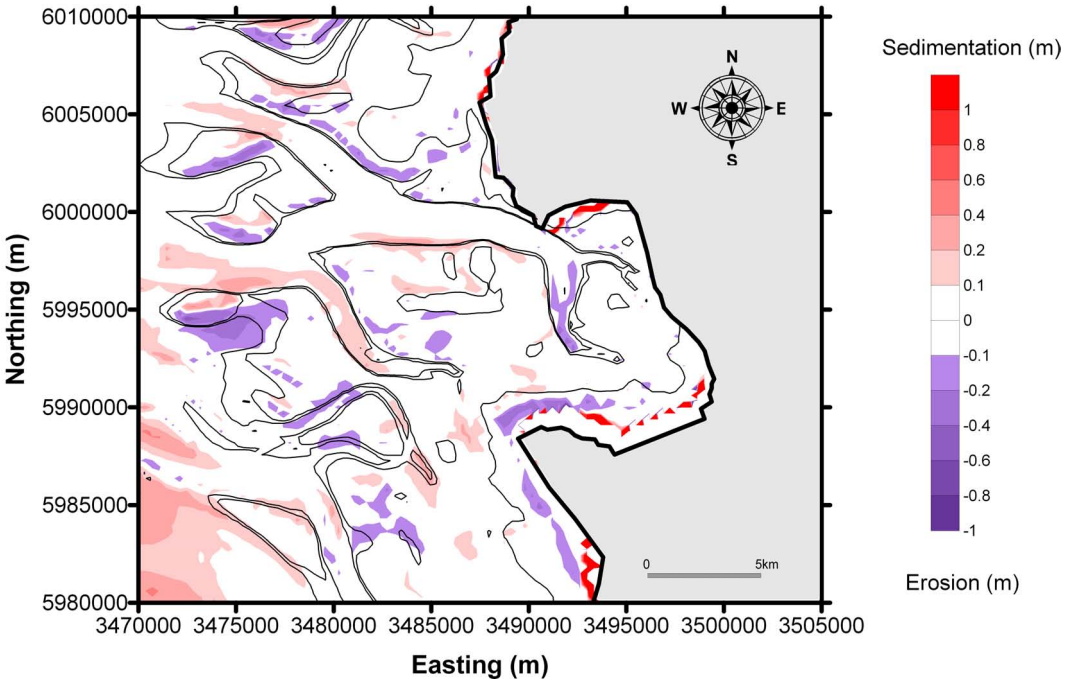

Figure 5.15: Bed level differences between 1994 and 1999 Storms

Fig. C.19 to C.21 (Appendix C) show comparisons of the variation in bed elevation at eight locations (see Fig. 5.8 and 5.9). It can be seen that the bed elevation changes during periods in which the tide is the only driving force (no wind, wave or so-called astronomical conditions) are up to few centimeters. On the other hand during the storm periods these changes may be up to about a meter in the more exposed sandbanks and tidal flats. Noteworthy, is the clear response of the model to the sudden changes in wind, water levels and waves. This is also can be seen from the bed shear stress results.

As it is described in Section 3.6.2, the seasonal (short-term) morphological changes in the Norderpiep tidal channel has a tendency for deposition. This is also valid from the storm events January 1994 and December 1999. It is clear from Fig. 5.20 that the deposition took place during both storms and it reached about 1m depth. The short-term measurement does not show clear evolution of the Suederpiep tidal channel (Section 3.6.2). It showed only that the morphological changes are in the range of 1 to 2m depth. The model results (Fig. 5.21) show also the same morphological changes in the order of 1 m with sedimentation tendency.

The same conclusion has been made for the Piep tidal channel from the short-term measurement analysis and the model results. From Fig. 5.22, it can be concluded that the Piep channel has a sedimentation pattern in the winter with a morphological changes in the order of 0.5 m (relatively stable).

For the Tertiussand sandbank, the model results showed that the erosion took place at the sandbank and accompanied with a pattern of morphological evolution in the landward direction (Fig. 5.23).

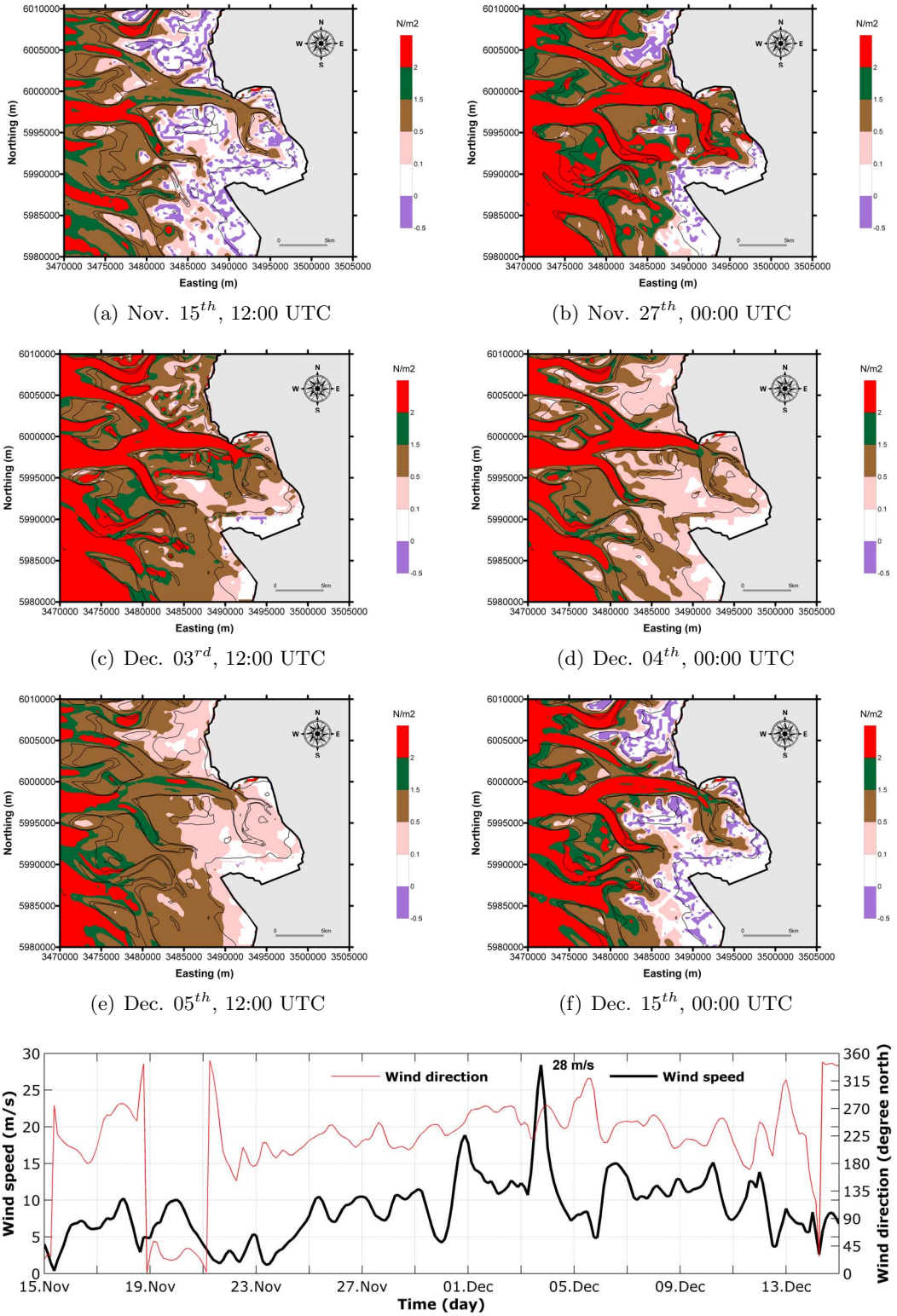

(a) Nov. 15^{th}, 12:00 UTC

(b) Nov. 27^{th}, 00:00 UTC

(c) Dec. 03^{rd}, 12:00 UTC

(d) Dec. 04^{th}, 00:00 UTC

(e) Dec. 05^{th}, 12:00 UTC

(f) Dec. 15^{th}, 00:00 UTC

(g) Wind speed

Figure 5.16: Bed shear stress resulting from the 1999 Storm

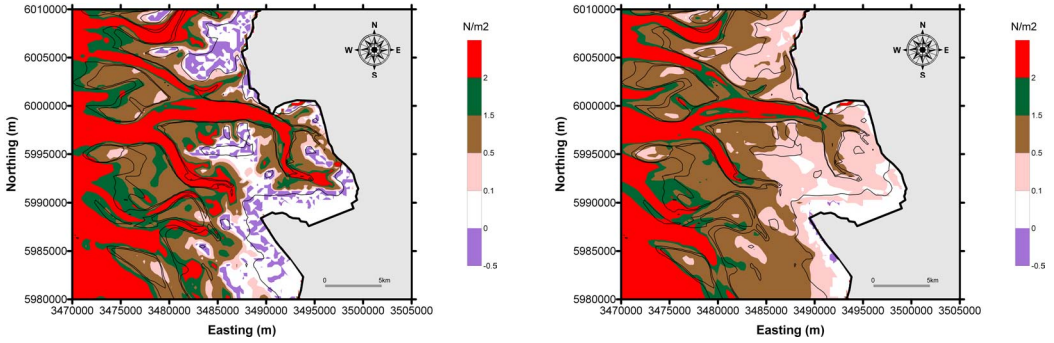

(a) Jan. 15^{th}, 12:00 UTC

(b) Jan. 25^{th}, 00:00 UTC

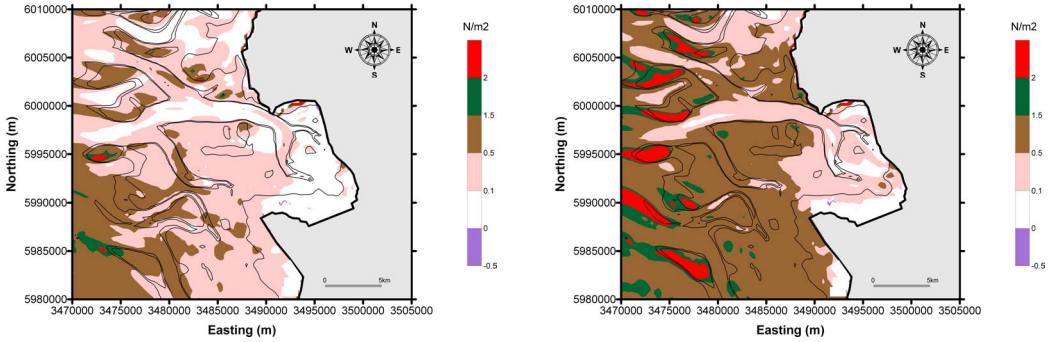

(c) Jan. 27^{th}, 12:00 UTC

(d) Jan. 28^{th}, 12:00 UTC

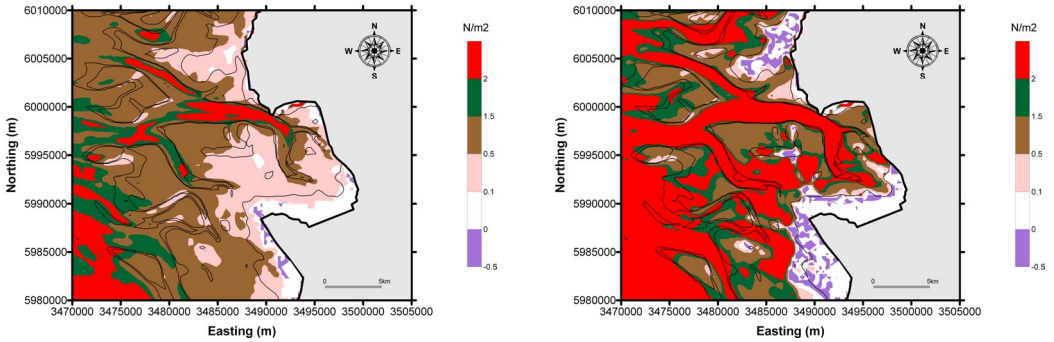

(e) Jan. 29^{th}, 12:00 UTC

(f) Feb. 14^{th}, 00:00 UTC

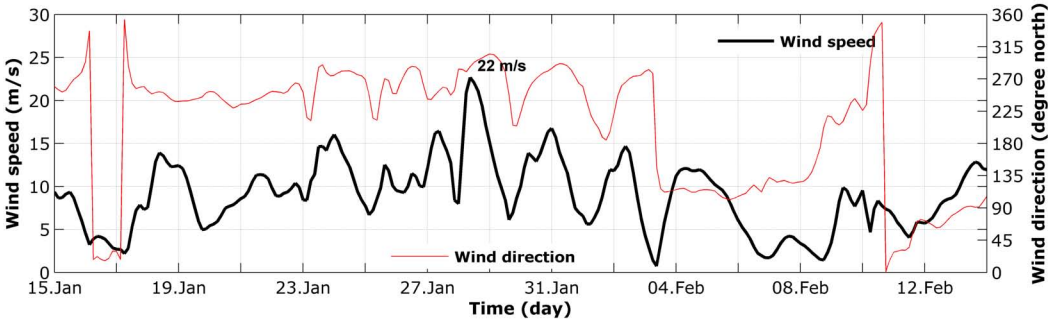

(g) Wind speed

Figure 5.17: Bed shear stress resulting from the 1994 Storm

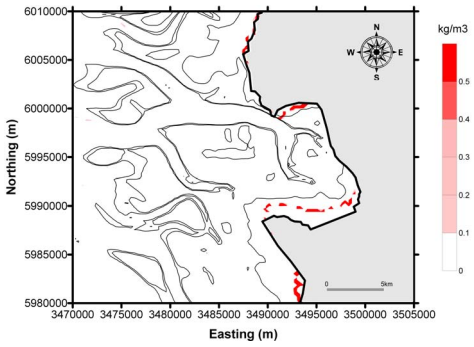

(a) Nov. 15^{th}, 12:00 UTC

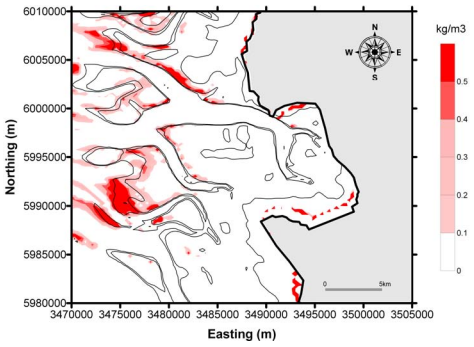

(b) Nov. 27^{th}, 00:00 UTC

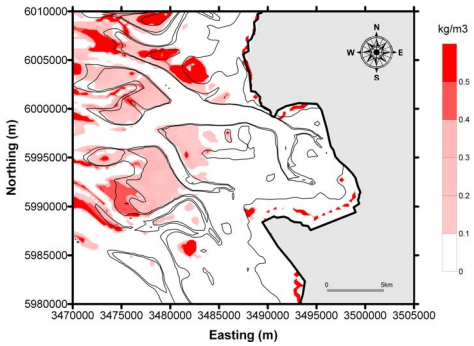

(c) Dec. 03^{rd}, 12:00 UTC

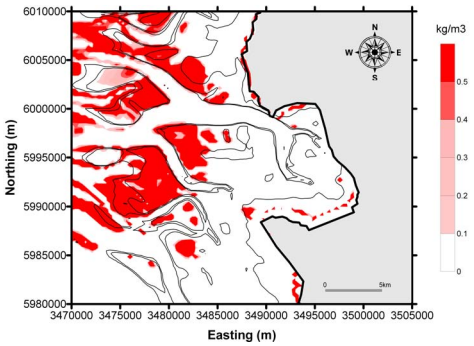

(d) Dec. 04^{th}, 00:00 UTC

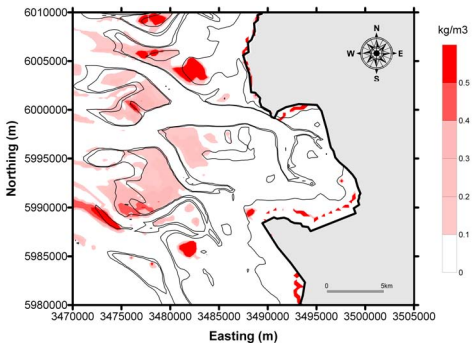

(e) Dec. 05^{th}, 12:00 UTC

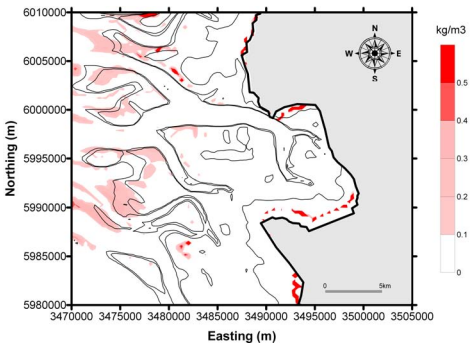

(f) Dec. 15^{th}, 00:00 UTC

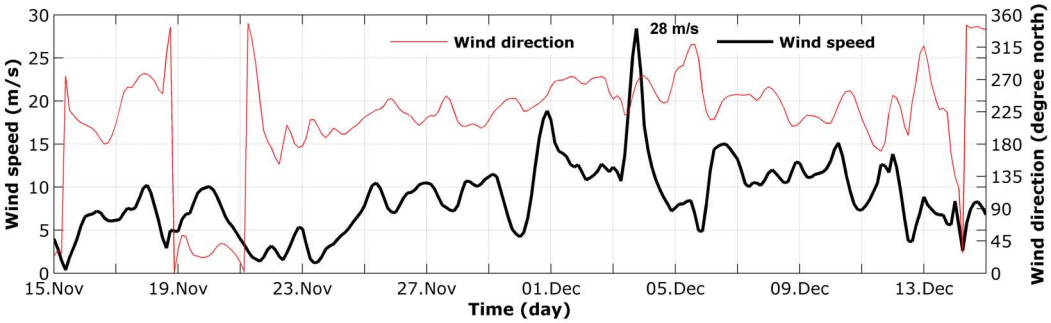

(g) Wind speed

Figure 5.18: Depth-averaged suspended sediment concentration resulting from the 1999 Storm

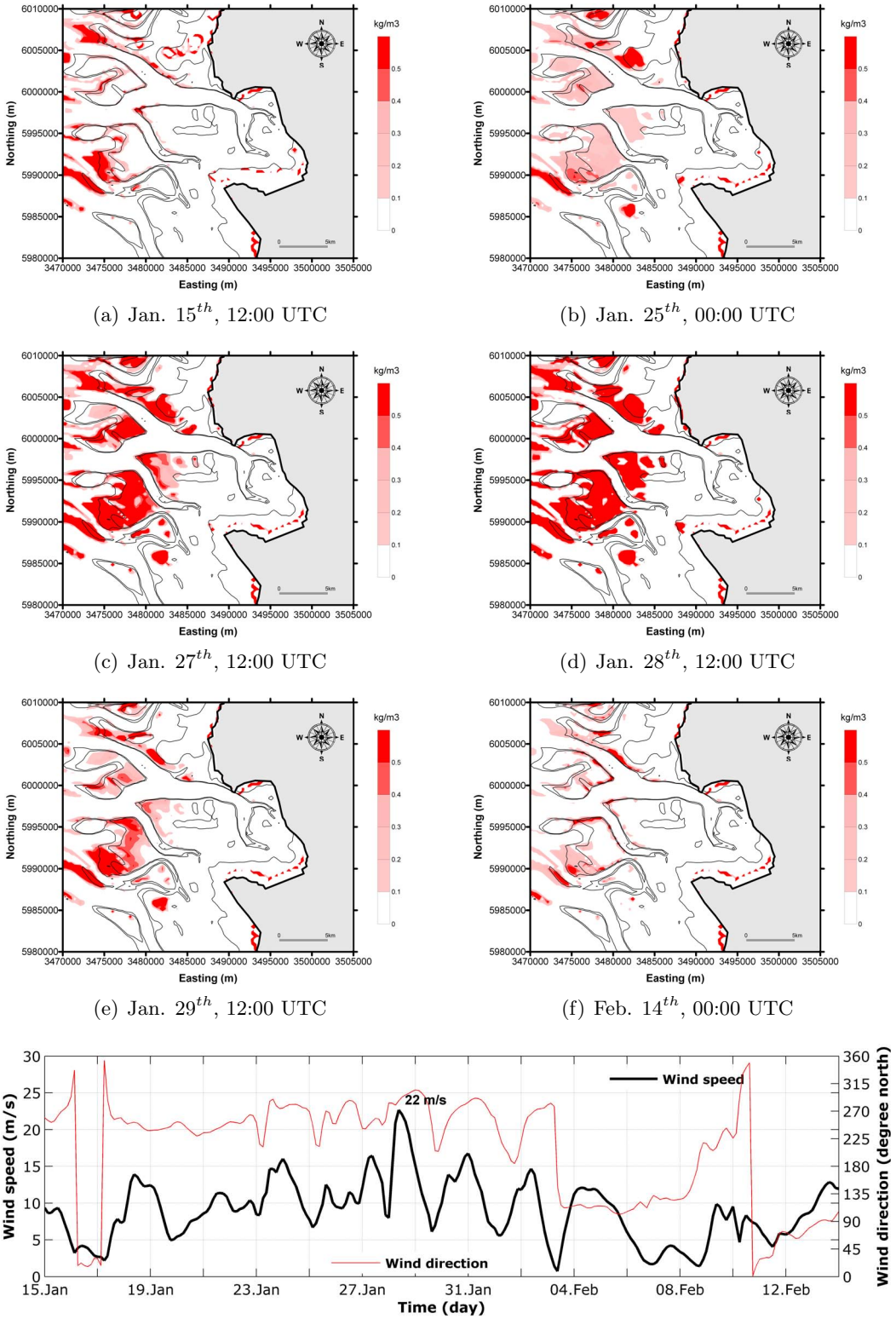

(a) Jan. 15^{th}, 12:00 UTC

(b) Jan. 25^{th}, 00:00 UTC

(c) Jan. 27^{th}, 12:00 UTC

(d) Jan. 28^{th}, 12:00 UTC

(e) Jan. 29^{th}, 12:00 UTC

(f) Feb. 14^{th}, 00:00 UTC

(g) Wind speed

Figure 5.19: Depth-averaged suspended sediment concentration resulting from the 1994 Storm

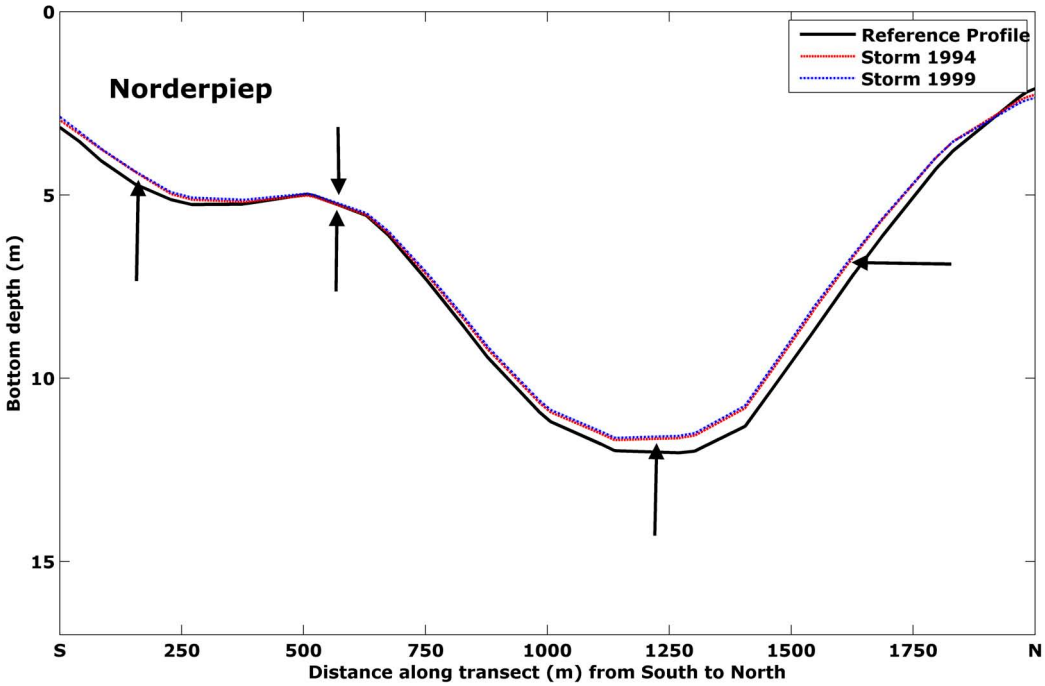

Figure 5.20: Modelled channel profile at cross-section in the Norderpiep

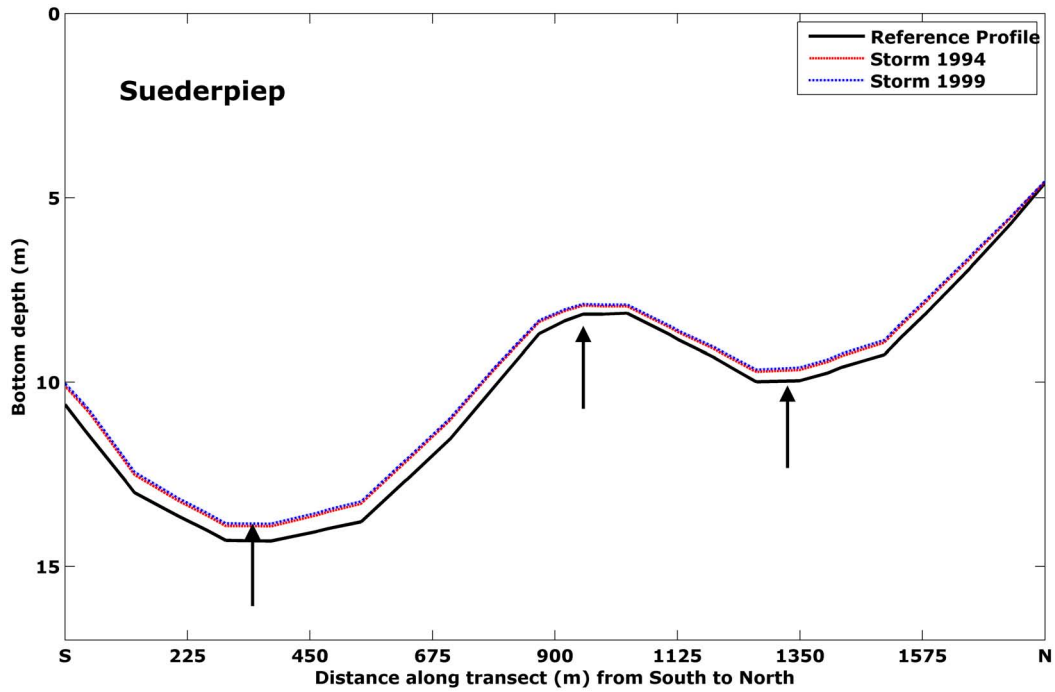

Figure 5.21: Modelled channel profile at cross-section in the Suederpiep

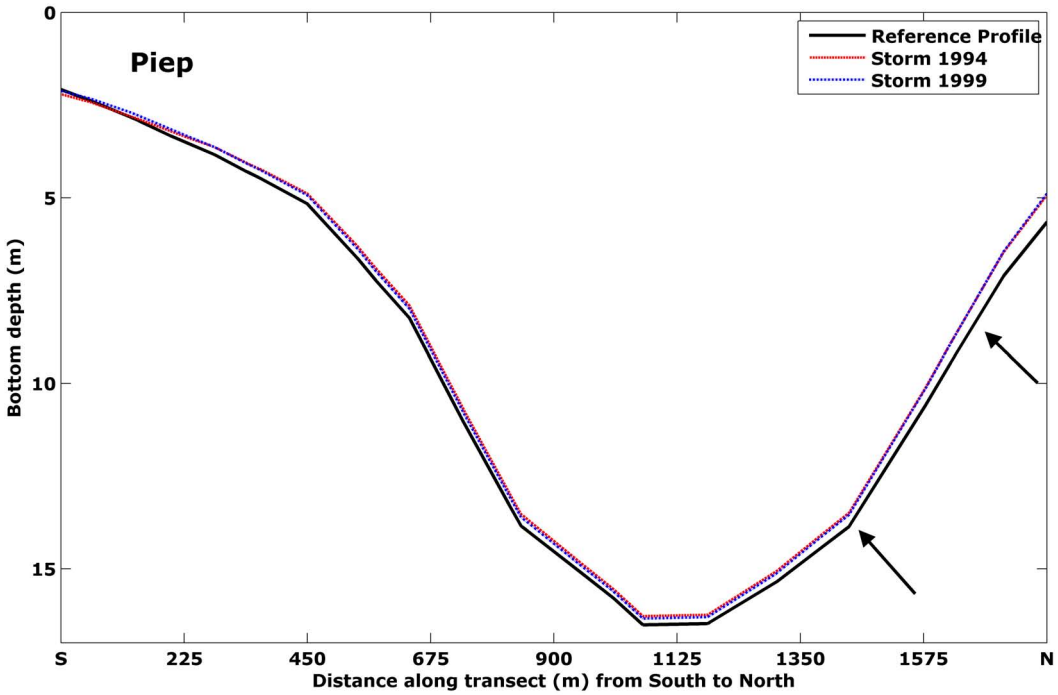

Figure 5.22: Modelled channel profile at cross-section in the Piep

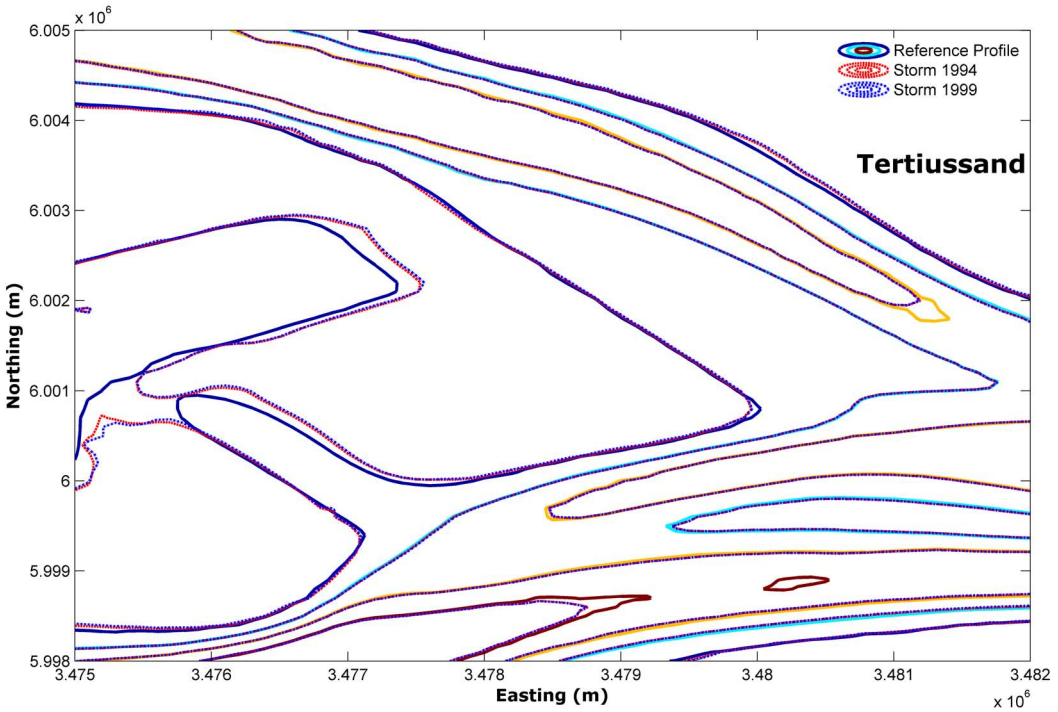

Figure 5.23: Modelled changes of 3 m depth contours near Tertiussand

5.4 Recovery of the bathymetry after the storms

From section5.3, it is evident how the effect of the storm events transform the morphology in the study area. Most important in this section is, how the system recovers after the storm events and their effects on the morphology.
Consequently, two simulations for a period of one year have been carried out to observe both, the transforming nature of severe storms and the post-storm recovery events that are relevant within the coastal area.

These simulations serve basically to understand what is expected to continue as what is defined as post-storm recovery. However, it should be considered that the recovery may be interrupted, and possibly delayed, due to the effects of future storm events that have an impact the coastal region.

The two simulations covered periods of one year each; between 15.Jan 1994 to 15.Jan 1995 and 15.Nov 1999 to 15.Nov 2000, respectively. The open-sea boundaries for the flow and the wave models were also determined according to the nesting sequence, as described in section 4.6.1, covering the entire North Sea.

As it can be seen from Fig.5.24, for both periods (1994-1995 and 1999-2000) two storm events with wind speed exceeding 20 m/s occurred during the simulation periods. Moreover, about 14 and 12 events for the first and the second periods are for wind speed between 20m/s and 15 m/s, respectively.

On one hand, the maximum wind speed for the period between 1994 and 1995 reaches a wind speed of about 22m/s in January 1994 and about 23m/s in January 1995 with a westerly wind direction. It is noticeable, for the same period, that wind speeds between April and July are about 10m/s wind speed with northerly wind direction.

On the other hand, the maximum wind speed for the period between 1999 and 2000 were about 28m/s at the beginning of December 1999 (Anatol storm) and 21m/s at the end of December 1999 with also a westerly wind direction. It is also clear that between March and April 2000 and between June and September 2000 the wind speed was about 10m/s with northerly wind direction.

Comparisons in terms of the modelled volumetric changes using Eq.5.1 over the same four areas (illustrated in Fig.5.10) for the two periods over one year are shown in Fig.5.25. It is very clear that when the storm events are taken place the erosion and the sedimentation patterns can be seen in the tidal channels and on the sandbanks, respectively.

An interesting observation can be also noted when the wind speed is in the order of 20m/s or higher; the highest bed level changes take place for the simulation of the period between 1994 and 1995 as well as for the period between 1999 and 2000. Additionally, it was found that the recovery process started immediately after the storm event ended.

Evidence of post-storm recovery was detected from April to October 1994 for the period of 1994-1999 and from March to September 2000 for the period of 1999-2000, respectively. Moreover, the relatively high severity of storms exerts a cumulative effect on and can significantly alter the bed elevation from month-to month (for more details see Fig.5.26 and 5.27).
The greatest and most dramatic changes occur during the period of 1999-2000. In this period and during the stormy season (from November 1999 to February 2000) up to 10% changes in the wet volume have been observed. It was also observed that up to 4% has been recoverd after the stormy season.

Comparisons of the changes in the wet volumes during the period between 1994-1999 showed less than 4% changes during the stormy season (from January to March 1994 and during January 1995) and 2% has been recovered after the stormy season. In addition it has been also concluded that some summer storms could cause a possible delay of the recovery process. From the simulation results, it is also obvious that the period of one year is not enough to recover the effect of the storm events during the stormy season. For the two periods, 1994-1995 and 1999-2000, longer simulations require to justify the period to recover the storm events.

5.5 Discussion

The effect of storms on short-term morphodynamics has been investigated with the help of a calibrated and validated process-based morphodynamic model. Simulations were carried out with continual full coupled model. In this study the analysis focused on two severe events that took place in January 1994 and December 1999. In order to analyse the effect of the storms, simulations were also carried out for the tide only situation.

The results showed that the morphological changes due to the tide only are quite small. Therefore the influence of the tide on the morphological changes during simulation period is limited.
The morphological changes during the storm reached up to about 1m in the more exposed areas. The model is capable of capturing the erosion on the sandbanks and the deposition in the tidal channels.

Comparisons of the morphological effects due to the two storms events indicate that more significant changes took place during the storm of December 1999. This probably occurred due to the sudden increases in westerly wind speeds in conjunction with neap tidal conditions result in the highest erosive activity in the area (1999 storm), whereas gradual changes in wind speed combined with spring tides leads to lower morphological activity (1994 storm).

To investigate the recovery from a storm event, two simulations during the periods 1994-1995 and 1999-2000 have been carried out. The simulation results showed clearly recovery after the storm event. Moreover, the recovery from the storm events requires more than one year for the two investigated periods.

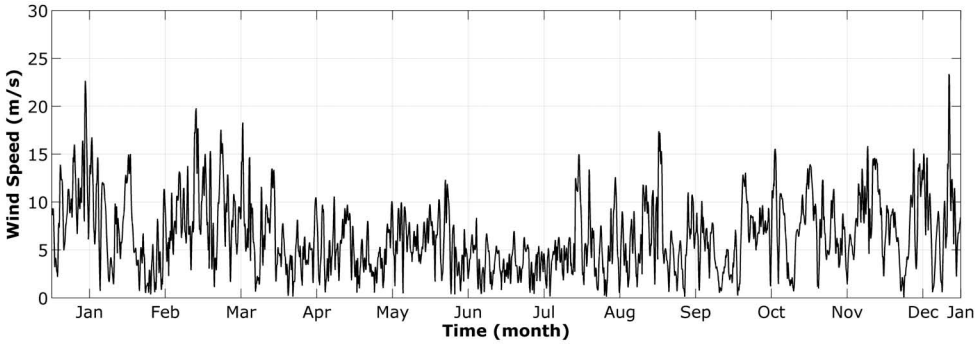

(a) PRISMA wind speed for 1994 Storm

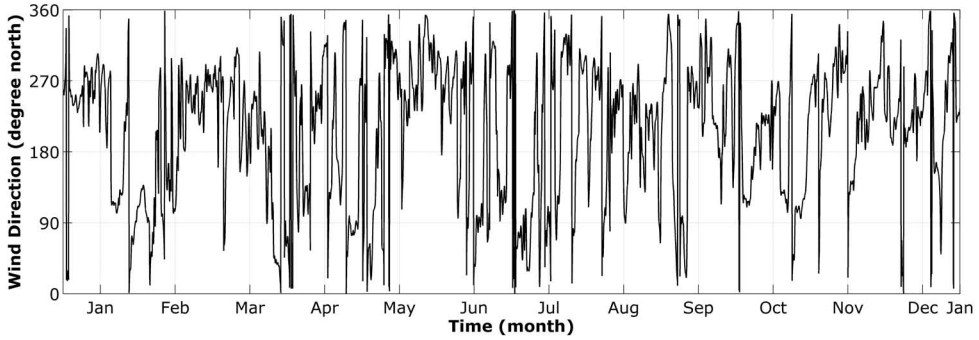

(b) PRISMA wind direction for 1994 Storm

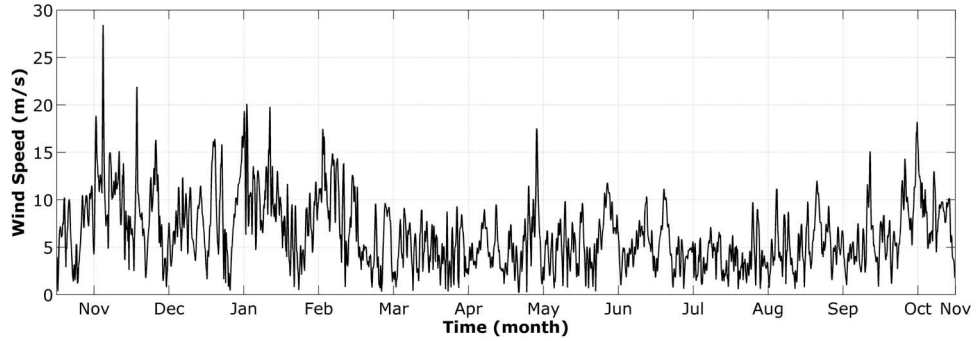

(c) PRISMA wind speed for 1999 Storm

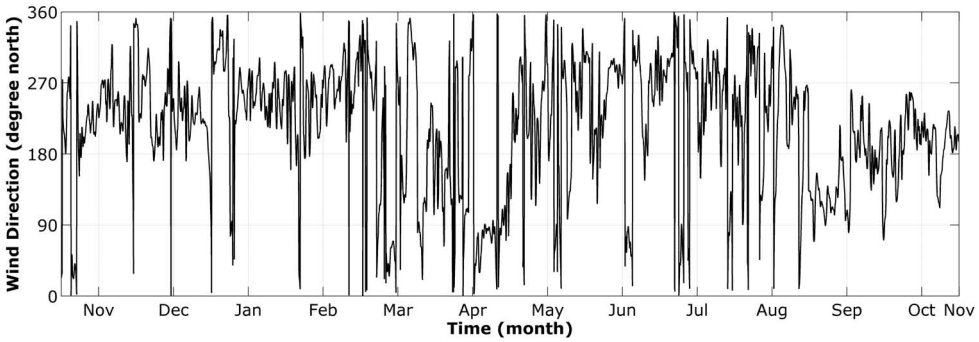

(d) PRISMA wind direction for 1999 Storm

Figure 5.24: PRISMA wind speed and direction for 1994 and 1999 Storms

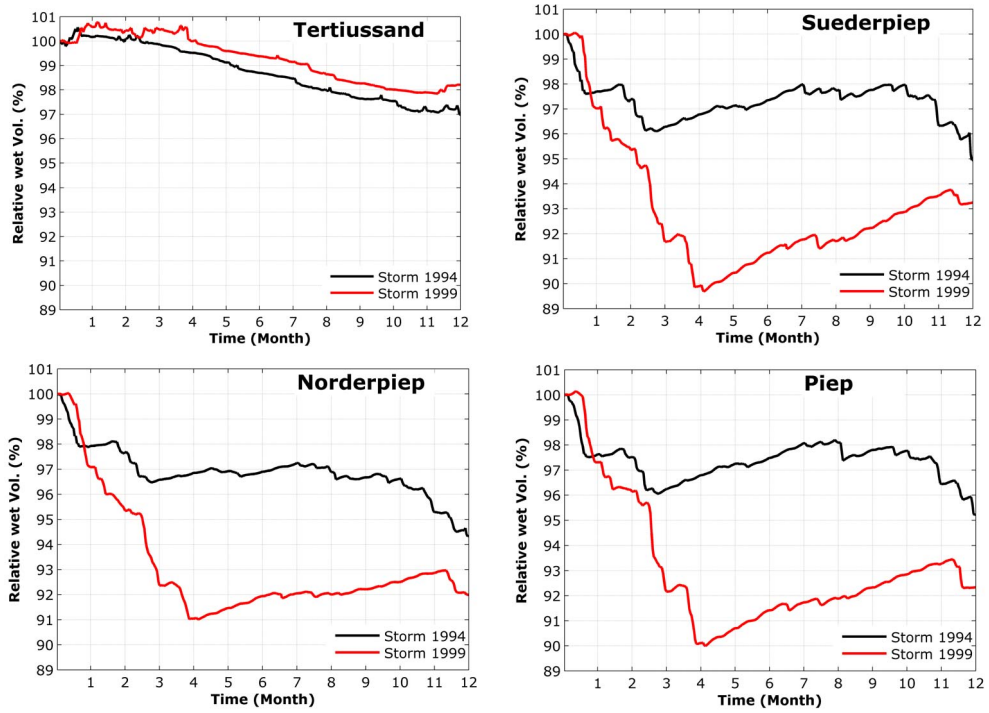

Figure 5.25: Relative wet volumes referred to at the beginning of the storm event

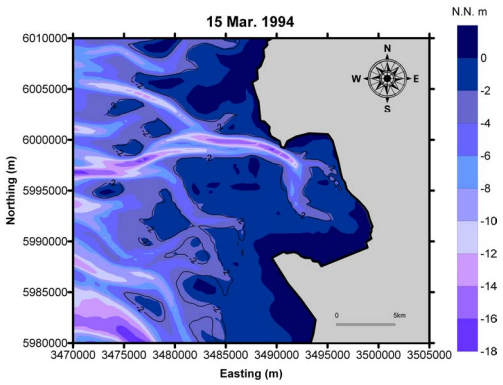

(a) Second month

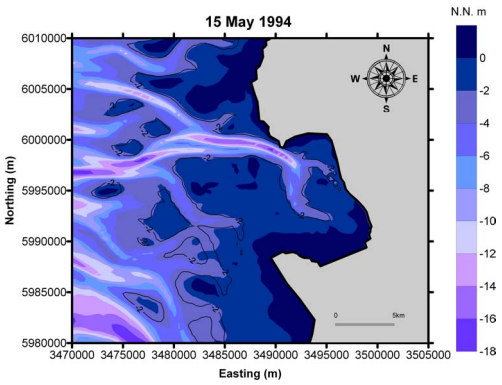

(b) Fourth month

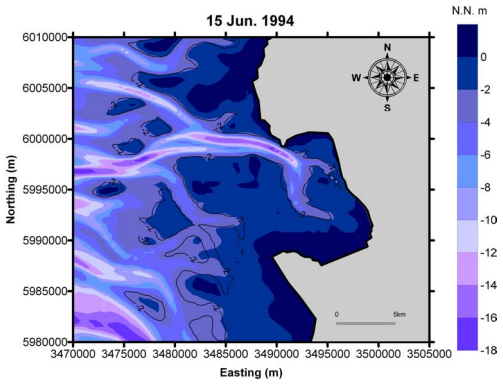

(c) Fifth month

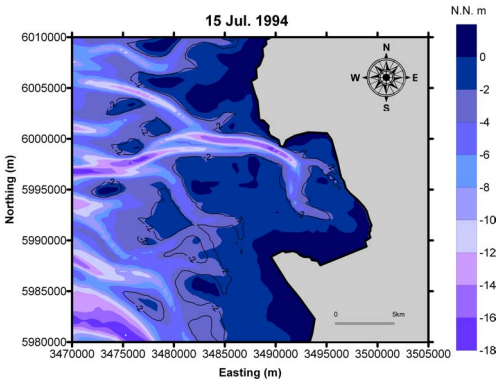

(d) Sixth month

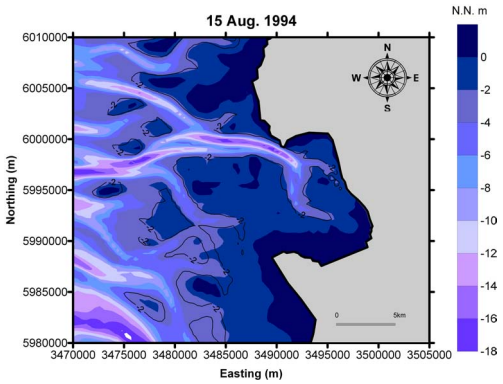

(e) Seventh month

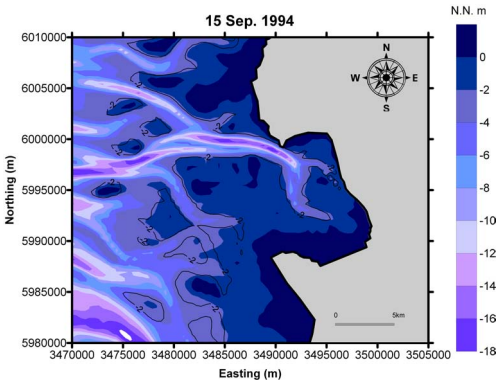

(f) Eighth month

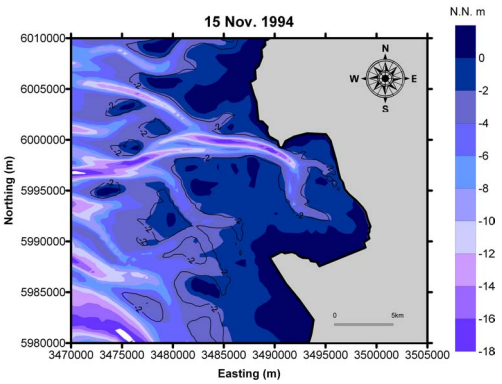

(g) Tenth month

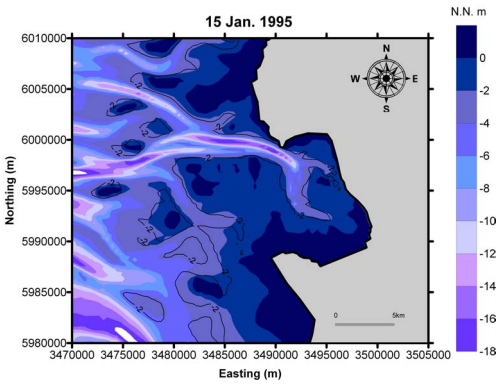

(h) Twelfth month

Figure 5.26: Bed level changes resulting from 1994-1995 simulation

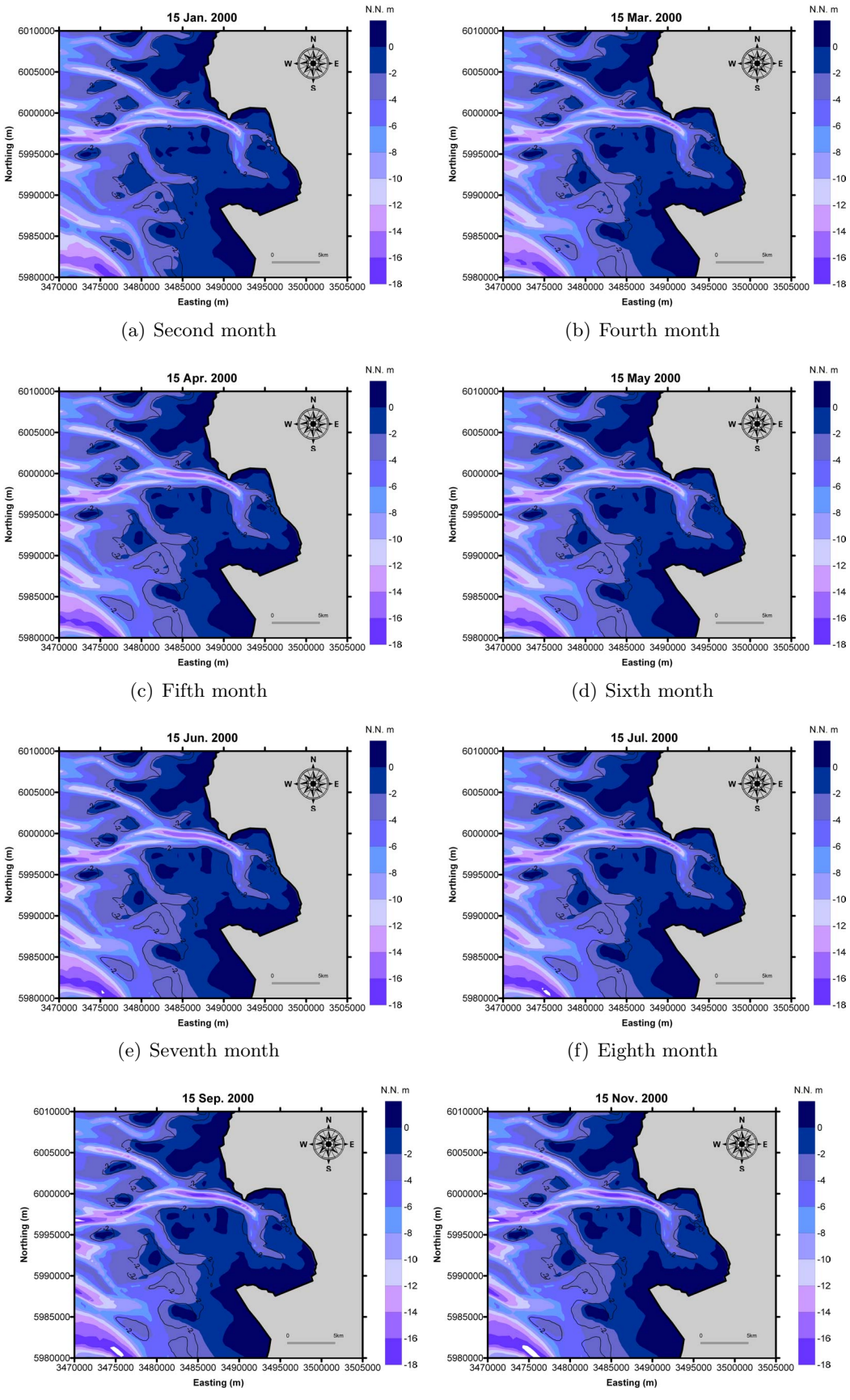

(a) Second month

(b) Fourth month

(c) Fifth month

(d) Sixth month

(e) Seventh month

(f) Eighth month

(g) Tenth month

(h) Twelfth month

Figure 5.27: Bed level changes resulting from 1999-2000 simulation

Chapter 6

Effects of storms on medium-term morphodynamics

6.1 Introduction

To improve our understanding of the effect of storms on the medium-term bed level changes of the central Dithmarschen Bight, the morphodynamic model has been extended to capture the bed elevation changes over periods of a few weeks to months. It has been based on the on-line approach with morphological factor as described in Section 2.3.3.2.
The coupling of the individual models (flow, wave, sediment transport and bed evolution models) into the morphodynamic model is discussed in Section 4.6.2. The process models are driven by conditions specified along the open sea boundaries and coupled to a model for calculation of morphological changes of the considered period of one year.

To assess the sensitivity of the morphodynamic model to the defined conditions, a study of storm chronology of a real storm has been carried out. Furthermore, a comparison has been made between the application of representative tidal conditions and a full neap-spring tidal cycle for one year simulation. Finally, the morphological changes due to the chronology of a wave climate over a period of one year have been studied.

6.2 Definition of the open sea boundary conditions

To study the medium-term bed level changes due to the storms, preparation is required to set-up the morphological model. This preparation covers the selection of representative tide that will be imposed on the open sea boundaries, definition of the morphological factor (morfac) for the calm and the active periods and the representative wave and storm conditions for the active periods. These three questions will define the scenarios of the imposed boundary conditions in the medium-term morphodynamic model.

6.2.1 Flow boundary conditions

6.2.1.1 Representative tide

The selection of the representative tide has been done based on the approach proposed by Steijn, 1992 (described in detail in Appendix B). This approach is the commonly accepted and applied concept of using representative boundary conditions (averaging tide). Moreover, it is based on the assumption that the long-term effect of natural tidal forcing can be approximated by a small number of tidal boundary conditions. This assumption is valid if their cumulative effect on morphology is close enough to that of the real signal throughout the whole period (Latteux, 1995). To find the representative tidal cycle the following sequence has been applied:

- Selection of representative locations on the domain for the tidal flats and channels as it is illustrated in Fig. 6.1 (14 on tidal flats and 17 in tidal channels). These locations have been chosen as Wilkens (2004);
- Sediment transport simulation for a period of 30 days has been carried out to cover complete neap-spring tidal cycle. This simulation allows to calculate the average sediment transport for each selected locations and for each tidal cycle as well for the entire neap-spring tide ;
- Calculation of the representative factors for each selected locations as follows:

$$\lambda_x(i,j) = \frac{\overline{S_x(i,j)}}{\overline{S_x(i,tot)}} \tag{6.1}$$

$$\lambda_y(i,j) = \frac{\overline{S_y(i,j)}}{\overline{S_y(i,tot)}} \tag{6.2}$$

where:

$\lambda_x(i,j)$ and $\lambda_y(i,j)$ = representative factor for tide j at point i in x-and y-direction

$\mathrm{S}_x(i,j)$ and $\mathrm{S}_y(i,j)$ = average sediment transport during tide j at point i in x-and y-direction

$\mathrm{S}_x(i,tot)$ and $\mathrm{S}_y(i,tot)$ = average sediment transport during whole neap-spring period in x-and y-direction

As is clearly shown in Eq. 6.1 and 6.2 if the value of λ equals or close to 1, the more representing for the average sediment transport rate.
The representative tide has to have tidal range between 7% and 20% (Latteux, 1995) and not higher than 10% (Steijn, 1992) compared to the mean tidal range for the southeren North Sea.

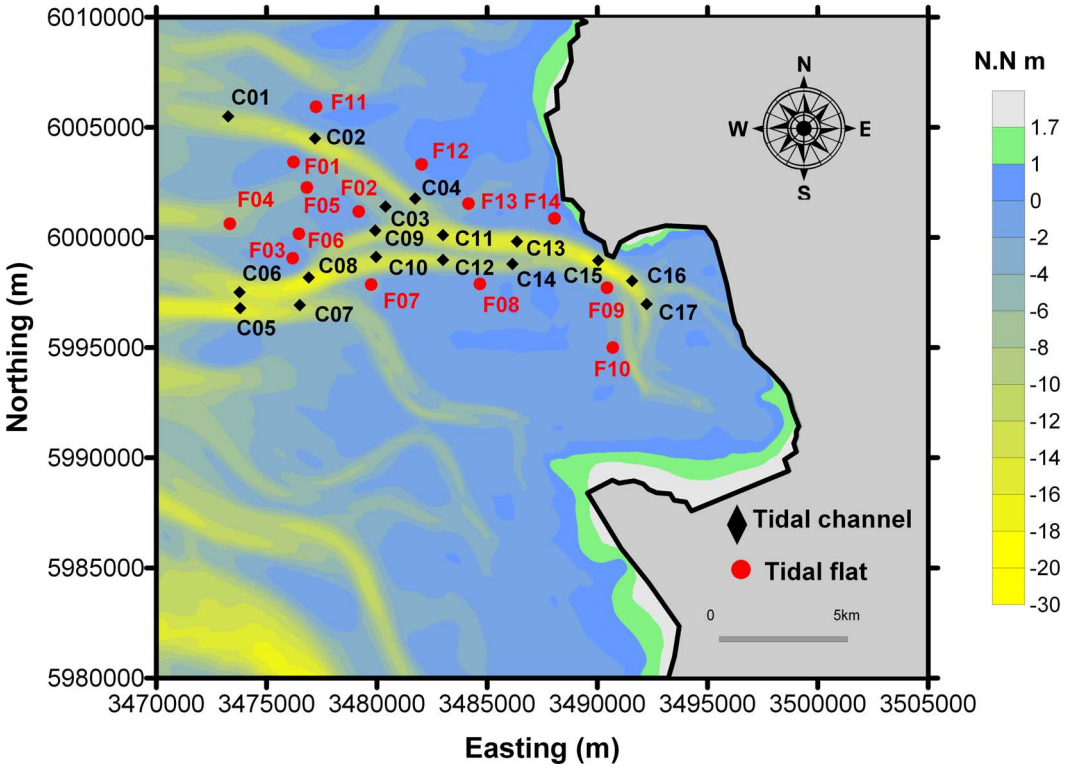

Figure 6.1: Location of the selected location for representative tide

Fig. 6.4 shows the tidal range of the representative tide at four different locations as shown in Fig. 6.2. It clearly shown that the representative tidal cycle at the four locations have tidal ranges 3.2, 3.0, 3.0 and 3.3m, respectively. These tidal ranges for the representative tidal cycle are very close to the mean tidal range (3.2m) of the Dithmarschen Bight and have 3% of maximum tidal range higher than the mean tidal range.

Fig. 6.5 summarizes the representative factors λ_x and λ_y at the selected locations. Also from the figure the selected tide (tide number 35 and indicated with vertical black line) has been chosen. It is clear that the tide number 35 showed good results for the representative tide factors along both directions.

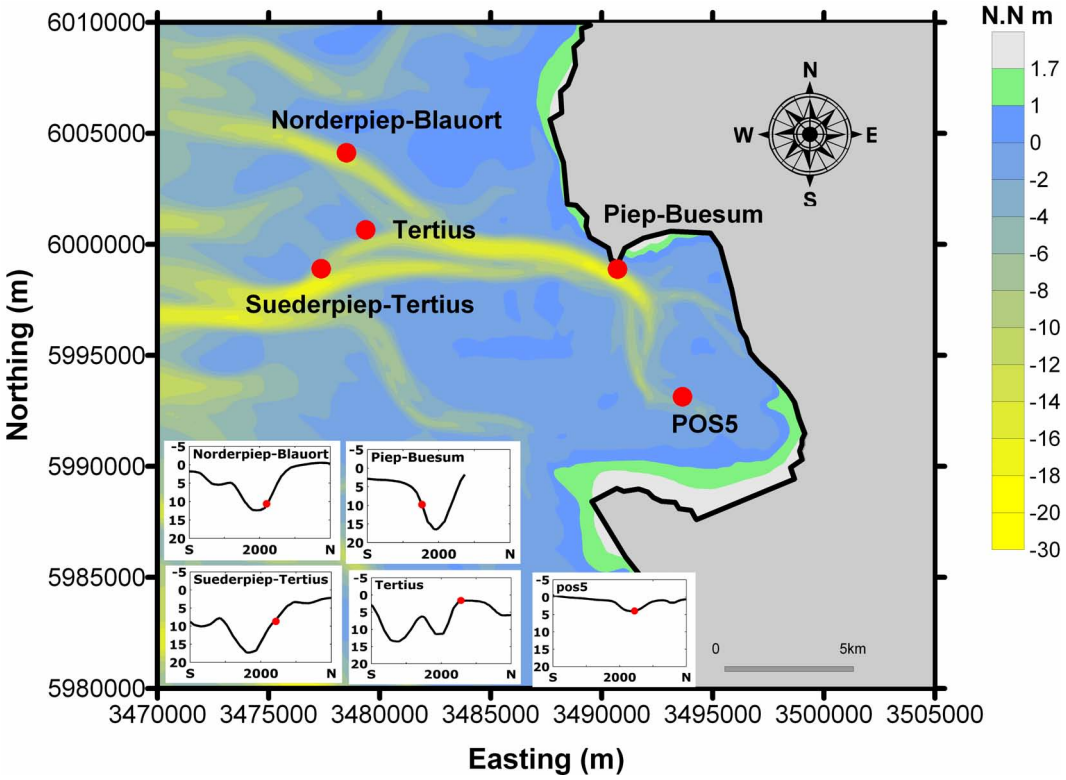

Figure 6.2: Location of the observation points

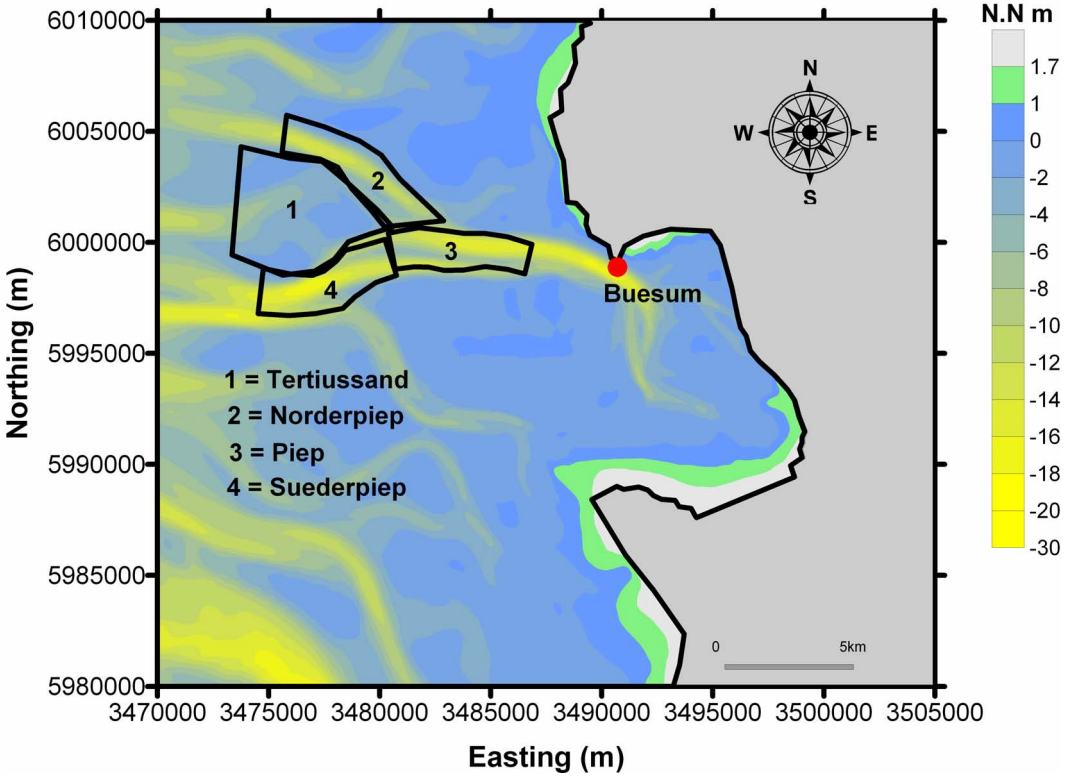

Figure 6.3: Location of the sub-domains for model results

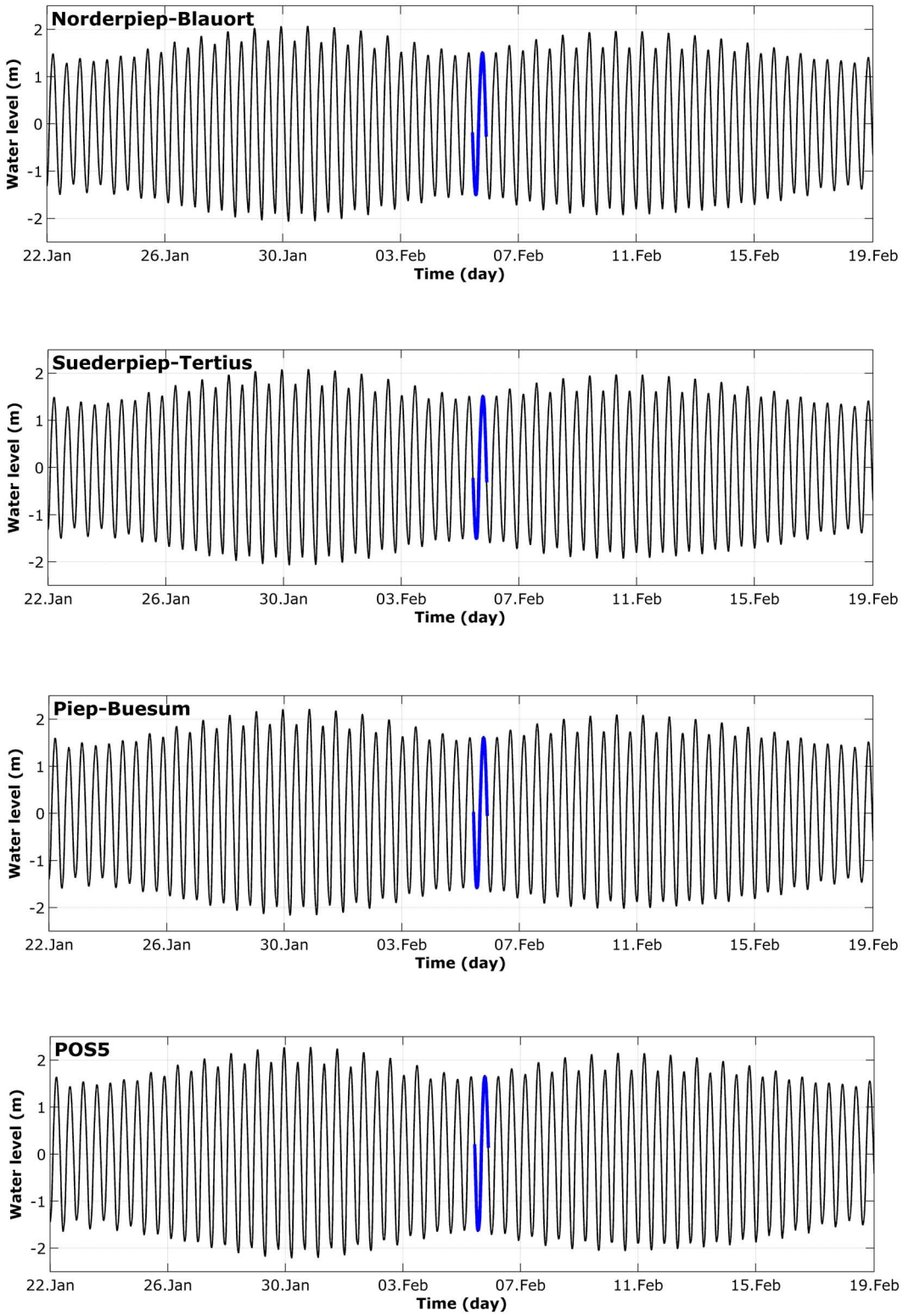

Figure 6.4: Computed water level for Spring-Neap period (1998) and the selected representative tidal cycle (blue line)

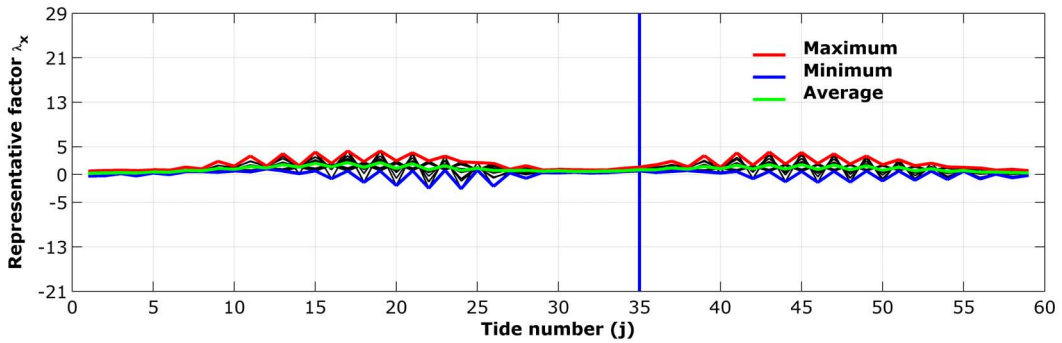

(a) x-component of tidal channel locations

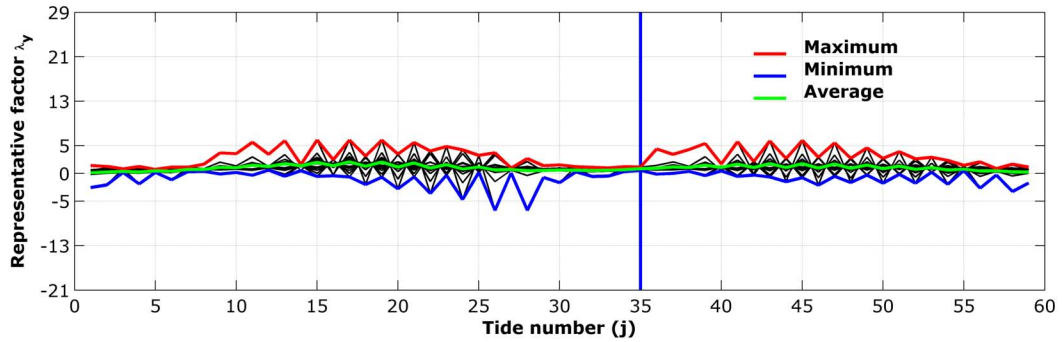

(b) y-component of tidal channel locations

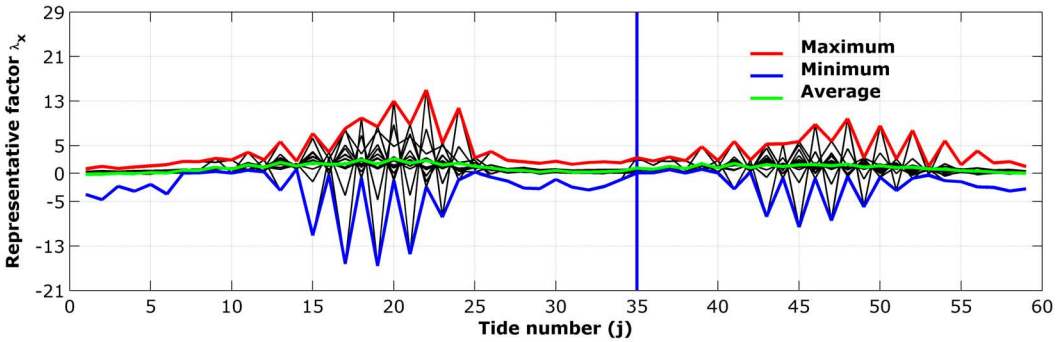

(c) x-component of tidal flat locations

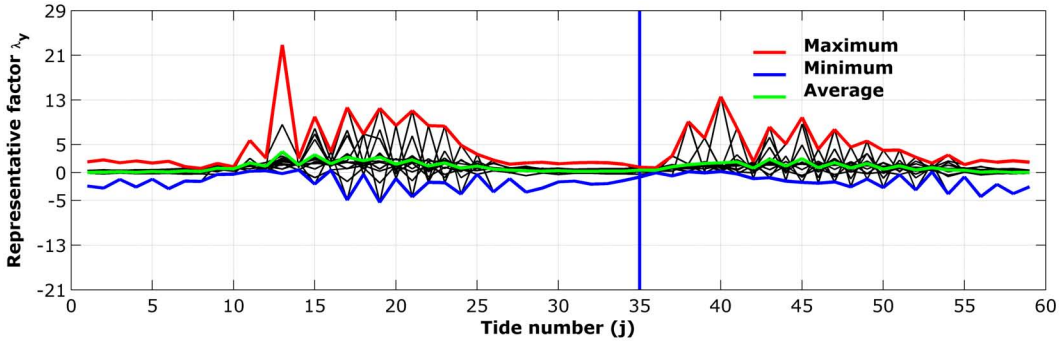

(d) y-component of tidal flat locations

Figure 6.5: Representative factors λ_x and λ_y at selected locations

6.2.1.2 Definition of morphological scale factor

One of the complications inherent in carrying out morphological projections on the basis of hydrodynamic flows is the morphological developments. They take place on time scale several times longer than typical flow changes. One technique to speed up the change in the morphology is the so-called morphological time scale factor approach (see Section 2.3.3.2). The speed of the changes in the morphology is scaled up to a rate that it begins to have a significant impact on on the hydrodynamic flow. This can be achieved by specifying a non-unity value for variable Morfac in the morphodynamic model(Delft3D-flow manual).
The maximum morphological time scale factor that can be included in a morphological model without affecting the accuracy of the model depends on the particular situation being modelled and will remain a matter of judgment. Therefore to use a morphological scale factor within acceptable accuracy, several simulations for different Morfac (1, 5, 10 and 30) have been carried out for one month period under conditions without wind or waves (calm period or tide only) and with wind and waves (active period). For the active period, the open sea boundaries for the wave and wind conditions have been chosen to be 1.0m significant wave height with 270 ^{o}N wave direction and 7.5 m/s wind speed with 240 ^{o}N wind direction.
Fig. 6.6 shows the results of the simulations in terms of volume changes considering different morphological scale factors for the previously described calm and active periods. The resulting wet volume have been extracted at selected areas only, where the size of the areas varies from 16 to 28 km^2. It can be seen that for the active period, the Morfac has a great influence on the results compared to the calm period. Moreover, higher Morfac values cause instability in the relative wet volume during the simulation period. Also it is clear that during the calm period, the Morfac could be as high as about 30. For Morfac values lower than 30 the results shows good agreement (less than 0.1% in reletive wet volume) with respect to real conditions (Morfac equals 1). On the other hand, the results for Morfac equals to about 30 show significant discrepancies in the relative wet volume, although, the differences in the relative wet volume was less than 0.25% compared to the real condition. It is also can be seen from Fig. 6.6 that the Morfac for the active period could be applied till Morfac equals to about 5. But for Morfac greater than 5 the result could not be reliable, where the differences in the relative wet volume up to about to 3% compared to the real condition (reference case).
In summary, for the conditions in question it was found that the morphological scale factor Morfac for the calm period can be as much as to 30 and for the active period it can be around 5. Therefore to increase the accuracy of the results for the coming simulation Morfac equal to 20 and 1 have been used for the calm and actives periods, respectively.

6.2.1.3 Combined representative tide and morphological scale factor

To study the effect of the selected representative tidal cycle and the lunar cycle (astronomical tide) on the morphological changes, two runs for a period of one year have been carried out. Based on the results obtained from Section 6.2.1.1 and 6.2.1.2 the flow open sea boundaries have been selected. For both cases the tidal cycles are repeated for one year period of time using Morfac value.

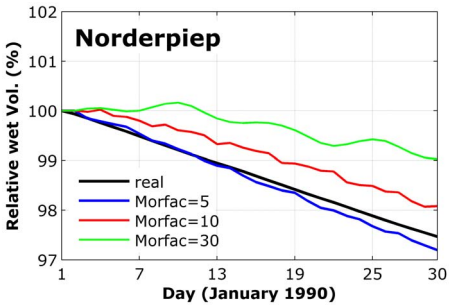

(a) Active period

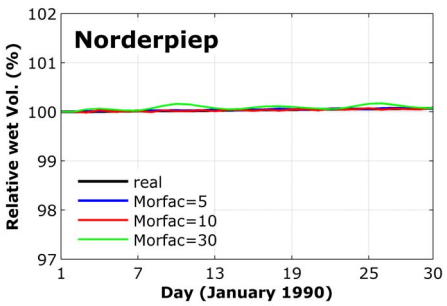

(b) Only tide (calm period)

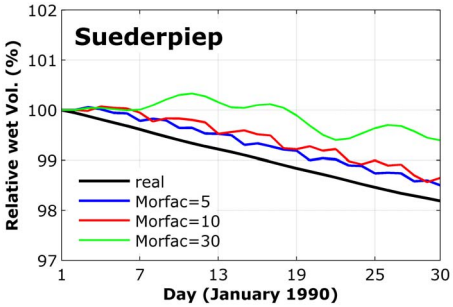

(c) Active period

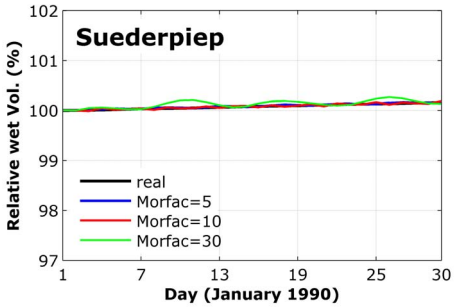

(d) Only tide (calm period)

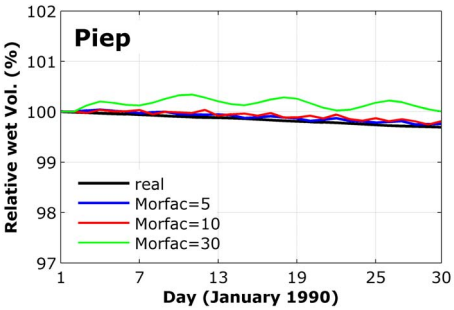

(e) Active period

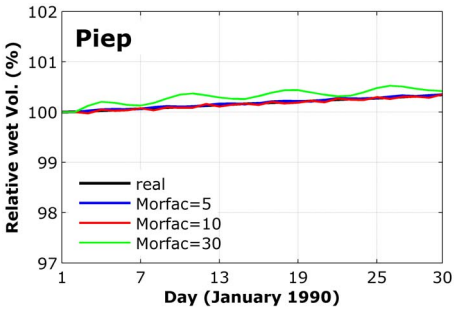

(f) Only tide (calm period)

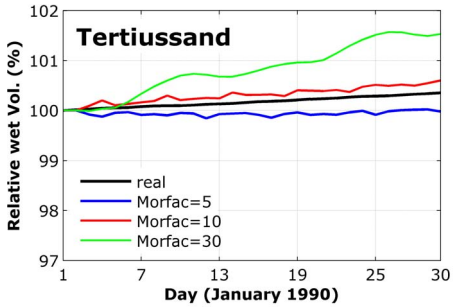

(g) Active period

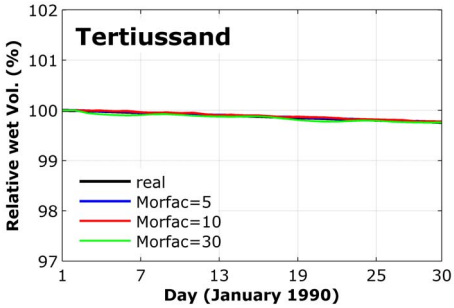

(h) Only tide (calm period)

Figure 6.6: Sensitivity analysis with respect to the morphological scale factor (Morfac) for calm and active periods

6.2.2 Storm conditions

To study the medium-term morphological changes due to storms, the Anatol storm in December 1999, as it is illustrated in Fig. 6.7, has been chosen. The storm has been applied in the medium-term Dithmarschen Bight model for a duration of 15 days from one year simulations with Morfac equals to 1. On the other hand, Morfac equals to 20 has been applied during the remaining period from the one year simulation with representative tide without any storms or waves.

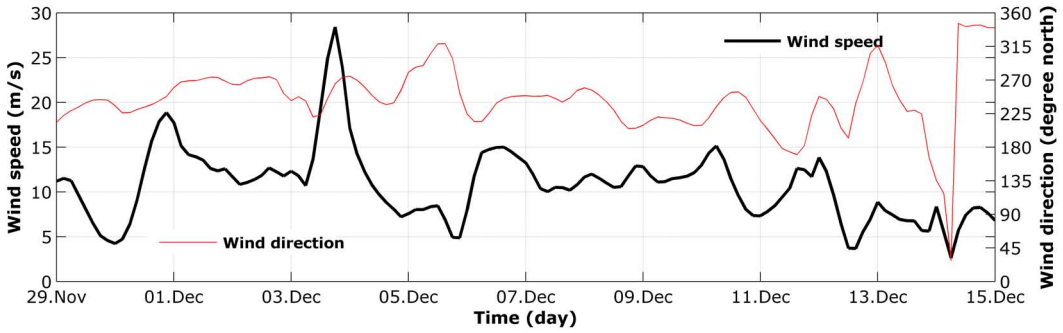

Figure 6.7: PRISMA wind speed and direction for 1999 storm

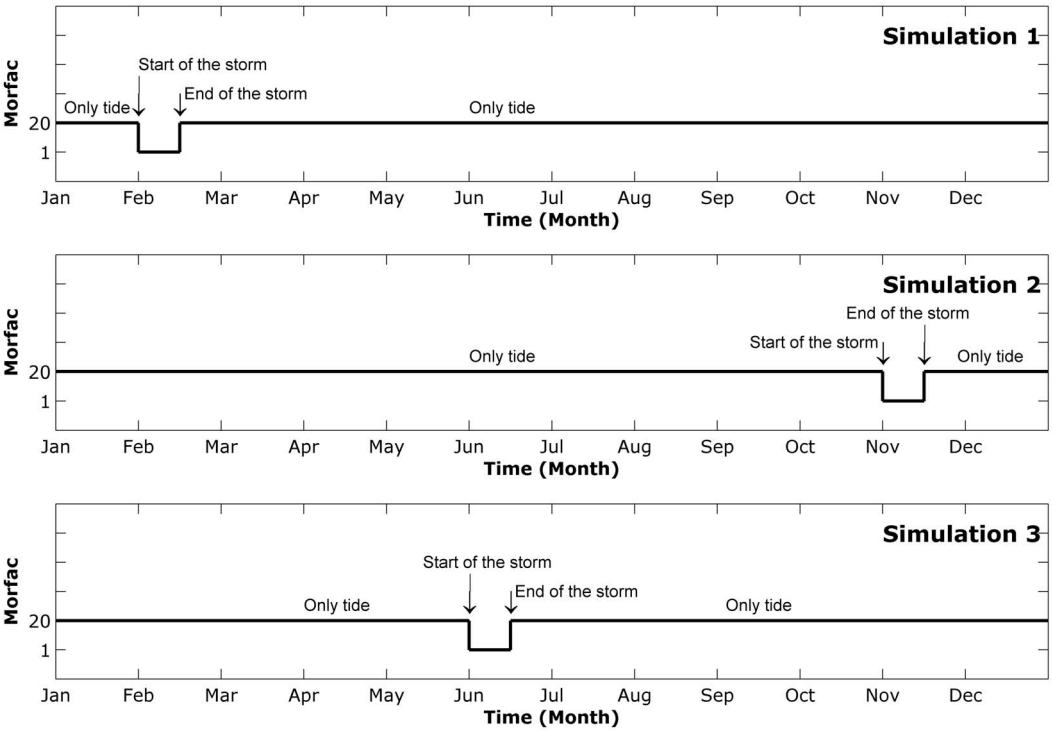

Figure 6.8: Schematic representation of the simulations and location of the Anatol storm

Fig. 6.8 shows a sketch describing the simulated conditions covering a one year period. Runs combining a period with tides only and one major storm were simulated. In the first case the storm occurs one month after the beginning of the simulation. Then this is set to take place in June and finally one month before the end of the period. The described simulations will show the effect of the storms as well as of the storm chronology on the morphological changes in the medium-term.

6.2.3 Wave climates

Similar to the previous section the effect of the waves on the medium-term morphological changes is studied. Since the swell wave conditions are stochastic, the schematisation of the expected wave climate can only be based on observations from the past. The wave climate that has been described in the Section 3.2.3.2 will be used. From Table 3.1 three wave conditions covering low, medium and high wave conditions have been chosen based on the probability of occurrence.

Table 6.1: Overview of the imposed wave conditions from HIPOCAS wave data set

Condition	**Description**	**H_s (m)**	**$\Theta(^oN)$**	**Probability (%)**
Low	Calm conditions	0.5	285	31
Medium	Intermediate wave	1.0	285	63
High	rough conditions	2.0	285	6

Table 6.1 summarizes the presented probability of occurrence (%) per wave direction and significant wave height at Station P7 from HIPOCAS wave data set (Table 3.1 at Section 3.2.3). Based on the selected wave conditions, three simulations with significant wave heights equal to 0.5, 1.0 and 2.0 m were carried out for a period of one year. To avoid any locally generated wave due to storms, these simulations have been carried out without any wind effects during the period of the simulation.

To study the effect of the wave chronology of the wave climate on the medium-term morphological changes, two additional simulations with two combined wave conditions have also been carried out.

Fig. 6.9 shows the sequence of the wave heights for two simulations with three wave segments. The first simulation is using 0.5, 1.0 and 2.0 m significant wave heights sequence and the second simulation is using 2.0, 1.0 and 0.5 m sequence. For both cases the over all period of the simulation is one year divided into three segments of different wave conditions (0.5, 1.0 and 2.0m) based on the probability of occurrence.

Therefore the simulation period for 0.5m, 1.0 and 2.0 significant wave heights were about 4 months, 7.5 months and 15 days, respectively.

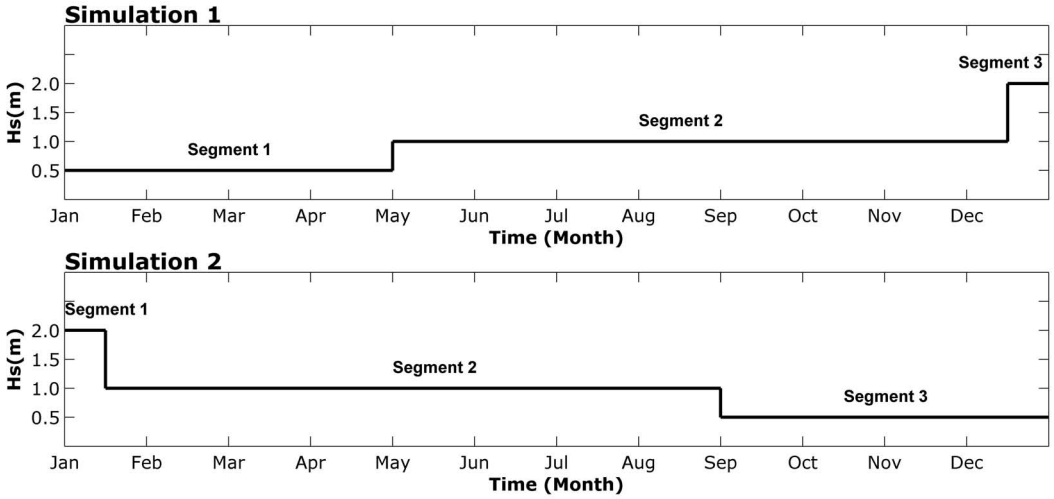

Figure 6.9: Sequence of wave heights showing partitions in 3 segments

6.3 Model results and analysis

6.3.1 Effect of tide on medium-term morphology

As it is described in Section 6.1 two cases have been taken to study the morphological changes due to tide only. The first case refers to the representative tide only that has been described in Section 6.2.1.1. The second case handles astronomical tide conditions. For both cases the simulations have been carried out for one year period. The computed sedimentation and erosion referred to the starting of the simulations for both cases are illustrated in Fig. 6.10 and Fig. 6.11. Since no wind or no wave have been imposed in these simulations, the modelled changes are purely based on the tide.

Fig. 6.12 shows the differences in the bed elevations between the two tidal conditions at the end of the simulation. It can be seen that the morphological changes for both cases are quite similar. In general the differences in the bed elevations at the end of the period do not exceed 0.1 m at some locations on the sandbank. In the remaining locations of the domain, it is difficult to recognize any differences in the morphological changes.

The results of the volume analysis for the four sub-domains (Fig. 6.3) are shown in Fig. 6.13. It is clear that also the volumetric changes indexed to the starting of the simulation at the four locations show very minor differences.

A number of locations has been selected throughout the study area, which consists of the main tidal channels and surrounding tidal flats. A total of 14 locations in the tidal channels and on the tidal flats has been defined. But the model performance showed similar tendency of erosion and depositions in the tidal channels and on the tidal flats. Therefore only 4 locations (Fig. 6.2) has been chosen to analyze the model results.

On one hand, the bottom depths at the four observation points (Fig. 6.2) showed that the maximum morphological changes at the end of the simulation were at most about 0.1m at the Norderpiep-Blauort location. On the other hand, the morphological changes (erosion and sedimentation) at the remaining three locations were relatively small (see Fig. 6.14).

In summary, the two test cases showed that there is no significant change in the computed morphological changes when representing the tidal conditions by a representative tidal cycle as against to a full astronomical tidal cycle.

It confirms that the on-line with morphological scale approach to impose the representative tidal conditions in the morphological simulations of the applied morphodynamic model is scientifically promising. Moreover the computational requirements are reduced significantly in the time needed for the simulations compared to the real time simulations.

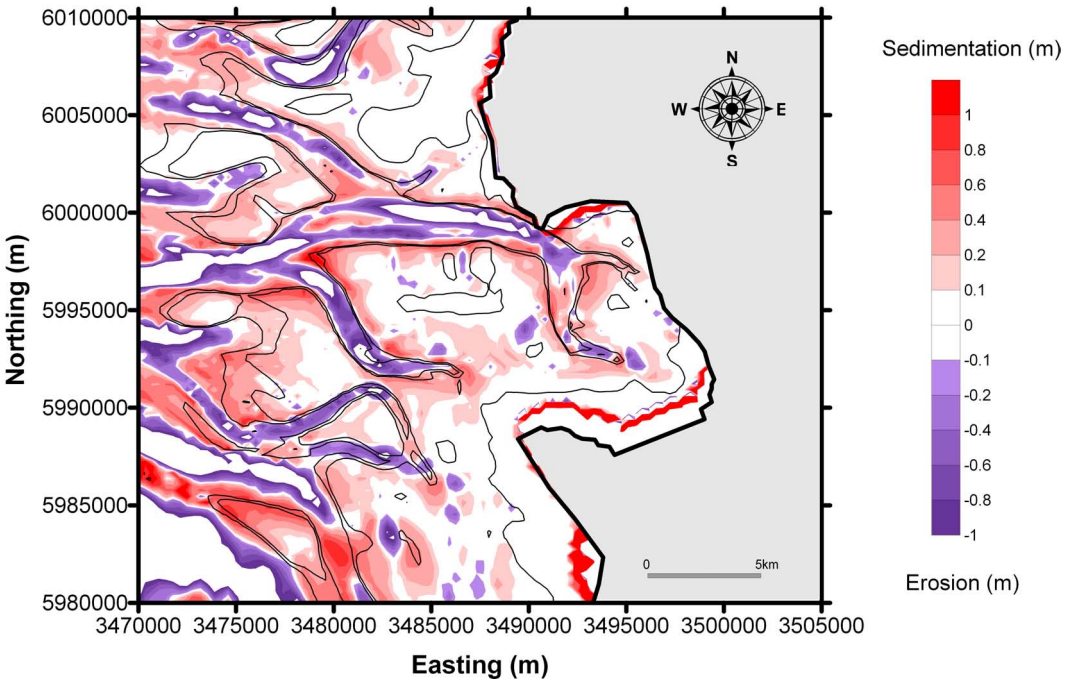

Figure 6.10: Bed level changes after one year due to astronomical tide

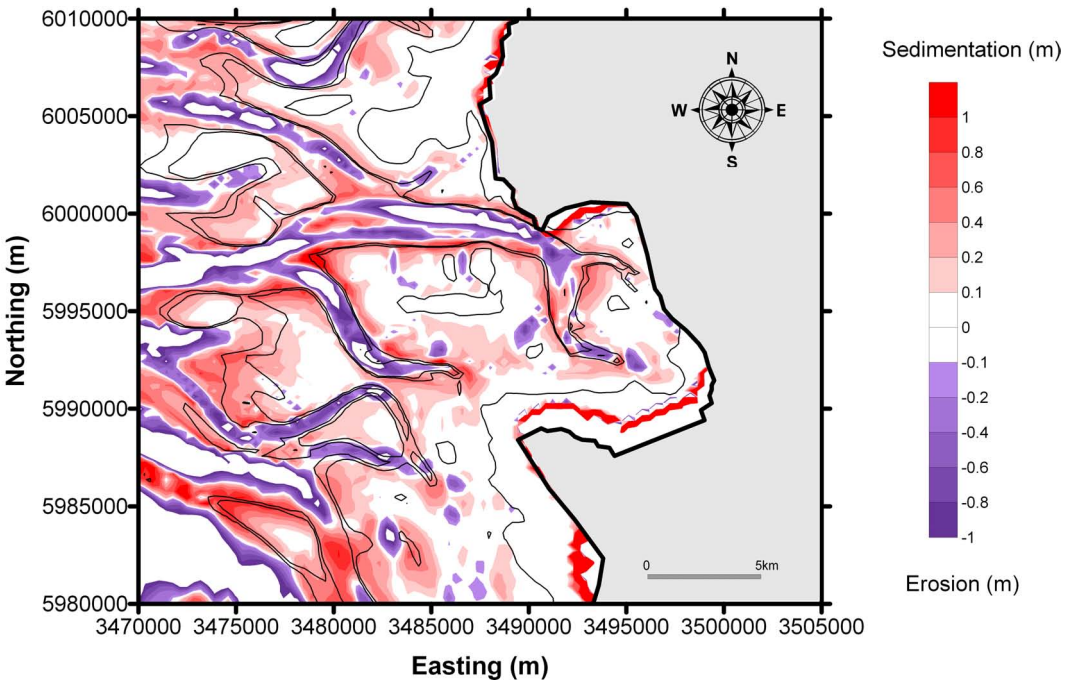

Figure 6.11: Bed level changes after one year due to representative tide

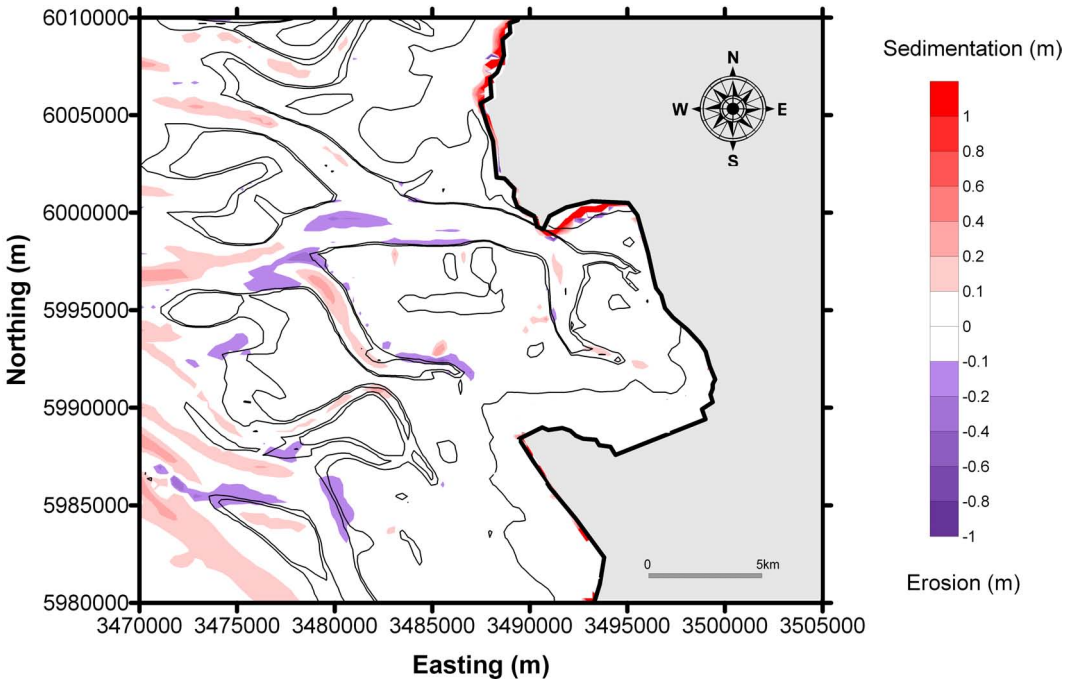

Figure 6.12: Bed level differences after one year between representative and astronomical tides

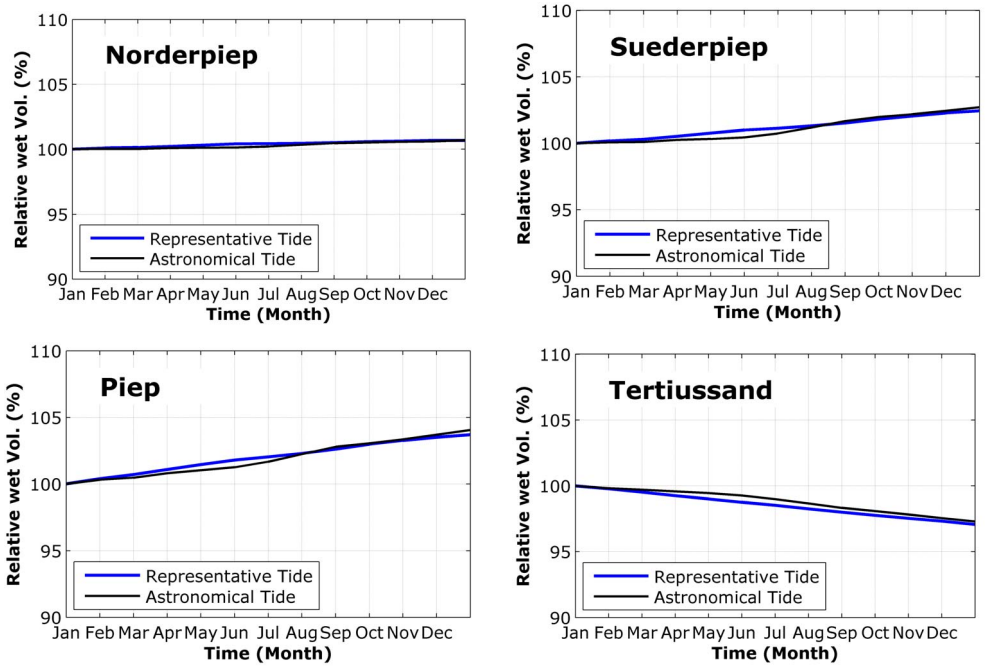

Figure 6.13: Relative wet volumes referred to the beginning of the simulation for astronomical and representative tides

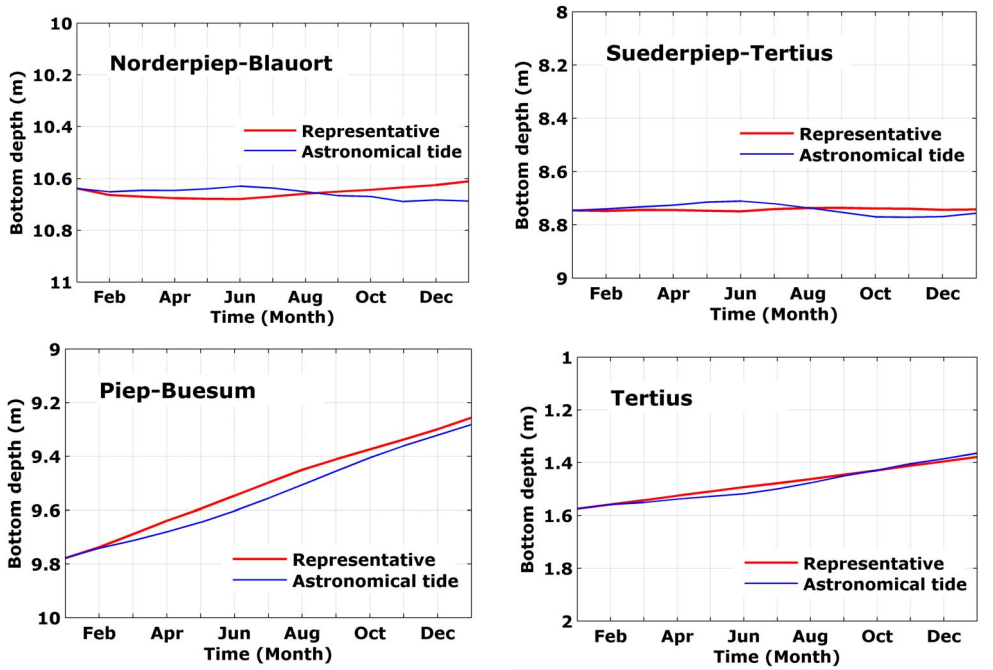

Figure 6.14: Bottom depth at selected locations for astronomical and representative tide

6.3.2 Effects of storm on medium-term morphology

The on-line morphological model with morphological scale factor has been used to simulate the storm effects on the morphological changes. The simulations have been carried out for one year by imposing the Anatol storm at the beginning, middle and at the end of the simulation.

The morphological changes after one year that resulted from the simulations are shown in Figs. 6.15 to 6.17. It is clear that when the storm conditions are imposed, much larger changes can be seen from the model results compared to simulations of the tide only.

The morphological changes over the considered period of one year for the the three storm sequences showed generally a tendency of deposition and erosion of about 1m and that most of the erosion takes place on the tidal flats with sedimentation in the surrounding channels.

The computed sedimentation and erosion differences referring to the case of the storm at the beginning of the simulation for the two remaining storm sequences are shown in Fig. 6.18 and Fig. 6.19. It can be noted that the maximum differences after one year in the bed elevations between the storm at the beginning and the storm at the end as well as between the storm in the middle are at most about 0.1m.

Fig. 6.20 shows the volumetric changes in the four sub-domains. It can be seen that the storm sequences do not affect significantly the morphological changes at the end of one year simulations. From the modelled conditions the results do not show any significant differences by means of storm chronology.

Fig. 6.21 shows the bottom depth at the four observation points (Fig. 6.2). It can be

seen that the storm sequences will not have an influence on the final morphological changes within the domain and for the simulation period. It has been also noted that in the Piep-Buesum location, when the storm hits, the bathymetry is slightly different. In other wards in places where the tide affects the bed and that are more exposed.
From the development of the profile at the cross-section Norderpiep in Fig. 6.22 it can be seen for the three simulated conditions that the channel has migrated from 1800 to 1250m (from north to south). On the one hand, this is caused by the progressing sandbank Tertiussand and one the other hand, by the sedimentation of the channel itself.
Fig. 6.23 shows the evolution of the channel at cross-section Suederpiep. It can be seen that the shape of the channel is rather stable and showing a decrease in the depth by about 1.25m for the three simulated conditions.
Fig. 6.24 shows the changes in the profile of the cross-section Piep. It is clear that the channel in general is moving gradually to the south. It can be seen that the depth at the middle of the channel decreased about 0.5m.
The 3m depth contours at the Tertiussand are shown in Fig. 6.25 for the three simulated conditions. Gradual progression of the sandbank towards the Northeast can be seen.
From the above, it is concluded that the inclusion of storm conditions in the medium-term morphodynamic simulations have significantly influenced the morphodynamic results within the current model set-up. But on the other hand the storm chronology does not significantly influences these results on the medium-term.

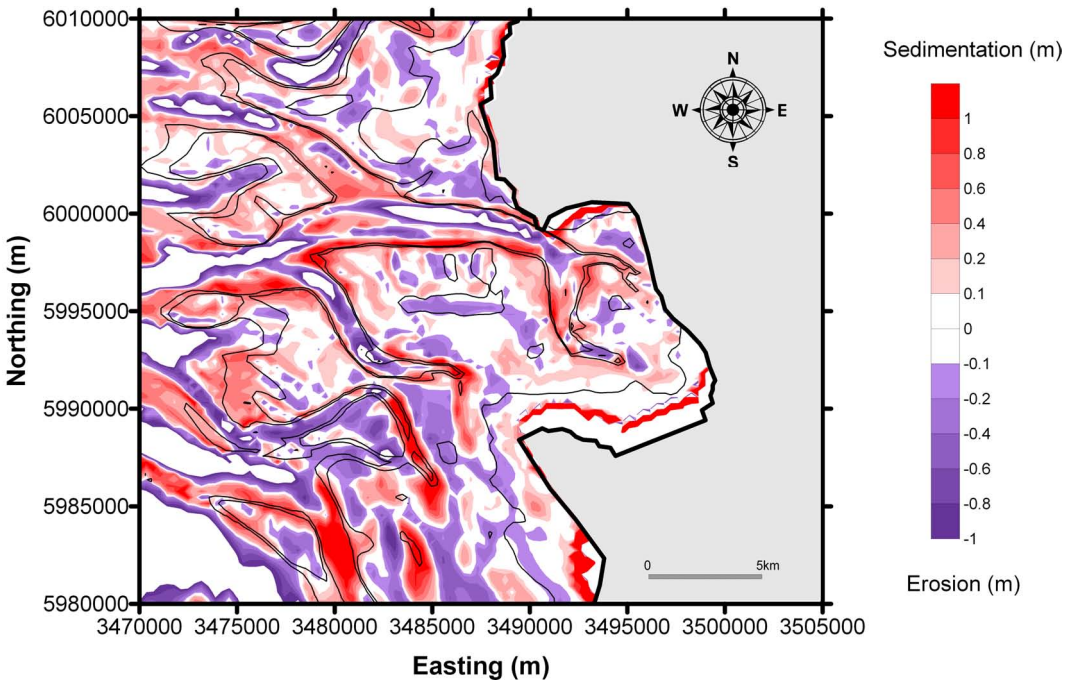

Figure 6.15: Bed level changes after one year resulting from the storm at the beginning of the period

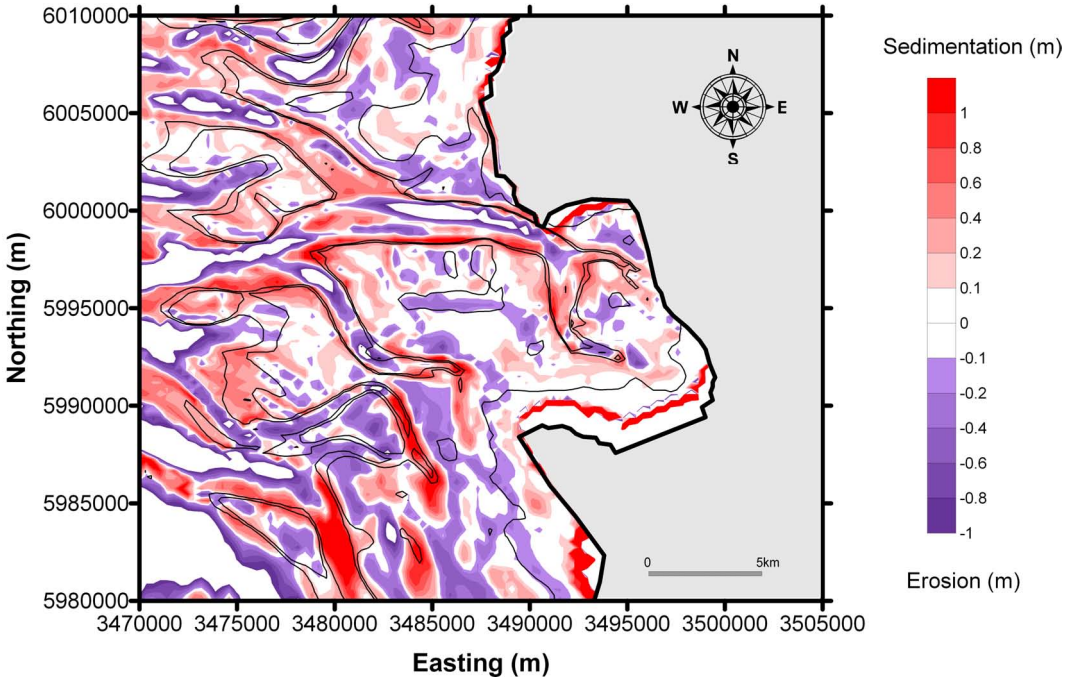

Figure 6.16: Bed level changes after one year resulting from the storm at the end of the period

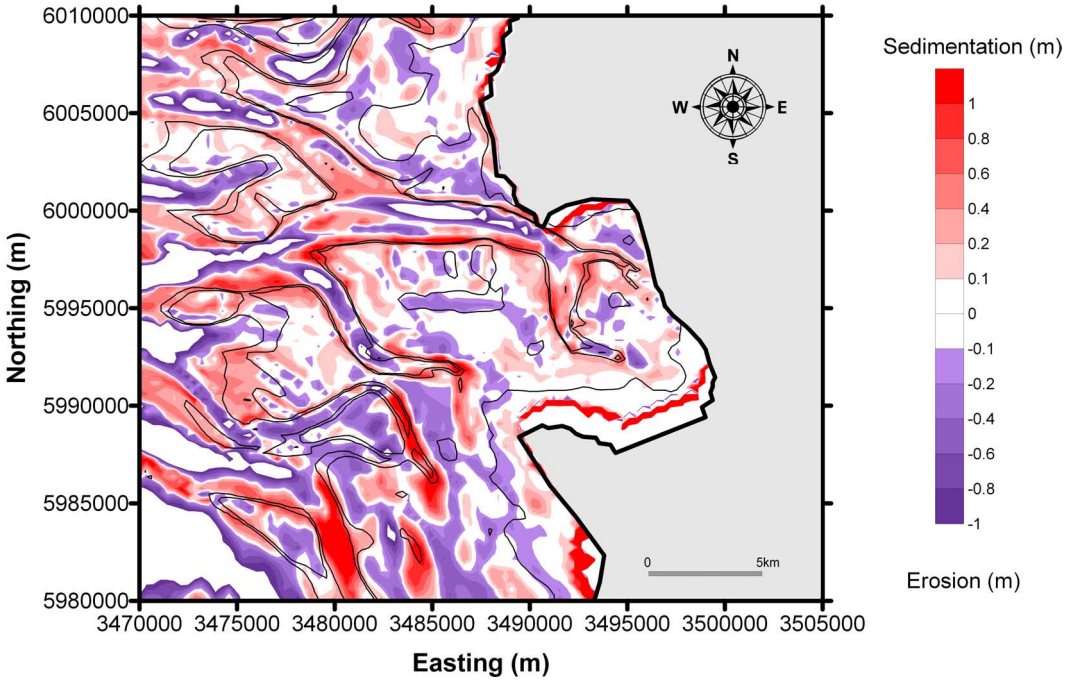

Figure 6.17: Bed level changes after one year resulting from the storm at the middle of the period

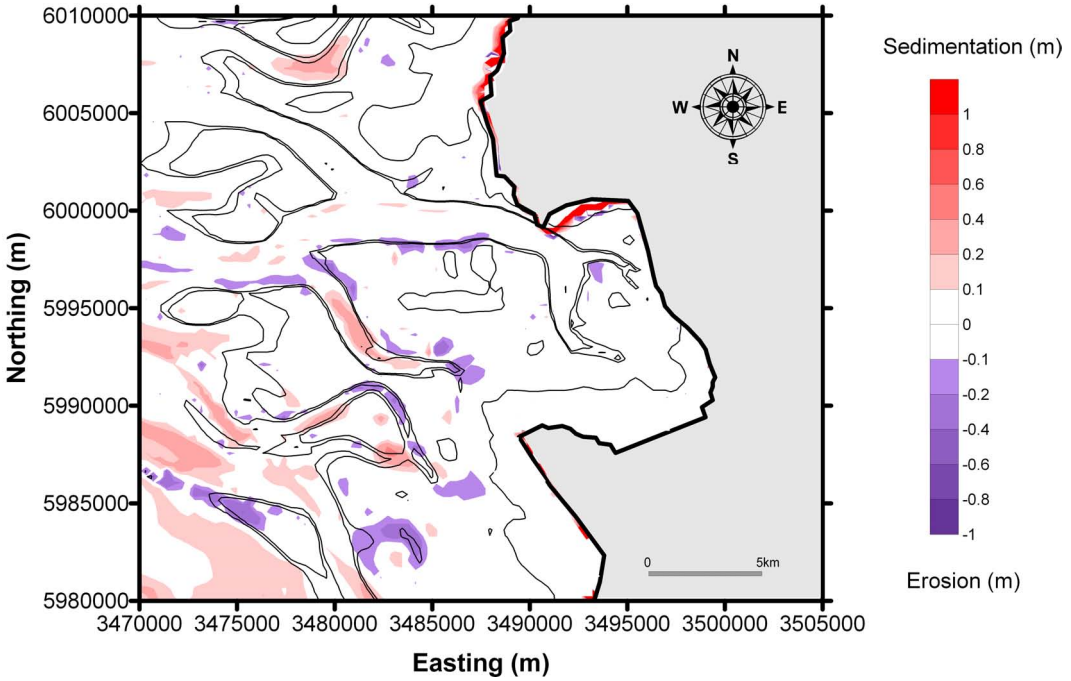

Figure 6.18: Bed level differences results from the simulations after one year between the storm at the beginning and the storm at end

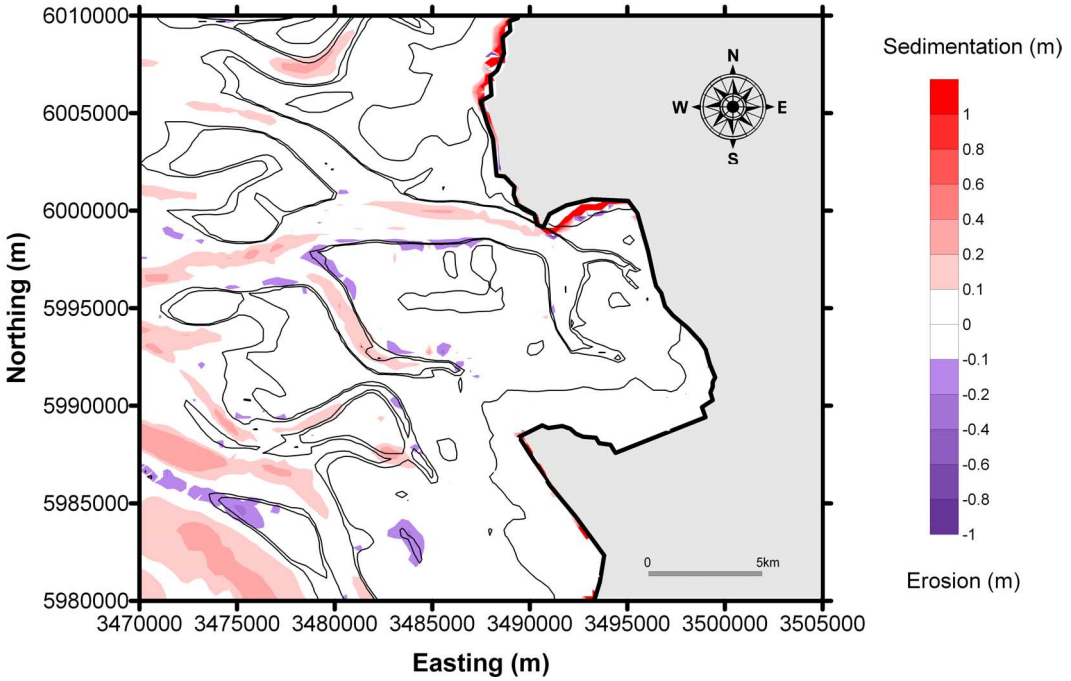

Figure 6.19: Bed level differences results from the simulations after one year between the storm at the beginning and the storm in the middle

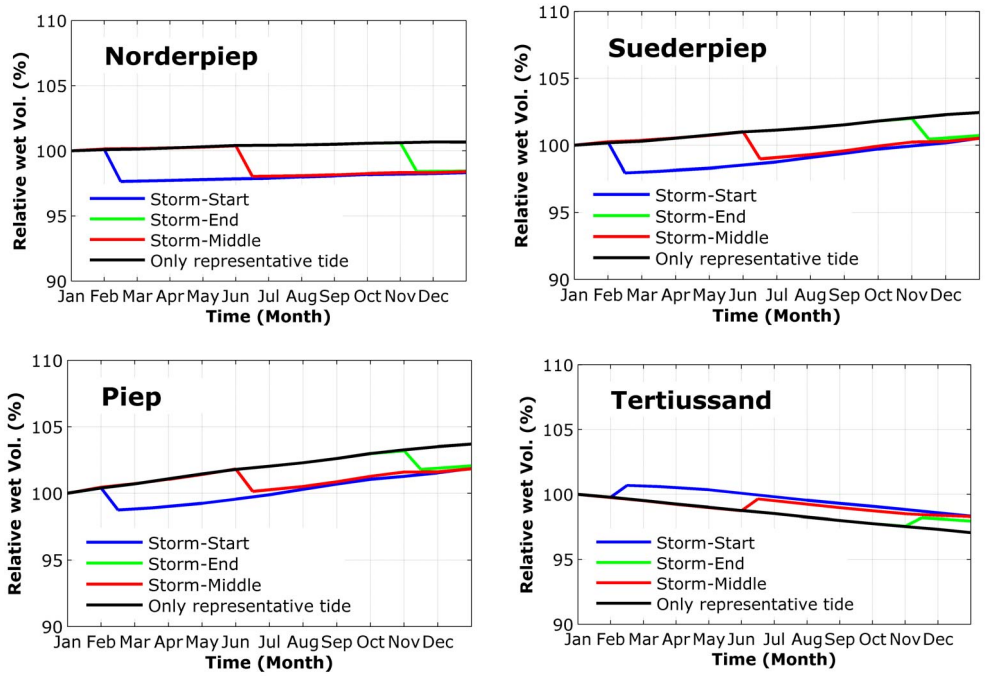

Figure 6.20: Relative wet volumes referred to the beginning of the simulation

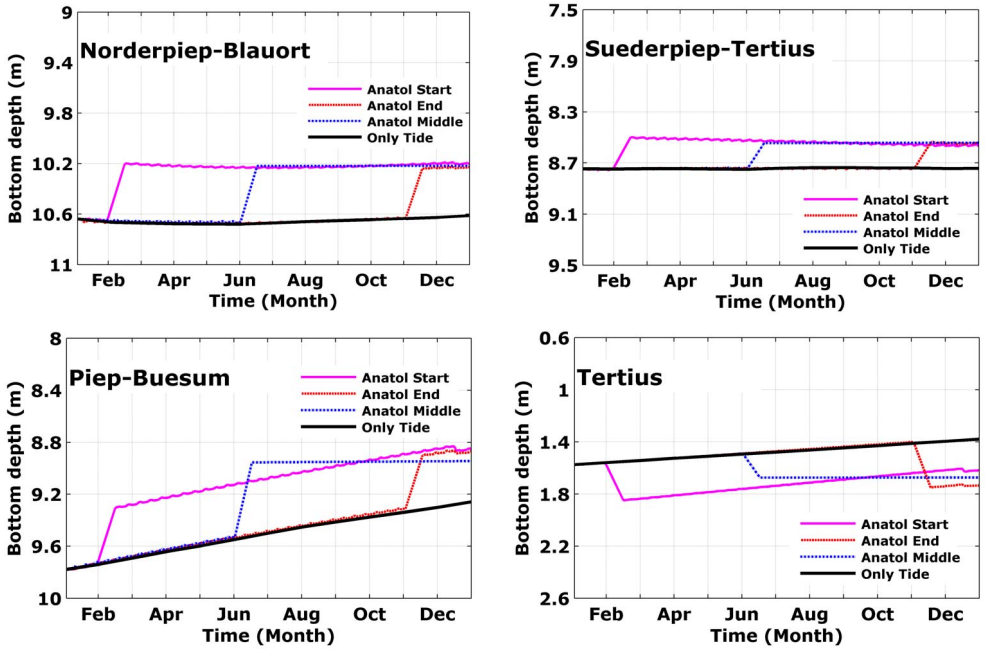

Figure 6.21: Bottom depth for three storm sequences

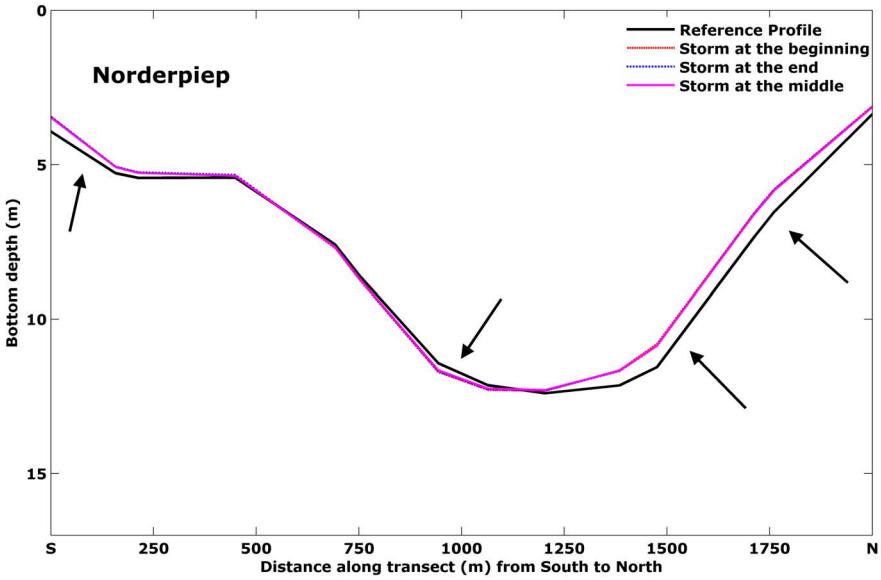

Figure 6.22: Modelled channel profile at cross-section in the Norderpiep for three storm sequences

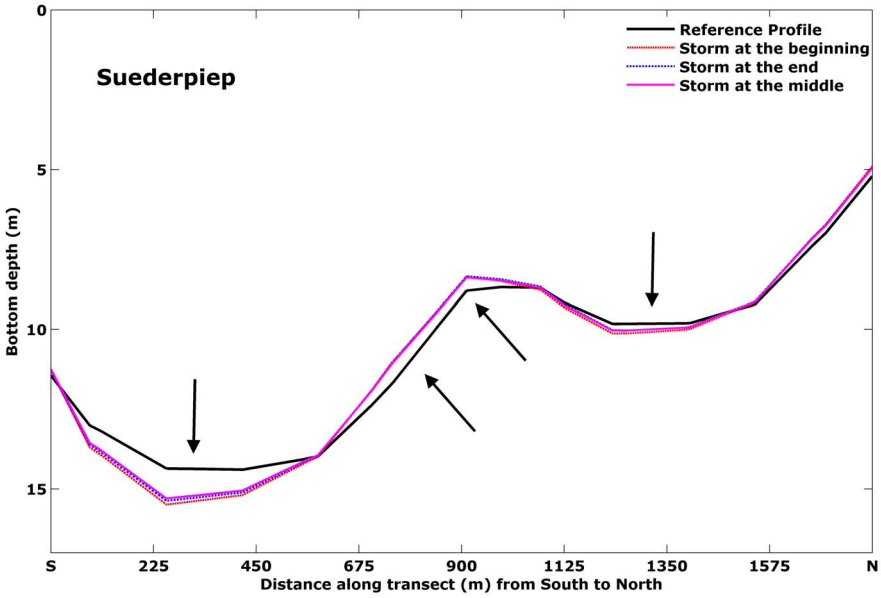

Figure 6.23: Modelled channel profile after one year at cross-section in the Suederpiep for three storm sequences

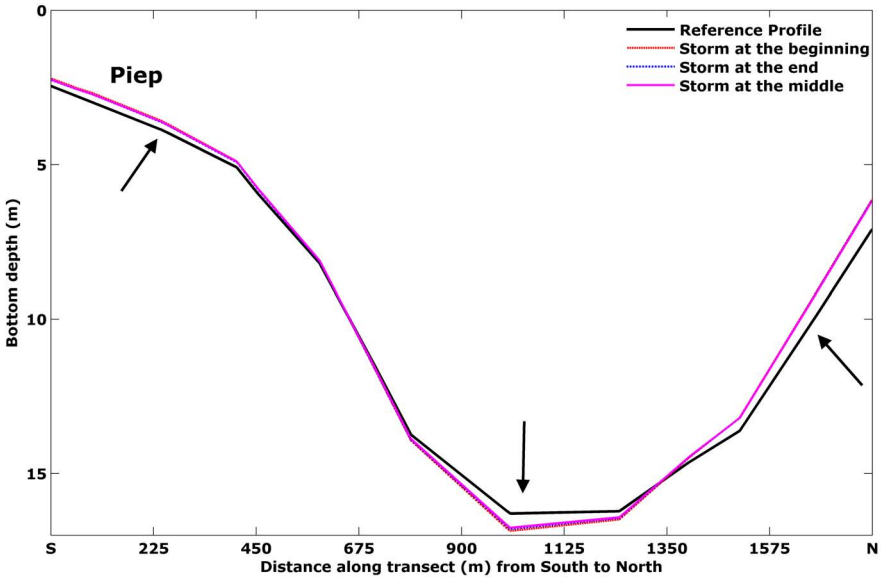

Figure 6.24: Modelled channel profile after one year at cross-section in the Piep for three storm sequences

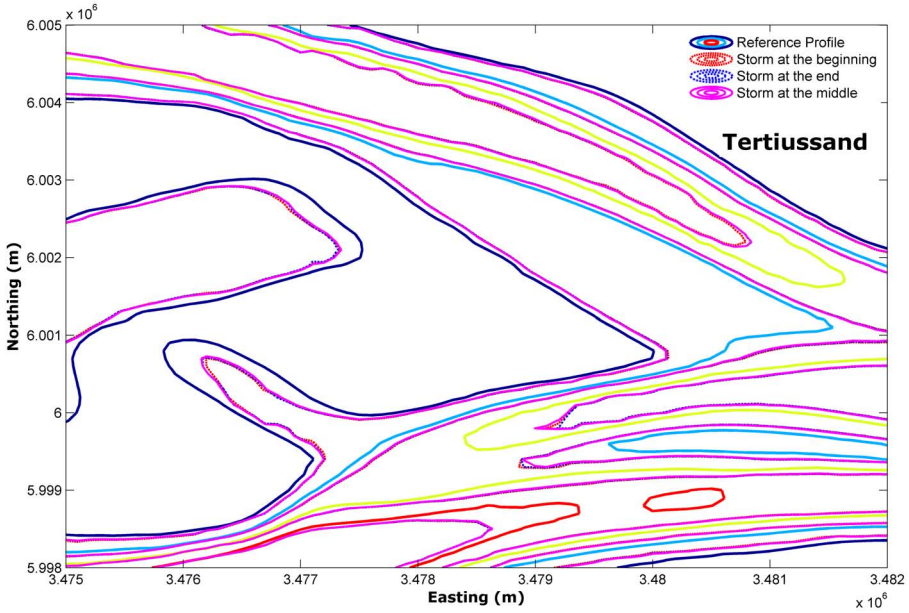

Figure 6.25: Modelled changes after one year of 3 m depth contours near Tertiussand for three storm sequences

6.3.3 Effects of wave climate and wave chronology on medium-term morphology

6.3.3.1 Effects of wave climate on medium-term morphology

As the waves have a significant influence on the morphological evolution of the Dithmarschen Bight (see Section 3.2.3), the effect of the waves on the medium-term morphodynamics is accounted for considering a wave climate which is based on results of model simulations (Section 6.2.3).

Figs. 6.26 to 6.28 show the results of the simulations of three wave climate conditions after one year referred to the starting of the simulations. It can be seen that the morphological developments as a result from wave climate along the open sea boundary have an important role compared to the tide only. It is also noted that the 0.5m significant wave height has similar morphological changes compared to the condition of tide only (see Fig. 6.10 and 6.11). It is clear that the erosion took place in the tidal channels and the sedimentation on the tidal flats.
In contrary to the 0.5m wave climate, the increase in the significant wave heights have an impact on the sedimentation and erosion patterns. It can be noted that for 1.0m and 2.0m wave climates the sedimentation took place in the tidal channel as a result of the erosion at the tidal flats and sandbanks.
As it is expected the most of the morphological developments were recorded from 2.0m wave climate (see Fig. 6.29 and Fig. 6.30).

Fig. 6.31 shows the relative wet volumes with respect to the starting bathymetry for the three different wave conditions. The figure shows an important influence of the wave conditions on the medium-term morphological changes within the model set-up. It is clear that the effect is getting more meaningful for the case of significant wave height equals to 2.0 m (rough wave conditions).

Fig. 6.32 shows the bottom depth at four observation points (Fig. 6.2). It can be seen that the depth variations at Buesum, Norderpiep and Suederpiep locations are in the order of few meters and in the Tertiussand is about one meter. One reason behind this behavior is that the eastern part of the domain is mostly dominated by the tide and any extreme wave conditions will have a clear influence on the morphological evolutions. On the other side, the western part of the domain is dominated by the combined effect of the wave and the tide.

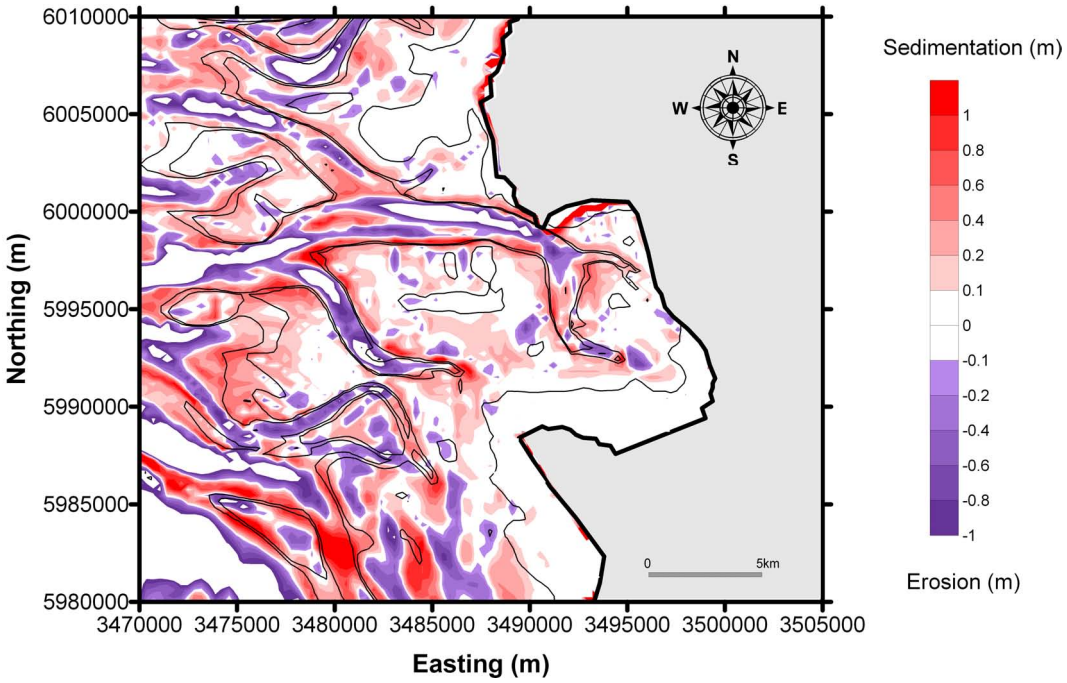

Figure 6.26: Bed level changes after one year resulting from a swell condition Hs=0.5m

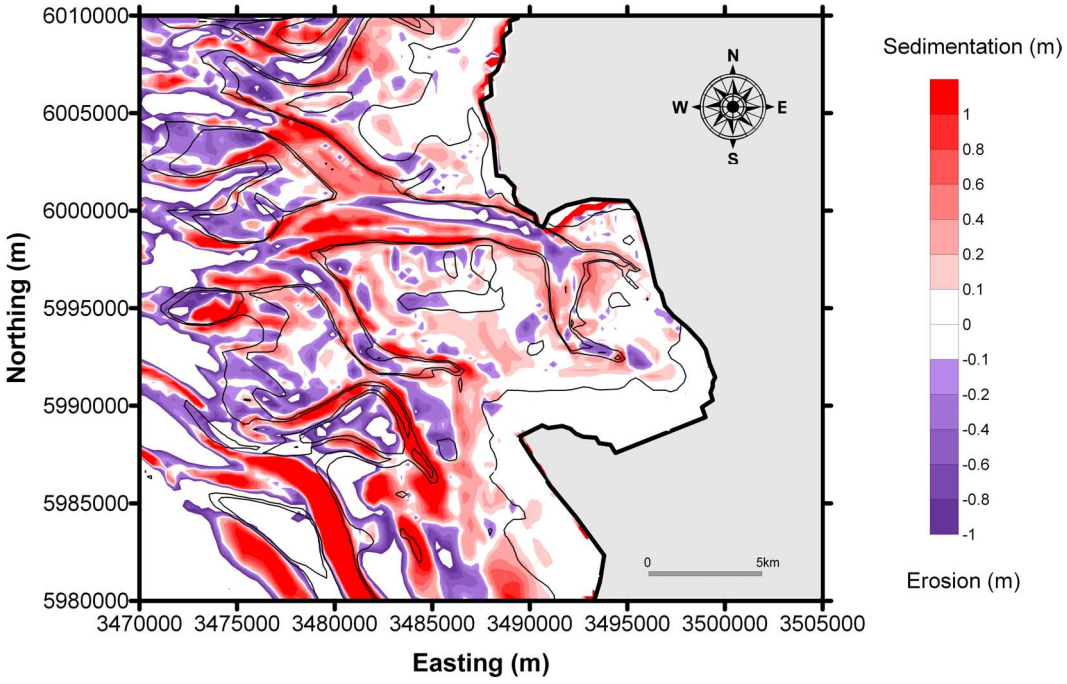

Figure 6.27: Bed level changes after one year resulting from a swell condition Hs=1.0m

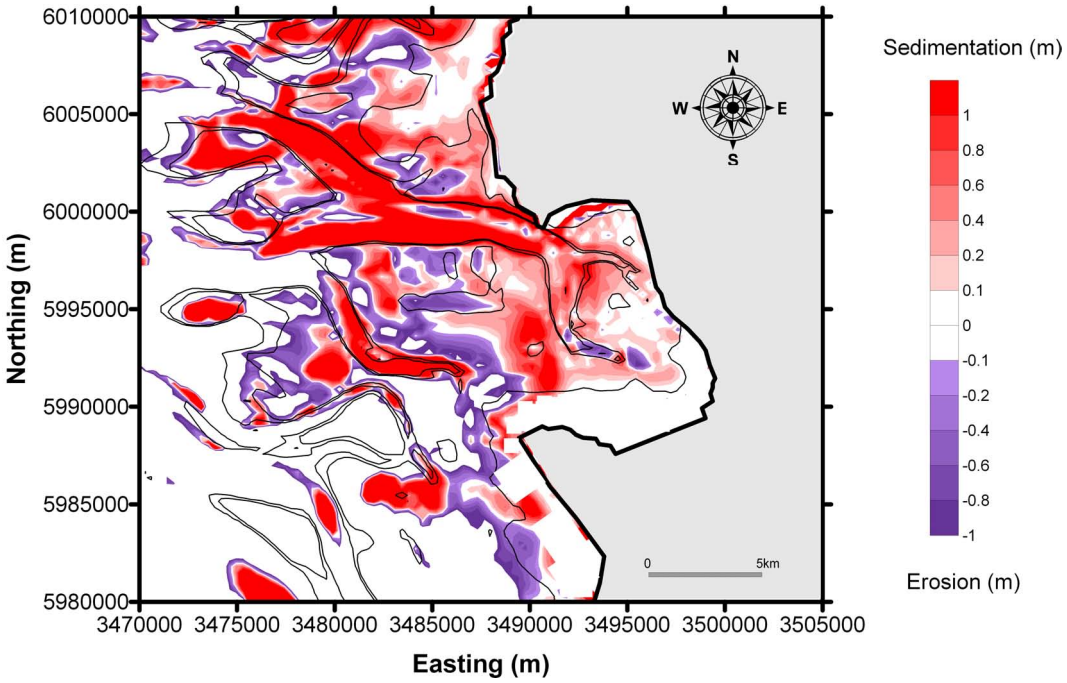

Figure 6.28: Bed level changes after one year resulting from a swell condition Hs=2.0m

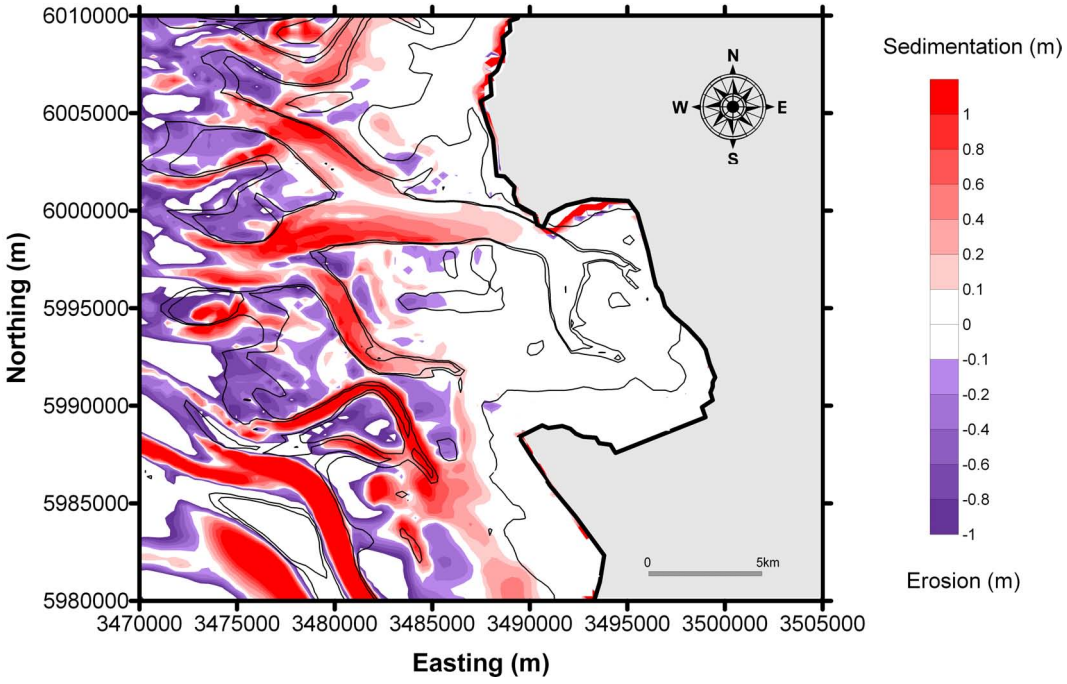

Figure 6.29: Bed level differences after one year between a swell conditions Hs=0.5m and 1.0m

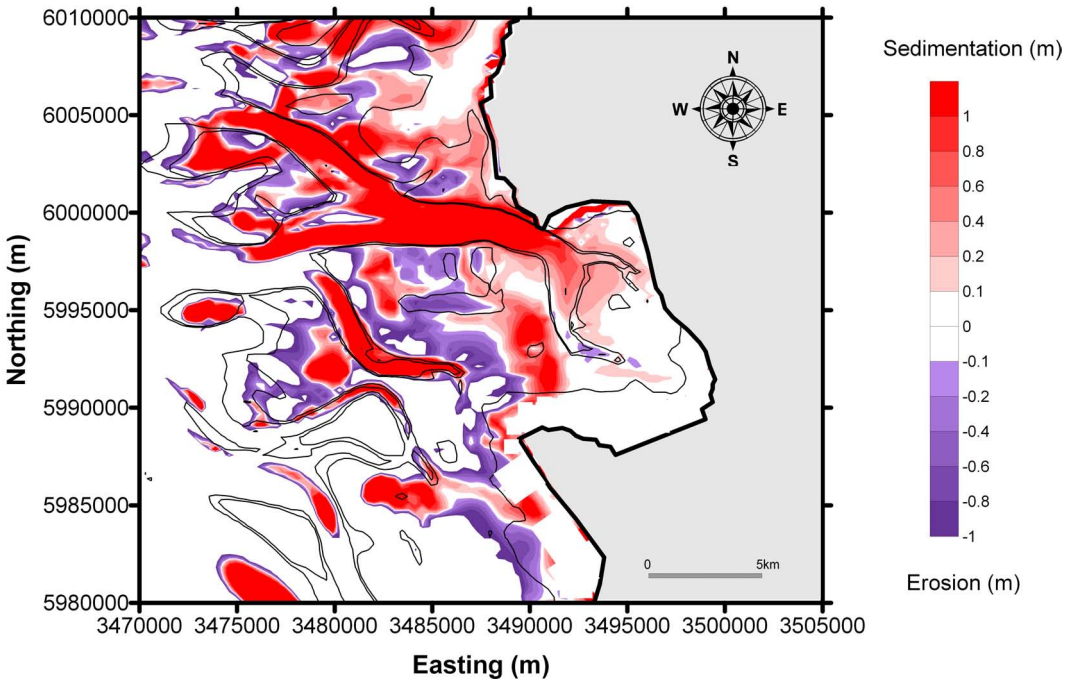

Figure 6.30: Bed level differences after one year between a swell conditions Hs=0.5m and 2.0m

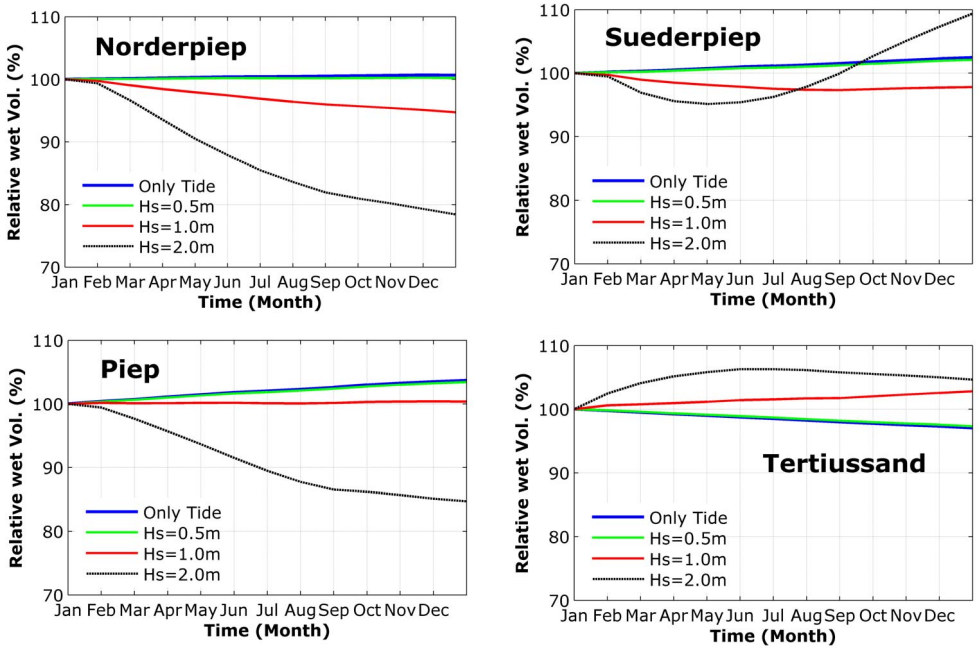

Figure 6.31: Relative wet volumes referred to the beginning of the simulation

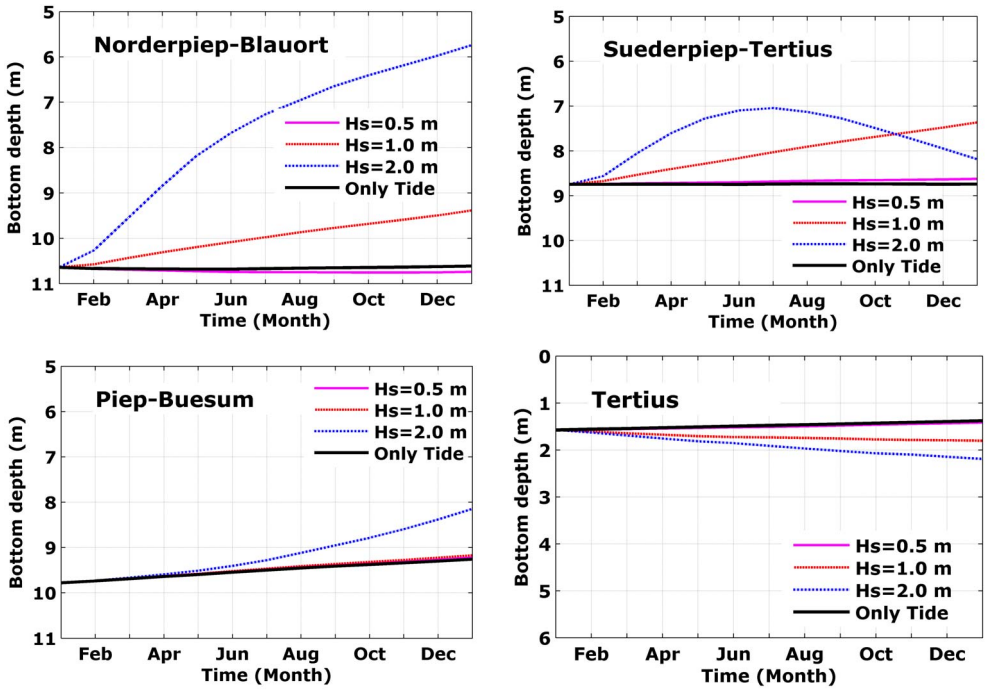

Figure 6.32: Bottom depth for different wave conditions

6.3.3.2 Effects of wave chronology on medium-term morphology

The order of the different wave conditions and probability of occurance is usually disregarded. In this section the chronology of the wave climate is investigated.
Fig. 6.33 and Fig. 6.34 show the bed level changes after one year referred to the starting of the simulation due to two chronology of wave climates (Section 6.2.3). It can be seen that the results are very similar for both wave climate sequences. This indicates that the final bed level are not sensitive to the choice of how the wave sequence is partitioned within the set-up of the used model.
The differences in the resulting bed levels between the two wave climate chronology are shown in Fig. 6.35. It shows that the differences can only be found in the south-western part of the domain with less than 0.1m sedimentation and erosion.

Fig. 6.36 shows the relative wet volume due to two different cases of wave sequences. It is acceptable to conclude that the defined wave chronology does not influence the computed morphological development. Also Fig. 6.37 verifies this conclusion.

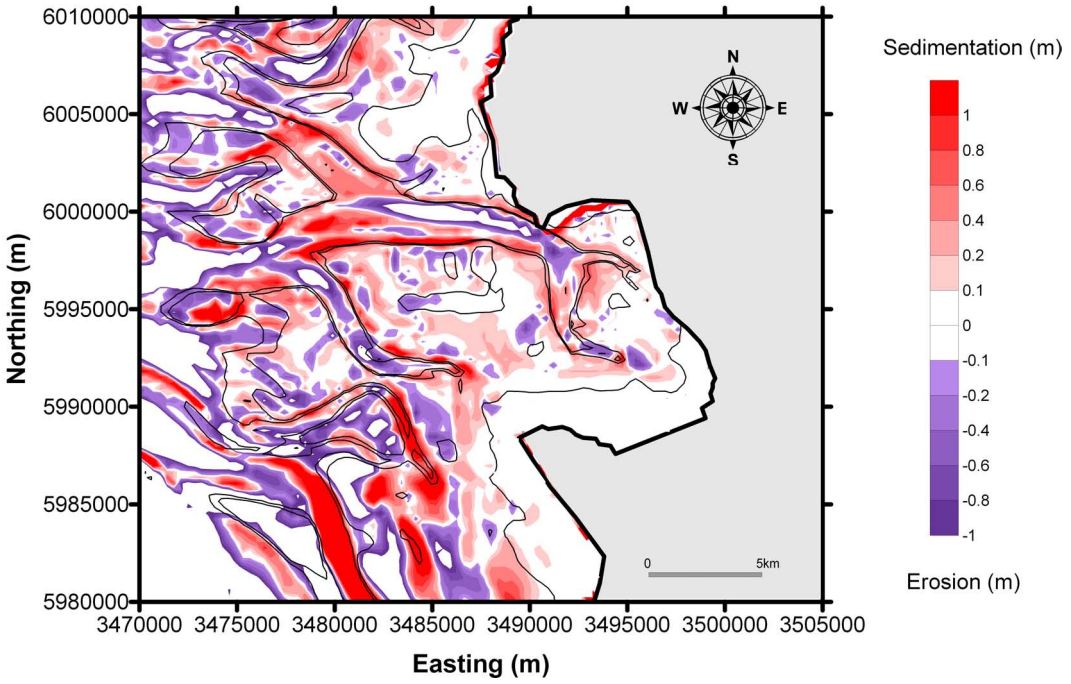

Figure 6.33: Bed level changes after one year resulting from first wave sequence (Hs(m)=0.5-1.0-2.0)

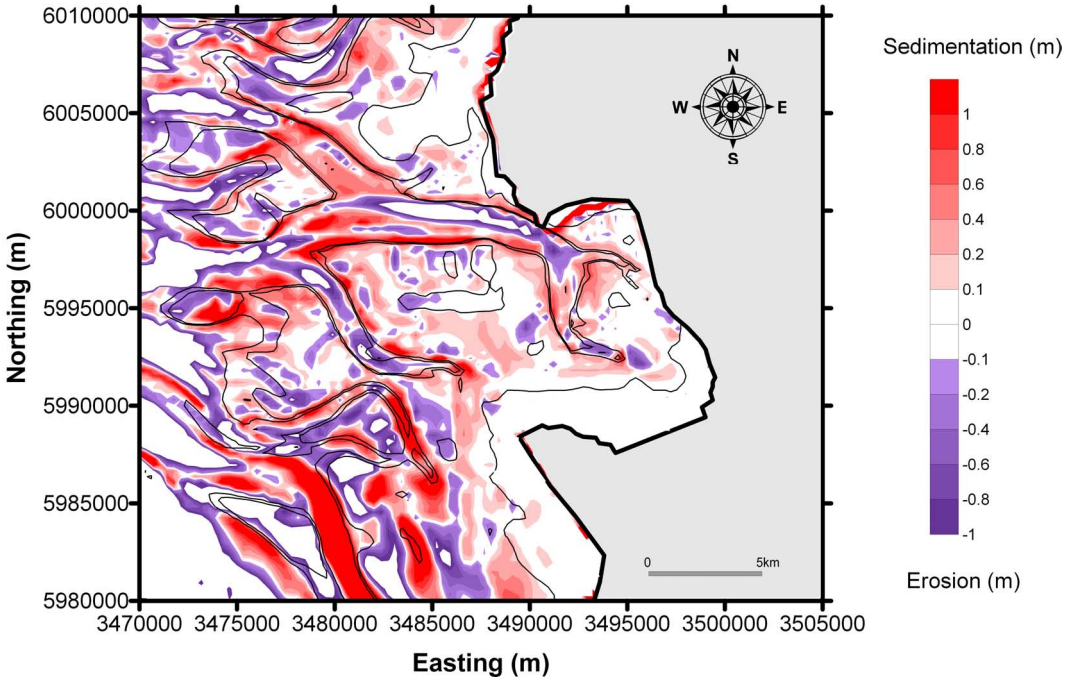

Figure 6.34: Bed level changes after one year resulting from second wave sequence (Hs(m)=2.0-1.0-0.5)

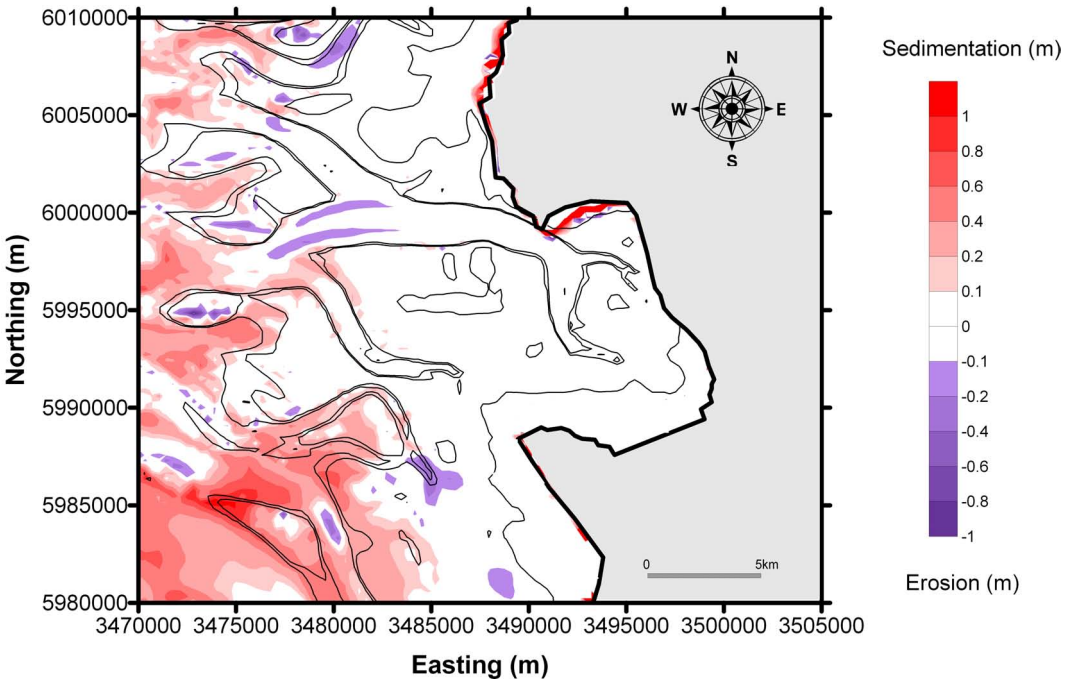

Figure 6.35: Bed level differences after one year between first and second wave sequences

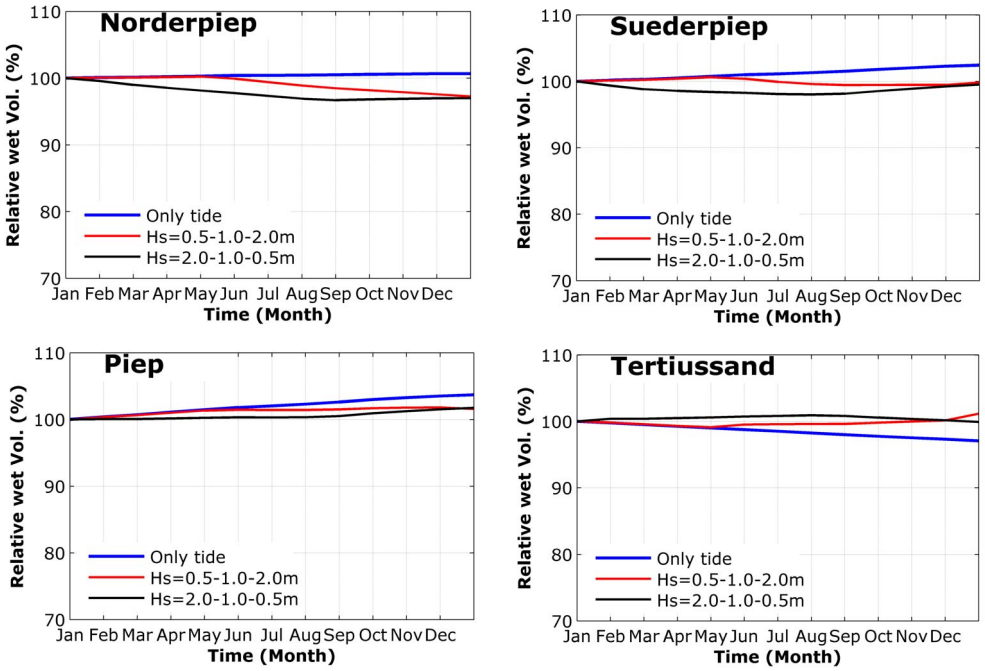

Figure 6.36: Relative wet volumes referred to the beginning of the simulation

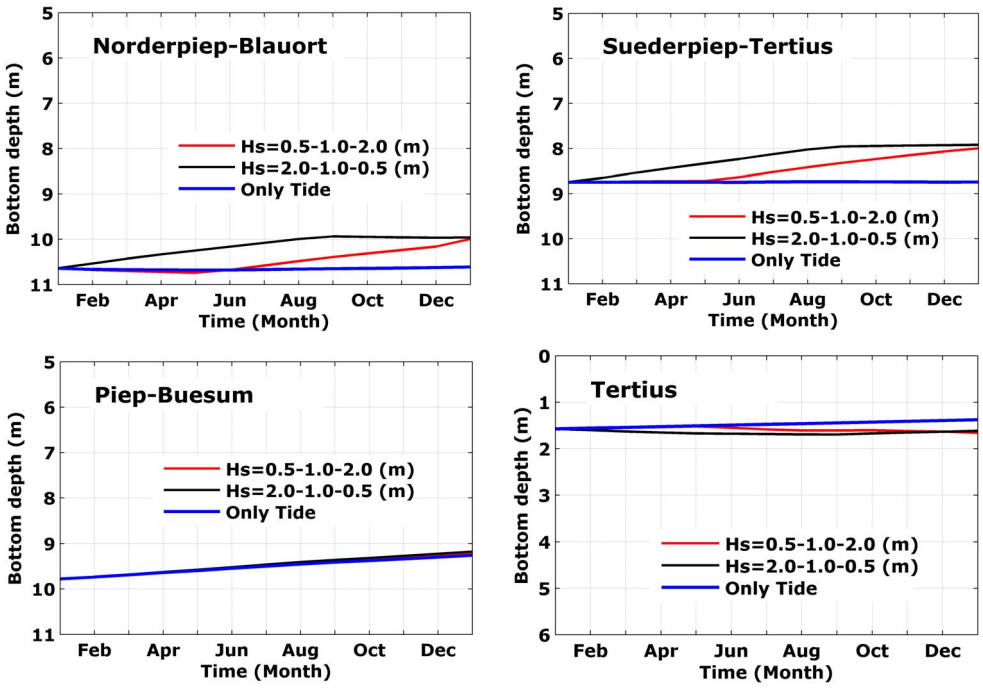

Figure 6.37: Bottom depth for different wave chronology

6.4 Discussion

The effect of storms on medium-term morphodynamics has been investigated by using a morphodynamic model with morphological acceleration factor approach. In this work the effect of the 1999 storm as well as the effect of the storm sequences on the morphological changes have been studied. In order to understand the effect of the storms on the morphological developments in the medium-term, simulations were also carried out for the tide only. Additional simulations to investigate the effect of the wave climates and the chronological effect of the wave climates have been done.

The results of the simulations showed that the tide only scenario is responsible for maintaining the tidal channels. On the other hand, the storms have an important influence on the medium-term morphodynamics where most of the morphological changes occur in the entire domain (tidal channel and tidal flats).

The simulation show that there is no indication that the storm sequences with a storm at the start or in the middle or at the end of the selected period have a markedly different effect on the morphodynamics.

The results show that the wave conditions cause an equalizing of the tidal flats and channels through erosion of the exposed tidal flats and sandbanks and filling of the channels. Moreover, the chronology of the wave climates does not show any important influence on the final morphology of the described model and for the simulation period. In summary, the results of the simulations show that the western part of the domain is clearly influenced by the wave conditions, the eastern part of the domain is highly tide-dominated and, the middle part is dominant by waves and locally generated waves due to storms.

Chapter 7

Conclusions and recommendations

7.1 Conclusions

The effectiveness of a process-based morphodynamic model for hindcasting bed elevation changes due to extreme storm events during short-term (a few days to a month) and medium-term (a few months to years) is demonstrated for a tidally dominated area on the German North Sea coast.
The results of the simulations served to improve our understanding of the underlying physical processes due to storm events.

Set-up of short-term morphodynamic model

The morphodynamic model was set-up based on the sensitivity studies for the main numerical and physical parameters, and the calibration and validation of the models against field data. In this study the cohesive material as well as the spatial distribution of several non-cohesive material classes were taken into account for the sediment transport model.

The results of individual models showed that each of the models was able to represent the behavior of the hydrodynamics and the sediment transport of the studied area in a detailed manner.

Not only the coupling of the models was carried out at every computing time step, the bathymetry was updated at every computing time step for the hydrodynamic and sediment transport as well. Therefore, the interaction between the models was properly represented in the results of the morphodynamic model.

To evaluate properly the effects of the storms two storm events (January, 1994 and December, 1999) were modelled. The two modelled storms not only showed the effect of the storms on the morphological changes, but also showed which storm event had a stronger influence on the morphology.

Two additional simulations using the same set-up short-term morphodynamic model but for one year period between 1994-1995 and 1999-2000 have been carried out. These simulations lead to comprehensive understanding of the recovery of the bathymetry after the storm events.

Morphological evolution due to storm events on the short-term

The short-term morphodynamic model has been applied to analyze the impact of the storm events on the morphological changes.
It is concluded that, due to the storms, there is a tendency towards erosion of the more exposed sandbanks and tidal flats, and deposition of the eroded material in the tidal channels. The morphological changes during the storm events were found to be in the order of 1m. This phenomena could be happened due to the fact that the waves break very close to the western boundaries, where the sandbaks are located. Approximately 80% of the total morphological changes, within the simulation period, took place during the storm event (from hours to a few days).

The results of the simulations showed that the intensity of the storm is one of the significant factors for the morphological changes. A similar morphological changes can be also obtained, when the characteristics of the storm itself is considered. It was found that sudden increases in the westerly wind speeds in conjunction with neap tidal conditions will lead to higher morphological activity (1999 storm). The gradual changes in the wind speed combined with spring tides results lower morphological changes in the area (1994 storm).

The morphological evolution due to the tide only shows very small changes, especially on the sandbank in the western part of the domain, where waves are the most dominant driving forces.

Morphological evolution due to recovery after the storms

The results of the numerical model for one year simulations between 1994-1995 and 1999-2000 showed different characteristics with regard to their morphodynamic behaviour, storm response and post-storm recovery.
In order to discriminate between the underlying reasons for the two periods different responses, one important factor that can be considered is the characteristics of the storm events during each period.
For both of the two periods the storm events occurred during the winter time but with different degree of intensity. The period with the higher intensity in terms of storm activity was during 1999-2000, and with storm number events as those present during the period of lower intensity (i.e. 1994-1995).

It is evident that the intensity of the storm events has an effect on the bed level changes. Additionally, it is clear that the return of the sediments during fair-weather conditions requires a longer period of time. It is also concluded that some summer storms could cause a possible delay of the recovery process.

Set-up of medium-term morphodynamic model

The medium-term morphodynamic model is based on the same individual process models that have been used in the short-term morphodynamic model. The process models are driven by specified open boundaries and coupled to a model for calculation of morphological changes of the considered period of one year.

The methodology presented in this study addresses the effects of the storms on the medium-term morphological development by carrying out several sensitivity simulations. A series of tests demonstrates different aspects of representative tides, storms, storm chronology, waves and wave chronology and the importance of each in the prediction of the morphological evolutions. The method provides means for both, understanding storms, waves, and their chronological effects, and predicting these effects in practical engineering problems involving medium-term changes to coastal morphology.

Morphological evolution due to storm events on the medium-term

The model runs show no significant variations in the computed morphological changes; either when the tidal conditions are represented by a representative tidal cycle or by astronomical conditions. Moreover, the effect of the tides only shows a high influence on the morphological changes in the tidal channels, where the erosion takes place.

It is concluded that the storm events has the most relevant influence on the medium-term morphodynamics (i.e. subject to one year). The maximum changes are in the order of 1 m and most of the erosion takes place on the tidal flats with sedimentation in the surrounding channels. Additionally, the storm will effect the tendency of the morphological evolution. Comparing the tendency resulting from the storm to that of the tide only conditions (erosion in the tidal channels and sedimentation on the sandbank), an opposite trend has been noticed.

There is no indication, with the used model set-up, that the sequences of the storm (storm at the beginning, at the middle and at the end of one year simulation) have markedly different effects on the final medium-term morphology.

Morphological evolution due to wave climate on the medium-term

It was shown that the wave conditions have a high influence on the medium-term morphology within the model set-up. It is concluded that the severe wave conditions has an extreme effect on the morphological changes compared to the medium and low wave conditions. Moreover, the low wave conditions proved to behave similarly to the tide only conditions.

It is also concluded that the final morphological changes are not sensitive to the way the wave sequence is partitioned (subject to the simulated wave conditions).

In other words, the wave chronology does not have a high influence on the final morphological changes within the model set-up.

7.2 Recommendations

This method of addressing the issue of storms and their sequencing in short- and medium-term morphodynamics and their effects on the morphology can be readily used for a better understanding of general types of morphodynamic behavior.

In the short-term morphodynamic model only two storm events have been imposed. Although a good understanding of the storm events was achieved, the application of the model to other storms from different years and different seasons may help to improve our understanding of storm effects on the morphological evolution.

The results of one year real time simulation, without using any morphological acceleration factor, for two different periods (1994-1995 and 1999-2000) give a clear idea of how recovery processes may happen after storm events. It would be important to extend the simulation for longer period to capture the recovery from the storms completely.

The results of one year simulation, using a morphological acceleration factor, show that there are significant effects due to the inclusion of the storms. It could also be important to study how the model would recover from the effect of the storms. This could be possible by extending the period of the simulation longer that one year.

In the wave model, the waves were constant in space along the open sea boundaries. Therefore imposing variable waves could improve the wave representation.

In the sediment transport model, the open sea boundaries for the sediment transport should be consider as this might particularly relevant for sedimentation along the boundaries.

In all of the simulations that have been carried out a two-dimensional depth-averaged (2Dh) approach has been applied. Although it was found that the 2Dh approximation seems to be appropriate for describing the morphological changes on the short- and medium-term, comparisons of the results with those using a 3D approximation is recommended.

References

Asp, N.E., 2004, Long to short-term morphodynamics of the tidal flats in the Dithmarschen Bight, German North Sea, Ph.D. thesis, University of Kiel, Germany.

Benkel, A. and Groβe,G., 2005, Meteorological data and wind field modelling in the Dithmarschen Bight, Die Küste, Heft 69, 129-140.

Bijker, E.W., 1971, Longshore transport computations, Journal of the Waterways, Harbors and Coastal Engineering Division, WW4, 687-701.

BMFT, 1994, Optimierung des Küstenschutzes auf Sylt - Phase II, Bundesministerium für Forschung und Technologie, Amt für Ländliche Räume, Husum, In German.

Booij, N., Ris, R.C., and Holthuijsen, L.H., 1999, A third-generation wave model for coastal regions, Part I, Model description and validation, Journal of Geophysical Research, Volume 104(C4), 7649-7666.

Chesher, T.J. and Miles, G.V., 1992, The concept of a single representative wave. In: R.A. Falconer, S.N. Chandler-Wilde and S.Q. Liu (Editors), Hydraulic and Environmental Modelling, Coastal Waters, Ashgate, Brookfield, VT, 371-380.

De Vriend, H.J., 1987, 2DH mathematical modelling of morphological evolutions in shallow water,Coastal Engineering, Volume 11, 1-27.

De Vriend, H.J., Zyserman, J., Nicholson, J., Roelvink, J.A., and Southgate, H.N., 1993, Medium-term 2DH coastal area modelling, Coastal Engineering, Volume 21, 193-224.

De Vriend, H.J., Capobianco, M., Chesher, T., De Swart, H.E., Latteux, B., and Stive, M.J.F., 1993, Approaches to long-term modelling of coastal morphology: a review, Coastal Engineering, Volume 21, 225-269.

De Vriend, H.J., 1997, Prediction of aggregated-scale coastal evolution (PACE), In: Thornton, M.B., and Huntley, D.A. (eds.), Coastal Dynamics 97.

De Vriend, H.J., 1998, Large-scale coastal morphological predictions: a matter of upscaling?, Proceeding of the third international conference on hydroscience and

engineering.

Deigaard, R. and Jϕrgen Fredsϕe, 1989, Shear stress distribution in dissipative water waves, Coastal Engineering, Volume 13, 357-378.

Dingemans, M.W., A.C. Radder and H.J. de Vriend, 1987, Computation of the driving forces of wave-induced currents, Coastal Engineering, Volume 11, 539-563.

Delft3D-Flow Simulation of multi-dimensional hydrodynamic flows and transport phenomena, including sediments, 2006, User Manual, November 2006, WL|Delft Hydraulics.

Delft3D-Wave Simulation of short-crested waves with SWAN, 2006, User Manual, November 2006, WL|Delft Hydraulics.

DWD, 2000, Orkantief Anatol vom 3./4. Dezember 1999, Homepage of the German Meteorological Service (Deutsche Wetter Dienst), In German.

Ehlers, J., 1988, The morphodynamics of the Wadden Sea, A.A. Balkema, Rotterdam, 397pp.

Escobar, C.A.S. and Mayerle, R., 2006, Procedures for improving the predection of equilibrium grain sizes, bed forms and roughness in tidally-dominated areas, Proc. of the 30^{th} International Conference on Coastal Engineering, ICCE 2006, San Diego, California, USA, 3092-3104.

Escobar, C.A.S., 2007, Modelling of sediment dynamics in the Dithmarschen Bight, German North Sea coast, Ph.D. thesis, University of Kiel, Germany.

Fredsoe, J. and R. Deigaard, 1992, Mechanics of Coastal Sediment Transport. Advanced Series on Ocean Engineering, Volume 3, World Scientific Singapore.

Hayes, M.O., 1979, Barrier island morphology as a function of tidal and wave regime, In: Leatherman, S.P. (eds.) Barrier Islands from the Gulf of St. Lawrence to the Gulf of Mexico.

Hofstede, J.L.A., 1997, Process-response analysis for the North Frisian supratidal sands (Germany), Journal of Coastal Research, Volume 13, 1-7.

Holthuijsen, L.H., Booij, N., and Herbers, T.H.C., 1989, A prediction model for stationary, short-crested waves in shallow water with ambient currents, Coastal Engineering, Volume 13, 23-54.

IPCC, 2007, M.L. Parry, O.F. Canziani, J.P. Palutikof, P.J. van der Linden and C.E. Hanson, Eds., Climate Change 2007: Impacts, Adaptation and Vulnerability. Contribution of Working Group II to the Fourth Assessment Report of the Intergovernmental Panel on Climate Change, Cambridge University Press, Cambridge,

UK, 976pp.

Kesper, J., 1992, Sedimentdynamik ausgewälter Auensände vor der Schleswig-Holsteinischen Westküste, Ph.D. thesis, University of Kiel, Germany, In German.

Latteux, B., 1995, Techniques for long-term morphological simulation under tidal action, Marine Geology, Volume 126, 129-141.

Lesser, G.R., Roelvink, J.A., van Kester, J.A.T.M. and Stelling, G.S., 2004, Development and validation of a three-dimensional morphological model, Coastal Engineering, Volume 51, 883-915.

Luthardt, H., 1987, Analyse der wassernahen Druck- und Windfelder über der Nordsee aus Routinebeobachtungen, Hamburger Geophysikalische Einzelschriften, Reihe A 83, In German.

Mayerle, R. and Zielke, W., 2005, Prediction of medium-scale morphodynamics: Project overview and executive summary, Die Küste, Heft 69, 1-23.

Mayerle, R., Wilkens, J., Escobar, C.A.S. and Windupranata, W., 2005, Hydrodynamics forcing along the open sea boundaries of small-scale coastal models, Die Küste, Heft 69, 203-228.

Nielinger, J., 1998, Kopplung numerischer Simulationsmodelle zur Regionalisierung von Ergebnissen globaler Klimaszenarien, Berichte des Instituts für Meteorologie und Klimatologie der Universität Hannover, Nr. 57, 131p, In German.

Niemeyer, H.D., Goldenbogen, R., Schroeder, E., and Kunz, H., 1995, Untersuchungen zur Morphodynamik des Wattenmeeres im Forschungsvorhaben WADE, Die Küste, Heft 57, In German.

OSPAR Commission, 2000, Quality Status Report 2000, Region II - Greater North Sea, OSPAR Commission, London, 136pp.

Phillips, O.M., 1957, On the Generation of Waves by Turbulent Winds, Journal of Fluid Mechanics, Volume 2, 417-445.

Phillips, O.M., 1960, On the Dynamics of Unsteady Gravity Waves of Finite Amplitude, 1. The Elementary Interactions, Journal of Fluid Mechanics, Volume 9, 193-217.

Palacio, C., Mayerle, R., Toro, M. and Jimènez, N., 2005, Modelling of flow in tidal flat area in the south eastern German Bight, Die Küste, Heft 69, 141-174.

Palacio, C., 2002, Calibration and validation of the flow model using extensive field measurement data, Coastal Research Laboratory (CORELAB), Germany, Report no. 15-01.

Palacio, C., Winter, C. and Mayerle, R., 2001, Set-up of a hydrodynamic model for the Meldorf Bight, Proceedings of the World Water and Environmental Resources Congress, ASCE/EWRI, Orlando.

Poerbandono, 2003, Sediment transport measurements and modelling in the Meldorf Bight tidal channels, German North Sea coast, Ph.D. thesis, University of Kiel, Germany.

Poerbandono and Mayerle, R., 2003, Field measurements of sediment dynamics in tidal channels: Preliminary results, Proc. of the 5^{th} International symposium on coastal engineering and science of coastal sediments process, Florida, USA.

Poerbandono and Mayerle, R., 2005, Composition and dynamics of sediments in tidal channels of the German North Sea Coast, Die Küste, Heft 69, 61-91.

Reimers, H.C., 2003, Sedimentverteilung und Benthosverbreitung in den Watten der Dithmarscher Bucht als Indikator für morphodynamische Veränderungen, Abschluβbericht zum Forschungsvorhaben SEDIMORV im GKSS-Hochschulprogramm, GKSS Research Centre Geesthacht, Germany, Report no. GKSS 2003/18, In German.

Reyes, J.L., Martins, J. T., Benavente, J., Ferreira, O, Gracia, F. J., Alveirinho-Dias, J. M. and Lopez-Aguayo, F., 1999, Gulf of Cadiz beaches: A comparative response to storm events, Boletin del Instituto Espanol de Oceanografia, Volume 15 (1-4), 221-228.

Ricklefs, K. and Asp, N.E.N., Geology and morphodynamics of a tidal flat area along the German North Sea coast, Die Küste, Heft 69, 93-127.

Ris, R.C., Booij, N., and Holthuijsen, L.H., 1999, A third generation wave model for coastal regions, Part II, Verification, Journal of Geophysical Research, Volume 104(C4), 7667-7682.

Roelvink, J.A. and Van Banning, G.K.F.M., 1994, Verwey, Minns, Babovic and Maksimovic (eds), Design and development of DELFT3D and application to coastal morphodynamics, Hydroinformatics 1994, Balkema, Rotterdam.

Roelvink, J. A., 2006, Coastal morphodynamic evolution techniques, Coastal Engineering, Volume 53, 277-287.

Soares, C. G., Carretero, J. C., Weiβe, R., Alvarez, E., 2002, A 40 years hindcast of wind, sea level and waves in European waters, Proceedings of 21^{st} international conference on offshore mechanics and arctic engineering, Oslo, Norway.

Sorensen, R. M., 2006, Basic coastal engineering, Third edition, Springer Science and Business Media, 324pp.

Soulsby, R.L., L. Hamm, G. Klopman, D. Myrhaug, R.R. Simons and G.P. Thomas, 1993, Wave-current interaction within and outside the bottom boundary layer, Coastal Engineering, Volume 21, 41-69.

Southgate, H. N., 1995, The effect of wave chronology on medium and long term coastal morphology, Coastal Engineering, Volume 26, 251-270.

SPM, 1984, Shore Protection Manual, Waterways Experiment Station, US Army Corps of Engineers, Vicksburg, MS.

Steijn, R.C., 1989, Schematization of the natural conditions in multi-dimensional numerical models of coastal morphology. Delft Hydraulics, Rept. H526-1.

Steijn, R.C., 1992, Input filtering techniques for complex morphological models. Delft Hydraulics, Rept. H824.53.

Steijn, R.C. and Hartsuiker, G., 1992, Morphodynamic response of a tidal inlet after a reduction in basin area, Delft Hydraulics, Coastal Genesis Rept. H840.00, 75pp.

Sündermann, J., Hesse, K.J., Beddig, S. and Wilkens, J., 1999, Coastal mass and energy fluxes in the southeastern North Sea, German Journal of Hydrography, Volume 51, No. 2/3, 113-132.

Toro, F., Mayerle, R., Poerbandono and Wilkens, J., 2005, Patterns of hydrodynamics in a tide-dominated coastal area in the south-eastern German Bight, Die Küste, Heft 69, 25-62.

Van Maren, D.S., 2004, Morphodynamics of a cyclic prograding delta: the Red River, Vietnam, Ph.D. thesis, Utrecht University, The Netherlands.

Van Overeem, J., Steijn, R.C. and Van Banning, G.K.F.M., 1992, Simulation of morphodynamics of tidal inlet in the Wadden Sea, In: H. Sterr, J. Hofstede and H.-P. Plag (Editors), Proc. Int. Coastal Congress, Kiel, Peter Lang Veflag, Frankfurt am Main, 351-364.

Van Rijn, L.C., Walstra, D.J.R., Grasmeijer, B., Sutherland, J., Pan, S., Sierra, J.P., 2003, The predictability of cross-shore bed evolution of sandy beaches at the time scale of storms and seasons using process-based Profile models, Coastal Engineering, Volume 47, 295-327.

Van Rijn, L.C., 1984, Sediment transport: Part I: Bed load transport; Part II: Suspended load transport, Journal of Hydraulic Engineering, 110.

Vela-Diez, S., 2001, Sediment mapping of the tidal flat channels of Büsum, MSc thesis, University of Kiel, Germany.

Verboom, G.K. and A. Slob, 1984, Weakly-reflective boundary conditions for two-dimensional water flow problems. 5^{th} Int. Conf. on Finite Elements in Water Resources, June 1984 Vermont, also Adv. Water Resources, Vol. 7, December 1984 Delft Hydraulics publication No. 322.

Verboom, G.K., Ronde, J.G. de and Dijk, R.P. van, 1992, A fine grid tidal flow and storm surge model of the North Sea, Continental Shelf Research, Volume 12, No. 2/3, 213-233.

Weiβe, R., Feser F. and Günther, H., 2003, Wind- und Seegangsklimatologie 1958-2001 für die suedliche Nordseee basierend auf Modellrechnungen, GKSS Research Centre Geesthacht, Germany, Report no. 2003/10, 38pp, In German.

Wilkens, J. and Mayerle, R., 2001, Wave modelling in the Dithmarschen Bight, Coastal Research Laboratory (CORELAB), Germany, Report no. 02-01.

Wilkens, J., 2004, Medium scale morphodynamics of the central Dithmarschen Bight, Ph.D. thesis, University of Kiel, Germany.

Wilkens, J., Junge, I. and Hoyme, H., 2005, Modelling of waves in a tidal flat area in the south-eastern German Bight, Die Küste, Heft 69, 175-201.

Wilkens, J. and Mayerle, R., 2005, Morphodynamic response to natural and anthropogenic influences in the German Bight, Die Küste, Heft 69, 311-337.

Winter, C. and Mayerle, R., 2003, Calibration and validation of a sediment transport model with extensive data-sets for a tidal channel system in German Wadden Sea, Proc. of the 5^{th} International symposium on coastal engineering and science of coastal sediments process, Florida, USA.

Winter, C., Chiou, M.Da, Riethmüller, R., Ernstsen, V.B., Hebbeln, D. and Flemming, B.W. (Editors), 2006, The concept of representative tides in morphodynamic numerical modelling, Geo-Marine Letters, Volume 26, Number 3, September, 2006, 125-132, Springer Berlin / Heidelberg, Germany.

Zanke, U. and Mewis, P., 2002, The morphodynamic simulation system TIMOR, Wasser und Boden, 54/4, 14-22, In German.

Zhang, K., Douglas, B. and Leatherman, S., 2002, Do storms cause long-term beach erosion along the U.S. east barrier coasts?, The Journal of Geology, Volume 110, 493-502.

Erklärung

Hiermit erkläre ich, dass die Abhandlung -abgesehen von der Beratung durch meine akademischen Lehrer, nach Inhalt und Form meine eigene Arbeit ist. Diese Arbeit hat an Keiner anderen Stelle im Rahmen eines Prüfungsverfahrens vorgelegen. Auβerdem erkläre ich, dass diese mein erster Promotionsversuch ist.

Kiel, den 24. Oktober 2007

Talal Etri

Curriculum Vitae

Personal details

Name:	TALAL A. MOHAMED **ETRI**
Date of birth:	05 September 1972
Place of birth:	Tripoli, Libya
Nationality:	Libyan
Sex:	Male
Marital statues:	Married
Address:	Jungmannstr. 21, 24105 Kiel, Germany
Phone:	+49 431 880 2797
Fax:	+49 431 880 7303
Email:	etri@corelab.uni-kiel.de

Academic qualification

2000-2002	M.Sc. degree, Computational Engineering, Ruhr-Universität Bochum, Bochum, Germany
1990-1995	B.Sc. degree, Civil Engineering, ALFATEH University, Tripoli, Libya
1987-1990	General secondary school certificate, scientific division, Tripoli, Libya
1984-1987	Preparatory secondary school certificate, Tripoli, Libya
1978-1984	Elementary secondary school certificate, Tripoli, Libya

Working experience

April 2003-2007	Research co-worker at the Coastal Research Laboratory, Christian-Albrechts-Universität zu Kiel, Germany
April 2002-September 2002	Master thesis at Okayama University, Okayama, Japan
October 2000-April 2002	Computational Eng., Ruhr Universität Bochum, Bochum, Germany
May 2000-September 2000	German language course, Berlin, Germany
August 1998-April 2000	National Consulting Bureau, Tripoli, Libya
July 1997-June 1998	Brega and Ras Lanuf Higher committee (National service), Brega, Libya
1995-May 1997	Free work, Libya

Appendix A

DELFT3D Modeling System

The two-dimensional depth-integrated process-based model implemented was developed on the basis of the on-line with morphological factor Delft3D modelling system (Lesser et al., 2004).

A.1 Hydrodynamic Model

The 2D or 3D flow model that has been developed by WL|Delft Hydraulics is based in general on the shallow water equations including the effects of tides, wind, density currents, waves, spiral motion and turbulence models including the k-ϵ model (Roelvink and van Banning, 1994).
The system equation even, in two (depth-averaged) or three dimensions, consist of the horizontal momentum equations, the continuity equation, the transport equation and a turbulence closure model. The vertical momentum equation is simplified assuming hydrostatic pressure relation as vertical acceleration are assumed to be small compared to gravitational acceleration and are not taken into account. Therefore the DELFT3D-FLOW model suitable for predicting the flow in shallow seas, coastal areas, estuaries, lagoons, rivers and lakes. It aims to model flow phenomena of which the horizontal length and time scales are significantly larger than the vertical scales (Lesser et. al, 2004).

The Delft3D-FLOW model, that has been used in this study, takes into account the following physical phenomena (Delft3D Flow manual, 2006):

- Free surface gradients (barotropic effects);
- The effect of the Earth's rotation (Coriolis force);
- Water with variable density (equation of state);
- Horizontal density gradients in the pressure (baroclinic effects);
- Turbulence induced mass and momentum fluxes (turbulence closure models);
- Transport of salt, heat and other scalar constituents;

- Tidal forcing at the open boundaries;
- Space and time varying wind shear-stress at the water surface;
- Space varying shear-stress at the bottom;
- Space and time varying atmospheric pressure on the water surface;
- Time varying sources and sinks (e.g. river discharges);
- Drying and flooding of tidal flats;
- Heat exchange through the free surface;
- Evaporation and precipitation;
- Tide generating forces;
- Effect of secondary flow on depth-averaged momentum equations;
- Lateral shear-stress at wall;
- Vertical exchange of momentum due to internal waves;
- Influence of waves on the bed shear-stress (2D and 3D);
- Wave induced stresses (radiation stress) and mass fluxes;
- Flow through hydraulic structures;
- Wind driven flows including cyclonic / hurricane / typhoon winds.

The model gives the possibility to solve the hydrodynamic equations on a cartesian rectangular, orthogonal curvilinear (boundary fitted), or spherical grid. For the orthogonal curvilinear grid the geographic space is defined in (ξ,η) coordinates along the grid and the shallow water equations are given as the following:

Continuity equation

The depth-averaged continuity equation is given by:

$$\frac{\partial \zeta}{\partial t} + \frac{1}{\sqrt{G_{\xi\xi}}\sqrt{G_{\eta\eta}}} \frac{\partial[(d+\zeta)u\sqrt{G_{\eta\eta}}]}{\partial \xi} + \frac{1}{\sqrt{G_{\xi\xi}}\sqrt{G_{\eta\eta}}} \frac{\partial[(d+\zeta)v\sqrt{G_{\xi\xi}}]}{\partial \eta} = Q \quad \text{(A.1)}$$

Where:

d : water depth below some horizontal plane of reference (datum) [m];

ζ : Water level above some horizontal plane of reference (datum) [m];

ξ, η : Horizontal curvilinear coordinates;

$\sqrt{G_{\xi\xi}}$: Coefficient used to transform curvilinear to rectangular coordinates [m];

u : Flow velocity in the ξ- direction [m/s];

v : Flow velocity in the η- direction [m/s];

Q : Global source or sink per unit area [m/s].

with Q representing the contributions per unit area due to the discharge or withdrawal of water, precipitation and evaporation and could be expresed in eq.A.2:

$$Q = (d + \zeta) \int_1^0 (q_{in} - q_{out}) d\sigma + P - E \tag{A.2}$$

where:
q_{in} : The local sources of water per unit of volume [1/s];

q_{out} : The local sinks of water per unit of volume [1/s];

P : The non-local source term of precipitation;

E : Non-local sink term due to evaporation;

σ : The vertical direction of the coordinate system, which described in eq.A.3

$$\sigma = \frac{z - \zeta}{d + \zeta} \tag{A.3}$$

Momentum equations in horizontal direction

The momentum equations in ξ - and η -direction are given by:

$$\frac{\partial u}{\partial t} + \frac{u}{\sqrt{G_{\xi\xi}}}\frac{\partial u}{\partial \xi} + \frac{v}{\sqrt{G_{\eta\eta}}}\frac{\partial u}{\partial \eta} + \frac{uv}{\sqrt{G_{\xi\xi}}\sqrt{G_{\eta\eta}}}\frac{\partial \sqrt{G_{\xi\xi}}}{\partial \eta}$$

$$-\frac{v^2}{\sqrt{G_{\xi\xi}}\sqrt{G_{\eta\eta}}}\frac{\partial \sqrt{G_{\eta\eta}}}{\partial \xi} - f_v = -\frac{1}{\rho_o \sqrt{G_{\xi\xi}}} P_\xi + F_\xi + M_\xi \tag{A.4}$$

and:

$$\frac{\partial v}{\partial t} + \frac{u}{\sqrt{G_{\xi\xi}}}\frac{\partial v}{\partial \xi} + \frac{v}{\sqrt{G_{\eta\eta}}}\frac{\partial v}{\partial \eta} + \frac{uv}{\sqrt{G_{\xi\xi}}\sqrt{G_{\eta\eta}}}\frac{\partial \sqrt{G_{\eta\eta}}}{\partial \xi}$$

$$-\frac{u^2}{\sqrt{G_{\xi\xi}}\sqrt{G_{\eta\eta}}}\frac{\partial\sqrt{G_{\xi\xi}}}{\partial\eta} - f_u = -\frac{1}{\rho_o\sqrt{G_{\eta\eta}}}P_\eta + F_\eta + M_\eta \tag{A.5}$$

Where:

f_u,f_v : Coriolis coefficient (inertial frequency) $[\frac{1}{s}]$;

ρ : reference density of water $[\frac{kg}{m_3}]$;

P_ξ : gradient hydrostatic pressure in ξ-direction $[\frac{kg}{m^2s^2}]$;

P_η : gradient hydrostatic pressure in η-direction $[\frac{kg}{m^2s^2}]$;

F_ξ : turbulent momentum flux in ξ-direction $[\frac{m}{s^2}]$;

F_η : turbulent momentum flux in η-direction $[\frac{m}{s^2}]$;

M_ξ : source or sink of momentum in ξ-direction $[\frac{m}{s^2}]$;

M_η : source or sink of momentum in η-direction $[\frac{m}{s^2}]$;

Hydrostatic pressure assumption

Under the shallow water assumption the vertical momentum equation reduces to the hydrostatic pressure equation. Under this assumption vertical acceleration due to buoyancy effects or sudden variations in bottom topography is not taken into account. The resulting expression is

$$\frac{\partial P}{\partial\sigma} = -\rho g h \tag{A.6}$$

in which the horizontal pressure terms, P_x and P_y are given by Boussinesq approximations (eqs.A.7 and A.8)

$$\frac{1}{\rho_o\sqrt{G_{\xi\xi}}}P_\xi = \frac{g}{\sqrt{G_{\xi\xi}}}\frac{\partial\xi}{\partial\zeta} + \frac{1}{\rho_o\sqrt{G_{\xi\xi}}}\frac{\partial P_{atm}}{\partial\xi} \tag{A.7}$$

$$\frac{1}{\rho_o\sqrt{G_{\eta\eta}}}P_\eta = \frac{g}{\sqrt{G_{\eta\eta}}}\frac{\partial\eta}{\partial\zeta} + \frac{1}{\rho_o\sqrt{G_{\eta\eta}}}\frac{\partial P_{atm}}{\partial\eta} \tag{A.8}$$

Coriolis force

The Coriolis parameter f depends on the geographic latitude and the angular speed of rotation of the earth, Ω: $f = 2\Omega\sin\phi$. For a curvilinear grid you should specify the space varying Coriolis parameter, using a suitable projection.

Reynolds stresses

The forces F_ξ and F_η in the momentum equations represent the unbalance of horizontal Reynold's stresses. The Reynolds stresses are determined using the eddy viscosity concept. This concept expresses the Reynolds stress component as the product between a flow-dependent eddy viscosity coefficient and the corresponding components of the mean rate-of-deformation tensor. Therefore for large-scale simulations, when shear stresses along closed boundaries may be neglected, the forces F_ξ and F_η reduce to the simplified formulations as in eqs.A.9 and A.10

$$F_\xi = v_H \left(\frac{1}{\sqrt{G_{\xi\xi}}\sqrt{G_{\xi\xi}}} \frac{\partial^2 u}{\partial \xi^2} + \frac{1}{\sqrt{G_{\eta\eta}}\sqrt{G_{\eta\eta}}} \frac{\partial^2 u}{\partial \eta^2} \right) \tag{A.9}$$

$$F_\eta = v_H \left(\frac{1}{\sqrt{G_{\xi\xi}}\sqrt{G_{\xi\xi}}} \frac{\partial^2 v}{\partial \xi^2} + \frac{1}{\sqrt{G_{\eta\eta}}\sqrt{G_{\eta\eta}}} \frac{\partial^2 v}{\partial \eta^2} \right) \tag{A.10}$$

In general the model solves the equations of motions and momentum using an *Alternating Direction Implicit* (ADI) finite-difference scheme. The numerical stability is not resticted by the time step Δt or by grid size, because the solution is implicit. However the accuarcy of the flow decreases with increasing Δt. In order to optimize the time step with which the model still produces accurate results the courant number c_rr is evaluated:

$$C_r = 2\Delta t \sqrt{gh} \sqrt{\frac{1}{\Delta x^2} + \frac{1}{\Delta y^2}} < 10 \tag{A.11}$$

Where Δx and Δy are the length of the grid cells in x and y direction in (m), respectively, g is the gravitational acceleration ($m^2 s^{-1}$) and h is the water depth (m) (van Maren, 2004).

A.1.1 Model grid and bathymetry

As mentioned before DELFT3D uses a curvilinear staggered grid (Arakawa C-grid) where the depth points are defined at the centre of each grid cell, velocity points at the mid-points of the grid cell side, and water level points at each grid cell corner (see Fig. A.1). The processes that can be accurately simulated with a numerical model depend on the grid cell size. The computational time increases with decreasing grid cell size for two reasons. The first reason is the computational time increases linearly with the amount of grid cells and the second reason is the computational time step Δt decreases with decreasing grid cell size. Moreover, the boundary conditions have to be sufficiently far away to avoid disturbances to enter the area of interest. The optimal grid design is therefore a compromise in which all relevant processes are accurately numerically simulated while the computational time remains acceptable.(van Maren, 2004).

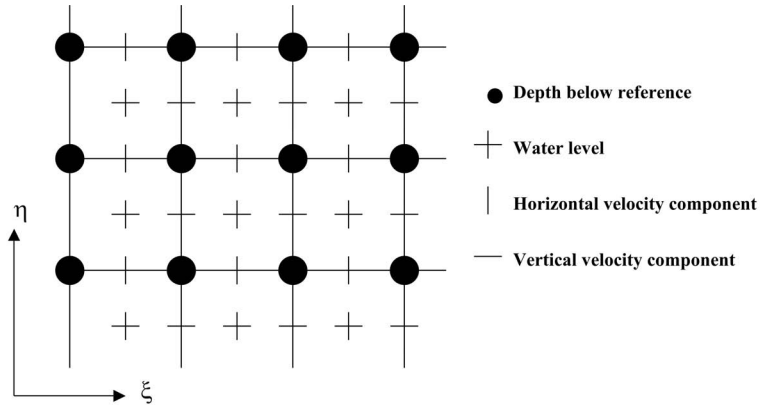

Figure A.1: DELFT3D staggered grid

A.2 Wave model

Wave effects can be also be included in DLFT3D simulation by running the separate DELFT3D-WAVE or on-line with flow model. The DELFT3D-WAVE model is performed using the second-generation Hindcasting Shallow Water Waves (HISWA) wave model (Holthuijsen et al., 1989) or the third generation Simulating Waves Nearshore (SWAN) wave model (Booij, et al., 1999 and Ris et al., 1999). A significant practical advantage of using the SWAN model is that it could run on the same curvilinear grids as are commonly used for DELFT3D-FLOW calculations.
In situations where the water level, bathymetry, or flow velocity field change significantly during the flow simulation, it is often desirable to call the wave model more than once (Lesser et al., 2004).
In coastal seas the wave action may influence morphology for a number reasons. The following processes are presently available in DELFT3D-FLOW (more details please see Section 2.3.2.1)

1. Wave forcing due to breaking (by radiation stress gradients);
2. Improvement of the bed shear-stress by wave;
3. Stokes drift and mass flux;
4. Streaming (wave-induced current in the bottom layer);
5. Wave-induced turbulence;

A.3 Sediment transport model

The total sediment transport is determined by the bed load transport and suspended load transport.

A.3.1 Suspended sediment transport

In the on-line sediment of DELFT3D FLOW, several formulations are required to fully describe the behaviour of the sediments as the following:

- Density effects;
- Settling velocity;
- Sediment exchange with the bed;
- Vertical diffusion coefficient for sediment;
- Suspended sediment correction vector.

A.3.2 Bedload sediment transport

For the bedload sediment the magnitude and direction of the bedload sand transport are computed using one of two formulations presented by van Rijn depending on whether waves are present in the simulation. The computed sediment transport vectors are then relocated from water level points t velocity points using an upwind computational scheme to ensure numerical stability. Finally the transport component are adjusted for bed-slope effects. Therefore the following effects should be taken into account:

- Simulation with or without wave;
- Upwind shift;
- Bed slope effect.

For more details about the different formulations, which have been used in the DELFT3D, could be found in the Flow manual of DELFT3D-FLOW.

A.4 Boundary conditions

The 2D depth-averaged shallow water or long-wave equations applied in Delft3D represent a hyperbolic (inviscid case) or parabolic (viscid case) set of partial differential equations. To get a well-posed mathematical problem with a unique solution, a set of initial and boundary conditions for water levels and horizontal velocities must be specified. To solve the system of equations the following boundary conditions are required.

A.4.1 Bed and free surface boundary conditions

The vertical velocities at these boundaries are simply:

$$\omega(surface) = 0 \qquad and \qquad \omega(bottom) = 0 \tag{A.12}$$

Friction is applied at the seabed as follows:

$$\frac{\nu_v}{(d+\zeta)}\frac{\partial u}{\partial \sigma} \mid_{bottom} = \frac{\tau_{b\xi}}{\rho_o} \qquad and \qquad \frac{\nu_v}{(d+\zeta)}\frac{\partial v}{\partial \sigma} \mid_{bottom} = \frac{\tau_{b\eta}}{\rho_o} \tag{A.13}$$

where $\tau_{b\xi}$ and $\tau_{b\eta}$ seabed shear stress component include the effect of wave-current interaction.
The friction due to wind stress at the water surface may be included in the similar manner. For the transport boundary conditions the vertical diffusive fluxes through the free surface and seabed are set to zero.

A.4.2 Lateral boundary conditions

Along closed boundaries the velocity component perpendicular to the closed boundary is set to zero, which known as free-slip condition. At the open boundaries one of the following types of boundary conditions must be specified, water level, velocity in the direction normal to the boundary, discharge or linearised Riemann invariant (weakly reflective boundary conditions; Verboom and Slob, 1984). For the transport boundary conditions the assumption, that the horizontal of dissolved substances is dominated by advection, is taken into account. For the sand sediment fractions the local equilibrium sediment concentration profile may be used (Lesser et al., 2004).

Appendix B

Representative Tide using Steijn approach

B.1 Introduction

In coastal morphodynamics two processes play a dominant role, currents and waves. The almost infinite number of hydraulic conditions that can be observed in a coastal area over a full year must be reduced to a manageable number of model input conditions. The selected conditions must be representative for the morphological changes. This goes for initial process-oriented morphology models (without any feedback of a change sea bed on the hydrodynamic computations) and for time-dependent dynamic morphology models (inclusive of this feedback). The selection of a few hydrodynamic input conditions for the model components is usually done in such a way that the annual sediment transport capacities are reproduced at a number of selected locations. This implies that the best we can do is to represent the annual sediment transport rather than the morphological evolutions (Steijn, 1992).

B.2 Representative Tide

Tidal currents are harmonic phenomena which reverse every slack water period. The tidal range, HW-LW cycle, varies as a function of the time mainly as a consequence of astronomical effects. For application in complex models the following two types of schematizations have to be made:

- Selection of a single representative tidal cycle;
- Discretization of this cycle in a number of steps.

B.2.1 Selection of a single representative tide

Tides are harmonic phenomena described by a large number of tidal components each with its own period, amplitude and relative frequency. Although multi-annual and fluctuations exist, most attention is paid to a correct schematization of a mean

neap-spring tidal cycle. In addition to the more theoretical selection of representative tide, more pragmatic reasons may also play a role.
The representative tide or morphological tide is defined as the HW-LW cycle whose tidal amplitude corresponds with the mean tidal amplitude by an amplification factor, which normally larger than 1. This factor can be computed by multiplying amplification factors for both the astronomical and the climatological effect. The computation of these factors requires long-term water level registrations for the determination of the mean value and the standard deviation. The representative tide turns out to be the tide with an approximately 10% higher amplitude than the average mean tide. This 10% is related to the difference in tidal range of the mean tide and the spring tide.
Also Latteux, 1990 reports that the representative tide in case of open estuary in coastal region is a tide in between mean tide and mean spring tide. He recommends that more than just one tidal cycle be used to represent the yearly tidal variations (Steijn, 1992).

B.2.2 Discretization of HW-LW tidal cycle

The total number of selected tidal conditions is important. If this number is taken large, the reproduction of the representative tide will be quite good but on the other side the computational effort will grow. And it is also correct when the number of tidal conditions is taken too small, the computed sediment transport may not be representative.
According to Steijn (1992) approach, the procedure for the selection of ten representative tidal conditions consists of the following steps:

- Select a number of location in the area of interest and determine water level, flow velocity and flow direction during the selected tidal cycle;
- Give scores to each half hour in the tidal cycle according to a list of criteria and for each location;
- Compute the total score for each half hour of the tide period by summing these scores;
- Select ten tidal conditions, in which the highest density is taken in the time intervals with the highest scores;
- Average the results obtained for the different locations.

When a proper representation of the tidal cycle is more critical at certain locations then a higher relative weight can be given to these specific locations.

Appendix C

Additional Figures of Chapter 5

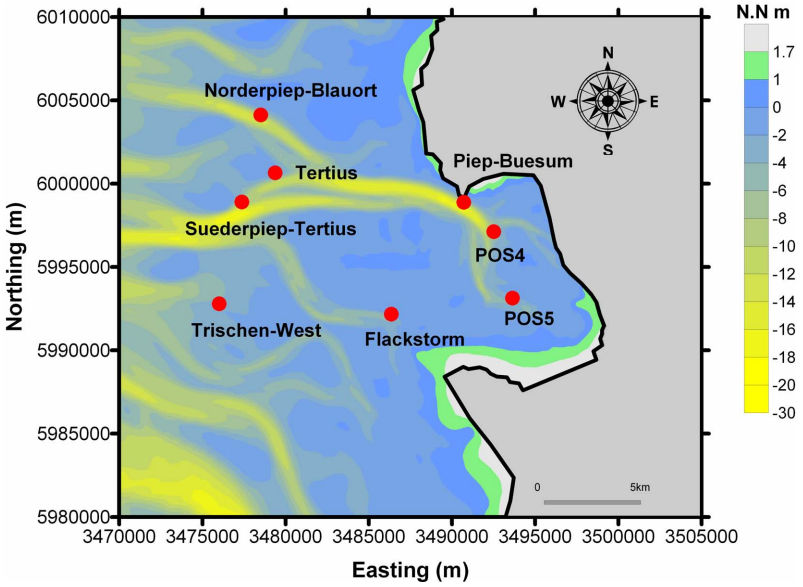

Figure C.1: Location of the observation points

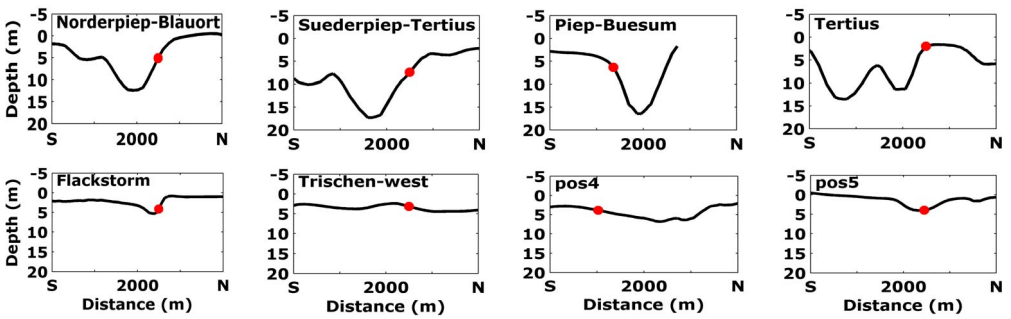

Figure C.2: Cross-sections including the location of the observation points

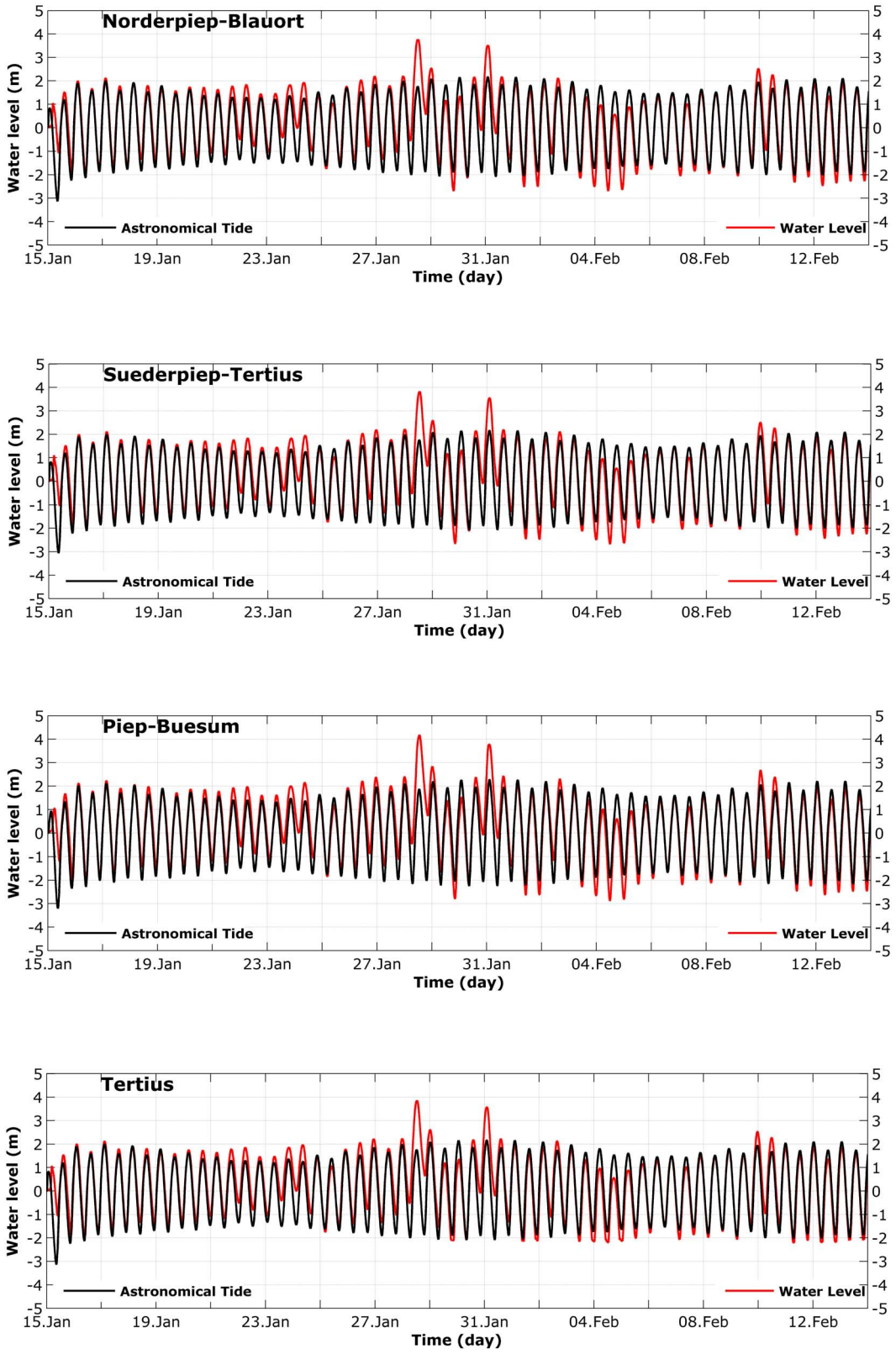

Figure C.3: Modelled water levels for 1994 storm

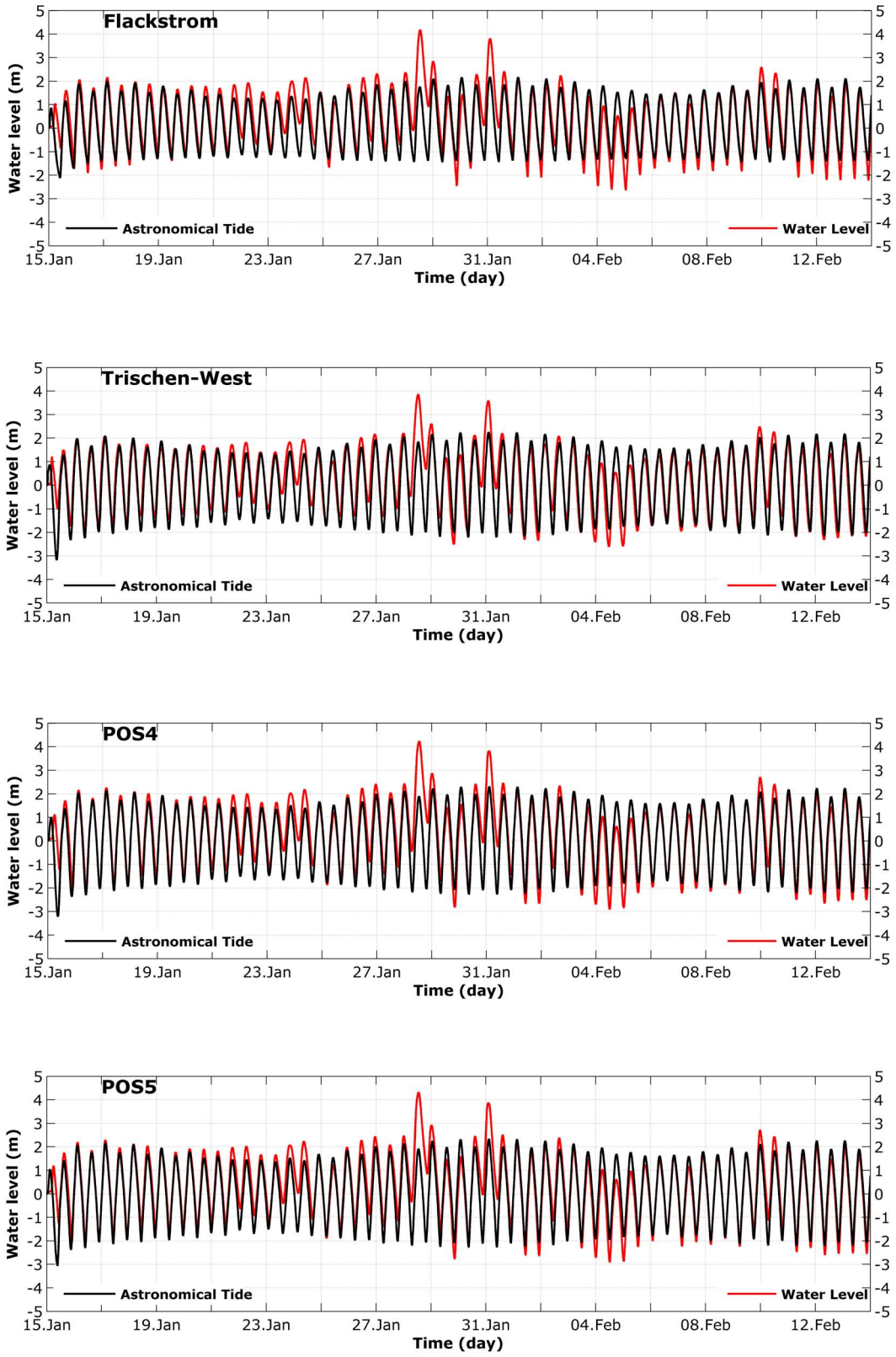

Figure C.4: Modelled water levels for 1994 storm (continue)

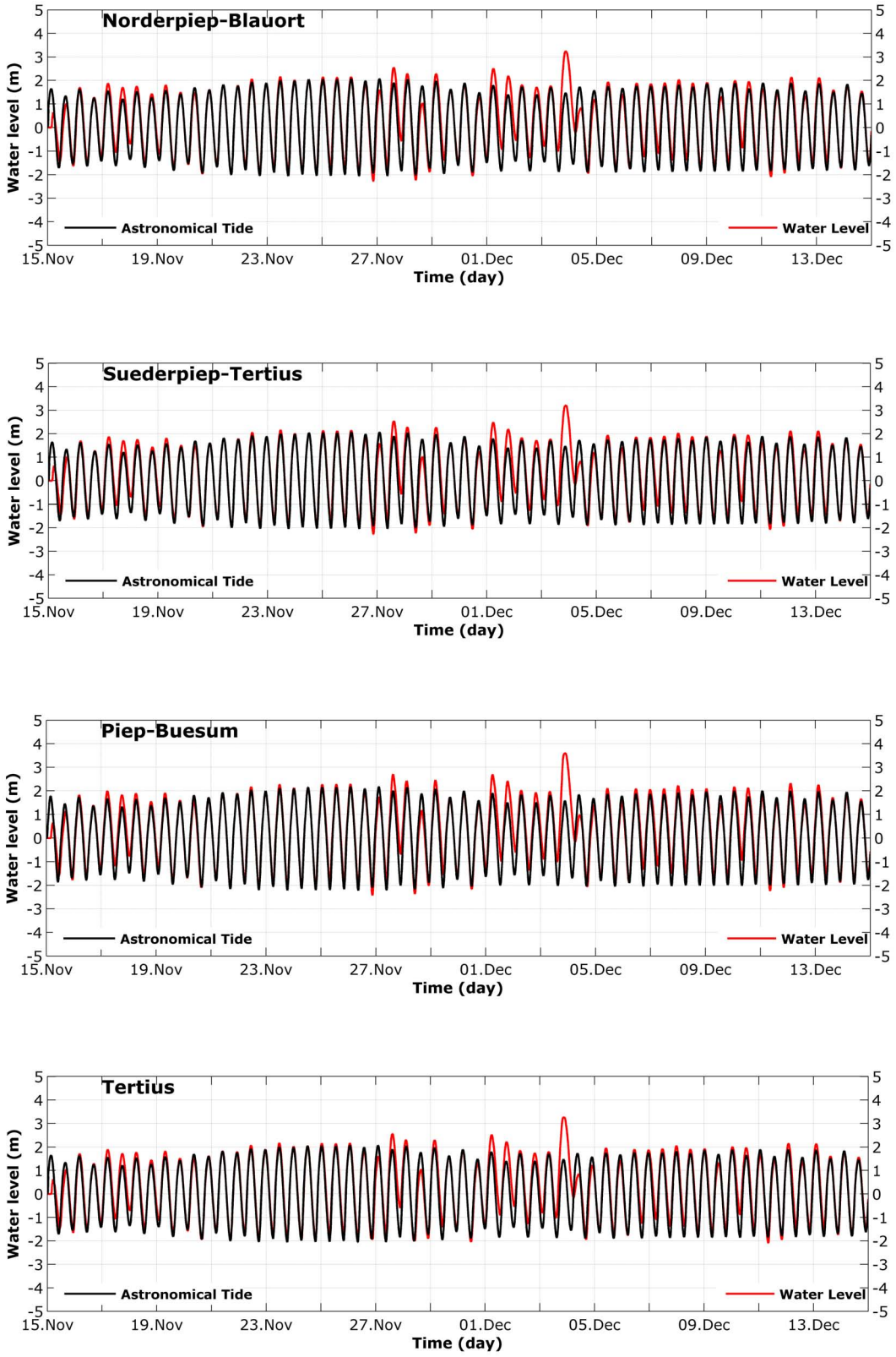

Figure C.5: Modelled water levels for 1999 Storm

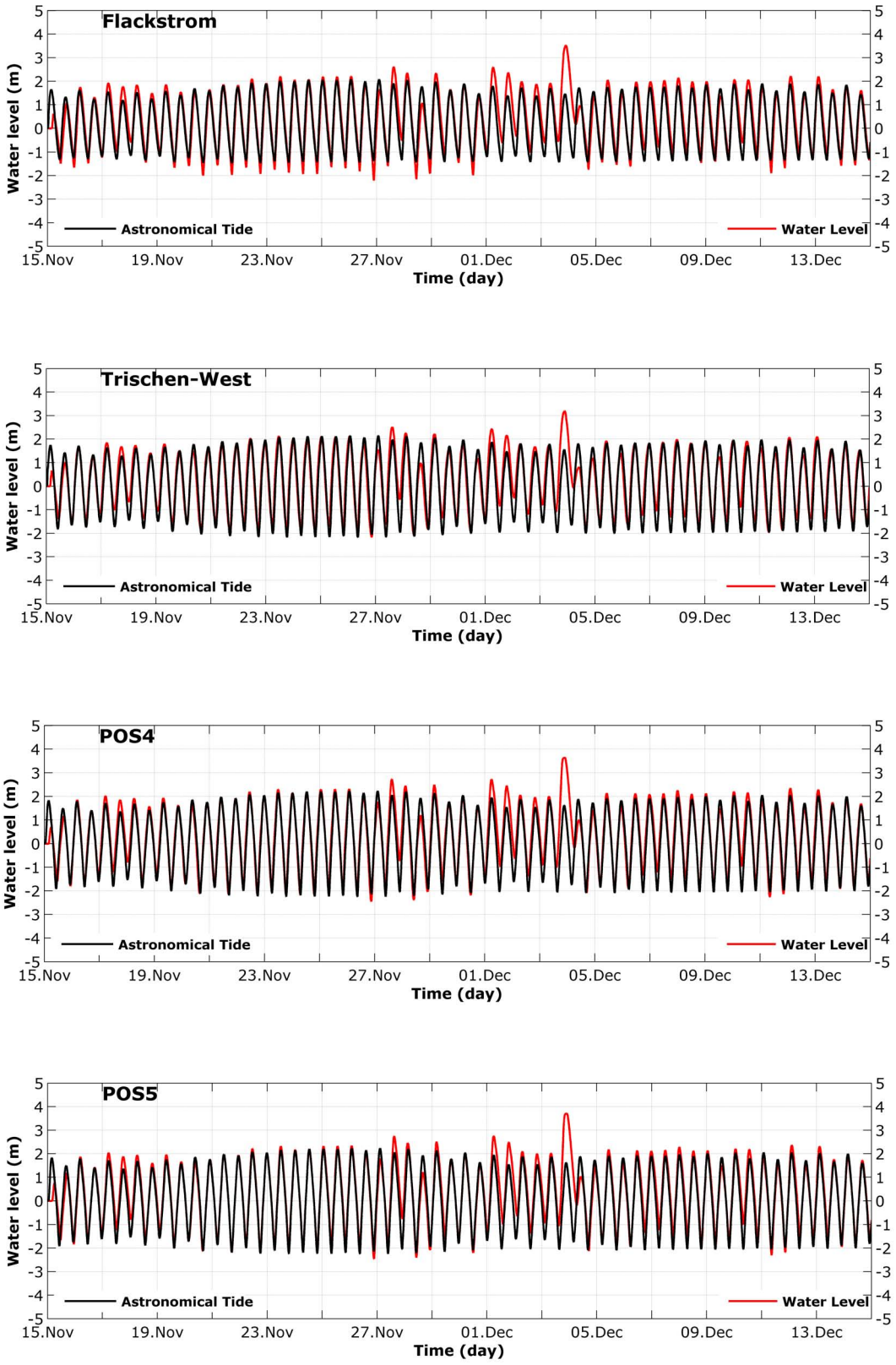

Figure C.6: Modelled water levels for 1999 Storm (continue)

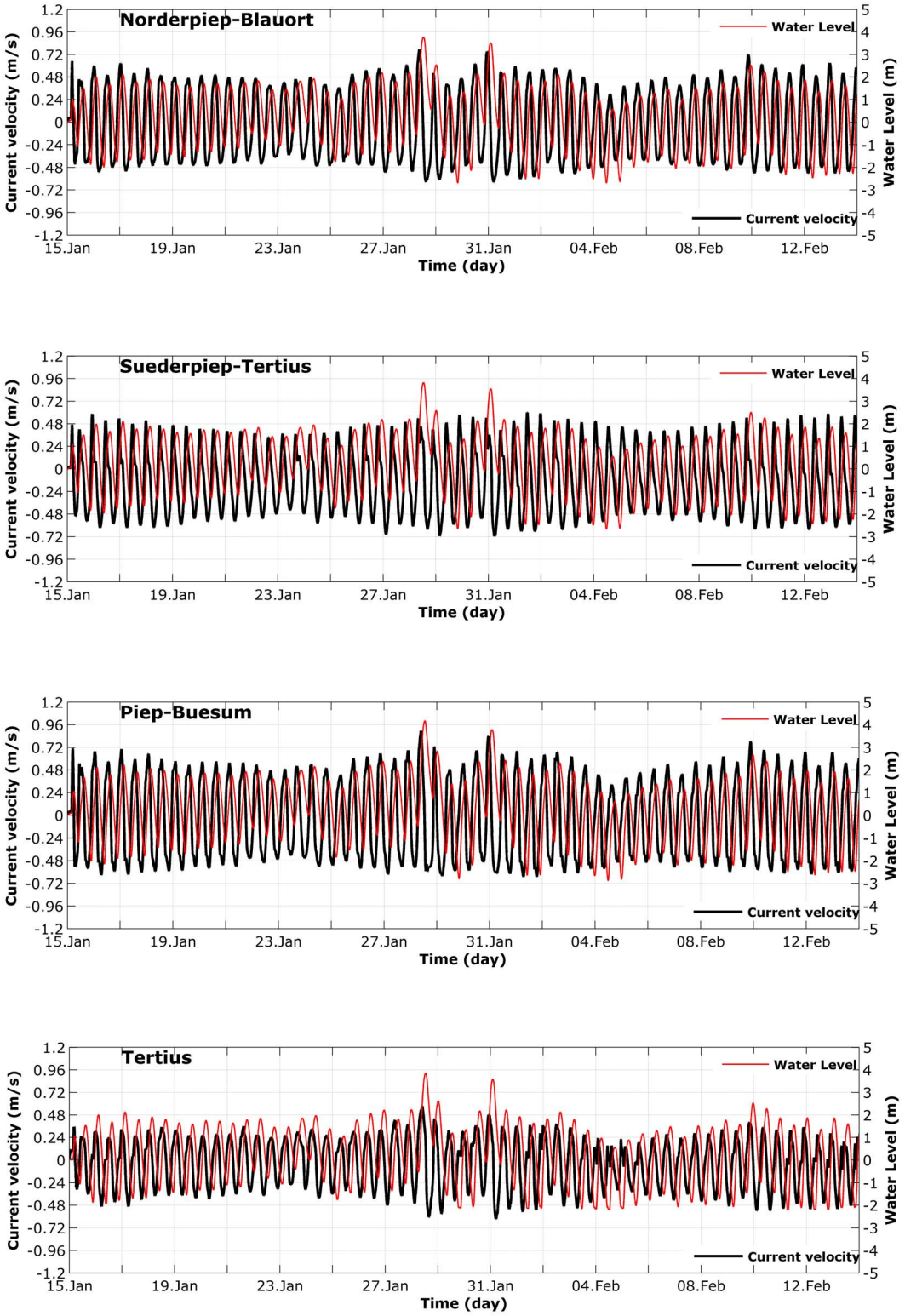

Figure C.7: Modelled current velocity for 1994 Storm

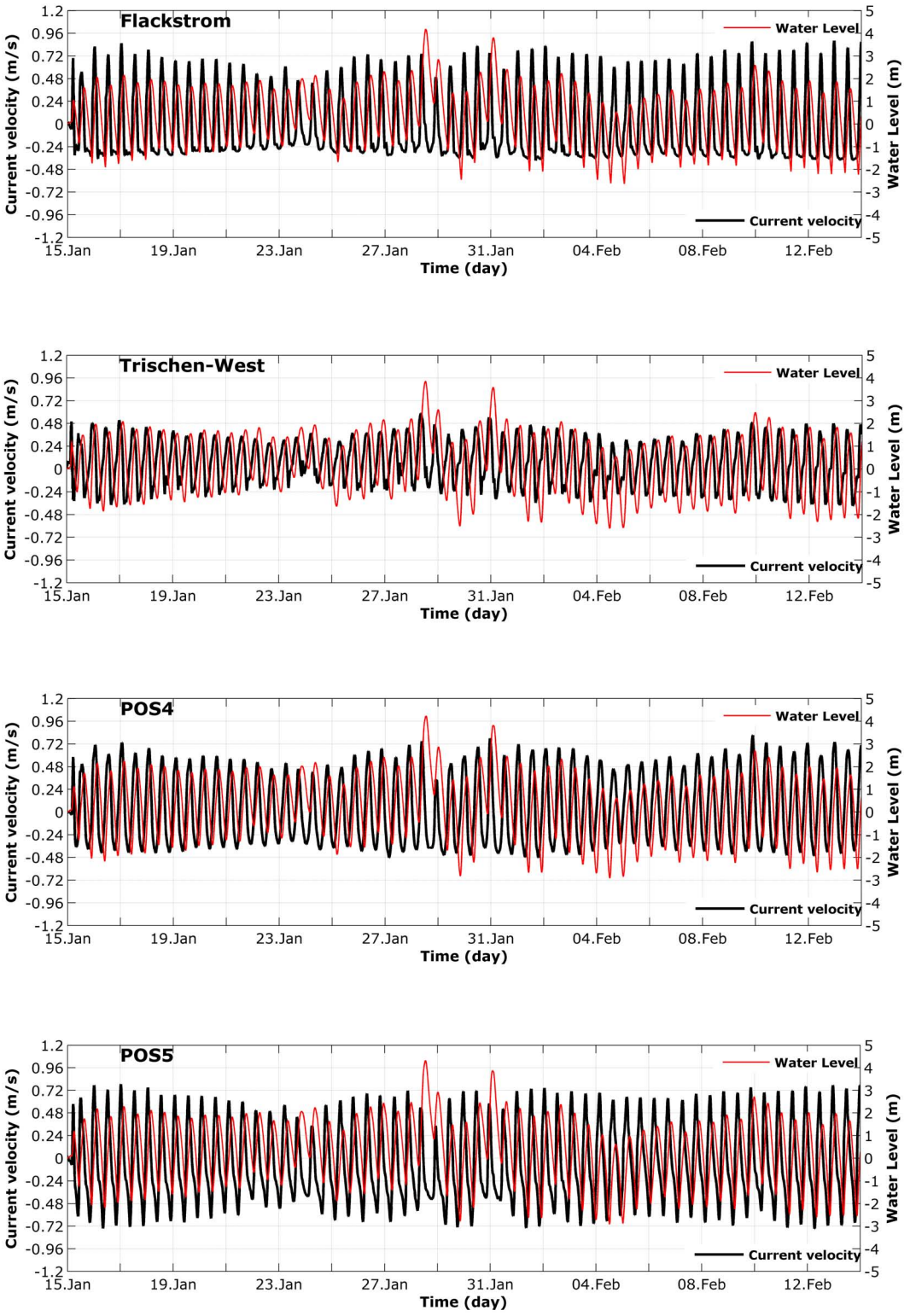

Figure C.8: Modelled current velocity for 1994 Storm (continue)

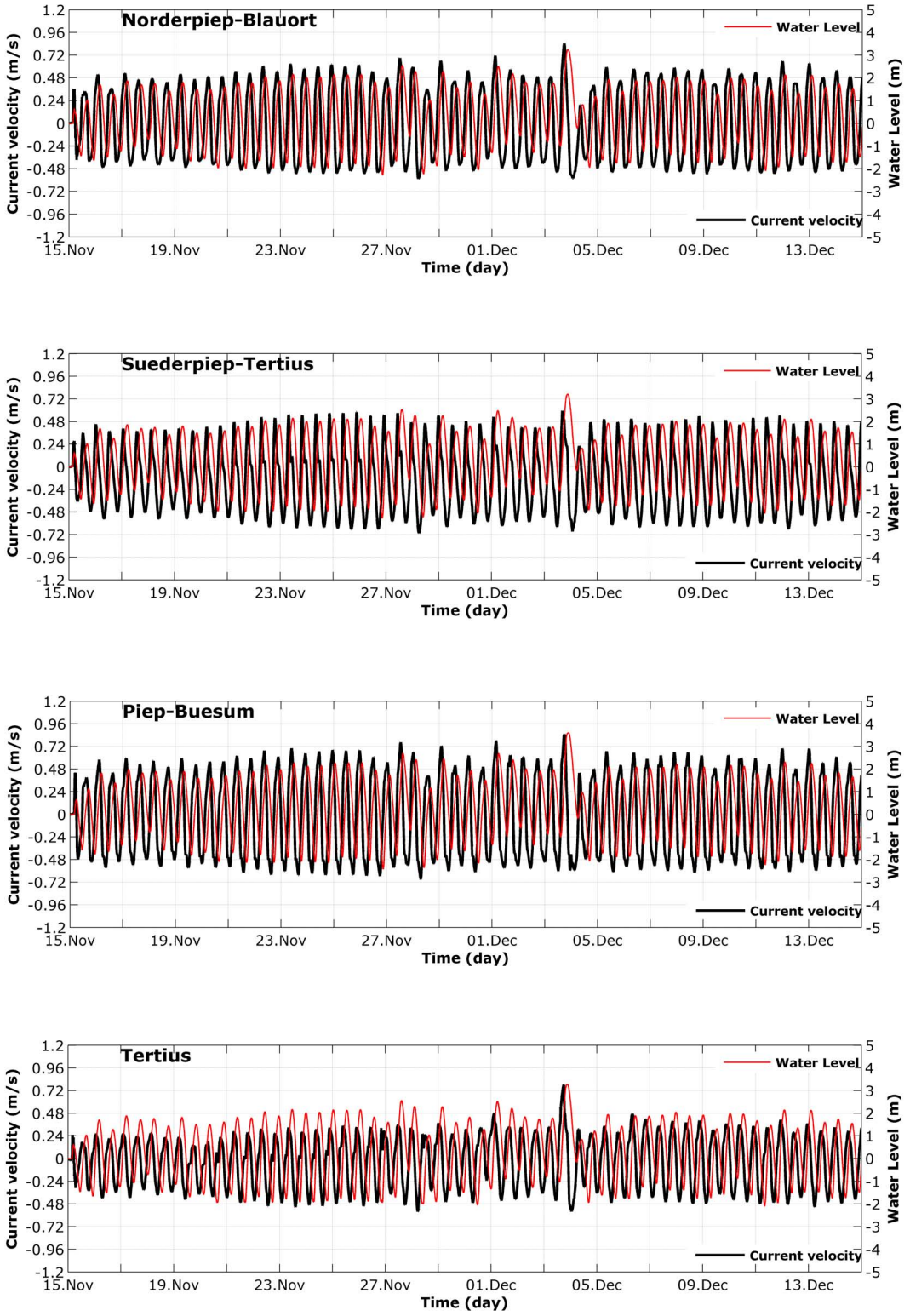

Figure C.9: Modelled current velocity for 1999 Storm

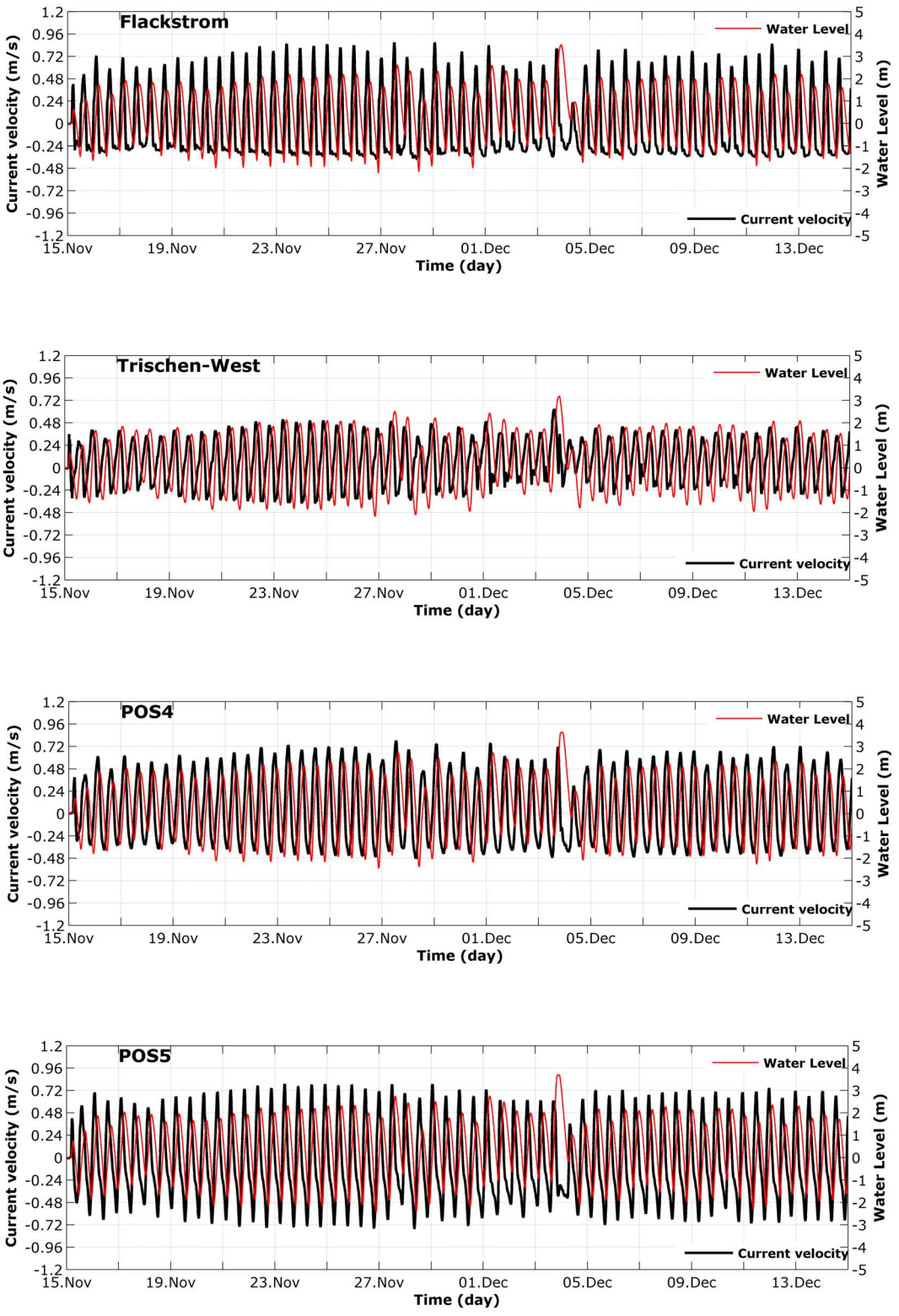

Figure C.10: Modelled current velocity for 1999 Storm (continue)

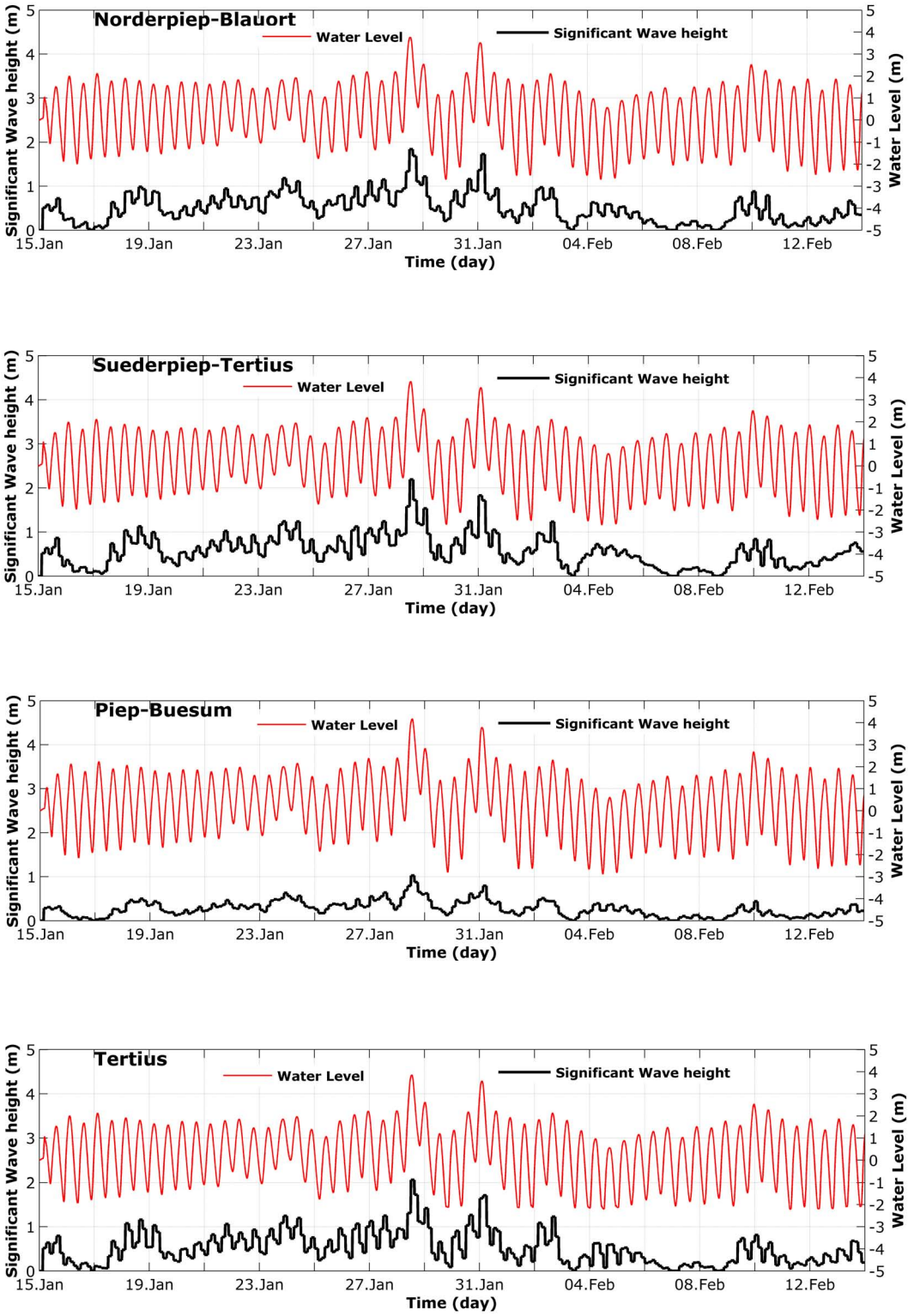

Figure C.11: Modelled significant wave height for 1994 Storm

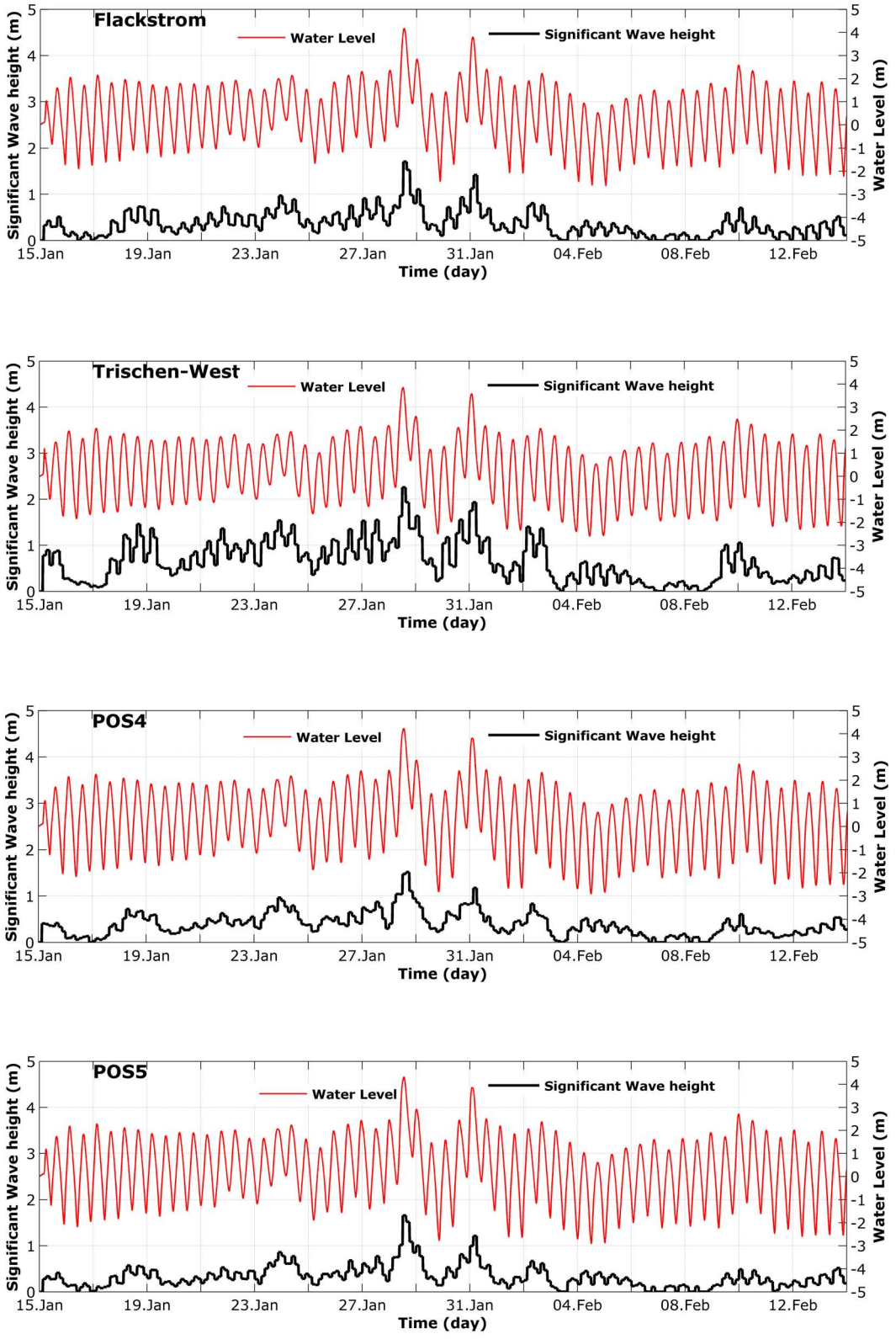

Figure C.12: Modelled significant wave height for 1994 Storm (continue)

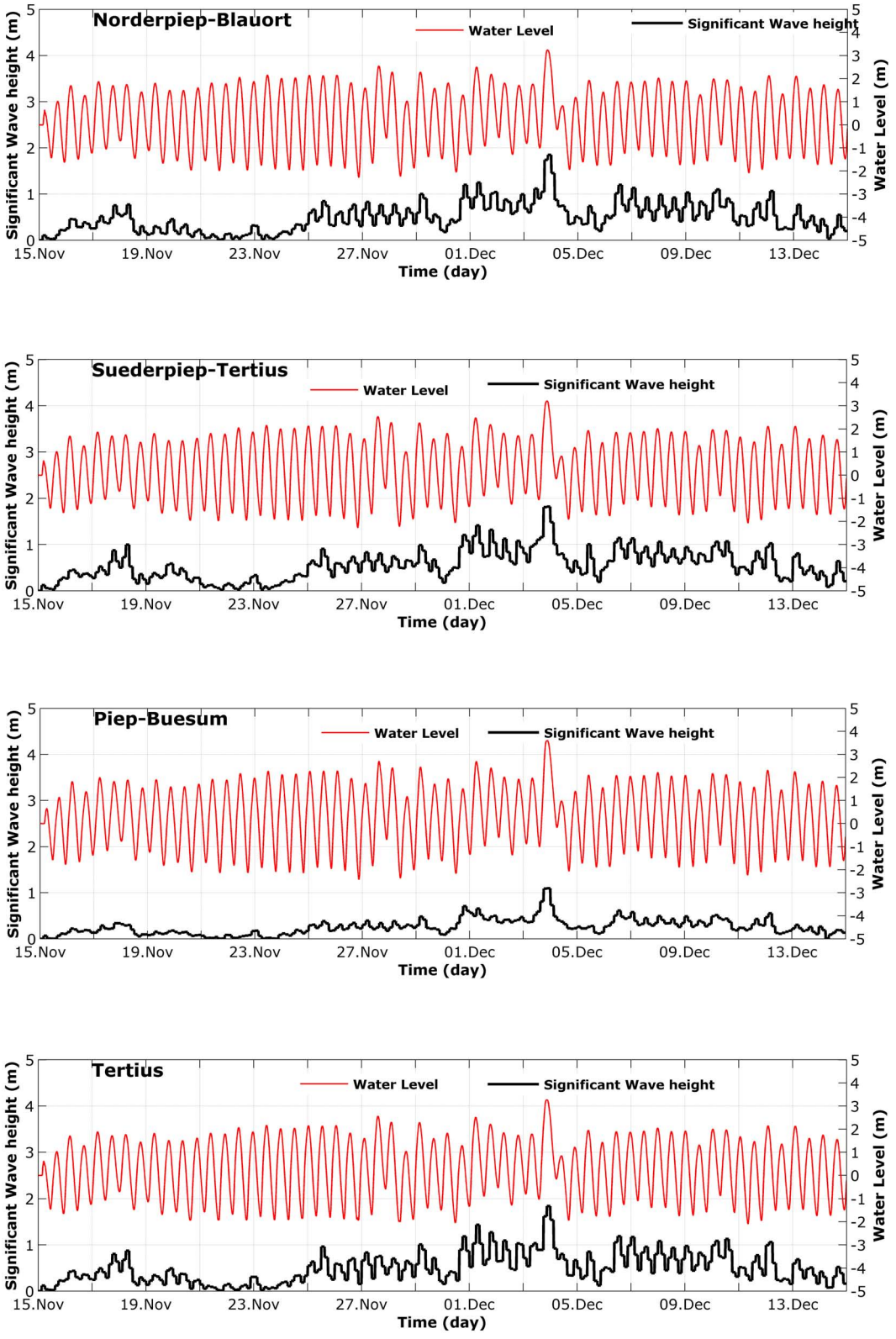

Figure C.13: Modelled significant wave height for 1999 Storm

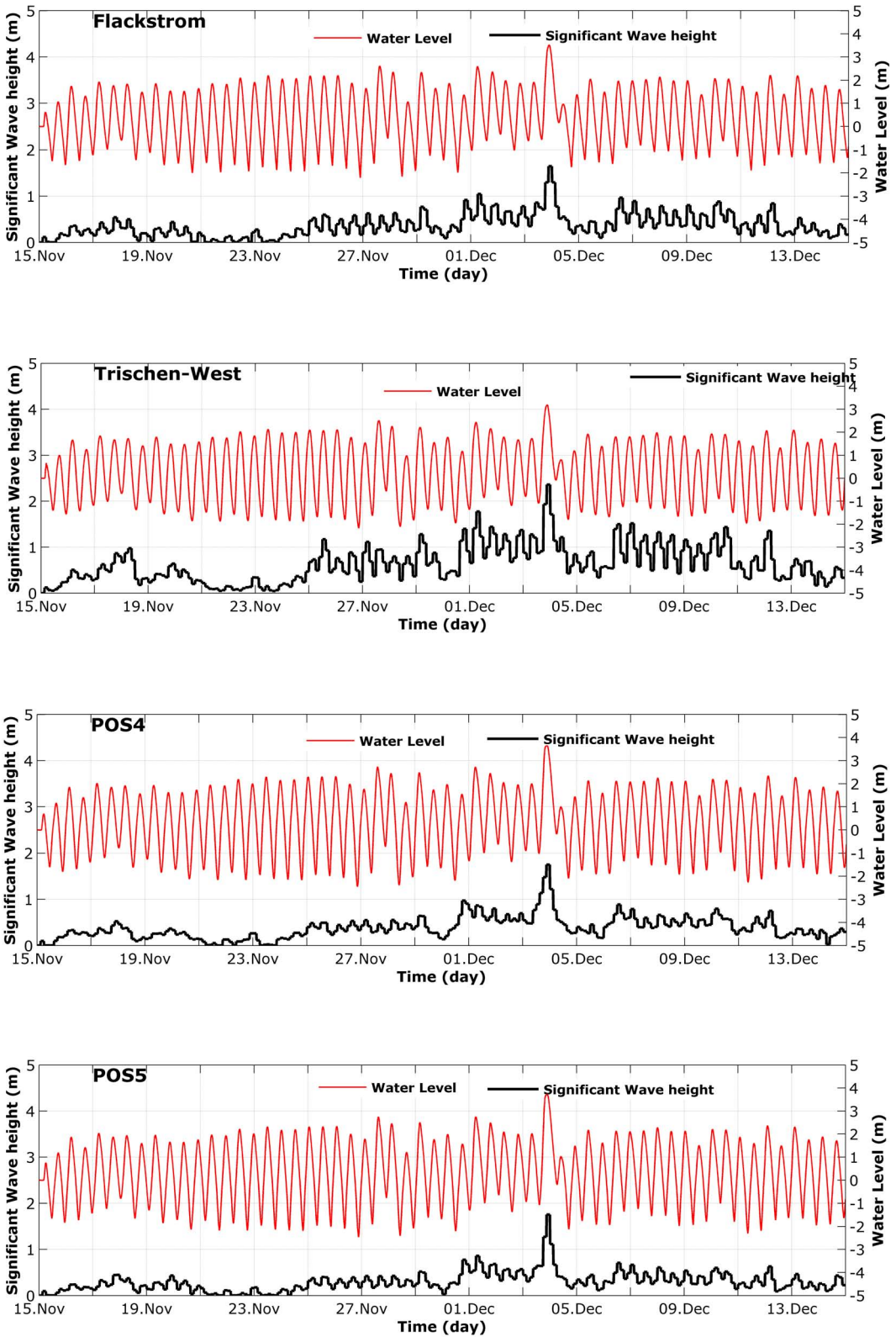

Figure C.14: Modelled significant wave height for 1999 Storm (continue)

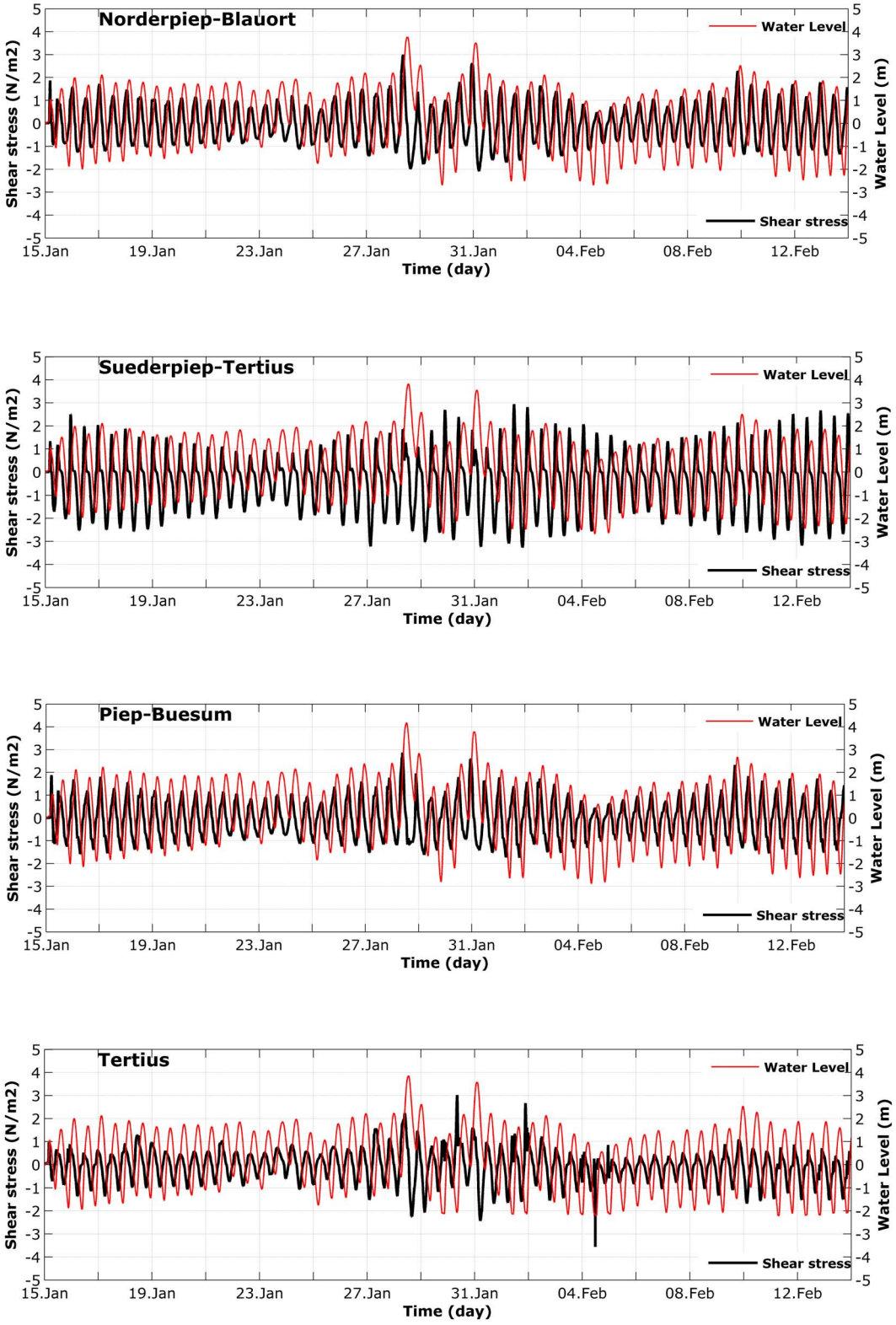

Figure C.15: Modelled bed shear stress for 1994 Storm

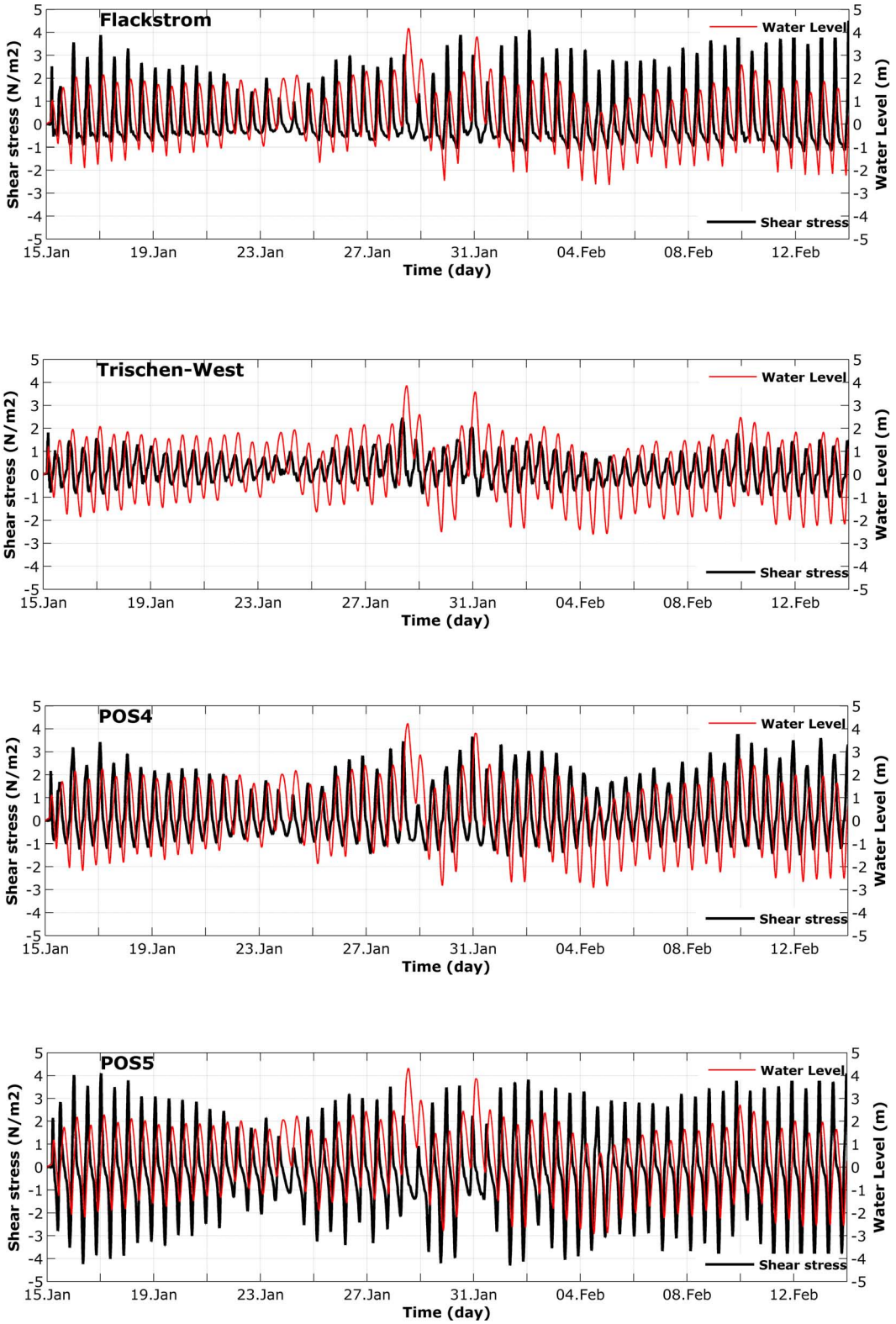

Figure C.16: Modelled bed shear stress for 1994 Storm (continue)

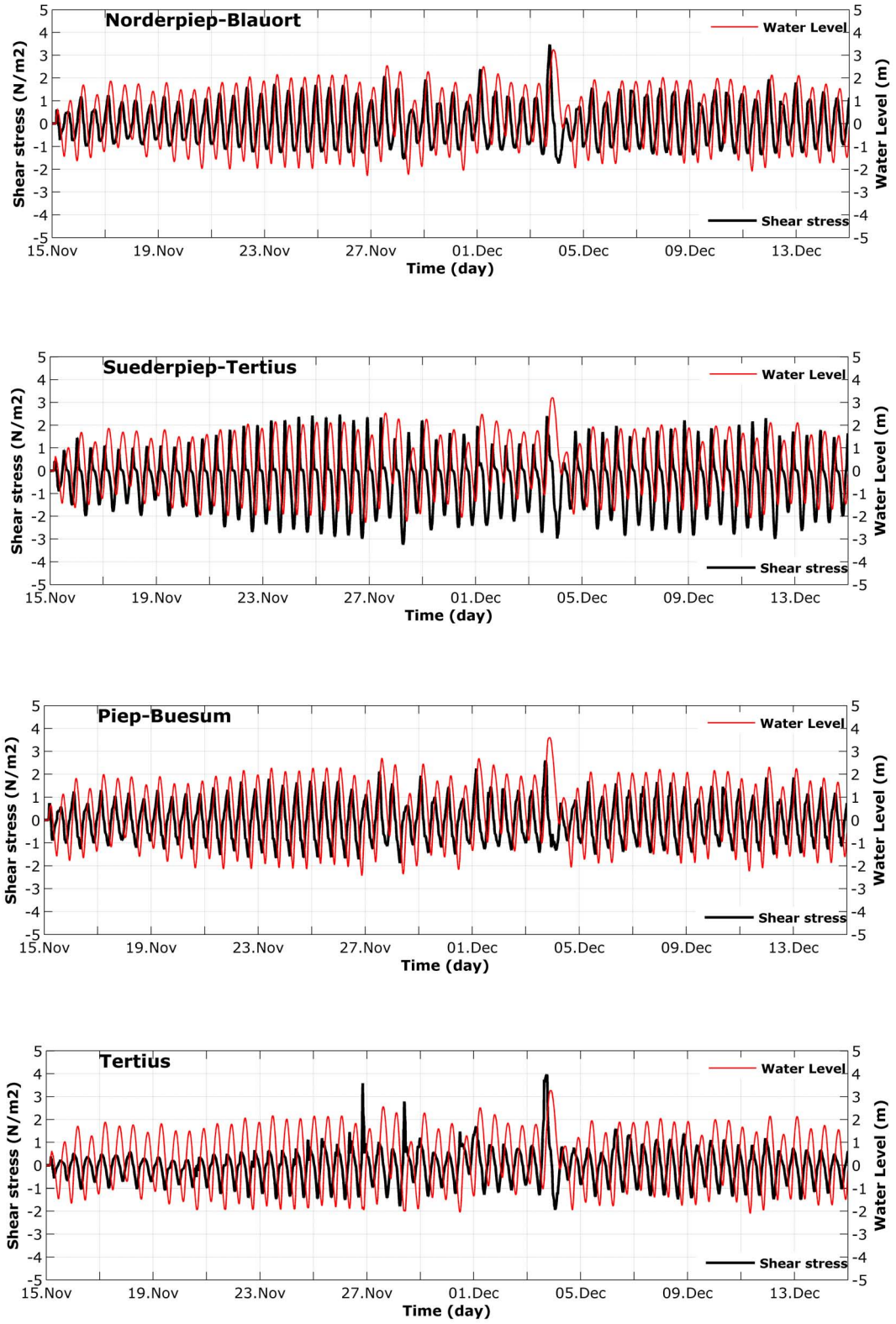

Figure C.17: Modelled bed shear stress for 1999 Storm

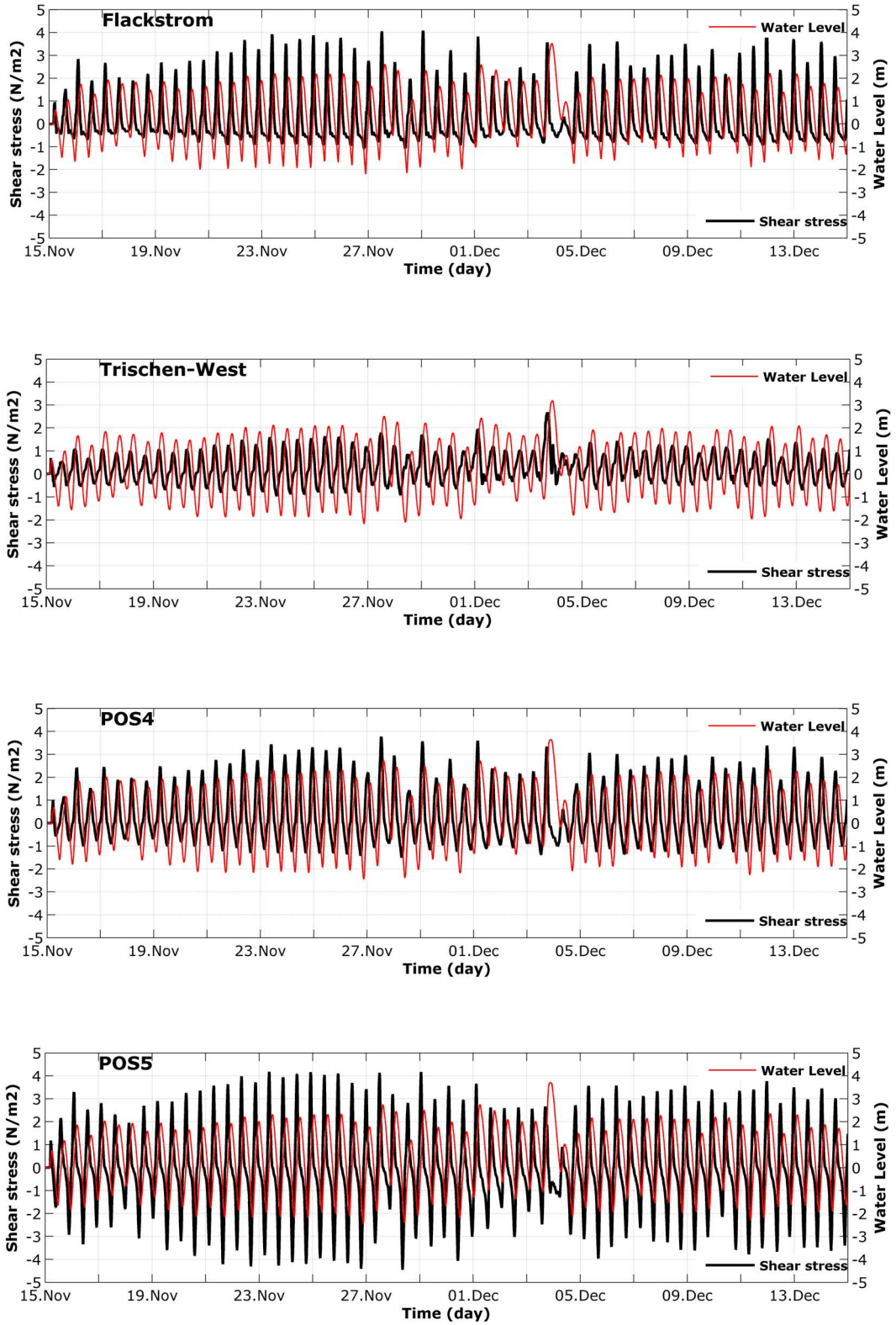

Figure C.18: Modelled bed shear stress for 1999 Storm (continue)

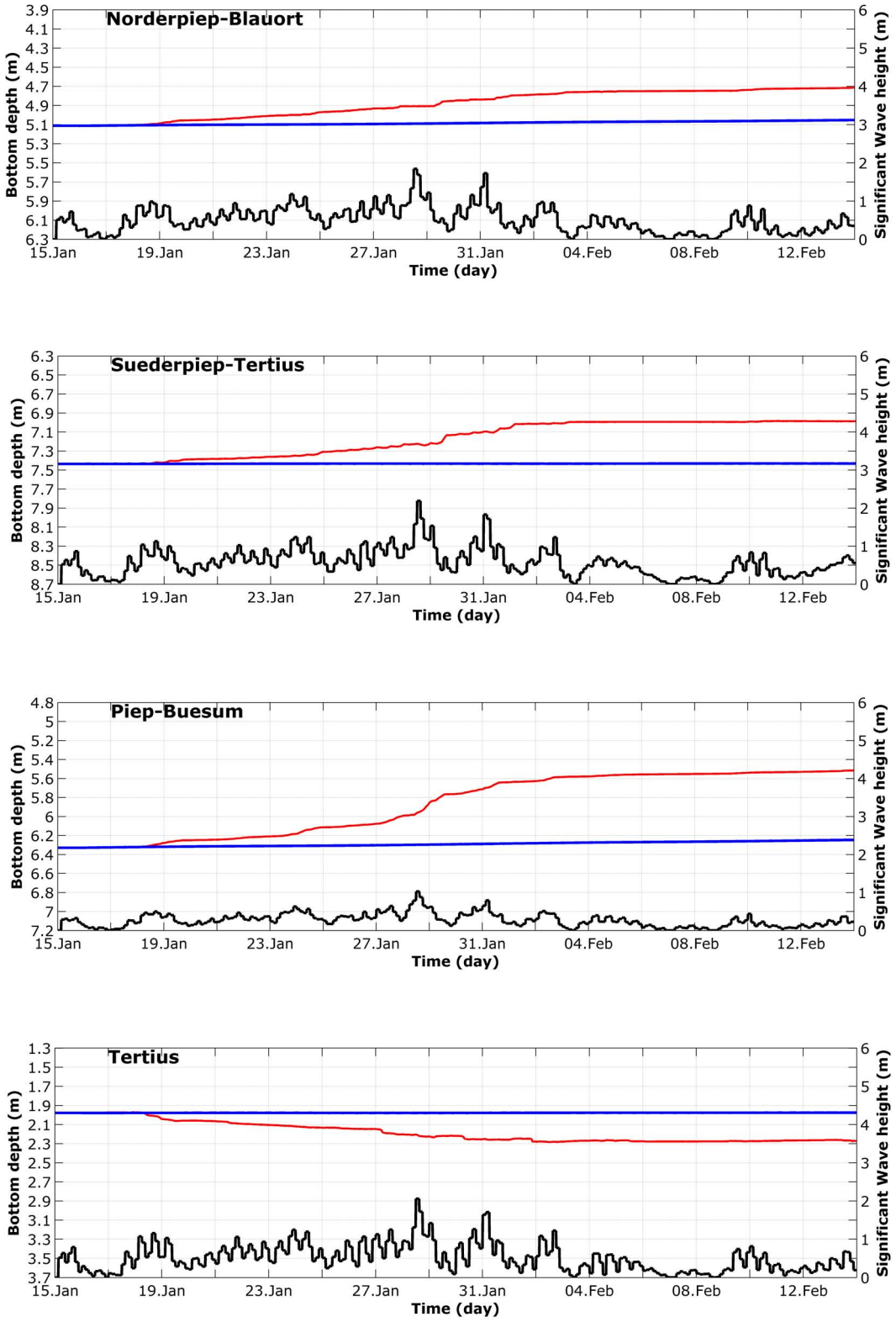

Figure C.19: Bottom depth for 1994 Storm

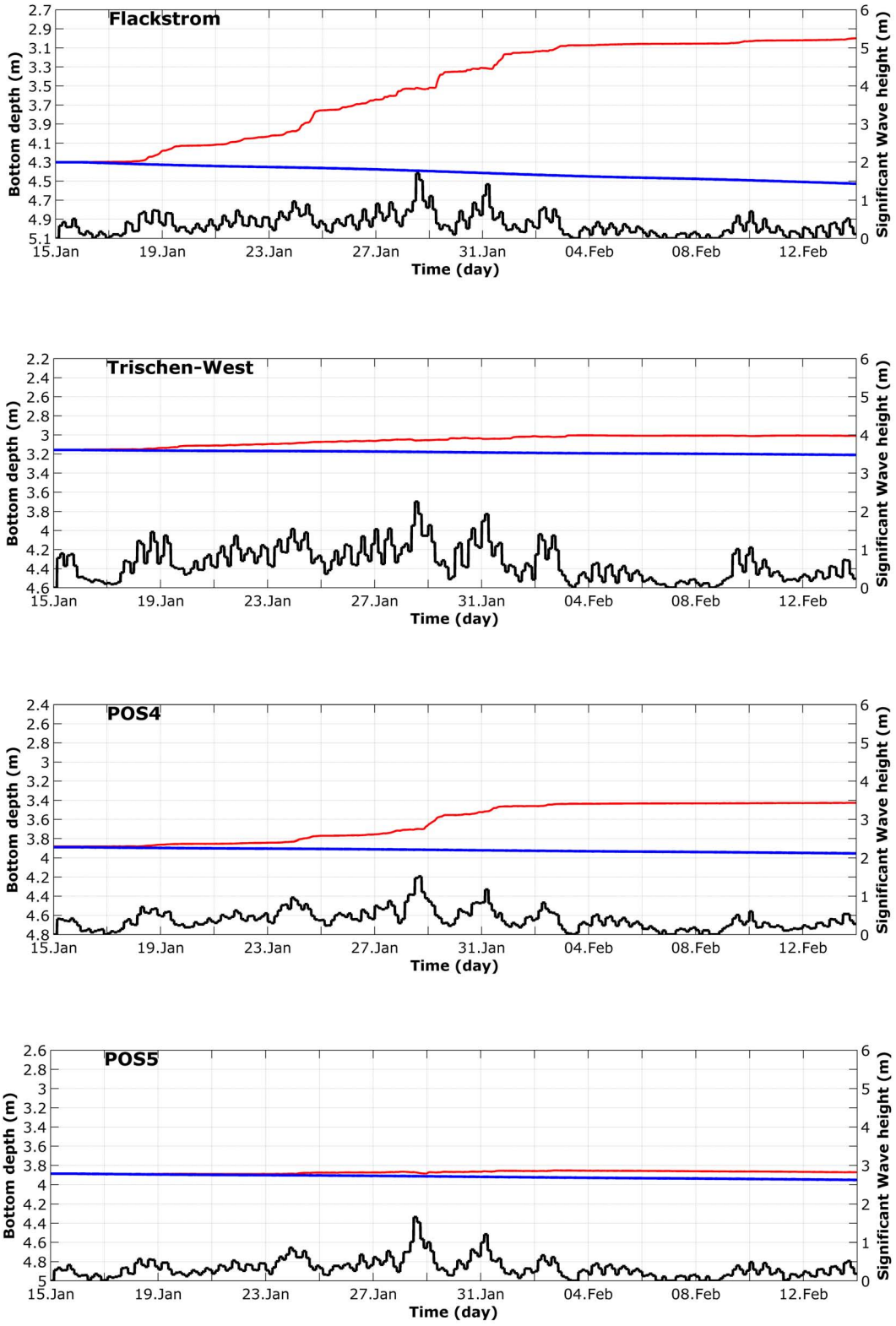

Figure C.20: Bottom depth for 1994 Storm (continue)

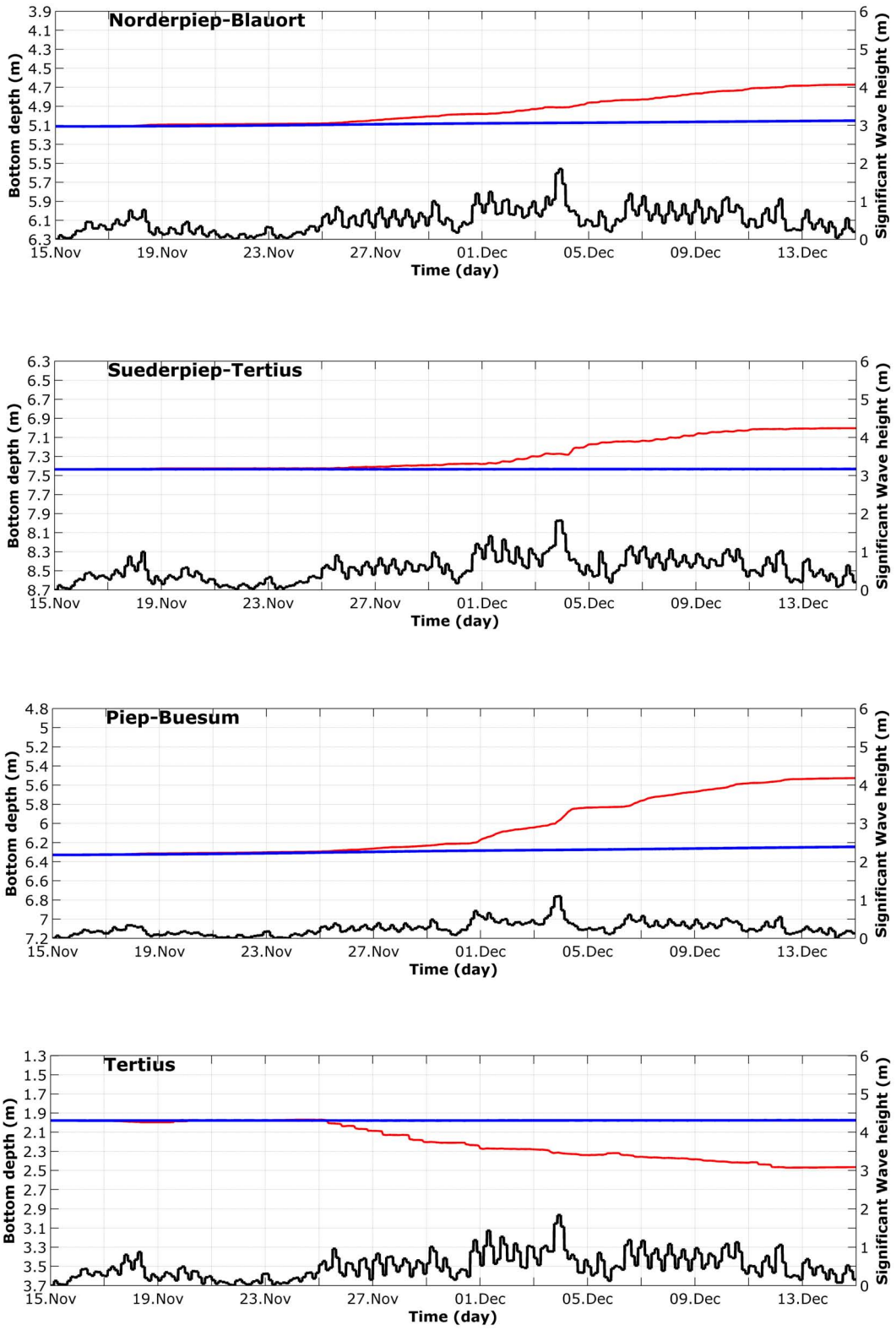

Figure C.21: Bottom depth for 1999 Storm

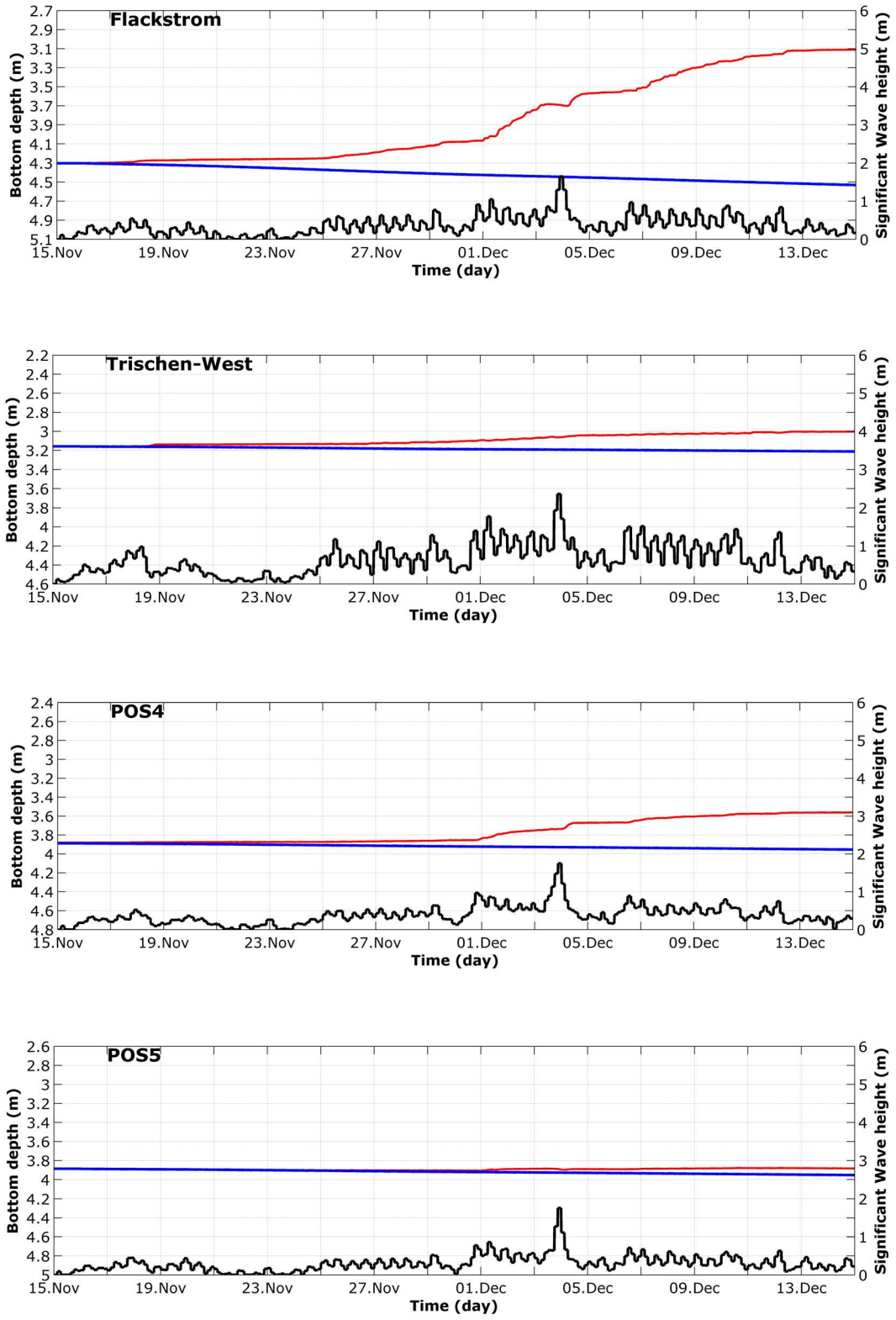

Figure C.22: Bottom depth for 1999 Storm (continue)

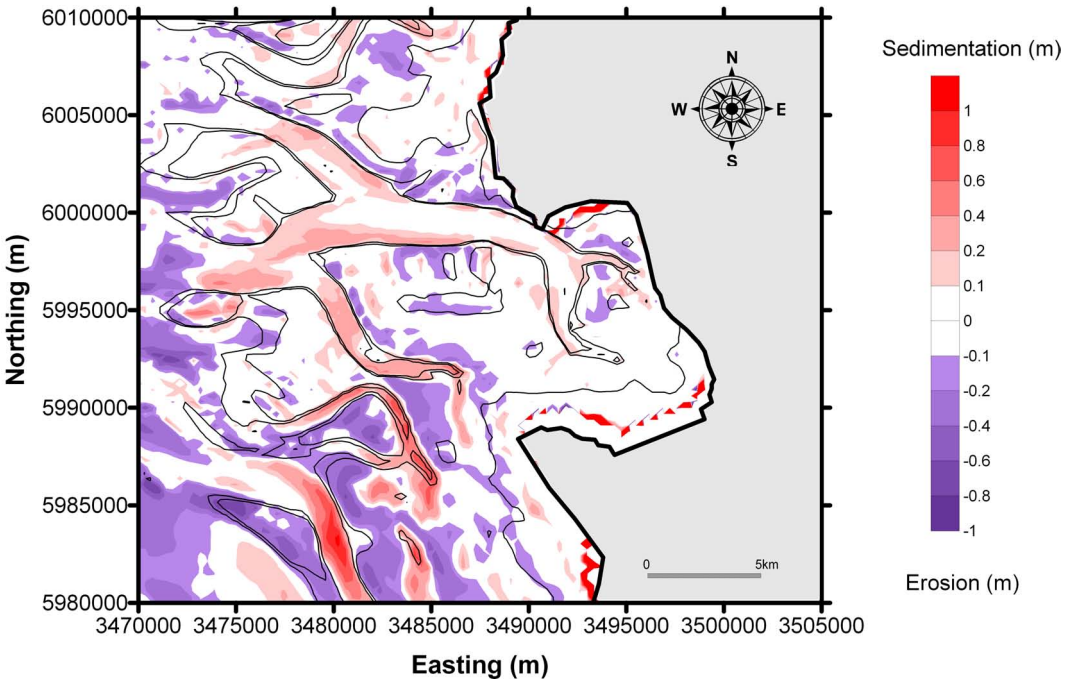

Figure C.23: Bed level changes resulting from one day before 1994 Storm

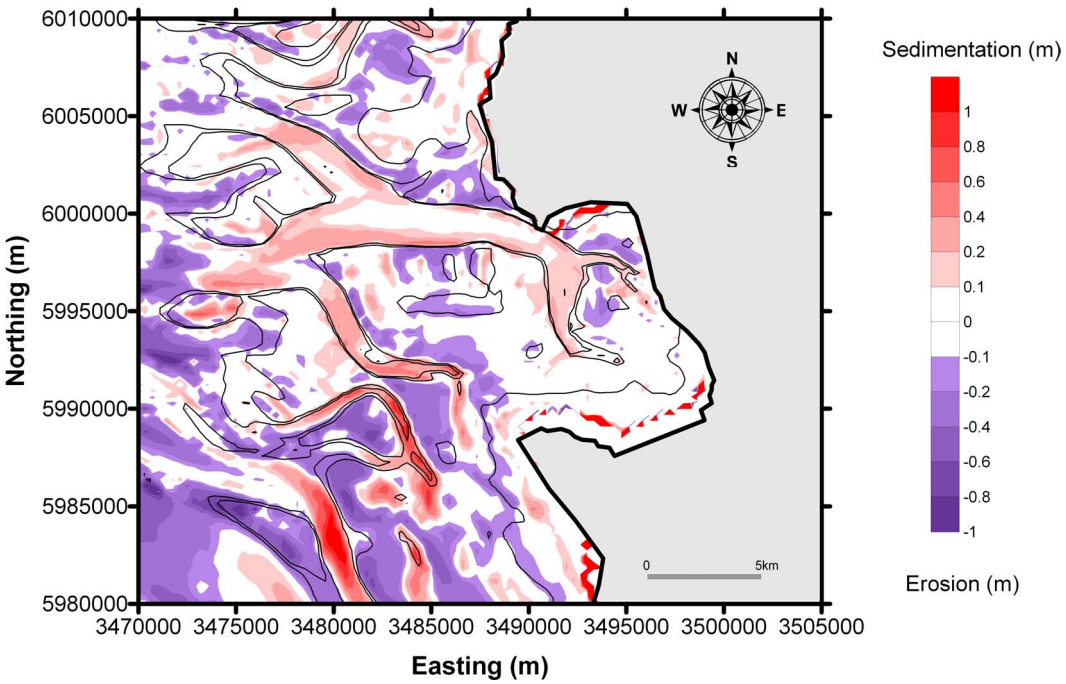

Figure C.24: Bed level changes resulting during the 1994 Storm

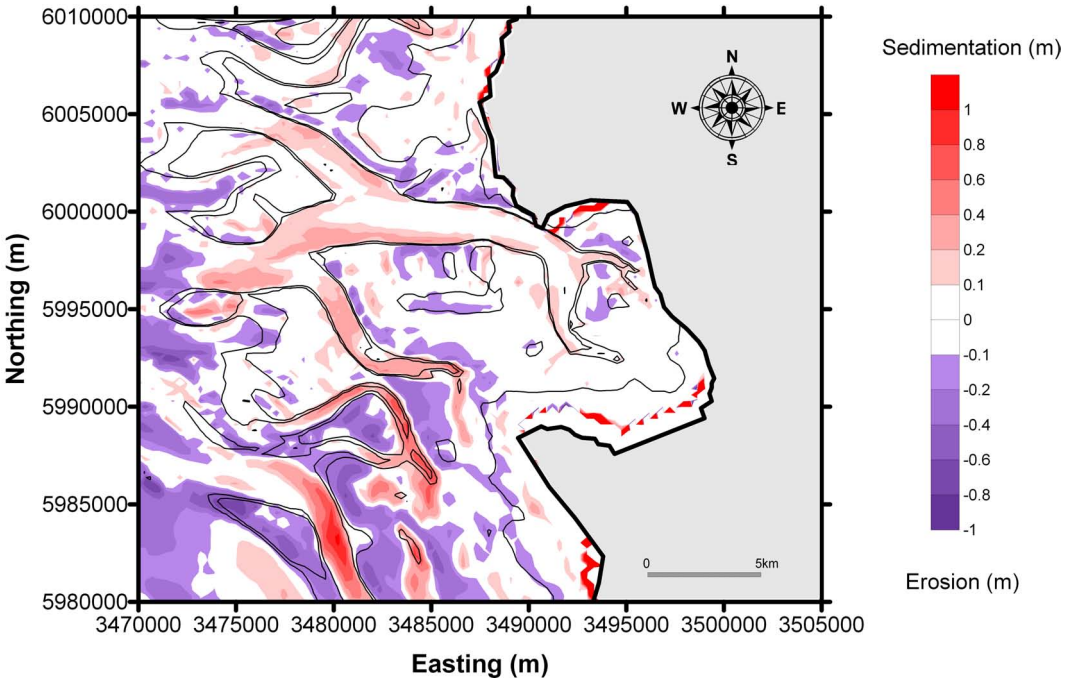

Figure C.25: Bed level changes resulting from one day after 1994 Storm

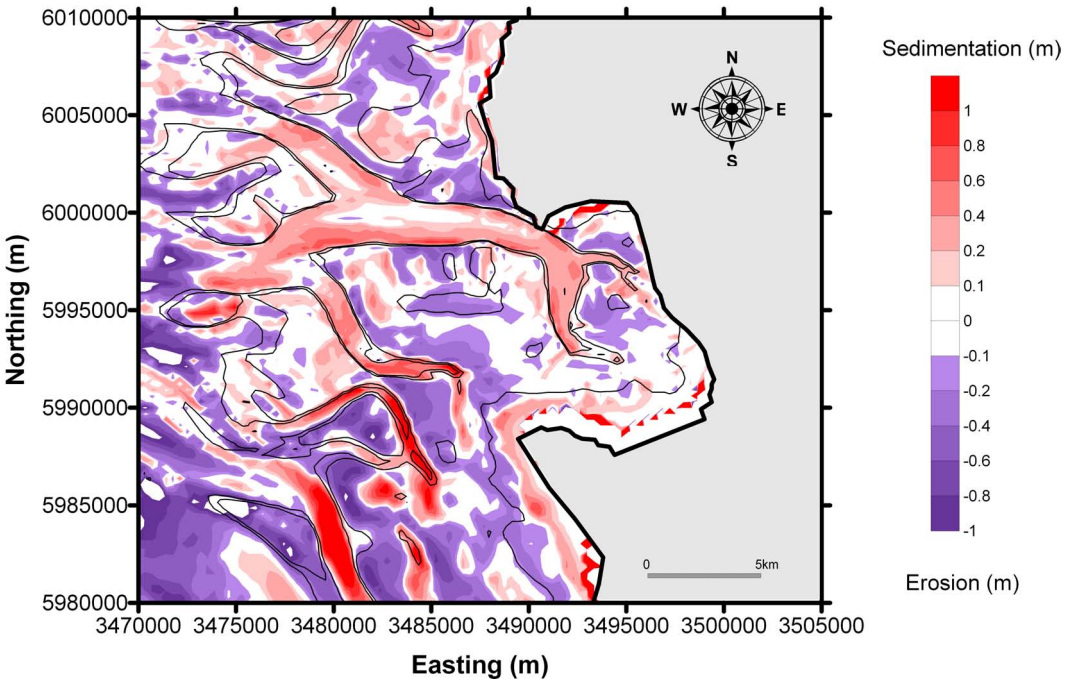

Figure C.26: Bed level changes resulting at the end of the simulation 1994 Storm (14.Feb)

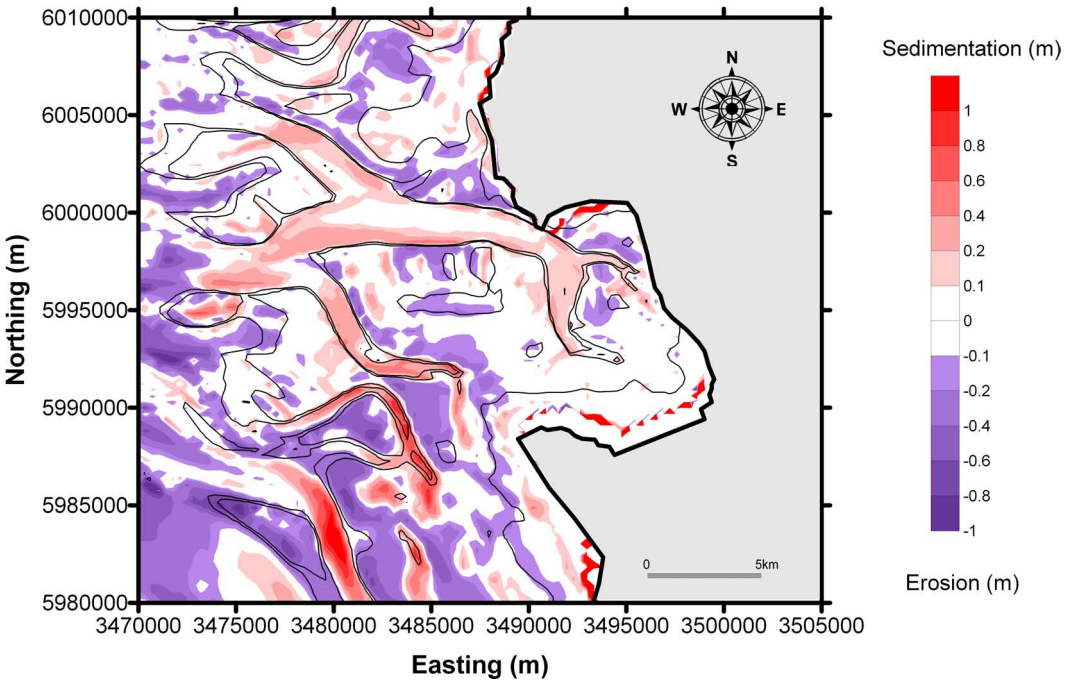

Figure C.27: Bed level changes resulting from one day before 1999 Storm

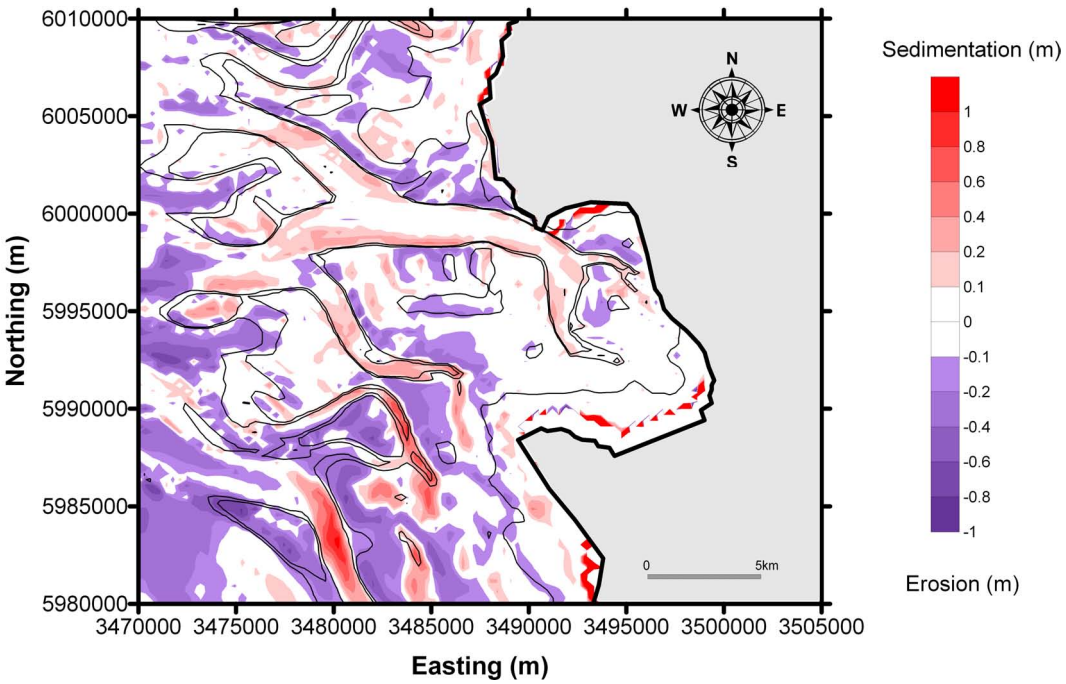

Figure C.28: Bed level changes resulting during the 1999 Storm

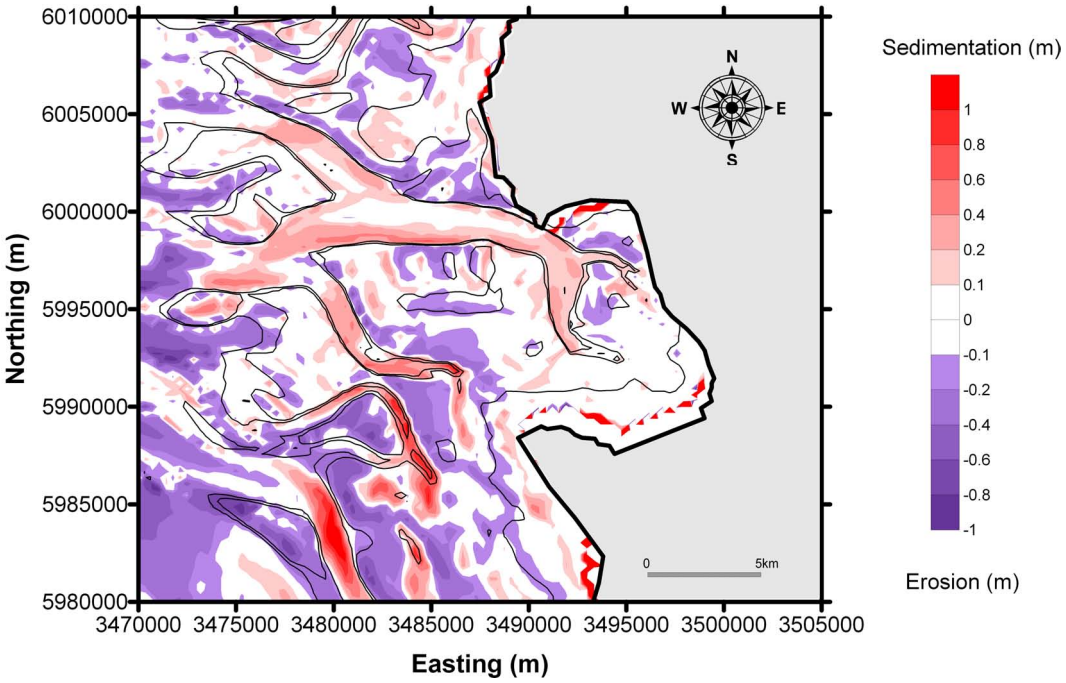

Figure C.29: Bed level changes resulting from one day after 1999 Storm

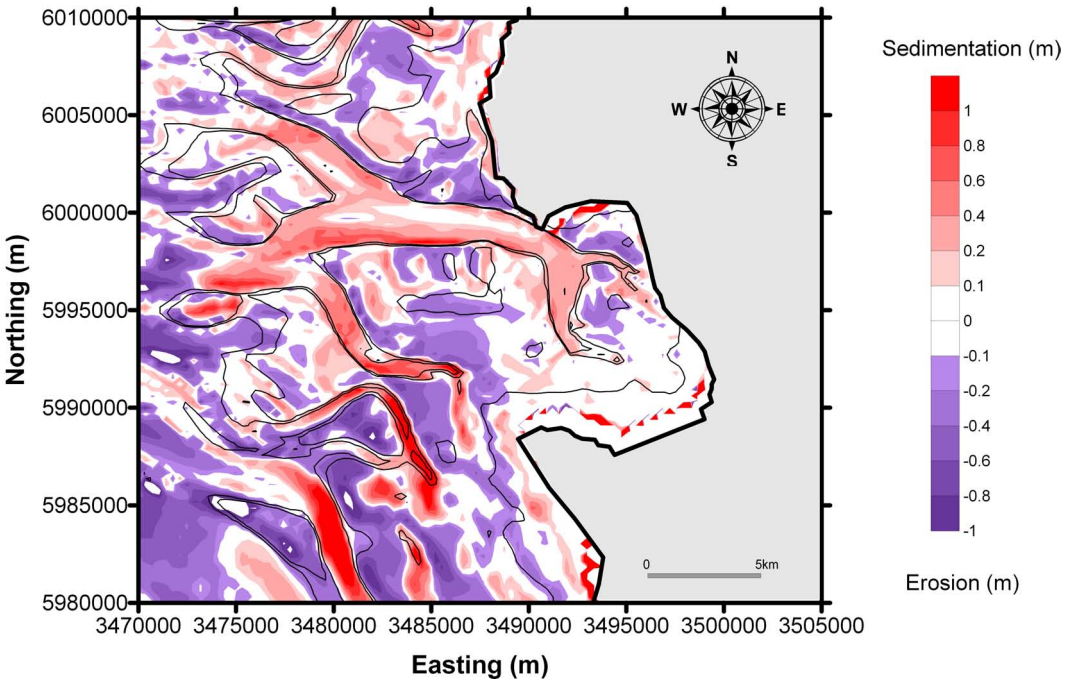

Figure C.30: Bed level changes resulting at the end of the simulation 1999 Storm (14.Dec)